GEOTECHNOLOGIES AND THE ENVIRONMENT

Pamela S. Showalter · Yongmei Lu (Eds.)

Geospatial Techniques in Urban Hazard and Disaster Analysis

Springer

Geospatial Techniques in Urban Hazard and Disaster Analysis

Geotechnologies and the Environment

Volume 2

Series Editors:

Jay D. Gatrell, *School of Graduate Studies and Department of Geography, Geology, and Anthropology, Indiana State University, Terre Haute, IN, USA*

Ryan R. Jensen, *Department of Geography, Brigham Young University, Provo, UT, USA*

The "Geotechnologies and the Environment" series is intended to provide specialists in the geotechnologies and academics who utilize these technologies, with an opportunity to share novel approaches, present interesting (sometimes counter-intuitive) case studies, and most importantly to situate GIS, remote sensing, GPS, the internet, new technologies, and methodological advances in a real world context. In doing so, the books in the series will be inherently applied and reflect the rich variety of research performed by geographers and allied professionals.

Beyond the applied nature of many of the papers and individual contributions, the series interrogates the dynamic relationship between nature and society. For this reason, many contributors focus on human-environment interactions. The series are not limited to an interpretation of the environment as nature per se. Rather, the series "places" people and social forces in context and thus explore the many socio-spatial environments humans construct for themselves as they settle the landscape. Consequently, contributions will use geotechnologies to examine both urban and rural landscapes.

For further volumes:
http://www.springer.com/series/8088

Pamela S. Showalter · Yongmei Lu
Editors

Geospatial Techniques in Urban Hazard and Disaster Analysis

Springer

Editors
Dr. Pamela S. Showalter
Texas State University
Department of Geography
San Marcos TX 78666-4616
USA
ps15@txstate.edu

Dr. Yongmei Lu
Texas State University
Department of Geography
San Marcos TX 78666-4616
USA
yl10@txstate.edu

ISBN 978-90-481-2237-0 e-ISBN 978-90-481-2238-7
DOI 10.1007/978-90-481-2238-7
Springer Dordrecht Heidelberg London New York

Library of Congress Control Number: 200992683

Cover image: Diamondhead Debris Sites-Post-Kalrina Imagery and Parcels, photo courtesy of Federal Emergency Management Agency, USA.

Printed on acid-free paper

Springer is part of Springer Science+Business Media (www.springer.com)

Preface

This book is the second in a series that examines how geographic information technologies (GIT) are being implemented to improve our understanding of a variety of hazard and disaster situations. The main types of technologies covered under the umbrella of GIT, as used in this volume, are geographic information systems, remote sensing (not including ground-penetrating or underwater systems), and global positioning systems. Our focus is on urban areas, broadly defined in order to encompass rapidly growing and densely populated areas that may not be considered "urban" in the conventional sense.

The material presented here is also unabashedly applied – our goal is to provide GIT tools to those seeking more efficient ways to respond to, recover from, mitigate, prevent, and/or model hazard and disaster events in urban settings. Therefore, this book was created not only with our colleagues in the academic world in mind, but also for hazards professionals and practitioners. We also believe graduate students will find the material presented here of interest, as may upper division undergraduate students.

Pamela S. Showalter
San Marcos, Texas Yongmei Lu

Acknowledgments

We are very grateful for the support of our colleagues, friends, and family members during the many months spent laboring on this book. Special thanks go to the following individuals (listed alphabetically), whose thoughtful suggestions vastly improved the effort presented here: Stephen D. Ambrose, Applied Sciences Program, NASA Headquarters; Lindsey Barnes, University of Colorado-Colorado Springs; Sally Caldwell, Texas State University-San Marcos; Richard Campanella, Tulane University; Xuwei Chen, Northern Illinois University; Thomas Cova, University of Utah; Ellen K. Cromley, The Institute for Community Research; Timothy J. Dolney, The Pennsylvania State University–Altoona College; David L. Eslinger, NOAA Coastal Services Center; Andrew Graettinger, University of Alabama; Ron Hagelman, Texas State University-San Marcos; Alisa Holloway, University of Cape Town; Mark W. Horner, Florida State University; Bo Huang, The Chinese University of Hong Kong; Chris J. Johannsen, Purdue University; Norman Kerle, International Institute for Geoinformation Science and Earth Observation (ITC), Enschede, the Netherlands; Michael Kevany, PlanGraphics, Inc.; Poh-Chin Lai, The University of Hong Kong; Jonathan Li, University of Waterloo, Canada; Ge Lin, University of Nebraska Medical Center; Susan Macey, Texas State University-San Marcos; Jeremy Mennis, Temple University; Robert J. Nicholls, University of Southampton; John Pine, Louisiana State University; Kathleen L. Purvis-Roberts, Claremont McKenna, Pitzer, and Scripps Colleges; Lynn M. Resler, Virginia Polytechnic Institute and State University (Virginia Tech); Jose L. Silván-Cárdenas, Texas State University-San Marcos; Susan I. Stewart, Northern Research Station, U.S. Forest Service; Jeannette Sutton, University of Colorado at Boulder; Lisa A. Taylor, NOAA National Geophysical Data Center; Jean-Claude Thill, University of North Carolina at Charlotte; Deborah S.K. Thomas, University of Colorado-Denver; Stefan Voigt, German Aerospace Center (DLR); William A. Wallace, Rensselaer Polytechnic Institute; Thomas J. Wilbanks, Oak Ridge National Laboratory; Olga Wilhelmi, National Center for Atmospheric Research (NCAR); F. Benjamin Zhan, Texas State University-San Marcos; and Sisi Zlatanova, Delft University of Technology, Delft, The Netherlands. Two additions to the above list are also the individuals responsible for instigating the entire enterprise: Jay D. Gatrell (Indiana State University) and Ryan R. Jensen (Brigham Young University) – thank you for encouraging us to take part in this venture.

We also wish to express our gratitude to the guidance of our sincere friends at Springer-Verlag. Special thanks go to Nina Bennink, Earth Sciences Publishing Assistant, and Robert K. Doe, Earth Sciences Publishing Editor, whose help and patience allowed us the time necessary to navigate the nuances of producing this book.

We are especially indebted to our loved ones. Pamela S. Showalter's deepest thanks go to her partner, Raylene, whose boundless support was offered from the moment the project was tackled. Yongmei Lu is in debt to her dearest husband, Shuwei, and her most lovely angels, Katie and Jeffrey, for their endless support and understanding during and beyond this book project. Both editors also wish to express their appreciation to Texas State University–San Marcos. Dr. Lu particularly appreciates the faculty development leave provided by Texas State University as well as the Visiting Professorship provided by Beijing Normal University, both of which greatly supported the second stage of her work on this project.

Finally, we acknowledge that no book is without its shortcomings – while we have attempted to keep errors of commission and omission to a minimum, we accept full responsibility for those that eluded us.

Contents

Contributors

Beverley J. Adams ImageCat Ltd., Communications House, Surrey, KT21 2BT, United Kingdom, bja@imagecatinc.com

Joshua S. Belhadj School of Planning, University of Cincinnati, Cincinnati, OH 45221-0016, USA, jsbelhadj@hotmail.com

Jean Pierre Bizimana Department of Geography, Faculty of Sciences, National University of Rwanda, Rwanda, Africa, bizijp@yahoo.fr

Molly E. Brown NASA Goddard Space Flight Center, Greenbelt, MD, USA, molly.brown@nasa.gov

Alexander Buyantuyev Sino-US Center for Conservation, Energy and Sustainability Science (SUCCESS), Inner Mongolia University, Inner Mongolia 010021, P.R. China, alexander.buyantuyev@asu.edu

Fernando López-Caloca Centro de Investigación en Geografía y Geomática "Ing. Jorge L. Tamayo A.C., Contoy 137 Lomas de Padierna Tlalpan 14240 México D.F., ferlopez@centrogeo.org.mx.

Lori Carter Malcom Pirnie, Inc., Austin, TX 78701, USA, lcarter@pirnie.com

Christopher Chamberlin NOAA/PMEL/NCTR/JISAO, Seattle, WA 98115 USA, Chris.Chamberlin@noaa.gov

Yunhao Chen College of Resources, Beijing Normal University, Beijing 100875, China, cyh@ires.cn

Jinmu Choi Department of Geosciences, Mississippi State University, MS 39762-5448, USA, jc778@msstate.edu

Gretchen Culp Earth and Environmental Sciences Program, City University of New York Graduate Center, New York, NY 10016, USA, gculp@gc.cuny.edu

Andrew J. Curtis Department of Geography, University of Southern California, Kaprielian Hall (KAP), Los Angeles, CA 90089-0255, USA, ajcurtis@usc.edu

Bruce A. Davis Infrastructure and Geophysical Division, Science and Technology Directorate, Department of Homeland Security, Washington, DC 20528, bruce.a.davis@dhs.gov

Philippe De Maeyer Department of Geography, Faculty of Sciences, Ghent University, 9000 Gent, Belgium, philippe.demaeyer@ugent.be

Pieter Deckers Department of Geography, Faculty of Sciences, Ghent University, 9000 Gent, Belgium, pieter.deckers@ugent.be

Ronald T. Eguchi ImageCat, Inc., Long Beach, CA 90802, USA, rte@imagecatinc.com

William F. Fagan Disaster Science and Management Program, CADGIS Research Laboratory, Louisiana State University, Baton Rouge, LA 70806, USA, fagan.brla@gmail.com

Yvette C. Feliberty Department of Geography, Northern Illinois University, DeKalb, IL 60115, USA, yvette.c.feliberty@monsanto.com

Michael P. Finn US Geological Survey, Rolla, MO 65401, USA, mfinn@usgs.gov

A. Stewart Fotheringham National Centre for Geocomputation, National University of Ireland, Maynooth, Co. Kildare, Ireland, stewart.fotheringham@nuim.ie

Christopher C. Funk University of California, Santa Barbara, CA, 93106, chris@geog.ucsb.edu

Shubharoop Ghosh ImageCat, Inc., Long Beach, CA 90802, USA, sg@imagecatinc.com

A-du Gong Academy of Disaster Reduction and Emergency Management, Beijing Normal University, Beijing 100875, China, gad@ires.cn

Susanne Grossman-Clarke Global Institute of Sustainability, Arizona State University, Tempe, AZ 85287-3211, USA, sg.clarke@asu.edu

Sharon L. Harlan School of Human Evolution and Social Change, Arizona State University, Tempe, AZ 85287-2402, USA, sharon.harlan@asu.edu

Michael E. Hodgson Department of Geography, University of South Carolina, Columbia, SC 29208, USA, hodgsonm@sc.edu

Charles K. Huyck ImageCat, Inc., Long Beach, CA 90802, USA, ckh@imagecatinc.com

Weiguo Jiang Academy of Disaster Reduction and Emergency Management, Beijing Normal University, Beijing 100875, China, jwg@ires.cn

Wim Kellens Department of Geography, Faculty of Sciences, Ghent University, 9000 Gent, Belgium, wim.kellens@ugent.be

Jitka Kotelenska CH2M HILL, WA 98004, USA, jitka.kotelenska@CH2M.com

Jiyeong Lee Department of Geoinfomatics, University of Seoul, Korea; Dongdaemun-gu, Seoul 130-743, Korea, jlee@uos.ac.kr

Michael Leitner Department of Geography and Anthropology, Louisiana State University, Baton Rouge, LA 70803, USA, mleitne@lsu.edu

Jing Li Academy of Disaster Reduction and Emergency Management, Beijing Normal University, Beijing 100875, China, lijing@ires.cn

Yongmei Lu Department of Geography, Texas State University-San Marcos, San Marcos, TX 78666, USA, yl10@txstate.edu

Juliana Maantay Environmental, Geographic, and Geological Sciences Department, Lehman College, City University of New York, NY 10468, USA, juliana.maantay@lehman.cuny.edu

Susan M. Macey James and Marilyn Lovell Center for Environmental Geography and Hazards Research, Department of Geography, Texas State University-San Marcos, San Marcos, TX, USA, sm07@txstate.edu

Andrew Maroko Environmental, Geographic, and Geological Sciences Department, Lehman College, City University of New York, NY 10468, USA, andrew.maroko@lehman.cuny.edu

Timothy McCarthy National Centre for Geocomputation, National University of Ireland, Maynooth, Co. Kildare, Ireland, tim.mccarthy@nuim.ie

Anneley McMillan ImageCat Ltd., Communications House, Surrey KT21 2BT, UK, am@imagecatinc.com

Nazila Merati NOAA/PMEL/NCTR/JISAO, Seattle, WA 98115, USA, nazila.merati@noaa.gov

Jacqueline W. Mills Department of Geography, California State University, Long Beach CA 90840-1101, USA, jacquelinewmills@gmail.com

Christopher Moore PMEL/NCTR/JISAO, Seattle, WA 98115 USA, Christopher.Moore@noaa.gov

Melany Noltenius Department of Geography, University of Tennessee, Knoxville, TN 37996-0925, USA, mnolteni@yahoo.com

Firooza Pavri Department of Geography-Anthropology, University of Southern Maine, Gorham, ME 04038, USA, fpavri@usm.maine.edu

John Pine Research Institute for Environment, Energy and Economics, Appalachian State University, Boone, NC 28608, USA, pinejc@appstate.edu

Bruce A. Ralston Department of Geography, University of Tennessee, Knoxville, TN 37996-0925, USA, bralston@utk.edu

Johan Reyns Department of Geography, Faculty of Sciences, Ghent University, 9000 Gent, Belgium, johan.reyns@ugent.be

Darren M. Ruddell School of Geographical Sciences, Arizona State University, Tempe, AZ 85287-0104, USA, darren.ruddell@asu.edu

Michele Schilling Chemin des Clotts, 05 160 Saint Apollinaire, France, schilligmichele@gmail.com

Pamela S. Showalter James and Marilyn Lovell Center for Environmental Geography and Hazards Research, Department of Geography, Texas State University-San Marcos, TX 78666, USA, ps15@txstate.edu

Vasily Titov PMEL/NCTR/JISAO, Seattle, WA 98115 USA, vasily.titov@noaa.gov

E. Lynn Usery U.S. Geological Survey, Rolla, MO 65401, USA, usery@usgs.gov

Tiffany C. Vance NOAA/NMFS/RACE, Seattle, WA 98115, USA, tiffany.c.vance@noaa.gov

Wouter Vanneuville Flanders Hydraulics Research, Antwerpen, Belgium, wouter.vanneuville@mow.vlaanderen.be

Elvia Martínez-Viveros Centro de Investigación en Geografía y Geomática “Ing. Jorge L. Tamayo A.C., Contoy 137 Lomas de Padierna Tlalpan 14240 México D.F., emartinez@centrogeo.org.mx

Fahui Wang Department of Geography and Anthropology, Louisiana State University, Baton Rouge, LA 70803, USA, fwang@lsu.edu

Xinhao Wang School of Planning, University of Cincinnati, Cincinnati, OH 45221-0016, USA, xinhao.wang@uc.edu

Steven M. Ward Department of Geography and Anthropology, Louisiana State University, Baton Rouge, LA 70803, USA, sward2@lsu.edu

Heng Wei Department of Civil and Environmental Engineering, University of Cincinnati, Cincinnati, OH 45221-0071, USA, heng.wei@uc.edu

Chapter 1
Introduction

Pamela S. Showalter and Yongmei Lu

1.1 Overview

This volume is a compilation of recent research using geographic information systems (GIS), remote sensing (RS), and other technologies such as global positioning systems (GPS) to examine urban hazard and disaster issues. The goal is to improve and advance the use of such technologies during the four classic phases of hazard and disaster research: response, recovery, preparation, and mitigation. Reflecting what has become common practice, the above technologies have been folded into a single term, "geographic information technology" (GIT), along with other spatial-technical aids that appear later in the book. We use GIT interchangeably, regardless of the number of technologies employed in any given study, or whether one or more is given primacy in the work. Chapters were solicited using a broad multidisciplinary call resulting in contributions from scholars representing Africa, Asia, Europe, Latin America and North America. All of the chapters underwent a double-blind peer-review process. It is every author's goal in this book to reduce the impact of future extreme events in urban environments by improving understanding of GIT and expanding its role at the local, regional, state, and federal levels.

The discipline of geography has developed broadly accepted meanings for the words "hazard", "disaster", and "urban", which we have expanded somewhat in order to embrace the range of work presented here. For example, a hazard is generally considered to be a component of the landscape that creates risk when it intersects with human activities. One example is a floodplain—unoccupied, it presents no risk; occupied it presents the risk of flooding and the potential for disaster. Conversely, terrorism is spatially indistinct because it can occur anywhere, any time, and is a direct result of human activities. An occupied floodplain and a terrorist

P.S. Showalter (✉)
James and Marilyn Lovell Center for Environmental Geography and Hazards Research, Department of Geography, Texas State University-San Marcos, San Marcos, TX 78666, USA
e-mail: ps15@txstate.edu

P.S. Showalter, Y. Lu (eds.), *Geospatial Techniques in Urban Hazard and Disaster Analysis*, Geotechnologies and the Environment 2, DOI 10.1007/978-90-481-2238-7_1,

represent potential problems. A disaster, however, is the embodiment of a real situation that must be addressed immediately (Tobin and Montz 1997) because it represents an event of such magnitude that it disrupts the social fabric (Stallings 2002).

An in-depth discussion of the many scholarly definitions of "urban" is far beyond the scope of this book. While Westerners have a tendency to associate the term "urban" with areas replete with high-rise building or skyscrapers, such is not the case in some rapidly expanding cities of the developing world. There, large numbers of people are urbanizing areas poorly equipped to absorb them, often resulting in the creation of "informal settlements". For our purposes, Hartshorn's (1992) concept that "urban" includes areas within or near a city (as opposed to a village, town, or hamlet) is appropriate, as well as the idea that cities, and/or areas considered to be urban, share broad characteristics such as population concentration; shared and distinctive employment patterns, lifestyle and land use; and the existence of a variety of institutions that coordinate the use of public facilities. The use of a broader definition allows the incorporation of studies that include extra-urban areas (e.g., stands of coastal mangroves) because there can be a direct relationship between the health of such ecosystems and the survival of nearby urban areas in the wake of a natural disaster such as a hurricane or tropical cyclone.

Due to the technical nature of this book, certain assumptions are made regarding the reader's familiarity with common GIT terminology and acronyms. For those readers unfamiliar with such terms, we recommend the glossaries and related chapters found in textbooks we have employed in our classrooms, such as DeMers (2008), Jensen (2000), Lillesand et al. (2008), and Longley et al. (2005).

The book is organized into five parts: sea level rise and flood analysis; metropolitan case studies; earthquakes, tsunamis, and international applications; hurricane response/recovery; and evacuation studies. The rationale for the book's organization is twofold. The first part addresses flooding because it is the most commonly experienced problem across the globe, both in terms of its frequency and spatial distribution. Not surprisingly, flood-related studies represented the largest number of submissions we received, resulting in that part containing the largest number of chapters in the book. Second, the book's focus on applied work led us to organize subsequent parts in such a manner that readers seeking specific guidance on, say, the use of GIT to address hurricane issues, would quickly be able to locate the majority of that material. However, we encourage such readers to look closely at the chapters in other parts because there is some "cross-over" work—for example, a chapter in the evacuation studies part is based on the scenario of a hurricane occurring in Key West, Florida while two in the flood analysis part address issues occurring in metropolitan locations.

Some readers may wish to quickly locate information regarding the basic contents of each chapter. Therefore, a brief description of each chapter follows describing the type of GIT employed (including new tools offered to advance our understanding of risk and vulnerability), as well as the spatial focus of the work.

1.2 Part Descriptions

1.2.1 Part I—Sea Level Rise and Flood Analysis

This part contains five chapters, beginning with Usery, Choi, and Finn's global animation of sea level rise. Their work is offered not as a predictive model but to demonstrate a methodology for using GIS data layers to create models, animate data, and provide the basis for more detailed modeling which can lead to improved coastal policy-making. In keeping with the theme of sea level rise but focusing on a more specific area, Pavri follows with an examination of sea level rise related flood vulnerability for Mumbai (Bombay), India using remote sensing. Through the use of readily available RS data and commonly employed classification methods, the author demonstrates that a relatively "low tech" approach yields results that can support the need for more aggressive flood control activities. Chapter 4 uses GIS to address the risk of flooding in Flanders, Belgium, a coastal area susceptible to sea-level rise as well as riverine floods. The team of Deckers, Kellens, Reyns, Vanneuville, and Maeyer developed a flood risk assessment tool (LATIS) to assess flood risk based on hydrologic models, land use information and socio-economic data with the goal of performing risk analysis quickly and effectively. Their chapter is followed by Maantay, Maroko, and Culp's examination of the flood risk in New York City. These authors developed the Cadastral-based Expert Dasymetric System (CEDS) and the New York City Hazard Vulnerability Index (NYCHVI) in order to more accurately estimate vulnerable populations in densely developed mega-cities, characterizing those populations based on measures of social, physical, and health vulnerability. The final chapter in this part presents the research of Bizimana and Schilling, who combined GIS, Quickbird imagery, GPS, and surveys to perform flood risk analysis for informal settlements in the Nyabugogo flood plain of Kigali City in Rwanda. Their work impacted local policy, resulting in the relocation of a major market and development restrictions within the flood plain.

1.2.2 Part II—Metropolitan Case Studies

Composed of five chapters, this part represents our "least traditional" portion of the book, describing the use of GIT in studying atmospheric pollutants, wild fire, and agriculture (vis a vis food security). Leading off is Chapter 7, where Macey uses GIS to examine the "respiratory riskscape" of five major metropolitan areas in Texas. The study utilizes readily available "criteria air pollution data" from federal government sources to determine the spatial pattern of urban air pollutants and combines this information with respiratory and nonrespiratory decedents' demographic characteristics to identify levels of variation between urban areas' pollution data and mortality rates. In a similar vein, Wang and Feliberty examine the spatial distribution of Chicago's toxic release inventory sites in an effort to identify whether environmental inequity exists in the area. The authors incorporate

data from the census and the Environmental Protection Agency's Toxic Release Inventory into a GIS to examine whether or not minority and low-income groups are disproportionately exposed to environmental hazards. Next, Ruddell, Harlan, Grossman-Clarke, and Buyantuyev examine risk and exposure to extreme heat in the semi-arid city of Phoenix, Arizona. The authors used the Weather Research and Forecasting (WRF) model to simulate air temperature variability throughout the region, and studied 40 diverse neighborhoods through survey analysis to better understand perceived temperatures and heat-related health problems during the summer of 2005. In keeping with the theme of heat, Lu, Carter, and Showalter follow with a wildfire risk analysis of Travis County's Wildland-Urban Interface (WUI). The authors combined historic wildfire records, land cover types, topographical characteristics, and housing density information into a GIS to create a wildfire risk profile and identified the need for expanded fire control and fire regulations in the WUI. The part closes with a chapter by Brown and Funk that details their use of GIT to investigate the growing food security crisis in Harare, Zimbabwe. Using MODIS NDVI data to estimate corn production shortfalls enabled early and decisive resource distribution by humanitarian groups to forestall a food crisis in 2007.

1.2.3 Part III—Earthquakes, Tsunamis, and International Applications

This part begins with a timely chapter by Li, Chen, Gong, and Jiang who studied the recent (May 2008) Wenchuan Earthquake in China. Beginning with a discussion of China's disaster management and emergency management systems, the authors relate how GIT was applied as a disaster relief tool following the earthquake, and conclude with a description of China's new "Small Satellite Constellation for Environment and Disaster Monitoring and Forecasting". The next chapter's focus is Mexico City, where Martínez Viveros and López Caloca discuss development of "Geodisplat"—an interactive, computerized tool that fuses data from multiple sources and models systems that interact during the disaster cycle. The goal of the tool is to efficiently support decision makers' information needs during all stages of the disaster cycle. Tsuami research is the focus of the next chapter, where Merati, Chamberlin, Moore, Titov, and Vance use geospatial data and GIS to build a tsunami forecasting system for US Tsunami Warning Centers. The authors discuss the use of open source and commercially available GIT to improve tsunami research and hazard mitigation as well as how they coupled tsunami model results with coastal risk, vulnerability, and evacuation models. The part concludes with a more general discussion of the use of GIT in managing hazards and disasters. Eguchi, Huyck, Ghosh, Adams, and McMillan pooled their efforts to introduce new and emerging technologies that have either proven effective in disaster management or show future promise. The authors conclude by addressing research/implementation issues as well as problems related to real-time event monitoring, privacy protection, information sharing, and trust management.

1.2.4 Part IV—Hurricane Response/Recovery

The fourth part of the book addresses hurricanes, and begins with a contribution by Hodgson, Davis, and Kotelenska who describe the use of GIT—with a focus on remote sensing—during the response and recovery phases of the disaster cycle. Analyzing three major hurricanes that impacted the US, they conclude GIT is still not uniformly implemented during those phases and work needs to be done to increase its use and acceptance by potential users. Hurricane Katrina's impact on the US Gulf Coast created the next two studies found in this part. Ward, Leitner, and Pine utilize GIT in New Orleans to assess the level of recovery, determine the most appropriate scale to use for studying the spatial aspects of recovery, and to identify spatial indicators of recovery. Curtis, Mills, McCarthy, Fotheringham, and Fagan follow with another New Orleans study that produced a Spatial Video Acquisition System. This system improved the collection of post-disaster geospatial damage assessment data in the spatially and temporally dynamic urban environment of a post-disaster neighborhood.

1.2.5 Part V—Evacuation Studies

The final part of the book contains three efforts to improve evacuation. Noltinius and Ralston test evacuation time estimates in Key West, Florida and found that there are three important aspects of pre-evacuation trip making behavior that run counter to common evacuation modeling assumptions. Incorporating these findings into future evacuation models will improve efforts to remove populations from harm's way. Choi and Lee create a 3D geometric network and agent-based evacuation model at the "micro-level"—buildings—in which they incorporate models of human behavior when attempts are made to exit the building. They found that the rate of building evacuation is greatly influenced by jamming situations, which are not uncommon under such circumstances. And, finally, Wang, Belhadj, and Wei developed a Community Evacuation Planning Support System (CE-PSS) to aid urban communities tasked with identifying likely terrorist targets as well as the optimum location for shelters following an attack. Developed with a GIS, the goal of the CE-PSS is to assist planners, citizens, and community leaders in their efforts to plan for possible terrorist attacks.

1.3 Closing Remarks

The maturity of GIT in hazards and disaster analysis is becoming more evident. As recently as six years ago, a book describing different methods applied to disaster research (Stallings 2002) devoted one chapter to the use of a single type of geographic technology, GIS (Dash 2002). Happily, there have been recent notable additions to the literature regarding the use of GIS, remote sensing, and other GIT in hazards and disaster analysis, e.g., Laben (2002), Cutter (2003), Mansor et al.

(2004), Van Oosterom et al. (2005), Adams and Huyck (2005), Li et al. (2007), National Research Council (2007), Shailesh and Zlatanova (2008), and Zlatanova and Li (2008). It is our hope that this volume makes a modest contribution to this growing body of literature, specifically through its focus on the application of GIT to urban hazard and disaster studies.

The chapters in this volume present a broad spectrum of applications of geographic information technologies to studies of various types of hazards and disasters in different urban settings. Our reading of the material has led us to conclude that there are several issues that warrant additional scrutiny by the community of hazards professionals. The first of these relates to the creation and dissemination of geographic information data that can be incorporated into GIT to reduce losses from urban hazards and disasters. This problem is twofold. On the one hand, in some urban areas (especially in the developing world) there is a lack of available information critical for understanding and preparing for hazard situations. This data shortage represents the major barrier to GIT's ability to contribute to urban hazard and disaster management in those locales. On the other hand, there is "an embarrassment of riches" in other parts of the world, where the amount of information is so great that there exists an urgent need to better oversee its proper dissemination and usage. How to ensure that appropriate geographic information and technologies are properly used in a proper manner at a proper time for a proper hazard and disaster reduction purpose? As we wrote in a recent column (Showalter and Lu 2009), we again urge the GIT community to address issues related to ready access to GIT information and how GIT is being used to communicate risk and other disaster-related data to non-professionals and members of the general public.

The second issue relates to urban hazard/disaster modeling that uses GIT. The combination of rapid development of computing power, richer data sets, and more efficient data collection/processing technologies, has led to models that tend to be more sophisticated, based on algorithms that can be extremely complicated, creating sometimes enormous data input demands, and perhaps hard-to-intepret results. While all of the above have the potential to advance scientific understanding of the specific disaster or hazard being investigated, we wish to reaffirm the applied nature of urban hazard and disaster analysis. Efforts linking advances in research labs with real-world hazardous event prediction, preparation, response, recovery, and overall loss reduction are encouraged. Some chapters in this book provide good examples of such efforts. We applaud research that both advances our scientific understanding of urban hazards and disasters, and attempts to determine the best manner of putting those scientific tools into public use to solve an actual problem. Significant contributions to urban hazard and disaster studies occur not only from the advancement of complicated models but also from their simplification and operationalization.

Last, GIT has helped, and will continue to help, strengthen the interdisciplinary nature of the study of urban hazards and disasters. As can be seen from the wide array of disciplines that form the roots of our chapter authors, the application of GIT to urban hazard and disaster analysis brings together social and physical scientists, engineers and planners, geographers and hydrologists, federal/regional/local public servants and the private sector, as well as many others not listed here. This

disciplinary "soup" not only has significant implications for education and training programs for specialists in urban hazard and disaster studies; it also signifies the importance of cross-disciplinary collaboration. In a sense, GIT's ability to absorb and massage data representing a variety of instruments, formats, scales, and levels of accuracy mirrors the field of urban hazard and disaster analysis, which absorbs input from a host of disciplines but has a singular two-pronged goal: saving lives and reducing losses.

References

Adams B.J. and Huyck C.K. 2005. The Emerging Role of Remote Sensing Technology in Emergency Management. In: C. Taylor and E. VanMarcke (eds.) *Infrastructure Risk Management Processes: Natural, Accidental, and Deliberate Hazards* (Monograph 1). Reston, VA: American Society of Civil Engineers, pp. 95–117.

Cutter S.L. 2003. GI Science, Disasters, and Emergency Management. Transactions in GIS 7(4): 439–446.

Dash N. 2002. The Use of Geographic Information Systems in Disaster Research. In: Robert A. Stallings (ed.) *Methods of Disaster Research*, pp. 320–333. International Research Committee on Disasters Bloomington, IN: Xlibris Corporation.

DeMers M. 2008. *Fundamentals of Geographic Information Systems* (4th edition). New York: John Wiley and Sons, Inc.

Hartshorn T.A. 1992. *Interpreting the City: An Urban Geography* (2nd edition). New York: John Wiley and Sons, Inc.

Jensen J. 2000. *Remote Sensing of the Environment: An Earth Resource Perspective*. New Jersey: Prentice Hall.

Laben C. 2002. Integration of Remote Sensing Data and Geographic Information System Technology for Emergency Management and Their Applications at the Pacific Disaster Center. Optical Engineering 41(9): 2129–2136.

Li J., Zlatanova S., and Fabbri A. 2007. *Geomantics Solutions for Disaster Management*. Berlin/Heidelberg: Springer-Verlag.

Lillesand T.M., Kiefer R.W., and Chipman J.W. 2008. *Remote Sensing and Image Interpretation* (6th edition). New Jersey: John Wiley and Sons, Inc.

Longley P., Goodchild M., Maguire D., and Rhind D. 2005. *Geographic Information Systems and Science*. New York: John Wiley and Sons, Inc.

Mansor S., Abu Shariah M., Billa L., Setiawan I., and Jabar F. 2004. Spatial Technology for Natural Risk Management. Disaster Prevention and Management 13(5): 364–373.

National Research Council (2007). *Successful Response Starts with a Map: Improving Geospatial Support for Disaster Management.* Committee on Planning for Catastrophe, Washington, DC: National Academies Press, 184p.

Shailesh N. and Zlatanova S. 2008. *Remote Sensing and GIS Technologies for Monitoring and Prediction of Disasters*. Berlin/Heidelberg: Springer-Verlag.

Showalter P., and Lu Y. 2009. Techno-Hyperactivity. GIM International. 23(1). http:www.gim-international.com/issues/articles/id1238-Technohyperactivity.htm. Last updated January 12.

Stallings R.A. (ed). 2002. *Methods of Disaster Research* (Volume Two). International Research Committee on Disasters Monograph Series. Bloomington, IN: Xlibris Corporation.

Tobin G.A., and Montz B.E. 1997. *Natural Hazards: Explanation and Integration*. New York/London: The Guilford Press.

Van Oosterom P., Zlatanova S., and Fendel E. 2005. *Geo-Information for Disaster Management*. Berlin/Heidelberg: Springer.

Zlatanova S. and Li J. 2008. *Geospatial Information Technology for Emergency Response*. London: Taylor and Francis Group.

Part I
Sea Level Rise and Flood Analysis

Chapter 2
Modeling Sea-Level Rise and Surge in Low-Lying Urban Areas Using Spatial Data, Geographic Information Systems, and Animation Methods

E. Lynn Usery, Jinmu Choi, and Michael P. Finn

Abstract Spatial datasets including elevation, land cover, and population of urban areas provide a basis for modeling and animating sea-level rise and surges resulting from storms and other catastrophic events. With a geographic information system (GIS), elevation data can be used to determine urban areas with large population numbers and densities in low-lying areas subject to inundation from rising water. This chapter provides details of the analysis and modeling procedure, as well as animations for specific areas of the world that are at risk from inundation from moderate rises or surges of sea level. The work is not an attempt to predict sea-level rise, but rather a methodological study of how to use GIS data layers to create the models and animations. Whereas global sea level rise is currently measured by millimeters per year, this work examines theoretical rise measured in meters as well as coastal threats posed by tsunamis, such as occurred in the Indian Ocean in 2004. Global, regional, and local animations can be created using widely available elevation, land cover, and population data. The models and animations provide a basis for determining areas with large population numbers in relatively low-lying areas and potentially subject to inundation risk, as was the case when Hurricane Katrina devastated New Orleans. This determination can provide a basis for more detailed modeling and policy planning such as development and evacuation.

Keywords Map projection · Global GIS data · Urban GIS data · Sea level rise · Modeling · Animation

2.1 Introduction

The development of high resolution geographical data (e.g., elevation, population, land cover) and geographical modeling and animation capabilities makes it possible to develop comprehensive spatial models of the effects of high surges and moderate

E.L. Usery (✉)
US Geological Survey, Rolla, MO 65401, USA
e-mail: usery@usgs.gov

P.S. Showalter, Y. Lu (eds.), *Geospatial Techniques in Urban Hazard and Disaster Analysis*, Geotechnologies and the Environment 2, DOI 10.1007/978-90-481-2238-7_2,

rises of sea level on human populations in areas of risk. This chapter makes no attempt to predict sea level rise, but rather provides a methodology for combining GIS data layers in a simulation and animation that reveals low-lying areas with large population numbers that may be subject to inundation and thus require evacuation planning. For global modeling, 30 arc-second resolution equiangular grid data from the US Geological Survey for elevation (GTopo30) and land cover (Global Land Cover), and population (Landscan 2005) from the Oak Ridge National Laboratory provide a basis for determining areas of land cover types and numbers of people below specific elevations that are subject to inundation. For regional areas outside the United States (US), 90-m resolution Shuttle Radar Topographic Mission (SRTM) elevation data are used and for US coasts, 30 m resolution elevation and land cover data are used with population converted to 30 m raster cells from the vector polygons of US Census block data. Whereas such global and regional datasets can be used to model sea-level rise, the resolution prohibits illustrating small increases as are now occurring. An extreme upper limit of 80 m, the approximate theoretical maximum rise in sea level if all icecaps and glaciers melt, is used for some of the global simulations because of resolution limitations. A limit of 30 m is used for the local and urban area simulations. The model of rising water is based only on elevation and does not attempt to account for tidal changes or the way a tidal wave would actually interact with coastal features.

The approaches discussed in this paper are most appropriate simulating large surges of sea water, such as the 30 m wave that occurred during the Indian Ocean Tsunami in 2004 and the 4 m inundation from hurricanes Katrina and Rita in 2005. With higher resolution data, for example a 10 cm resolution elevation grid from LIDAR data, the same methods can be used to model small rises of a few millimeters, as are now occurring each year. It is the purpose of this paper to present these global and regional modeling techniques and methods of animating the results of the models as potential tools for risk assessment, development, and evacuation planning.[1]

The next section of this chapter provides a motivation for the work and a brief discussion of the history and potential heights of sea-level rise. The third section provides information regarding storm surge and potential surge levels. Section 2.4 of the chapter discusses data preparation methods, particularly projection and resampling of raster data. The fifth section examines the multiscale modeling approach and includes discussion of the visualization and animation methods. A final section draws conclusions, discusses limitations, and provides recommendations for future research.

2.2 History and Potential Heights of Sea-Level Rise

Global sea level and the Earth's climate are intricately linked. With the consistent trend towards higher temperatures, conditions are less icy in the Artic regions as seen in increasing melt areas over the Greenland ice sheet, retreating glaciers,

[1] Animations are available at http://cegis.usgs.gov/sea_level_rise.html.

reduced sea ice coverage, and permafrost thawing (Arctic Climate Impact Assessment 2005). Comiso et al. (2008) determined that the extent of Arctic sea ice coverage was 24 percent lower in September 2007 than September 2005, the previous record low.

The Intergovernmental Panel on Climate Change (IPCC) Fourth Assessment Report (IPCC 2007) estimates of sea-level rise range from 0.18 to 0.59 m by the 2090s from the average level between 1980 and 2000. The Greenland and West Antarctica ice sheets may be collectively adding 0.35 mm/yr to sea-level rise in recent years (Shepherd and Wingham 2007). Because it is unknown how these ice sheets may respond to the increased polar temperatures expected during this century, it is essential that ice sheet monitoring be expanded (Horton et al. 2008).

Estimates of current (2008) rates of global sea-level rise vary from 1.0 to 3.1 mm/yr (Douglas et al. 2001; Miller and Douglas 2004; Wadhams and Munk 2004; Church and White 2006; Holgate 2007; IPCC 2007). The 20th century acceleration of sea-level rise appears to be a global phenomenon (Gehrels et al. 2008). This rise is likely associated with the concurrent upsurge in global temperatures and is demonstrated by Gehrels et al. (2008) by the rate of sea-level rise in New Zealand, which was determined as approximately 2.8 mm/yr. In the Mediterranean Sea and Atlantic Ocean, Marcos and Tsimplis (2007) determined that the residual sea-level rise corrected for post-glacial rebound processes were 0.9 and 1.3 mm/yr, respectively.

Research by Beckley et al. (2007) determined a global sea-level rise rate of 3.36 $\pm$ 0.41 mm/yr during 14 years from 1993 to 2007, whereas Chao et al. (2008) show an essentially constant rate of rise for global sea level of +2.46 mm/yr during at least the past 80 years. Chambers (2008) provides a description of methods for measuring global sea-level rise using satellite altimetry and reports that a rise of 3.5 $\pm$ 0.5 mm is the average for the entire ocean. Chambers (2006) indicates that the rise rate is not constant across the oceans, but is affected by temperature and salinity, that affect gravity measurements.

One of the most important consequences of diminishing mountain glacier cover is rising sea level (Arendt et al. 2002). Schiefer et al. (2007) determined that between 1985 and 1999 the rate of glacier loss in the Coast Mountains of British Columbia approximately doubled that observed for the previous two decades and could account for about 8.3 percent of the contribution from mountain glaciers and ice caps. For example, the retreat of the Grinnell Glacier since the early 1900s is shown in Fig. 2.1. The images show the former extent of the glacier in 1938, 1981, 1978, and 2006. Mountain glaciers are excellent monitors of climate change; the worldwide shrinkage of mountain glaciers is thought to be caused by a combination of a temperature increase from the Little Ice Age (which ended in the latter half of the 19th century) and increased greenhouse-gas emissions (Poore et al. 2000).

Small magnitude changes in the rate at which sea level is observed to rise enhance the ability to monitor sea level and predict its change (Cazenave and Nerem 2004). Jenkins and Holland (2007) put bounds on potential sea-level rise associated with ice shelf melting, icebergs, and sea ice currently afloat in the world's oceans.

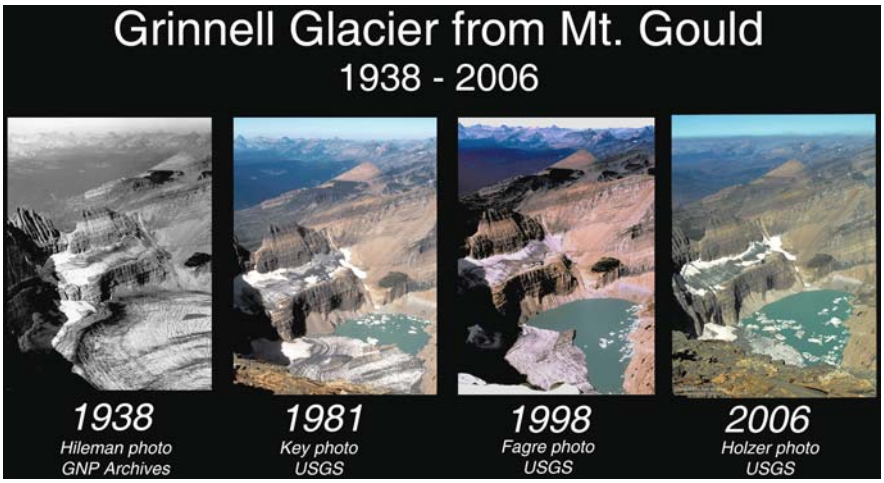

Fig. 2.1 The melting of the Grinnell Glacier from 1938 to 2006 in Glacier National Park (USGS)

Kolker and Hameed (2007) also find that beyond broad climatologic data there is a meteorological driver of sea-level trends through atmospheric centers of action that have some affect on winds, pressure, and sea-surface temperatures, thereby influencing sea level via a suite of oceanographic processes.

Most current (2008) global land ice mass is in the Antarctic and Greenland ice sheets (Fig. 2.2). Complete melting of these ice sheets would cause a maximum sea-level rise of 80 m (Table 2.1). Whereas today's rates of sea-level rise are only a few millimeters per year, the geological record shows a 20 m rise over a 500 year period, resulting from Meltwater Pulse 1A during the collapse of Earth's former ice sheets (Weaver et al. 2003).

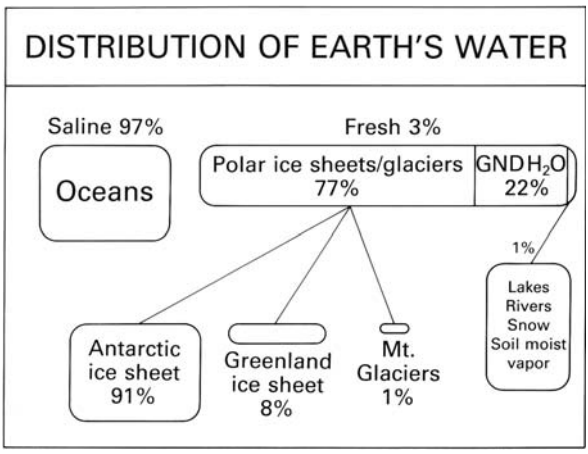

Fig. 2.2 Distribution of Earth's water showing most of the freshwater is in the Antarctic and Greenland ice sheets (Thomas, 1993)

Table 2.1 Potential sea-level rise from the Earth's ice sheets

Location	Volume	Potential sea-level rise (m)
East Antarctic Ice Sheet	26,039,200	64.80
West Antarctic Ice Sheet	3,262,000	8.06
Antarctic peninsula	227,100	0.46
Greenland	2,620,000	6.55
Other ice caps, fields, glaciers	180,000	0.45
Total	32,328,300	80.32

Source: Thomas (1993).

Ice sheets are composed of a largely homogeneous material and move so slowly that turbulence, Coriolis, and other inertial effects can be ignored by climate modelers; yet rooted within ice sheets are outlet glaciers (Vaughan and Arthen 2007). These glaciers, for example, those flowing from the Greenland Ice Sheet, discharge ice directly into the ocean at 200 to 12,000 mm/yr (Joughin et al. 2008). Recent reports record the rapidly escalating discharge of Greenland's outlet glaciers (Joughin et al. 2004; Rignot and Kanagaratnam 2006; Truffer and Fahnestock 2007). Data indicate summer increases of 50 to 100 percent of the volume of surface meltwater reaching the ice-bedrock interface of the ice sheet (Joughin et al. 2008). Current (2008) observations demonstrate that the ice flow all along western fringe of Greenland's ice sheet accelerates all through the summer as surface meltwater lubricates sliding at the interface (Zwally et al. 1998; Joughin et al. 2008). Das et al. (2008) described the swift drainage of a 5.6 km^2 supraglacial lake on the Greenland Ice Sheet signifying that an efficient drainage system dispersed the meltwater subglacially. Such findings can clarify calculations regarding observed net regional summer ice flow increase by incorporating the impact from multiple lake drainages. Variation on the Antarctic Ice Sheet surface noted from satellite observations also seems to indicate moving subglacial water under a huge ice stream (Fricker et al. 2007).

2.3 Storm Surge and Effects: Tsunamis and Hurricanes

Across our planet, civilization is vulnerable to disaster events that can annihilate because they catch individuals by surprise. Sea waves act to dissipate concentrations of energy in the Earth's dynamic systems that stem from various meteorological or geophysical sources, and can sometimes result in a natural disaster (Zebrowski 1999). Tsunamis are seismic sea waves generated spontaneously by a rapid release of energy from submarine earthquakes, explosions of sea-level volcanoes, and by undersea landslides along the continental shelves. Tsunamis have long wavelengths and periods, i.e., the time for passage of one wavelength, and the first wave peak hitting land is not necessarily the largest (Zebrowski 1999). These long periods often cause unexpected wavefronts to hit local populations.

In 2004, a massive tsunami occurred in the Indian Ocean. Coastal areas in Indonesia, Thailand, India and surrounding locations received significant inundation including a 30 m wave that hit Banda Aceh on the northwestern tip of the island of Sumatra in Indonesia. In Sri Lanka and other locations the wave heights crested 10 m or more. Wave heights at these levels can inundate large coastal areas causing significant loss of life and damage to property and infrastructure (as of this writing, a selection of before/after images of the tsunami's impact on Banda Aceh were available on the World Wide Web at http://homepage.mac.com/demark/tsunami/9.html; Demark 2005).

While tsunamis are particularly devastating with high surges of sea water, hurricanes occur more frequently, in more world locations, and can also cause high water surges. The 1900 Galveston hurricane is on record as the worst natural disaster in US history with an estimated loss of life of between 6000 and 12,000 persons (McGee 1900; Zebrowski 1999). Barrier islands, similar to the one on which Galveston is built, are found along the coasts of the US Atlantic Ocean and Gulf of Mexico, and are areas most prone to hammering by high-energy waves and storm surges (Zebrowski 1999).

On August 28, 2005, Hurricane Katrina passed across the Gulf of Mexico and became a Category 5 storm on the Saffir-Simpson hurricane scale, with winds estimated at 175 miles per hour (NOAA 2007). Hurricane Katrina devastated New Orleans and other Gulf Coast areas destroying lives, homes, and city infrastructure. As of this writing, many people are still coping with Katrina's devastation. The storm surge was particularly destructive (see http://www.snopes.com/katrina/photos/surge.asp), flooding a large area around New Orleans. Coastal storm surge flooding was 7 to 10 m (20 to 30 feet) above normal tide levels (FEMA 2007). In the same year that Katrina hit the Gulf Coast, Hurricane Rita caused a second wave of devastation a few months later. A series of before and after maps and images of the effects of Katrina and Rita are available from the USGS (2008a).

The potential for damage from hurricanes and tsunamis becomes apparent from these few examples. To better perform risk assessment, understand development opportunities and challenges, and improve evacuation routing, it is necessary to develop methods to model areas subject to inundation that include the number of persons who could be affected, various land covers (that can impede or exacerbate the movement of coastal surges), and infrastructure at risk. Following is a description of methods employed for global, regional, and local areas.

2.4 Global, Regional, and Local Modeling of Sea-Level Rise

The availability of global elevation, land cover, and population datasets at 30 arcsec (approximately 1 km at the Equator) resolution have made it possible to model inundation effects globally and regionally. The SRTM elevation data are available at 90 m resolution for much of the world, and provide a basis for more accurate modeling in regional areas. In the US, higher resolution 30 m elevation and land-cover data can be augmented with population numbers from the US Census block converted to 30 m raster cells (Table 2.2).

Table 2.2 Datasets used in models and animations

Area	Elevation	Land cover	Population
Global	Gtopo30 30 arc-sec	USGS Global Land Cover 30 arc-sec	LandScan 2005 30 arc-sec
Regional	SRTM 90 m	USGS Global Land Cover Resampled to 90 m	LandScan 2005 Resampled to 90 m
US Coasts/ Local	National Elevation Dataset 30 m	National land Cover Dataset 30 m	US Census Block Numbers Converted to 30 m

2.4.1 Problems and Solutions for Global Projection and Resampling

In order for global, regional, and local models to be created, the data used in these models must be resampled to a standard projection. Whereas elevation data can be resampled with an averaging resampler (e.g., bilinear interpolation), land cover and population data require different methods. Categorical (land cover) data must be resampled with a nearest neighbor algorithm causing significant pixel gain/loss in some locations (Seong and Usery 2001; Seong et al. 2002). Population data (numbers of people in each raster cell) cannot be resampled with averaging or nearest neighbor methods, but instead require an additive resampler. In the additive resampler, the output pixel value is a result of combination of multiple input pixel values. The software adds all complete input pixels that map to the area covered by a single output pixel. We proportionally assign input pixels that are split across output pixel boundaries. Thus, each output pixel has a unique value (number of people) that results from the additive combination of the appropriate set of input pixels. We validate the process by checking the total number of people in the output image against the total number from the input image. These must exactly match so we do not loose or gain people in the resampling process.

For global projections, significant problems were encountered with commercial software when attempting to resample and project the 2 Gb elevation and 1 Gb land cover/population raster files. Software problems included unreliable global projections, inability to account for singularities such as the North and South Poles, and specific projections unable to process to completion (aborting before the plane representation is complete). Inverse projection results moved North America across the Atlantic to the Greenwich meridian, increased file sizes by orders of magnitude, and repeated areas at edges of a global projection (i.e., caused both Alaska and Siberia to appear on both edges of the map). Computation time was also an issue because it can be extensive, lasting up to 200 hours or more on high-end desktop computers (Usery and Seong 2001; Usery et al. 2003).

To solve such problems, a USGS software package called mapIMG was used (available from http://carto-research.er.usgs.gov/projection/acc_proj_data.html). To account for pixel loss and gain in categorical data, the resampling method uses a statistical strategy, such as the modal category or some other user-defined strategy.

For example, to down-sample the data from a 30 arc-sec to an 8 × 8 km pixel, 64 input values are used to determine a single output value. The mapIMG software examines the 64 values and tabulates the number of values in each category. The user can then assign the modal category (the value that occurs the highest number of times) to the output cell. The result is a smoother image of categorical data with a reduction in pixel loss and gain (Steinwand 2003). For population data, an additive resampler was used. Using the above example of 64 input pixels to one output pixel, the mapIMG software adds the values of the 64 pixels to create one output value. MapIMG, is available for various computing platforms and can be downloaded without charge.

2.4.2 Multi-Scale Modeling Approach

Global and regional effects of rising sea level are modeled using elevation, population, and land cover data at 30 arc-sec spatial resolution projected and resampled to 1 km cells as described in the previous section. The datasets were transformed to the Mollweide projection to provide a global view with equal areas of land cover (Fig. 2.3), using a decision support system for map projection selection that is freely available to users of global and regional raster/vector datasets (USGS 2008b).

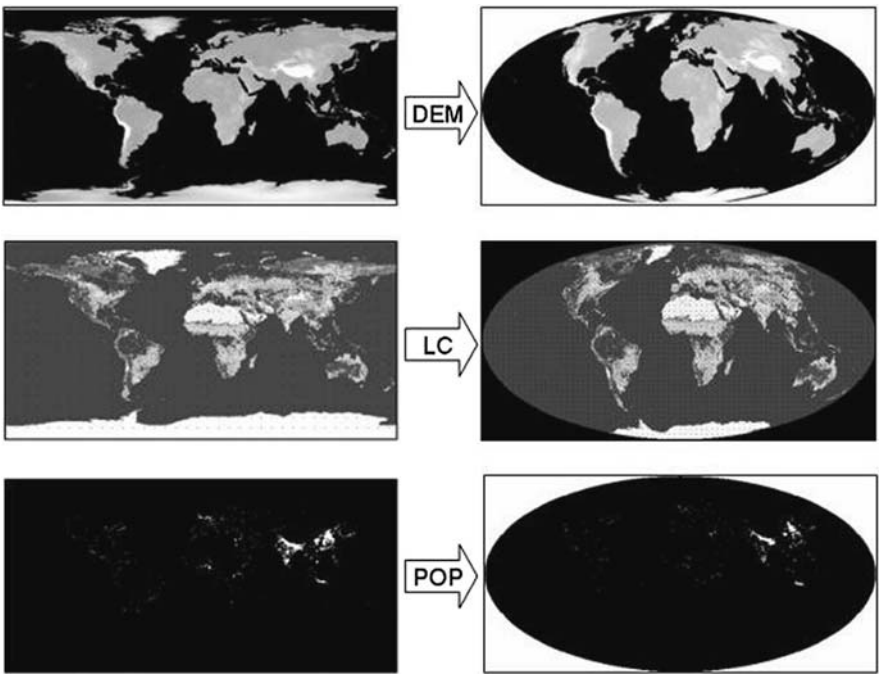

Fig. 2.3 Transformation of the global datasets for elevation, land cover, and population from geographic coordinates to the Mollweide projection

The subsequent modeling effort utilizes statistical summaries and animations. Statistical summaries show sea-level rise effects at global and regional scales, as well as surge effects in low-lying urban areas at local scales and in relation to affected populations and land cover loss. Animations are used to illustrate the locations of affected areas; a blue mask aids the visualization of rising water as it "inundates" existing land cover. One caveat regarding the simulations, animations, and statistical models presented here is that their accuracy is dependent on the resolution and accuracy of the elevation data. Determining the extent of land classes and numbers of people affected depends on the resolution and accuracy of the land cover and population data. As with all models, any errors in these data will be propagated throughout the models, and may invalidate the results.

To determine areas of inundation and affected land cover types, and to extract the number of people in inundation areas of specific levels of rise, a conditional overlay and global summation operation are used (Fig. 2.4). The model is established to operate on intervals of sea-level rise and create an output map for each interval. For example, on a 1 m interval, individual maps are created for 1, 2, 3, 4, 5 m and so forth. To extract the number of people residing in the inundation area, the first conditional overlay uses population and elevation data. A population value is assigned to an output pixel only when the location is at an elevation equal to, or lower than, the specified elevation in the condition. Otherwise, a 0 value is assigned to the pixel. The second conditional overlay considers both elevation and land cover type from the 25 land cover categories in the Global Land Cover dataset as listed

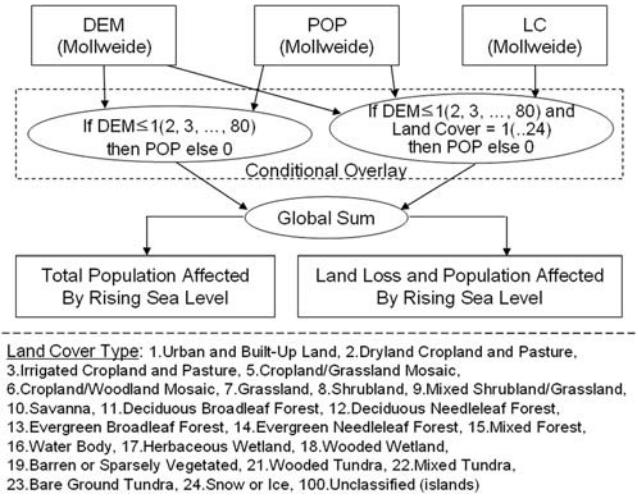

Fig. 2.4 A schematic of the conditional model used to determine areas of land cover and numbers of people in areas of inundation. The if-then conditional on the *left side* of the figure assigns population numbers as pixel values when the elevation of the pixel is below a specified value or a 0 otherwise. The conditional on the *right side* assigns land cover values if the elevation is above a specified value, otherwise a 0 is assigned. The global summation function tabulates numbers of people and total areas of each land cover category at below specified elevations

in the figure. If a pixel value is a specified land cover type and meets the elevation condition, the overlay assigns the population value at the location in the result data. Otherwise, a 0 is also assigned. The population in the area that is inundated, assigned a blue mask color, is totaled and shown in the running counter and the land cover categories outside the inundation area are used to set colors for the remainder of the map in the animations.

2.5 Sea-Level Rise Effects at Global and Regional Scales

Approximately 11 percent of the world's population lives in areas subject to a 5 m rise in sea level (Table 2.3). Nearly 1.5 billion people, or approximately 23 percent of the world's population, live in areas that would be inundated area in the event of a 30 m rise in sea level. The model used in this study indicates that there is a linear relationship between rising sea level and the number of people affected by that rise. As people become affected, so too will be their surroundings, including homes, infrastructure, critical facilities (e.g., hospitals), and schools. Community cohesion may be ruptured as relocation becomes necessary, and social stressors may increase as cities attempt to absorb the displaced.

Rising sea level impact on people and land cover was examined by exploring the 25 land-cover categories of the Global Land Cover dataset shown in Fig. 2.4. Among these categories, urban and built-up areas contain the highest population densities (about 3600 people per km^2); over 960 million people (about 16 percent of the world's population) live in those areas (Table 2.4). With a 5 m rise in sea level, 125 million people (about 2 percent of world population) living in urban and built-up areas are affected, or approximately 13 percent of the total urban population. Other land cover categories with high population densities include three cropland areas, Dry Land Cropland and Pasture, Irrigated Cropland and Pasture, and Crop Land/Woodland Mosaic, that are residence to more than 50 percent of the world's population. While population densities are not as high in these areas as in the Urban and Built-up Land, more land falls into this category. Therefore, should sea levels rise 5 m in these three cropland areas, over 250 million people would be affected.

Table 2.3 Population affected by rising sea level

Water level increase (m)	Area of land loss (km^2)	Number of people affected (percent)
5	5,431,902	669,739,183 (10.8)
10	6,308,676	870,751,960 (14.0)
20	7,888,233	1,176,709,476 (18.9)
30	9,459,562	1,405,824,876 (22.6)
Total world population		6,228,997,089 (100)

Table 2.4 Population affected with major land cover types by rising sea level

Land cover	Total land area (km^2)	POP density (per km^2)	Total population (percent)*	Population affected by rising sea level		
				5 m (percent)	10 m (percent)	20 m (percent)
Urban and Built-up land	3,100,287	3629	966,920,555 (15.5)	125,426,492 (2.0)	167,534,955 (2.7)	225,034,603 (3.6)
Irrigated Cropland and Pasture	3,811,178	392	1,285,065,525 (20.6)	146,650,929 (2.3)	231,800,008 (3.7)	353,447,741 (5.7)
Dryland Cropland and Pasture	14,141,964	121	1,480,209,129 (23.8)	90,514,229 (1.4)	117,463,463 (1.9)	169,232,478 (2.7)
Cropland/ Woodland Mosaic	5,086,575	90	394,546,228 (6.3)	18,977,528 (0.3)	28,429,804 (0.5)	46,827,725 (0.8)
Total			6,228,997,089(100)	669,739,138 (10.8)	870,751,960 (14.0)	1,176,709,476 (18.9)

*Percentage of total population residing in this land cover type.

2.5.1 Surge Effects at Local and Urban Scales

The impacts of 2004's Indian Ocean Tsunami and 2005's Hurricanes Katrina and Rita indicate the importance of local flood simulation. From the model, estimates of the number of people affected by 1−30 m flooding in the Los Angeles, Washington, DC, and New York areas are shown in Tables 2.5, 2.6, and 2.7, respectively (note that the numbers reflect the areas selected for modeling and do not apply to urban areas as defined by the US Census or other spatially defined boundaries). The highest surge flooding from Hurricane Katrina was 13 feet (approximately 4 m) along the coasts of Louisiana and Mississippi. Using 4 m as a "design surge" in Los Angeles produces an impact on about 276,000 people; in Washington, DC on about 1,500,000; and in the New York area on about 1,300,000. If the flooding is increased to 30 m, the approximate number of people living in these areas that would be affected is 3,600,000; 7,000,000; and 12,000,000, respectively.

Table 2.5 Population affected by urban flooding in the Los Angeles area

Flooding height (m)	Population affected	Percent of total population*
1	95,443	0.79
2	114,583	0.94
3	198,879	1.64
4	276,014	2.28
5	350,898	2.89
6	433,352	3.57
8	602,799	4.97
10	851,246	7.02
12	1,117,857	9.22
14	1,379.794	11.38
16	1,668,664	13.76
18	1,956,670	16.16
20	2,218,638	18.29
22	2,497,027	20.59
24	2,844,003	23.45
26	3,126,605	25.78
28	3,380,608	27.87
30	3,677,386	30.32
Total population*	12,128,147	100.00

* Total number of people in the area used for the model and animation

2.5.2 Visualization with Animation

Animations can be created using elevation and land cover data by taking "snapshots" of inundated land cover at particular elevations/water levels. The snapshot images are imported into animation software such as Macromedia® Flash® or Microsoft®

Table 2.6 Population affected by urban flooding in the Washington, DC area (including Baltimore, Philadelphia, Richmond)

Flooding height (m)	Population affected	Percent of total population*
1	220,811	1.22
2	542,712	3.00
3	1,042,825	5.76
4	1,503,203	8.30
5	1,907,150	10.53
6	2,376,907	13.12
8	2,901,938	16.02
10	3,395,204	18.75
12	3,917,752	21.63
14	4,322,253	23.86
16	4,676,841	25.82
18	5,041,001	27.83
20	5,399,400	29.81
22	5,750,108	31.75
24	6,092,345	33.64
26	6,458,236	35.66
28	6,781,498	37.44
30	7,095,692	39.18
Total population*	18,112,065	100.00

* Total number of people in the area used for the model and animation

Table 2.7 Population affected by urban flooding in the New York area

Flooding height (m)	Population affected	Percent of total population*
1	240,798	1.17
2	478,033	2.32
3	963,085	4.67
4	1,344,586	6.52
5	1,832,608	8.89
6	2,502,664	12.14
8	3,497,555	16.96
10	4,652,513	22.57
12	5,655,103	27.43
14	6,477,280	31.42
16	7,376,777	35.78
18	8,256,420	40.05
20	9,022,190	43.76
22	9,816,514	47.62
24	10,466,181	50.77
26	11,103,041	53.86
28	11,672,852	56.62
30	12,184,647	59.10
Total Population*	20,616,311	100.00

* Total number of people in the area used for the model and animation

Powerpoint®. The images are arranged sequentially to simulate the rise of sea level from 1−30 m (or, 80 m in the case of some of the global and regional animations). Finally, the sequential images are exported to an animation file such as .avi or .wmv to create a flipbook animation.

Figure 2.5 illustrates land covered by rising sea levels of 5, 10, 20, and 30 m in several areas including Florida in the US, the Netherlands in Europe, and China in East Asia. The figure includes the number of people worldwide who would be affected by each level of rise. Most areas in Florida would be flooded by a 30-m rise in sea level. Beijing and Shanghai, the two largest cities in China, would be flooded by 10−20 m rises. And, in Europe, the western one-half of the Netherlands would be flooded by a 5-m rise in sea level.

More moderate rises were also modeled to examine localized results. Although the western coast of the US does not normally experience hurricanes, severe storms can occur in the area, including tropical cyclones and tsunamis (Butler 2005). Figure 2.6 displays simulated storm surge flooding in Los Angeles, California. As flood levels increase, the southern part of the city is increasingly flooded. With 30 m flooding, about half the city is inundated.

Simulations for Washington, DC (Fig. 2.7) and New York (Fig. 2.8) show significantly larger land areas affected by sea level rise. Examining these figures with Tables 2.6 and 2.7 demonstrates how low east coast elevations expose more people to inundation at low levels of rise.

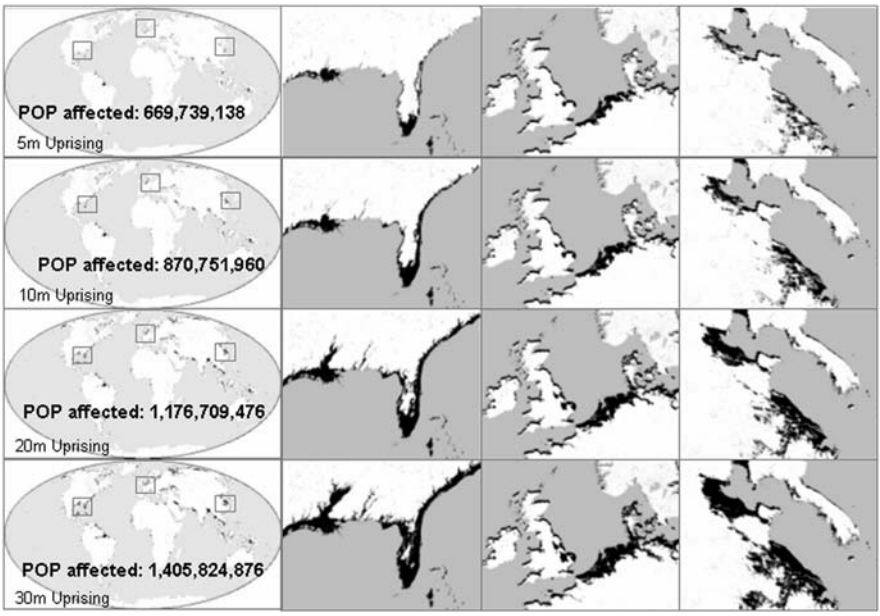

Fig. 2.5 Land loss in selected areas and global population affected

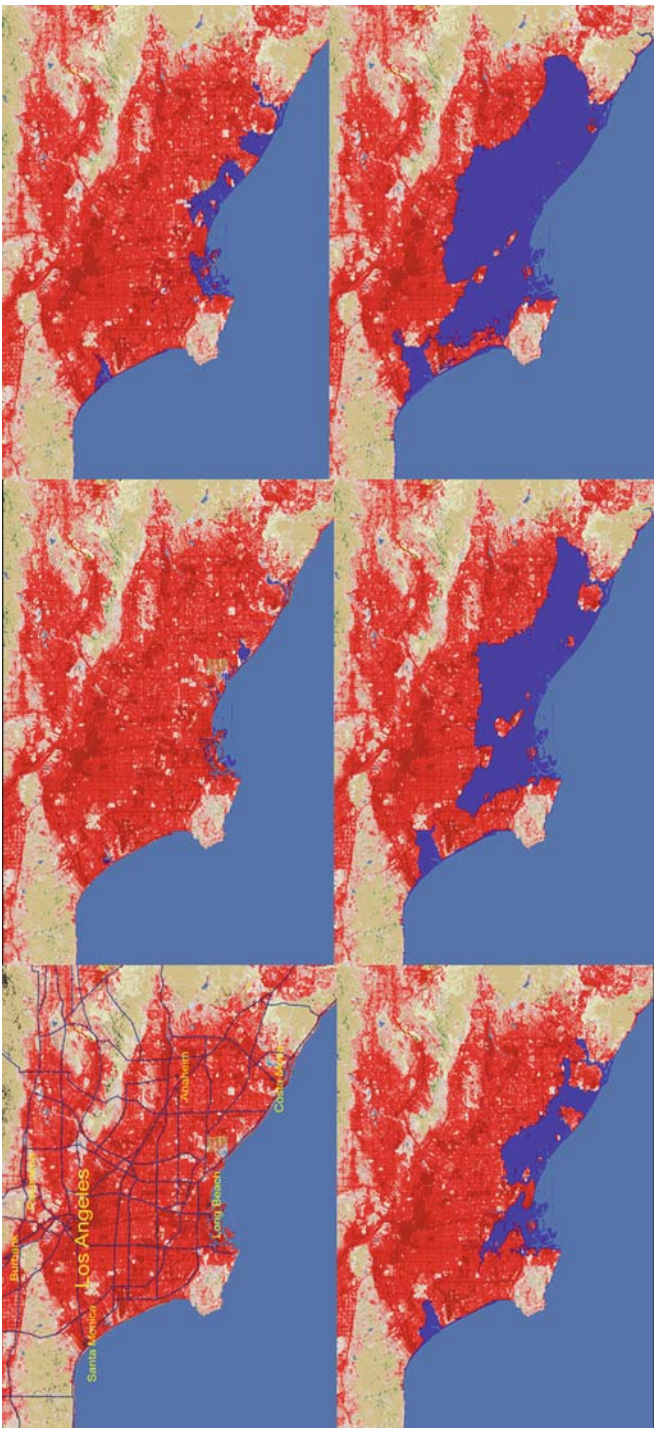

Fig. 2.6 Storm surge flooding simulation in the Los Angeles, California area

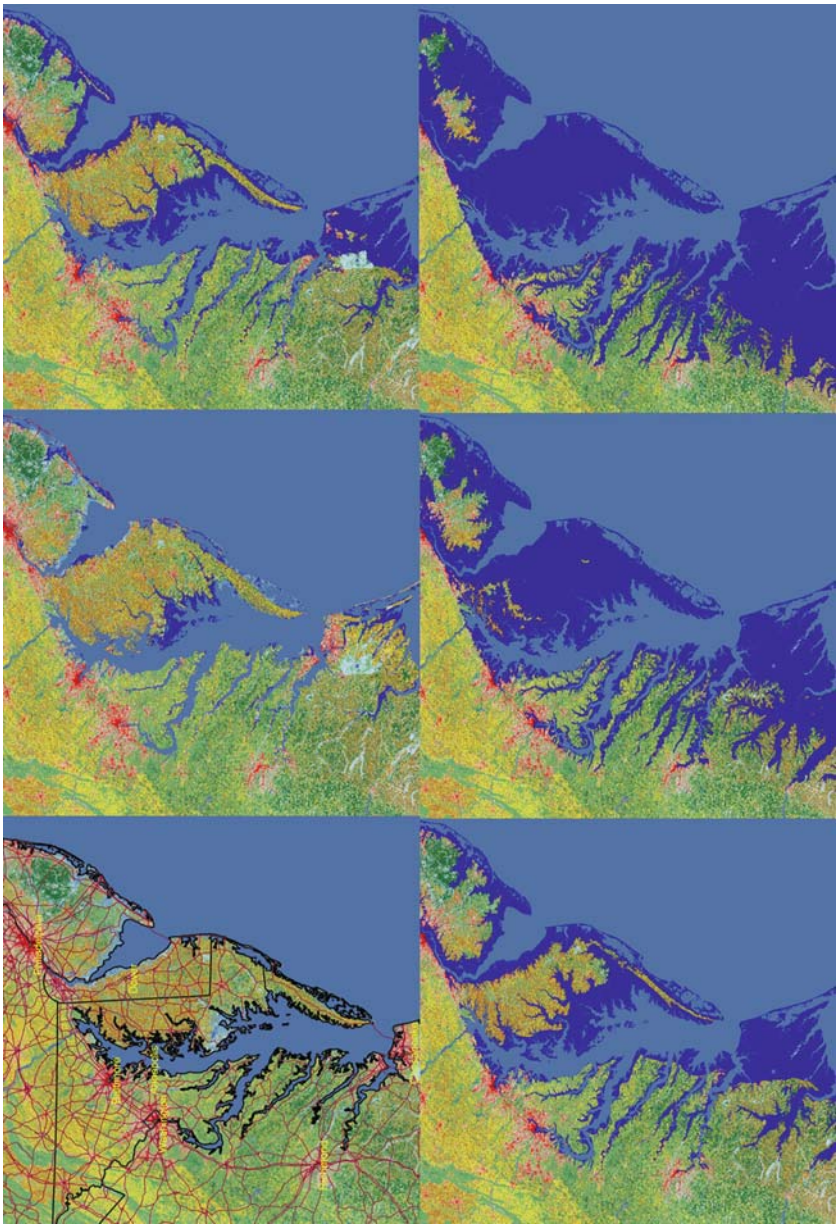

Fig. 2.7 Storm surge flooding simulation in the Washington, DC area

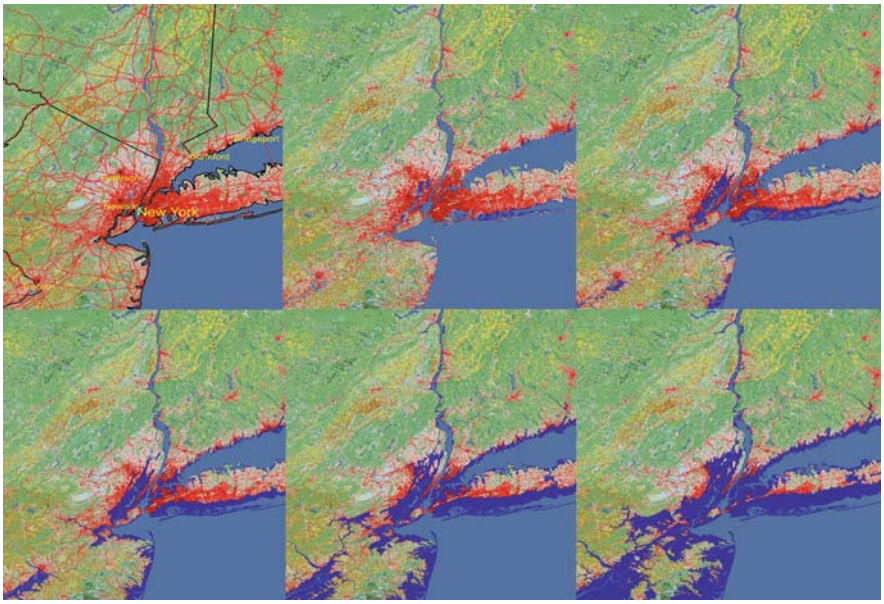

Fig. 2.8 Storm surge flooding simulation in the New York area

Flood simulations such as those shown in Figs. 2.6, 2.7, and 2.8 can help planners focus on areas that may experience inundation, plan evacuation routes, and undertake appropriate mitigation measures. The US Geological Survey is currently producing flood simulation animation files for all US coastal areas using 30 m elevation, land cover, and population data. The 90 m SRTM data are being used to produce animations for major urban areas along the world's coasts. These global animations with regional enlargements have been created with data at 30 arc-sec resolution for elevation, land cover, and population. All of these animations are available at http://cegis.usgs.gov/sea_level_rise.html.

2.6 Conclusion

Large numbers of people living in rural and urban coastal areas are at risk from sea-level rise and storm surge. Using a multi-scale approach, sea-level rise at global and regional scales and storm surge effects at local and urban scales were modeled. Modeling sea-level rise effects across the globe utilized land cover, elevation, and population at 30 arc-sec resolution projected and resampled to 1 km raster cells. Results show that a 5 m rise in sea level would potentially affect about 700 million people; of these, 125 million live in urban and built-up areas. A 30 m rise places 1.4 billion, or 23 percent, of the world's people in areas of risk.

Storm surge modeling for Los Angeles, Washington, DC, and New York is based on 30 m resolution data for land cover, elevation, and population. Southern Los

Angeles has relatively low elevation so that area is easily flooded. Raising sea level 1 m in the Los Angeles area would inundate locations occupied by over 95,000 people; a 1 m rise in Washington, DC and New York will affect over 220,000 and 240,000 people, respectively. In Los Angeles, a 5 m rise would affect over 350,000 people, whereas, in Washington, DC and New York, a similar rise inundates over 1,900,000 and 1,800,000 people, respectively. And a 10 m rise in global sea level would affect more than 8 million people in these three urban areas.

The methods presented in this chapter are used with available global and regional datasets, limiting the ability to model small sea level change, such as the 3.5 mm that is now occurring each year. Higher resolution datasets, such as elevation data from LIDAR placed on a 10 cm grid, can be used to model small rises in sea level using the same methods outlined here. These methods provide a basis for visualizing risk and can help guide urban planning, development and evacuation decisions.

Future research includes the development of complete datasets at 30 m resolution for the United States and at 90 m for selected parts of the world where large coastal populations are found. An interactive capability allowing users to access these datasets on the World Wide Web to conduct user-selected area of interest simulations is also being developed. Such an interactive capability will permit GIS laymen and the general public to educate themselves and others to the potential harm of global warming through "playing" with the website with different simulations, adjusting areas to those of immediate interest. Additionally, simulations incorporating high resolution LIDAR data are being created and further refinements are being added, such as data layers containing boundaries and place names.

References

Arctic Climate Impact Assessment. (2005). *Arctic Climate Impact Assessment*. Cambridge: Cambridge University Press, 1042.

Arendt, A.A., Echelmeyer, K.A., Harrison, W.D., Lingle, C.S., and Valentine, V.B. (2002). Rapid wastage of Alaska glaciers and their contribution to rising sea level. *Science*, Volume 297. no. 5580, 382–386.

Beckley, B.D., Lemoine, F.G., Luthecke, S.B., Ray, R.D., and Zelensky, N.P. (2007). A reassessment of global and regional mean sea level trends from TOPEX and Jason-1 altimetry based on revised reference frame and orbits. *Geophysical Research Letters*, Volume 34, L14608.

Butler, R. (2005). Hurricane could hit San Diego. Web document. mongabay.com. http://news.mongabay.com/2005/0908-san_diego.html.

Cazenave, A., and Nerem, R.S. (2004). Present-day sea level change: Observations and causes. *Reviews of Geophysics*, Volume 42, RG3001.

Chambers, D. (2008). Causes and effects of sea-level rise. Presentation to the National Research Council Mapping Sciences Committee, April 24, 2008.

Chambers, D.P. (2006). Observing seasonal steric sea level variations with GRACE and satellite altimetry. *Journal of Geophysical Research*, Volume 111, C03010.

Chao, B.F., Wu, Y.H., and Li, Y.S. (2008). Impact of artificial reservoir water impoundment on global sea level. *Science*, Volume 320, 212–214, 11 April.

Church, J.A., and White, N.J. (2006). A 20th century acceleration in global sea-level rise. *Geophysical Research Letters*, Volume 33, L01602.

Comiso, J.C., Parkinson, C.L., Gersten, R., and Stock, L. (2008). Accelerated decline in the Arctic sea ice cover. *Geophysical Research Letters*, Volume 35, L01703.

Das, S.B., Joughin, I., Hehn, M.D., Howat, I.M., King, M.A., Lizarralde, D., and Bhatia, M.P. (2008). Fracture propagation to the base of the Greenland ice sheet during Supraglacial Lake drainage. *Science*, Volume 320, 778–781, 9 May.

Demark, T. (2005). Before and after images of areas affected by the Indian Ocean Tsunami, Web document. http://homepage.mac.com/demark/tsunami/9.html.

Douglas, B.C., Kearney, M.S., and Leatherman, S.P. (2001). *Sea-level rise: History and consequences*. New York: Academic Press.

FEMA. (2007). About Louisiana Katrina flood recovery maps. Web document. FEMA. http://fema.gov/hazard/flood/recoverydata/katrina/katrina_la_index.shtm.

Fricker, H.A., Scambos, T., Bindschadler, R., and Padman, L. (2007). An active subglacial water system in West Antarctica mapped from space. *Science*, Volume 315, 1544–1548, 16 March.

Gehrels, W.R., Hayward, B.W., Newnham, R.M., and Southall, K.E. (2008). A 20th century acceleration of sea-level rise in New Zealand. *Geophysical Research Letters*, Volume 35, L02717.

Holgate, S.J. (2007). On the decadal rates of sea level change during the twentieth century. *Geophysical Research Letters*, Volume 34, L01602.

Horton, R., Herweijer, C., Rozenzweig, C., Liu, J., Gormitz, V., and Ruane, A.C. (2008). Sea-level rise predictions for current generation CGCMd based on the semi-empirical method. *Geophysical Research Letters*, Volume 35, L02715.

Intergovernmental Panel on Climate Change (IPCC). (2007). *Climate change 2007: The physical science basis*. In S. Solomon, D. Qin, M. Manning, M. Marquis, K. Averyt, M. Tignor, H.L. Miller, Jr., and Z. Chen (Eds.). Cambridge: Cambridge University Press. Web document. http://ipcc-wg1.ucar.edu/wg1/wg1-report.html. Accessed 10 May 2008.

Jenkins, A., and Holland, D. (2007). Melting of floating ice and sea-level rise. *Geophysical Research Letters*, Volume 34, L16609.

Joughin, I., Abdalati, W., and Fahnestock, M. (2004). Large fluctuations in speed on Greenland's Jakobshavn Isbræ glacier. *Nature,* Volume 432, 608–610, 2 December 2004.

Joughin, I., Das, S.B., King, M.A., Smith, D.E., Howat, I.M., and Moon, T. (2008). Seasonal speedup along the western flank of the Greenland ice sheet. *Science*, Volume 320, 781–783, 9 May.

Kolker, A.S., and Hameed, S. (2007). Meteorological driven trends in sea level rise. *Geophysical Research Letters*, Volume 34, L23616.

Landscan. (2005). 2005 Global Population Database Release, Web document. http://www.ornl.gov/sci/landscan/landscanCommon/landscan05_release.html. Accessed 8 December 2008.

Marcos, M., and M. N. Tsimplis (2007). Forcing of coastal sea level rise patterns in the North Atlantic and the Mediterranean Sea. *Geophysical Research Letters*, Volume 34, L18604.

McGee, W.J. (1900). The lessons of Galveston. *National Geographic*, October, 377–378.

Miller, L., and Douglas, B.C. (2004). Mass and volume contributions to twentieth-century global sea-level rise. *Nature*, Volume 428, 406–409, 25 March.

NOAA. (2007). Hurricane Katrina—Most destructive hurricane ever to strike the US Web document, NOAA. http://www.katrina.noaa.gov.

Poore, R.Z., Williams, R.S., Jr., and Tracey, C. (2000). Sea level and climate. *USGS Fact Sheet 002–00*.

Rignot, E., and Kanagaratnam, P. (2006). Changes in the velocity structure of the Greenland ice sheet. *Science*, Volume 311, 986–990, 17 February.

Schiefer, E., Menous, B., and Wheate, R. (2007). Recent volume loss of British Columbian glaciers, Canada. *Geophysical Research Letters*, Volume 34, L16503.

Seong, J.C., and Usery, E.L. (2001). Modeling raster representation accuracy using a scale factor model. *Photogrammetric Engineering and Remote Sensing*, Volume. 67, no. 10, 1185–1191.

Seong, J.C., Mulcahy, K.A., and Usery, E.L. (2002). The Sinusoidal Projection: A new meaning for Global Image Data. *The Professional Geographer*, Volume 54, no. 2, 218–225.

Shepherd, A., and Wingham, D. (2007). Recent sea-level contributions of Antarctic and Greenland ice sheets. *Science*, Volume 315, 1529–1532, 16 March.

Steinwand, D. (2003). A new approach to categorical resampling, Proceedings. American Congress on Surveying and Mapping Annual Convention, Phoenix, AZ. Web document. http://www.acsm.net/sessions03/NewMethodologies41.pdf. Accessed April 2007.

Thomas, R.H. (1993). Ice Sheets. In R.J. Gurney, J.L. Foster, C.L., and Parkinson (Eds.), *Atlas of Satellite Observations Related to Global Change*. Cambridge, UK: Cambridge University Press, 385–400.

Truffer, Martin and Mark Fahnestock. (2007). Rethinking ice sheet time scales. *Science*, Volume 315, 1508–1510, 16 March.

Usery, E.L., and Seong, J.C. (2001). All equal area map projections are created equal, but some are more equal than others. *Cartography and Geographic Information Science,* Volume 28, no. 3, 183–193.

Usery, E.L., Finn, M.P., Cox, J.D., Beard, T., Ruhl, S., and Bearden, M. (2003). Projecting global datasets to achieve equal areas. *Cartography and Geographic Information Science*, Volume 30, no. 1, 69–79.

USGS. (2008a). Products related to Hurricanes Katrina and Rita. Web document. http://store.usgs.gov/mod/HurricaneAreas.html.

USGS. (2008b). Decision support system for map projections of small scale data. US Geological Survey. Web document. http://mcmcweb.er.usgs.gov/DSS/, Accessed May.

Vaughan, D.C., and Arthern, R. (2007). Why is it hard to predict the future of ice sheets? *Science*, Volume 315, 503–1504, 16 March.

Wadhams, P., and Munk, W. (2004). Ocean freshening, sea level rising, sea ice melting. *Geophysical Research Letters*, Volume 31, L11311.

Weaver, A.J., Saenko, O.A., Clark, P.U., and Mitrovica, J.X. (2003). Meltwater pulse 1A from Antarctica as a trigger of the Bølling-Allerød warm interval. *Science*, Volume 299, no. 5613, 1709–1713.

Zebrowski, E., Jr. (1999). *Perils of a Restless Planet: Scientific Perspectives on Natural Disasters*. Cambridge: Cambridge University Press (First paperback edition).

Zwally, H.J., Brenner, A.C., and DiMarzio, J.P. (1998). Growth of the southern Greenland Ice Sheet. *Science*, Volume 281, 1251a, 28 August.

Chapter 3
Urban Expansion and Sea-Level Rise Related Flood Vulnerability for Mumbai (Bombay), India Using Remotely Sensed Data

Firooza Pavri

Abstract Rapid growth and expansion of the developing world's urban areas has both social and biophysical consequences such as increased population density, inadequate infrastructure and services, the expansion of impermeable surfaces, and habitat fragmentation with a loss of green space. Data from NASA's Landsat and Shuttle Radar Topography Mission (SRTM) programs are employed to examine urban patterns between 1973 and 2004 for the coastal mega-city of Mumbai (formerly Bombay), India. By 2015 Mumbai is expected to be the world's second largest city containing 22.6 million people with one of the highest population densities (UN Population Division 2006). This chapter considers the city's ongoing and future vulnerability to flood hazards in the light of climate change models predicting an increased intensity of monsoonal storms, as well as a 0.38−0.59 m sea level rise by the end of the 21st century. Landsat MSS and ETM+ data are used to map change in urban patterns, while an unsupervised classification produces a land use map for the city and its environs. SRTM data are used to build an elevation model which is analyzed in conjunction with the land use map. Zones of vulnerability to floods are identified for the city and its environs. The results suggest that the predicted consequences of climate change will exacerbate the city's ongoing vulnerability to flooding if urgent measures are not taken to improve storm water drainage systems and shore up other flood control defenses.

Keywords Urban expansion · Vulnerability · Sea-level rise · Satellite data · Mumbai (Bombay) · India

3.1 Introduction

On July 26, 2005 a severe 24-hour monsoon event resulted in close to 965 mm of rain falling in the city of Mumbai (formerly Bombay), the commercial and financial

F. Pavri (✉)
Department of Geography-Anthropology, University of Southern Maine, Gorham, ME 04038, USA
e-mail: fpavri@usm.maine.edu

P.S. Showalter, Y. Lu (eds.), *Geospatial Techniques in Urban Hazard and Disaster Analysis*, Geotechnologies and the Environment 2, DOI 10.1007/978-90-481-2238-7_3,

capital of India. The ensuing disastrous flooding led to loss of life, property damage that rose into the millions, epidemic threats, and the city coming to a grinding halt for days (TNN 2005a). While the monsoonal event was unusual in its severity and was coupled with astronomical high tides, the vulnerability of the city to climate hazards is not new. The city has long struggled with regular monsoon-related floods owing to antiquated sewer and flood control infrastructure, now clearly unable to cope with the level of population explosion and development witnessed over the past 50 years.

The most recent and definitive (to date) report by the Intergovernmental Panel on Climate Change (IPCC) has confirmed the global threat of rising sea levels and extreme weather patterns to coastal regions (Nicholls et al. 2007). Across South Asia, research suggests that sea level rise will test the coping capacity of coastal cities to their limits, while a study ranking India's coastal zones by their vulnerability found Mumbai to be the most likely to experience considerable damage from sea level rise (Nicholls 1995; Nicholls et al. 2007; TERI 1996; Wilbanks et al. 2007). A recent United Nations' report on World Urbanization Prospects has projected that by 2015 the Mumbai Metropolitan region of India will be the world's second largest urban agglomeration with 22.6 million people, up from its current 18 million residents (UN Population Division 2006). This increase will only add to already overburdened city services and result in predictable demands on housing, infrastructure and transportation. Added to this, Mumbai's island orientation, high population density, lack of suitable housing for a vast section of its population, and its vulnerability to persistent flooding will further complicate planning efforts.

The growth and expansion of urban areas creates a variety of impacts with both social and biophysical consequences. In the 21st century, the mega cities of the world will be primarily concentrated in developing nations where resources are limited and the ability of local governments to provide services are already stretched to their breaking point (UN Population Division 2006). Population density is particularly high in the developing world's cities and can be problematic on a number of fronts. Governments often fall short in providing infrastructure and services, preserving intra-city green space, and crafting adequate disaster management plans (Demographia 2007). Furthermore, urban sprawl leads to leapfrog development as the growth of satellite towns and bedroom communities expand into the rural hinterlands, consuming essential agricultural land. The expansion of urban surfaces also reduces ground permeability and increases runoff and the risk for flooding. The semi-variable predictability of seasonal rainfall like the monsoon, while providing residents with some opportunity for preparation, can still have very different impacts even within neighborhoods and households based on housing structure, the floor a resident occupies, and socio-economic status.

Historically, hazards researchers have sought to identify and provide practical risk reduction alternatives to perilous environmental conditions including severe meteorological, hydrological or geological events and their consequences. This work commonly provided human-engineered solutions to minimize threats faced by populations (Barrows 1923; White 1964). The now well established field of vulnerability research traces its roots back to this earlier hazards work. Vulnerability

research recognizes that human systems are inextricably linked to understanding the variable impact of hazards on individuals and their abilities to cope, resist and recover from these hazards (Blaikie et al. 1994, p. 9; Burton et al. 1993; Cutter 1996; Cutter et al. 2000; Few 2003; Hewitt 1997; Kasperson et al. 1995; Smith 1992).

More generally, vulnerability research helps clarify and make explicit the connections between hazard events and their impact on the coping capacity of populations based on their socio-economic and demographic characteristics. Hazard events have traditionally been considered momentous events such as earthquakes and tsunamis or extreme weather related occurrences such as hurricanes. Recent vulnerability research has expanded the definition of hazard to include longer term evolving conditions such as drought, desertification, pollution, deforestation, and more recently conditions related to climate change such as sea level rise and changing precipitation patterns. Vulnerability research has much to contribute in terms of assessing the impact of a changing environment on affected populations. Furthermore, the focus on coping capacities and adaptations to these changing conditions offers important policy prescriptions to help tackle this situation.

The use of satellite imaging technology to monitor urban environments in the developing world is rapidly expanding (Alrababah and Alhamad 2006; Al Rawashdeh and Saleh 2006; Ji et al. 2001; Kaya 2007; Kwarteng and Chavez 1998; Maktav and Erbek 2005; Mundia and Aniya 2005; Weber et al. 2005; Zhang et al. 2002). Remote sensing technology can be particularly useful given the paucity and limited accessibility of data from some parts of the developing world. Vulnerability research, in particular, has been hindered by the dearth of reliable data to feed its data rich models. Analysis of satellite imagery provides one step toward filling this data void. This technology also allows for quick assessments and hence can be practical for post-hazards adaptation and rescue and recovery operations. Thus far, systematic studies using satellite imagery to monitor urban growth patterns and map flood vulnerability zones for Mumbai and its immediate surrounding are largely lacking (TNN 2005b). As researchers have suggested, such assessments provide necessary information for decision-makers and are an important first step to identifying effective urban planning options in the face of hazard events (Maktav et al. 2005). Mumbai is often promoted as the financial and commercial capital of one of the world's fastest growing economies. If the city is to sustain such growth and provide an acceptable quality of life for its citizens, its planners, as a first step, will need to monitor existing sprawl patterns and their impact on habitat fragmentation, flood vulnerability and the population's ability to cope with changing environmental conditions.

3.2 Background

Located on the west coast of India by the Arabian Sea, Mumbai's history can be traced back to seven original islands reclaimed and filled-in over centuries. The seven original islands currently contain most of the older part of the city and its central business district (CBD). Ruled by various regional Hindu and Muslim rulers,

it was not until the landing of Francis Almeida and the Portuguese take-over in 1534 that this deep natural harbor was named *Bom Bahia* (the Good Bay). In 1668 the islands were acquired by the British East India Company, who later shortened the name to Bombay, and made it their Company headquarters. This marked the turning point in Bombay's history. Thereafter the city grew in size from 13,726 in 1780 to 977,822 by 1906, fed largely by early merchant migrants and those interested in commerce (TIFR 1999a). Post-independence expansion and the large influx of rural migrants contributed to the current approximate size of 18 million (MMRDA 2003). In 2001, population density for the Greater Mumbai Metropolitan region was reportedly at 27,715 people per square kilometer, and second only to Hong Kong, China (Demographia 2007; MMRDA 2003).

Today, Mumbai is a microcosm of larger India. It has an ethnically and religiously diverse population, tens of different languages spoken by its newer migrants, and citizenry living at the extremes of staggering wealth or abject poverty typical of the developing world. Aptly named "Maximum City" in a recent account of the metropolis, the city's "larger than life" aura is apparent to even the most casual visitor (Mehta 2004). Geographically, the greater metropolitan region of Mumbai spans approximately 482 km^2 with much of the city's coastline at or just above sea level. The island of Mumbai has an average elevation ranging between 10 and 15 m with the highest point found in the city's northern section at 460 m. Mumbai experiences southwest monsoons between the months of June through September, with an average rainfall of 1800 mm (TIFR 1999b).

The rapid urbanization experienced by the city and its environs over the past four decades has left planners struggling to cope. Development is often unplanned with once small suburbs and neighboring towns becoming overnight bedroom communities and cities in their own right with minimal improvements in infrastructure and amenities. Recent data indicate that the rate of growth in the outlying suburbs and satellite towns has far outpaced that observed within the city (MMRDA 2003). For example, Navi Mumbai (formerly New Bombay), conceived in 1971, is one of the largest planned cities in the world and was designed to accommodate approximately 2 million residents and alleviate some of the population pressures experienced by Mumbai (MMRDA 2003). Today, however, it is widely recognized that even though the planned city contained approximately 704,000 residents in 2001, it failed to draw some of the more important business and employment opportunities away from Mumbai (MMRDA 2003). For the most part, Navi Mumbai serves as a bedroom community to its larger neighbor across the creek. On the other hand, Mumbai's shanty town or slum population has steadily increased to a staggering 50% of the city's population (MMRDA 2003). These densely packed parcels of land contain makeshift huts and inadequate infrastructure (Leahy 2008). One example is Dharavi, also infamously known as Asia's largest slum, which houses approximately 60,000 families and is located in a low lying district close to the center of the city (Leahy 2008). For the most part, slums are interspersed on open land throughout the city and abut high rise apartments, which themselves command astronomical prices comparable to many of the developed world's megalopolises.

The island orientation of the main city of Mumbai, with limited space for expansion, has led to a steady destruction of green space and fringing coastal wetlands, compounding the effects of habitat fragmentation and stretching ecosystem resources and services to their breaking point. Despite this, Mumbai is one of the few mega cities of the world with a National Park within its geographic boundaries. Besides being the largest park in the world within a metropolitan city, the Sanjay Gandhi National Park (SGNP) occupies a vast section of the north-central portion of the city and houses three important water reservoirs specifically for the city's populace. However, the encroachment of shanty towns and housing developments within and along the park boundary has been steady and unabated, spurred on by strong development pressures (Zerah 2007). Likewise, fringing coastal mangroves on both the eastern and western coasts of the city, while theoretically protected by coastal zone development moratoriums, face constant development and encroachment pressures.

The Mumbai Metropolitan Region Development Authority (MMRDA) is responsible for the planning goals of the city. The Authority includes an Emergency Operations Center and develops emergency management and hazard response plans. This agency also assesses risk and vulnerability to a myriad of hazards including cyclones, earthquakes, epidemics, and industrial disasters and outlines response scenarios (MMRDA 1999). Even with these agencies in place, inadequate response during the catastrophic flooding of July 2005 made obvious the deficiencies in the city's emergency response infrastructure (TNN 2005c). Basic emergency response systems such as ambulance, fire and rescue services were unable to operate; rail and other transport links stalled, and electricity for vast sections of the city was not restored for days. Despite India having much past experience coping with natural disasters, researchers have puzzled over the weak response of the Indian government to hazard events in general (Ray-Bennett 2007).

This chapter uses data from the US National Aeronautics and Space Administration's (NASA) Landsat and Shuttle Radar Topography Mission (SRTM) programs to analyze urban sprawl patterns for Mumbai city and its surroundings from 1973 through 2004. Particular attention is given to the contraction of green space due to sprawl, in-filling of open city space, leapfrog urban development patterns, and identifying flood vulnerable zones. Recent climate models predict a global sea level rise of anywhere between a 0.38 and 0.59 m by the end of the 21st century with significant local variations (Meehl et al. 2007). In the case of Mumbai not only would sea level rise have a very significant impact, but additionally, more severe monsoonal activity and increased precipitation as also predicted by general circulation climate models would compound its vulnerability (Meehl et al. 2007). By using readily downloadable multispectral data through NASA's Landsat mission and merging these with elevation data through the SRTM program, this chapter employs methods tested and accepted in the conventional literature to assess the potential impact of predicted sea-level rise for the greater Mumbai Metropolitan region. In so doing, it provides a template for similar such studies for the developing world's coastal cities.

3.3 Data and Methods

Data used for this study were derived from the Landsat program's long historical archive of multispectral imagery. The first image is a Multispectral Scanner (MSS) four band dataset from 9 January 1973 at 79 m spatial resolution and obtained through the Earth Science Data Interface (ESDI) at the Global Land Cover Facility website supported by NASA (GLCF 1997). This image is used primarily to assess the city's urban extent in 1973. The image is one of the earliest cloud-free and downloadable images of the city available from the Landsat archive and provides an important glimpse of the city's geographical extent prior to the recent exponential growth in population. The coarse spatial and spectral resolution of these data, however, limits detailed analyses. Additionally, the lack of data in the region of 400−500 nm limits its use for urban applications.

The second image is a 17 October 2004 gap-filled six band dataset from the Enhanced Thematic Mapper + (ETM+) sensor at 30 m spatial resolution obtained from the Earth Resources Observation and Science (EROS) Data Center (USGS EROS 2006). These data were captured after the ETM+ sensor developed the Scan Line Corrector (SLC) problem, which compensated for the forward movement of the satellite. To correct this problem, the US Geological Survey (USGS) now provides ETM+ gap filled data products using an average DN from previous passes over the same area. In this case, values from a previous pass were used to fill in the SLC missing data. However, filling in these data sometimes causes striping to occur and this is evident on the 2004 ETM+ image. While data from both time periods (1973 and 2004) are not captured during the same time of year, they are acceptable because both were obtained during the dry season. However, because the ETM+ image was acquired in October, it should be noted that the recent end of the monsoons in September of that year will significantly influence the vegetation signal. Given the mismatch in terms of time of capture and the lack of any sensor calibration data for the MSS image, the two images were only visually compared to assess obvious changes in the spatial extent of the city. Most analytical efforts focused on the 2004 ETM+ image to map land use and identify zones of vulnerability.

In addition to the imagery, an SRTM elevation dataset also obtained via the USGS EROS website at 3 arcsec (90 m spatial resolution) is used to construct a digital elevation model for the city and aid in identifying zones of vulnerability to sea level rise and flood events (SRTM 2006). At present, these elevation data are only available at 1 m z-value increments. Consequently, mapping fine-scale vulnerability zones is limited by the dataset and to 1 m increments. While some issues have been raised about the accuracy of the SRTM dataset (Rabus et al. 2003), SRTM are the *only* systematic elevation dataset freely downloadable for most of the globe and as such provide an enormously rich source of information for data poor regions across the developing world. Given the 90 m spatial resolution for these data, they are coarser than that captured by ETM+ and the dataset does contain a few gaps in terms of dropped pixels. However, for the study site, these gaps are minimal and appeared mostly in non-urban areas. Reference data for ground control points

and for accuracy assessments were obtained through a topographic map and high resolution Google Earth™ imagery. All image processing and analysis was conducted using ERDAS® Imagine® software and ESRI's ArcGIS™ was used for an overlay analysis and to produce vulnerability data.

The paper uses existing methodologies and analytical tools established in the literature (Auch et al. 2004; Jensen et al. 2005). False color composites (FCC) for both the 1973 and 2004 datasets using standard stretching and contrast techniques are examined and findings reported. An unsupervised classification procedure is used to build a land use map from the 2004 ETM+ dataset. The Iterative Self Organizing Data Analysis (ISODATA) algorithm in ERDAS®, which uses a minimum distance function to assign pixels to a cluster, is employed (Lillesand et al. 2008). To appropriately capture land surface variability, selecting a suitable number of clusters is an important parameter to take into account when running the ISODATA routine (Mundia and Aniya 2005). After experimentation, 15 clusters were determined to be the most appropriate number for the ETM+ image. After visually inspecting and naming the clusters, the 15 were further reclassed into eight clusters. Accuracy assessments were performed on the ETM+ classified dataset using 256 points generated using a stratified random sample, while high spatial resolution Google Earth™ imagery, local knowledge, and topographic maps of the area were used for verification. The final unsupervised classification results were imported into ArcGIS™ to be analyzed in conjunction with the SRTM elevation dataset. ArcGIS's Spatial Analyst module was used to overlay the SRTM elevation data with land use classes to map and examine vulnerability zones to sea level rise across the city and its environs. Attention was focused on simulating flood vulnerability zones from 1 to 4 m above sea level. While the predicted rise in sea level is less than 1 m over the next 100 years, the ensuing vulnerability to flooding will likely spread across low lying regions. Spatial Analyst's raster calculator functionality is used to calculate land use impacted within the flood vulnerable zones and the areas are mapped to assess their spatial distribution across the city.

3.4 Analysis and Results

The data analysis proceeds in four stages. First, a visual assessment of the 1973 MSS and 2004 ETM+ false color composites are presented, focusing in particular on deciphering urban patterns and changes therein. Next, results of the unsupervised classification and accuracy assessments for the 2004 ETM+ image are discussed. Third, an SRTM elevation model is constructed for the greater metropolitan area. Finally, results from the land use analysis and the SRTM elevation model are combined in ArcGIS's Spatial Analyst to assess the impact of potential climate change on land use activities across the region and identify zones of flood risk.

3.4.1 False Color Composites for 1973 and 2004

A visual assessment of the 1973 MSS false color composite (FCC) of Bands 1, 2, 3 (Fig. 3.1) shows most of the city of Bombay contained within the southern portion of

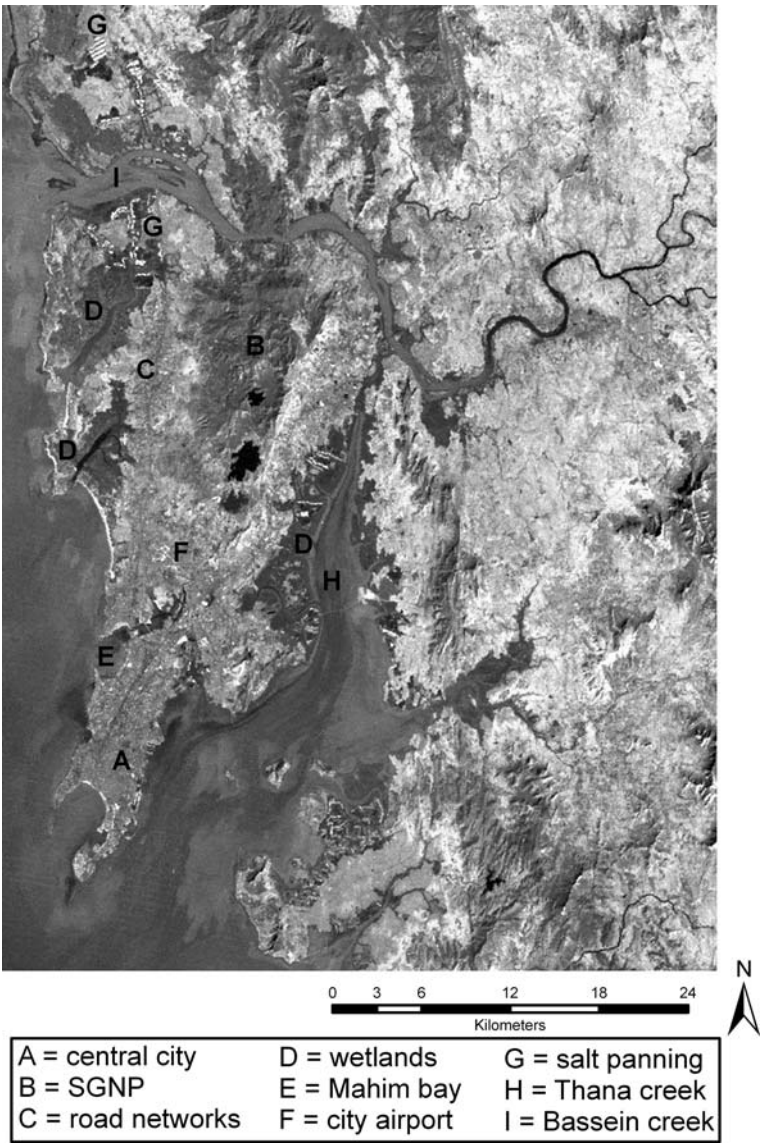

Fig. 3.1 Landsat MSS false color composite for the Greater Mumbai Metropolitan region and surrounding, 1973

the island peninsula ("A" on the bottom left of the figure). Key arterial expressways can be seen extending out from the city center into the northern suburban sections of the island on either side of the Sanjay Gandhi National Park (SGNP; "B"), with some suburban development along either side of these expressways (C). The image shows green space interspersed throughout the city. The SGNP covers a vast section

of the north-central portion of the image. Taken in the month of January, the image displays some mixed tropical deciduous tree cover with leaf-off conditions. Development activities, including cleared tracks, are seen interspersed within and adjacent to the park's boundaries. Also noteworthy are the robust coastal mangroves and estuarine wetlands that border the northeastern and northwestern sections of the island city (D). These habitats are an essential and important protective buffer from tidal surges and cyclonic activity and appear relatively healthy. Extensive mudflats appearing during low tide conditions are also apparent along the eastern coast of the island.

The southern end of the island, south of Mahim bay (E), contains the city's core central business district and original residential areas. It is also in the south end of the island that most reclamation activities were undertaken, and where the original seven islands of Bombay were eventually joined together. In this case, the FCC suggests a fairly dense urban landscape. Urban density declines north of the city's airport (F), which is typified by greater expanses of green space.

Overall, the MSS image from 1973 suggests that the densest concentration of urban activity was largely limited to the southern section of the island. While development is clearly expanding outward from the core old city, it is mostly restricted to areas along the western and eastern expressways that make their way out of the central city and into the island's suburban northern reaches. The mainland to the north of Bassein creek (I) and east of Thana creek (H) is typified by the city's rural hinterland. Agricultural activities dominate here, but for the most part, the data indicate fallow agricultural fields yet to be planted with the winter crop. At this spatial resolution, smaller towns in the rural hinterland are difficult to distinguish. The city of Navi Mumbai across the harbor to the east of the island has not yet been developed. Urban development on the mainland north of the city is also largely absent. For the most part, this land is used for salt panning activities (G). In 1971 the Mumbai Metropolitan Region's population stood at approximately 7.8 million with an annual growth rate of 3.7%, the highest it had seen in its history (MMRDA 2003).

A cursory visual comparison between in the 1973 MSS (Fig. 3.1) and the 2004 ETM+ false color composite (Fig. 3.2) reveals dramatic shifts in land cover over the 30 year period. The obvious changes are in the expansion and intensification of developed land surface across the city and its outlying townships. Also observed is an ensuing contraction of the city's green space. As indicated earlier, the vegetation signal is quite strong because the 2004 image was taken at the end of the monsoon season where almost every non-paved surface is taken over by ephemeral shrubs and grasses. The 2004 image also indicates that the vital coastal mangroves along the main island have are encroached upon by development activities since the time of the 1973 image.

By 2004 the city of Mumbai has seen a tremendous boom in suburbs on the island itself, now occupying virtually all of the open space on the island with the exception of the SGNP. Moreover, the larger region has also witnessed an expansion of new suburbs and satellite towns on the mainland. The cities of Navi Mumbai (A), Thane (B), Kalyan (C), Dombivili (D), Bhiwandi (E) and Panvel (F) on the mainland to the northeast of the city and Mira (G) and Nalasopara (H) to the north of the

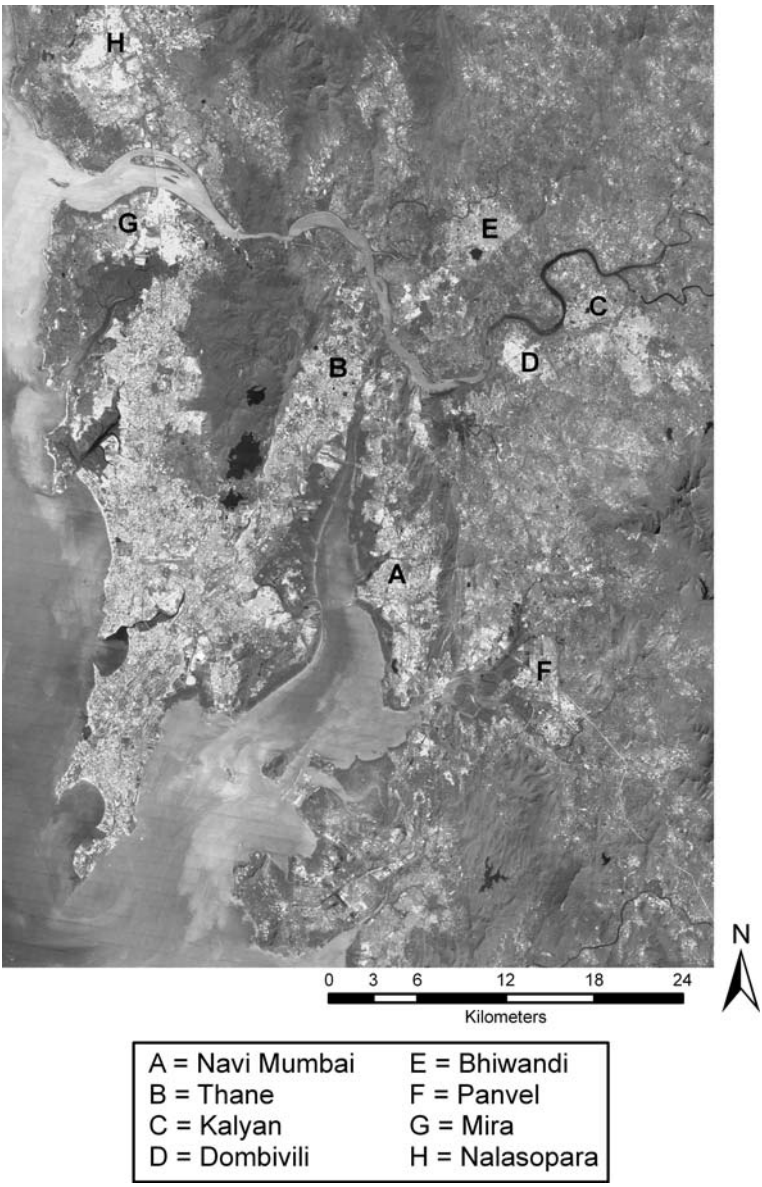

Fig. 3.2 Landsat ETM+ false color composite for the Greater Mumbai Metropolitan region and surrounding, 2004

city were small towns in the 1973 image. Today, they all contain populations of over 100,000 residents, with Thane and Kalyan containing over 1 million residents each (MMRDA 2003). A visual analysis of the changes between 1973 and 2004 indicates these dramatic shifts. Urban expansion for the city and its environs has

been typified by intensification across the island, encroachment into open space along coastal mangroves and green pockets across the city, expansion into outlying suburban areas, and leapfrog development into the rural hinterland especially across the mainland east of the island.

3.4.2 Land Use Classification

Land use classification maps are an effective way to observe spatial patterns. In this case, an ISODATA routine is employed to arrive at a land use map for the city and its surroundings using the 2004 ETM+ dataset. The routine was originally run with a large number of clusters and later collapsed into eight classes representing land use patterns for the city (Fig. 3.3).

Quantifying the accuracy of any classification routine is a necessary step toward building confidence in the results. For the accuracy assessment, a stratified random sample of 256 pixels with a minimum of 20 pixels per class was generated to ensure coverage of all eight cover classes and to minimize bias. These reference pixels are checked against 3 m high spatial resolution Google Earth^{TM} imagery and substantiated by extensive local knowledge and topographic maps. The results of the error matrix generated indicate an overall classification accuracy of 83.5% (Table 3.1). The overall Kappa index of agreement, which indicates the extent to which the assignment of pixels in the error matrix were due to "true" versus "chance" agreement, was reported at 0.81 (Lillesand et al. 2008). In terms of Producer's Accuracy all classes were above 70% with the exception of the Encroaching Development class at 60.71%. All classes were above 70% in terms of User's Accuracy. The important Urban/Developed class was at 81.25 and 72.22% for Producer's and User's Accuracy respectively. Overall, the ISODATA routine, a simple yet powerful algorithm, provided better than expected results in terms of producing a final land cover map. The map was exported into ArcGIS's Spatial Analyst for further analysis.

3.4.3 SRTM Elevation Model

SRTM data were downloaded and imported into ArcMap for further analysis (Fig. 3.4). Figure 3.4 uses a color palette to distinguish elevation above sea level, and large expanses of land can be seen at or just above sea level for the greater metropolitan region of Mumbai.

Table 3.2 reports the spatial coverage of elevation zones across the image. Particularly noteworthy is the extent of land under a 4 m elevation cut-off. On the main island of Mumbai, these areas are also some of the more densely packed sections of the city and with low to middle income housing. Strikingly, this section of the island city was particularly impacted by the severe monsoon event and flooding of 2005 referenced at the beginning of this chapter. Low lying areas across the city

Fig. 3.3 Land use map using ETM+ data for the Greater Mumbai Metropolitan region and surrounding, 2004

are already prone to flooding. In many cases, this area houses some of the city's poorer shanty town residents who are already economically vulnerable and whose ability to cope with and recover from hazard events is very limited. The flood of 2005 produced large numbers of fatalities from these areas (TNN 2005d).

Table 3.1 Error matrix for the Greater Mumbai Metropolitan region land use map derived from Landsat ETM+ data

Land-use class	1	2	3	4	5	6	7	8	Total	Producer's accuracy	User's accuracy	Kappa statistic
1	*38*	0	0	0	0	0	0	0	38	100.00	100.00	1
2	0	*20*	0	0	0	0	0	0	20	100.00	100.00	1
3	0	0	*18*	0	2	1	0	0	21	81.82	85.71	.84
4	0	0	0	*23*	1	1	3	2	30	92.00	76.67	.74
5	0	0	2	0	*26*	6	2	0	36	81.25	72.22	.68
6	0	0	1	0	3	*17*	3	0	24	60.71	70.83	.67
7	0	0	1	1	0	0	*36*	2	40	70.59	90.00	.87
8	0	0	0	1	0	3	7	*36*	47	90.00	76.60	.72
Total	38	20	22	25	32	28	51	40	–	–	–	–

Overall classification accuracy = 83.5%
Kappa Index of Agreement = 0.81

Land Use Class Index: 1 Water; 2 Inland Waterways; 3 Mud flat/urban surface; 4 Coastal/ Riverine marsh/Green cover; 5 Urban/Developed; 6 Encroaching Development; 7 Agricultural Land/Undeveloped Urban; 8 Green space

3.4.4 Land Use and SRTM Overlay Analysis

The SRTM elevation model is used in conjunction with the land use map to calculate the areal size of each of the land use classes contained within 0−1 m, 1−2 m, 2−3 m and 3−4 m elevation zones (Table 3.3). These are identified as critical, severe, high and moderate risk zones for flooding, respectively.

Given the predicted 0.38−0.59 m rise in sea level over the next 100 years and increased severity of storms, these zones will be subject to the most hazardous flood conditions. It is here that efforts need to be focused to build more effective flood control measures, redesign housing structures, or perhaps even resettle populations and development activities over the next 50–100 years. While the total amount the of Urban/Developed land use class within the 0−1 m critical flood vulnerability zone comprises a relatively small area of 3.05 km^2, when one considers the high population density for the metropolitan region at 27,715 km^2 reported in 2001 (Demographia, 2007), that area could amount to as many as approximately 83,000 affected people (see Table 3.3). Additionally, vulnerability will not just be contained to the predicted approximate 0.58 m sea level rise zone – its effects would permeate across most low lying areas of the city, with its impact compounded in economically poor neighborhoods.

The two land uses affected the most significantly between 0 and 4 m in elevation vulnerability zones include the Coastal/Riverine marsh/Green cover class for a total of 12.7 km^2 and the Urban/Developed class for a total of 11.6 km^2 (see Table 3.3). This finding suggests that mangrove areas already under pressure from present development will face additional pressures from sea level rise and flood vulnerability and perhaps, as observed elsewhere, will affect the configurations of

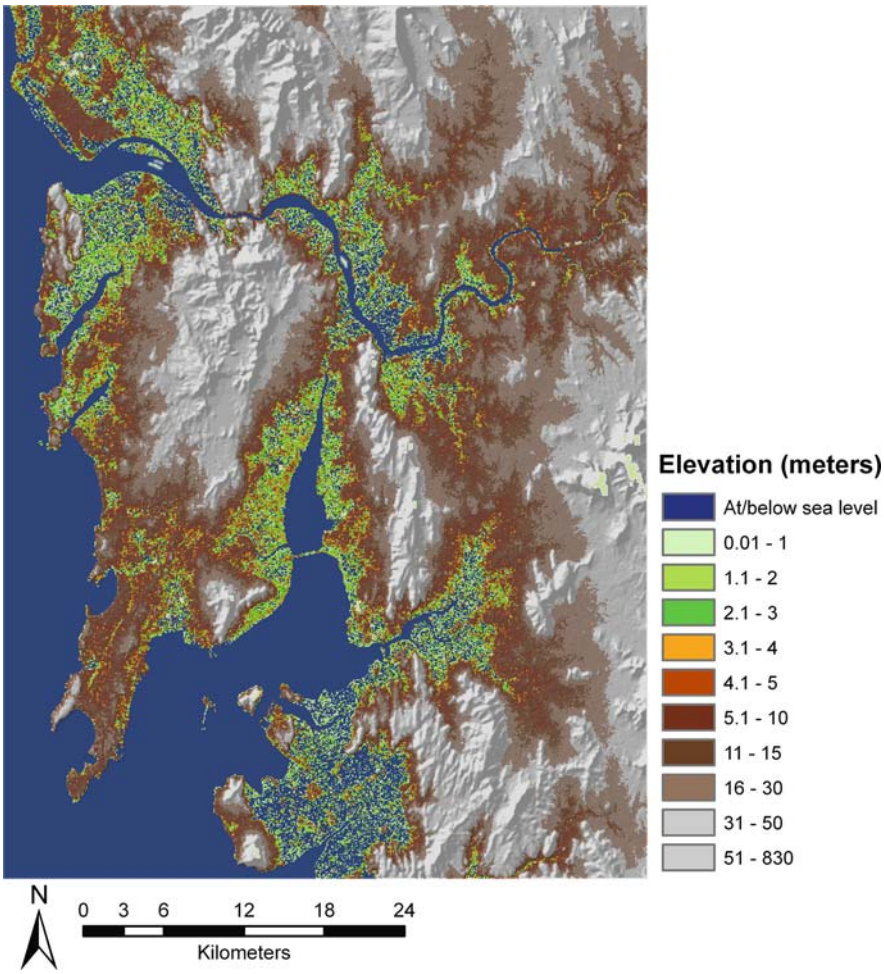

Fig. 3.4 SRTM elevation model for the Greater Mumbai Metropolitan region and surrounding

wetland species. Of more concern would be the area of the Urban/Developed class that falls within the 4 m vulnerability zone. The coping strategies and local response to these conditions at present involve ad-hoc household level adaptations and a reliance on kinship networks to survive periodic flood conditions. However, with the increased severity and frequency of these conditions, longer term response measures will need to be developed. The data from this analysis suggest that a very significant proportion of the city and its suburbs will be subject to more persistent hazardous conditions based on climate predictions for the next 50–100 years.

To date, Mumbai has utilized large World Bank loans for piecemeal improvements in potable water and drainage infrastructure. However, as most citizens will attest, these improvements are short lived as population densities increase and sheer numbers of people overwhelm city services. To have more long lasting benefits,

Table 3.2 Land area at or above sea level for the Greater Mumbai Metropolitan region using SRTM data

Elevation (m)	Area coverage (in km^2)
0–1	101.5
1–2	95.5
2–3	85.3
3–4	74.7
4–5	67.8
5–10	320.8
10–15	276.0
15–30	495.3
30–50	275.9
50–150	375.0
50–830	181.6

Table 3.3 Extent of land use (in square kilometers) within flood vulnerability risk zone

Land use	0−1 m (critical)	1−2 m (severe)	2−3 m (high)	3−4 m (moderate)
Mud flat/urban surface	1.28	1.01	0.82	0.61
Coastal/Riverine marsh/Green cover	3.79	3.40	2.73	1.87
Urban/Developed	3.05	3.05	2.82	2.69
Encroaching Development	0.75	0.81	0.97	0.76
Agricultural Land/Undeveloped Urban surfaces	1.09	1.21	1.34	1.50
Green space	0.37	0.45	0.45	0.47

efforts to tackle flood vulnerability need to be considered from several angles. The city's planners and governance bodies need to give more serious consideration to updating and expanding storm drainage systems and flood control barriers and defenses, protect the city's natural mangrove defenses from development activities and expand mangrove coverage, engage in politically charged slum redevelopment schemes to provide adequate housing, and shore up the city's disaster response systems, all of which have been promised for decades. Perhaps the information from recent climate models suggesting higher sea levels and the increased intensity and frequency of storms, coupled with the results of studies such as the present one, will provide the impetus to address, with some urgency, the city's vulnerability to persistent flood events.

3.5 Conclusion and Future Recommendations

The analysis conducted for this study provides a synoptic view of a developing world city and its environs. Such an approach to understanding the landscape can be useful as it offers a comprehensive look at the interconnection of systems within

an urban environment, helps identify areas that require quick attention or target others for further analysis. Classification techniques, such as the one used in this study, form an important aspect of image interpretation and pattern recognition. Such analyses provide quantifiable information on land use activities and provide planners with essential data when crafting development plans. Regional or urban land use planning is a multi-faceted process that requires economic, social, demographic and spatial data to inform the planning process. The application of remote sensing data as demonstrated in this chapter provides one approach to analyze urban systems, illustrating its usefulness for planners, environmentalists, developers, and even non-government groups engaged in improving land use conditions in urban areas.

There is much scope for future remote sensing applications research on hazards and vulnerability for the city of Mumbai. With over 50% of the city's population living in shanty towns lacking basic infrastructure, future efforts must focus on more detailed analyses of these zones. As was pointed out in this chapter, shanty towns often occupy the city's low lying regions and face the persistent threat of monsoonal flooding. As a start, these areas need more fine scale mapping using high resolution imagery. Likewise, the city's few remaining green spaces require protection from development activities. Intra-urban green space is fundamental to the health of urban ecosystems and must be paid more attention by planning efforts. In the case of Mumbai, fringing coastal wetlands will serve as important natural barriers as the city copes with rising sea levels over the next century. City planners must not only protect remaining coastal marshes, but also engage in active wetland regeneration activities where encroachment has caused losses. Finally, as planning efforts focus on the city, satellite towns must not be inadvertently overlooked, as these are the growth areas of the 21st century. Planning lessons learned for the metropolis should be heeded and transferred as attention shifts to these newer cities.

Remote sensing technology has revolutionized the way we can assess change in land use and land cover over time. Imagery has provided scientists with a data rich environment to examine parts of the world that have heretofore been overlooked. Data scarcity is particularly problematic in the developing world and as a result, until very recently, vulnerability and hazards studies were mostly focused on the developed world. This chapter demonstrates that the use of readily available remotely sensed data coupled with conventional techniques can prove informative. Today, the proliferation of high spatial resolution data makes it possible to engage in analyses at higher levels of detail that enhance our ability to decipher fine-scale patterns and thereby improve policy recommendations. While the costs associated with such data are still high, increased future competition in the private remote sensing sphere and increased demand for such products will undoubtedly reduce prices. The limited number of spectral bands available through commercial enterprises, however, still provides an essential role for Landsat data. Moreover, the recent USGS announcement to make all of its Landsat data archive available free of cost to users, now makes virtually every part of the globe accessible to those with the necessary theoretical and technical skills to contribute to Land Use and Land Cover Change science in general and hazard vulnerability research in particular.

References

Alrababah, M. A. and M. N. Alhamad. (2006). Land use/cover classification of arid and semi-arid Mediterranean landscapes using Landsat ETM. *International Journal of Remote Sensing*, 27(13), 2703–2718.

Al Rawashdeh, S. and B. Saleh. (2006). Satellite Monitoring of urban spatial growth in the Amman area, Jordan. *Journal of Urban Planning and Development*, 132(4), 211–216.

Auch, R., J. Taylor and W. Acevedo. (2004). *Urban Growth in American Cities: Glimpses of US Urbanization*. USGS Circular 1252: US Department of the Interior.

Barrows, H. (1923). Geography as human ecology. *Annals of the Association of American Geographers*, 13, 1–14.

Blaikie, R., T. Cannon, I. Davis and B. Wisner. (1994). *At Risk: Natural Hazards, People's Vulnerability and Disasters*. London: Routledge.

Burton, I., R. W. Kates and G. F. White. (1993). *The Environment as Hazard.* New York: Guilford Press, p. 240.

Cutter, S. L. (1996). Vulnerability to environmental hazards. *Progress in Human Geography*, 20, 529–539.

Cutter, S. L., J. T. Mitchell, and M. S. Scott. (2000). Revealing the vulnerability of people and places: A case study of georgetown county, south carolina. *Annals of the Association of American Geographers*, 90(4), 713–737.

Demographia. (2007). *World Urban Areas*. http://www.demographia.com/db-worldua.pdf Accessed April 24, 2008.

Few, R. (2003). Flooding, vulnerability and coping strategies: local responses to a global threat. *Progress in Development Studies*, 3(1), 43–58.

GLCF (Global Land Cover Facility) (1997). *Data and Products.* http://glcf.umiacs.umd.edu/data/ Accessed November 6, 2007.

Hewitt, K. (1997). *Regions of Risk: A Geographical Introduction to Disasters.* Essex: Longman.

Jensen, R., J. Gatrell and D. McLean (eds.). (2005). *Geo-Spatial Technologies in Urban Environments.* Heidelberg: Springer Verlag.

Ji, C. Y., Q. Liu, D. Sun, S. Wang, P. Lin, and X. Li. (2001). Monitoring urban expansion with remote sensing in China. *International Journal of Remote Sensing*, 22(8), 1441–1455.

Kasperson, J. X., R. E. Kasperson and B. L. Turner II. (1995). *Regions at Risk: Comparisons of Threatened Environments.* Tokyo: United Nations University Press.

Kaya, S. (2007). Multitemporal analysis of rapid urban growth in Istanbul using remotely sensed data. *Environmental Engineering Science*, 24(2), 228–233.

Kwarteng, A. Y. and P. S. Chavez, Jr. (1998). Change detection study of Kuwait City and environs using multi-temporal Landsat Thematic Mapper data. *International Journal of Remote Sensing*, 19(9), 1651–1662.

Leahy, J. (2008). Riches rise from Mumbai slum clearance. *Financial Times*, May 6, 2008.

Lillesand, T. M., R. W. Kiefer, and J. W. Chipman. (2008). *Remote Sensing and Image Interpretation*. 6th edition. New York: Wiley.

Maktav, D., F. S. Erbek, and C. Jurgens. (2005). Remote sensing of urban area. *International Journal of Remote Sensing*, 26(4), 655–659.

Maktav, D. and F. S. Erbek. (2005). Analysis of urban growth using multi-temporal satellite data in Istanbul, Turkey. *International Journal of Remote Sensing*, 26(4), 797–810.

Mehta, S. (2004). *Maximum City: Bombay Lost and Found*. New York: Alfred A. Knopf.

Meehl, G. A., T. F. Stocker, W. D. Collins, P. Fiedlingstein, A. T. Gaye, J. M. Gregory, A. Kitoh, R. Knutti, J. M. Murphy, A. Noda, S. C. B. Raper, I. G. Watterson, A. J. Weaver and Z. C. Zhao. (2007). Global climate projections. In Solomon, S., D. Qin, M. Manning, Z. Chen, M. Marquis, K. B. Averyt, M. Tignor and H. L. Miller (eds.), *Climate Change 2007: The Physical Science Basis. Contribution of Working Group I to the Fourth Assessment Report of the Intergovernmental Panel on Climate Change.* Cambridge University Press, Cambridge, United Kingdom and New York, USA.

Mundia, C. N. and M. Aniya. (2005). Analysis of land use/cover changes and urban expansion of Nairobi city using remote sensing and GIS. *International Journal of Remote Sensing*, 26(13), 2831–2849.

MMRDA (Mumbai Metropolitan Region Development Authority). (1999). *Regional Plan for Mumbai Metropolitan Region, 1996–2011.* http://www.regionalplan-mmrda.org / Accessed May 1, 2008.

MMRDA (Mumbai Metropolitan Region Development Authority). (2003). *Population and Employment Profile of Mumbai Metropolitan Region*. http://www.mmrdamumbai.org/docs/Population%20and%20Employment%20profile%20of%20MMR.pdf Accessed May 1, 2008.

Nicholls, R. (1995). Coastal megacities and climate change. *GeoJournal*, 37(3), 369–379.

Nicholls, R. J., P. P. Wong, V. R. Burkett, J. O. Codignotto, J. E. Hay, R. F. McLean, S. Ragoonaden and C. D. Woodroffe. (2007). Coastal systems and low-lying areas. In M. L. Parry, O. F. Canziani, J. P. Palutikof, P. J. van der Linden and C. E. Hanson (eds.), *Climate Change 2007: Impacts, Adaptation and Vulnerability. Contribution of Working Group II to the Fourth Assessment Report of the Intergovernmental Panel on Climate Change*, Cambridge University Press, Cambridge, United Kingdom and New York, USA.

Rabus, B., M. Eineder, A. Roth, and R. Bamler. (2003). The shuttle radar topography mission – a new class of digital elevation models acquired by spaceborne radar. *ISPRS Journal of Photogrammetry and Remote Sensing*, 57, 241–262.

Ray-Bennett, N. S. (2007). Environmental disasters and disastrous policies: An overview from India. *Social Policy and Administration*, 41(4), 419–424.

SRTM (Shuttle Radar Topography Mission). (2006). *Shuttle Radar Topography Mission – Finished.* http://edc.usgs.gov/products/elevation/srtmbil.html Accessed November 22, 2007.

Smith, K. (1992). *Environmental Hazards: Assessing Risk and Reducing Disaster*. London: Routledge, p. 324.

TERI (Tata Energy Research Institute). (1996). *The Economic Impact of a One Meter Sea Level Rise on the Indian Coastline: Method and Case Studies.* Report submitted to the Ford Foundation.

TIFR (Tata Institute for Fundamental Research). (1999a). *The History of Mumbai.* http://theory.tifr.res.in/bombay/history /Accessed May 4, 2008.

TIFR (Tata Institute for Fundamental Research). (1999b). *The Geography of Mumbai.* http://theory.tifr.res.in/bombay/physical /Accessed May 4, 2008.

TNN (Times News Network). (2005a). Mumbai is down under. *The Times of India*, Thursday July 28, 2005, p. 1.

TNN (Times News Network). (2005b). Could technology have stemmed the tide of Mumbai's misery? *The Times of India*, Thursday July 28, 2005, p. 6.

TNN (Times News Network). (2005c). Where's the government? Public rage against administration spills onto streets. *The Times of India*, Sunday July 31, 2005, p. 1.

TNN (Times News Network). (2005d). Island city, for real. *The Times of India*, Thursday July 28, 2005, p. 6.

United Nations, Population Division, Department of Economic and Social Affairs. (2006). *World Urbanization Prospects: The 2005 Revision*. CD-ROM Edition data in digital form POP/DB/WUP/Rev.2005. http://www.un.org/esa/population/publications/WUP2005/2005wup.htm Accessed April 24, 2008.

USGS EROS (United States Geological Survey – Earth Resources Observation Science). (2006). *Satellite Products*. http://eros.usgs.gov/products/satellite.html Accessed February 4, 2007.

Weber, C., C. Petropoulou and J. Hirsch. (2005). Urban development in the Athens metropolitan area using remote sensing data with supervised analysis and GIS. *International Journal of Remote Sensing*, 26(4), 785–796.

White, G. F. (1964). *Choice of Adjustment to Floods*. Department of Geography Research Paper No. 93. Chicago: University of Chicago Press, p. 149.

Wilbanks, T. J., J. T. Ensminger, and C. K. Rajan (2007). Climate change vulnerabilities and responses in a developing country city: Lessons from Cochin, India. *Environment*, 49(5), 22–33.

Zhang, Q., J. Wang, X. Peng, P. Gong, and P. Shi. (2002). Urban built-up land change detection with road density and spectral information from multi-temporal Landsat TM data. *International Journal of Remote Sensing*, 23(15), 3057–3078.

Zerah, M.-H. (2007). Conflict between green space preservation and housing needs: The case of the Sanjay Gandhi National Park in Mumbai. *Cities*, 24(2), 122–132.

Chapter 4
A GIS for Flood Risk Management in Flanders

Pieter Deckers, Wim Kellens, Johan Reyns, Wouter Vanneuville, and Philippe De Maeyer

Abstract In the past decades, Flanders, a region of north Belgium that extends from the coastline inland (in northwest Europe), has suffered several serious riverine floods that caused substantial property damage. As Flanders is one of the most densely populated regions in the world, a solid water management policy is needed in order to mitigate the effects of this type of calamity. In the past, Flemish water managers chose to drain off river water as quickly as possible by heightening the dikes along the rivers. However, this method leads to a higher flood probability further downstream. Moreover, water defence infrastructure can always suffer from technical failures (e.g., breaching) creating even more damage than would have occurred if no defences were in place. In a search for a better solution to this recurring problem, the Flemish administration proposed a new approach in the 1990s. This approach focuses on minimizing the consequences of flooding instead of attempting to prevent floods. To implement this approach, large amounts of data were gathered for the Flemish Region. Using a Geographic Information System (GIS), a risk-based methodology was created to quantitatively assess flood risk based on hydrologic models, land use information and socio-economic data. Recently, this methodology was implemented in a specifically designed GIS-based flood risk assessment tool called *LATIS*. By estimating the potential damage and number of casualties during a flood event, *LATIS* offers the possibility to perform risk analysis quickly and effectively. This chapter presents a concise overview of *LATIS*' methodology and its implementation for flood risk management in Flanders.

Keywords Floods · Damage · Risk · Flanders · GIS · Modeling

P. Deckers (✉)
Department of Geography, Faculty of Sciences, Ghent University,
Krijgslaan 281, 9000 Gent, Belgium
e-mail: pieter.deckers@ugent.be

P.S. Showalter, Y. Lu (eds.), *Geospatial Techniques in Urban Hazard and Disaster Analysis*, Geotechnologies and the Environment 2, DOI 10.1007/978-90-481-2238-7_4,

4.1 Introduction

Flanders is located in the centre of northwest Europe, in the low-lying northern part of Belgium, bordering the North Sea (Fig. 4.1). The region is characterised by a number of river valleys with moderate slopes and minor elevation differences. During heavy torrents or long-lasting rainy weather, parts of Flanders are regularly flooded due to overflow (and in rare occasions by breaching) of river dikes. For example, the Dender catchment (the dark grey region west of Brussels indicated by the "D" in Fig. 4.1) suffered heavy floods in 1995, 1999 and 2002–2003.

As Flanders is one of the most densely populated and industrialised regions in the world, adequate flood risk management is necessary. In the past, the solution of the Flemish administration to the flood problem was to drain the water downstream as quickly as possible by heightening the dikes along the river banks. However, experience showed that this was far from an ideal solution. It has become clear that this method leads to higher water levels and a higher flood risk downstream. Moreover, water defence infrastructure can collapse due to technical failure such as breaching, often creating more damage than would have occurred if no flood defence infrastructure had existed.

The Flemish minister responsible for addressing these types of issues launched a new approach in the governmental note, "Mobility and Public Works 2000−2004" (Vanneuville et al. 2003). The new idea was a paradigm shift away from attempting to protect against high water levels to reducing damages caused by the water. This

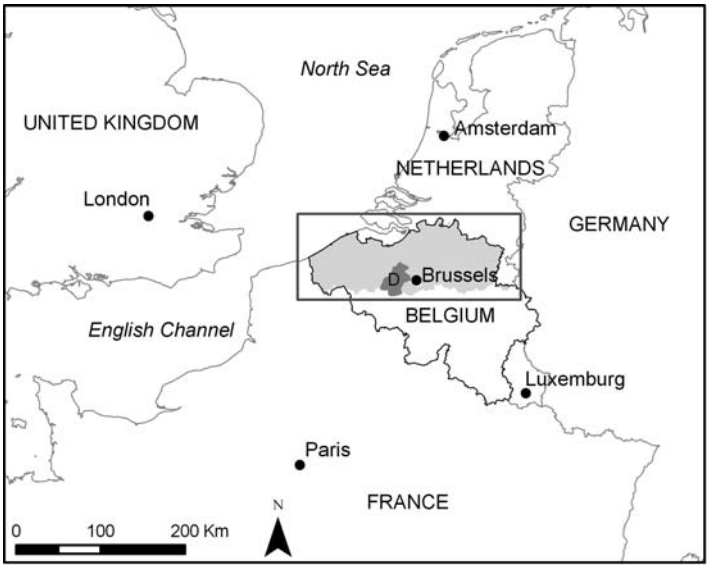

Fig. 4.1 Situation of the region of Flanders (the *gray* region in the *rectangle*) in northwest Europe Source: Vector versie van het "Voorlopig Referentiebestand Gemeentegrenzen", AGIV, toestand 22/05/2003 (GIS-Vlaanderen) and – Vectoriële versie van de "VHA-waterlopen and –zones", Vlaamse Milieumaatschappij – Afdeling Operationeel Waterbeheer (AGIV)

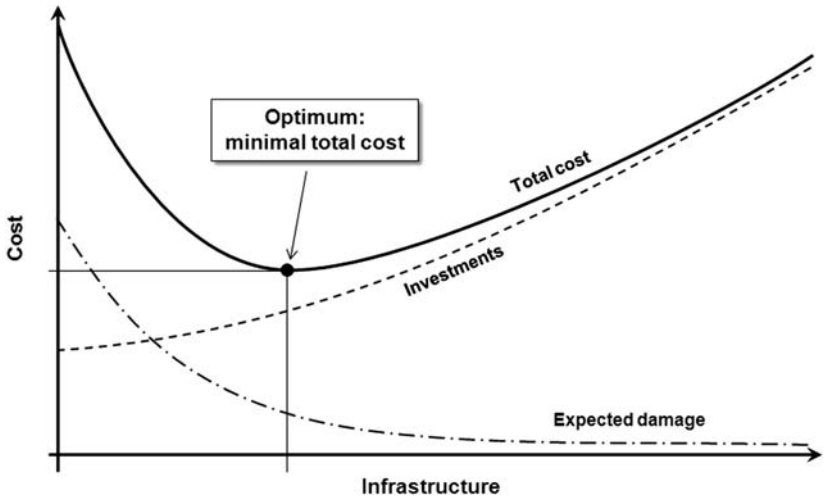

Fig. 4.2 Economic optimum in a cost benefit analysis for water infrastructure

shift created the need to identify the level of investment represented on the landscape (e.g., buildings, infrastructure) and the cost of repairing those investments following a flood. Figure 4.2 provides a graph of this cost benefit analysis, where a point has been placed on the "Total cost" to illustrate the "Optimum minimal total cost". The lower the investment in flood defence infrastructure, the higher the expected costs for damage. As investments in infrastructure increase, expected damage decreases as does the total cost. At a certain point, higher investments no longer lead to major decreases in expected damages and the total cost begins to increase again. At this point, the total cost of investments and expected damage is minimal (De Nocker et al. 2004).

In agricultural areas, the impacts of floods are limited due to low population density, fewer buildings, and reduced amounts of infrastructure. In other areas (e.g., nature conservation zones), flooding can even have positive effects. The opposite is true in densely populated areas or in areas with important industrial activities. In these areas, extra effort and investment must be made to try to reduce the effects of flooding, such as delineating controlled inundation areas to provide short term storage for large volumes of water. In order to estimate and compare the benefits from each of different types of measures, a uniform risk analysis approach is necessary. In this context, several objectives were set by policy makers in the governmental note described earlier (Vanneuville et al. 2003):

- The development of a methodology for the uniform calculation of damage and risk for the whole of Flanders;
- Use of this methodology to calculate change in flood risk and damage due to change in local infrastructure works and/or land use; and,
- A definition of data and software necessary for running the equations in a geographic information technology (GIT) environment.

To meet these goals, Flanders Hydraulics Research,[1] in cooperation with the Department of Geography at Ghent University, developed a risk-based methodology to assess potential flood damage. This chapter describes how the risk-based methodology was implemented via the assessment tool *LATIS*, providing an overview of the input data, chosen assumptions, and different calculations performed. The methodological framework is provided, as well as how flow velocity was modeled as a damage factor and how flood casualties are calculated. Because there is a need for more effective and adaptable tools, *LATIS* is offered as a substitute for earlier GIS-based models. The capability of using *LATIS* to calculate flood risk scenarios with regard to climate change is also demonstrated. The chapter concludes by discussing methodological issues and future research.

4.2 Overview of the Risk-Based Methodology

Generally, risk is defined by the probability of an event (e.g., a flood) and the magnitude of its consequences (Jacobs and Worthley 1999). These consequences can be measured in terms such as buildings damaged or lives lost (Ahola et al. 2007). Although some researchers have added additional criteria to the definition of risk, flood risk studies in European countries are usually performed using the combination of probability and consequences (Verwaest et al. 2008). The methodology described in this chapter follows this general definition.

Several steps are required to calculate damage and risk (Vanneuville et al. 2005), as is shown in Fig. 4.3. The first step requires the generation of a set of flood maps, each representing the extent of a flood with a certain return period, using hydrological, hydraulic, and digital elevation models. Second, different land use maps are combined with a variety of socio-economic data resulting in a maximum damage map. This maximum damage map is subsequently combined with the different flood maps to create damage maps for each return period. In the final phase, these damage maps are combined into a single risk map.

4.2.1 Flood Map Calculations

Before calculating damage and risk, it is necessary to estimate an area's flooding probability through statistical analysis of past water levels and flow rates. First, the return period, or average period of time in which a particular maximum water level and discharge may occur, is calculated. Higher water levels and discharge volumes correspond to longer return periods of occurrence. Calculating probability of occurrence is performed using composite hydrographs, which are synthetic hydrographs integrated from Quantity/Duration/Frequency (QDF)-relationships. These

[1] Flanders Hydraulics Research is part of the Department of Mobility and Public Works of the Flemish Government and is responsible for the navigable waterways in Flanders.

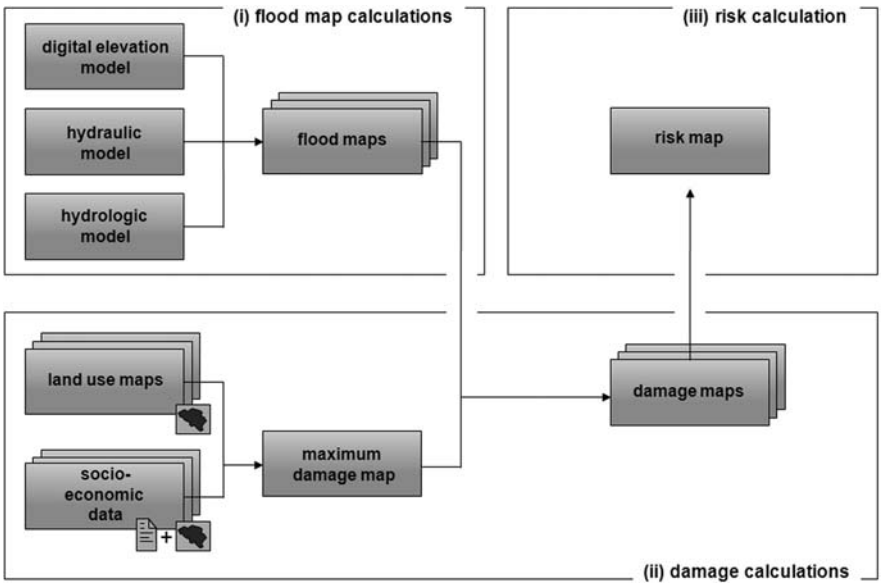

Fig. 4.3 Framework for risk mapping (to be read counterclockwise, starting at *upper left*)

QDF-relationships statistically link every river discharge with its duration and return period. Composite hydrographs have the advantage that in every point along the waterway (and in the flood zones) the calculated water levels have the same return period. Only one calculation is required for every return period, resulting in more rapid risk calculation models (Vaes et al. 2002).

As stated above, flood maps are created using hydrological, hydraulic, and digital elevation models. These maps show maximum water levels and flooding extent. Additional information such as flow velocity and the "rise velocity" of water (especially important for casualty assessment) can also be obtained. Thus for each return period, a set of maps is available indicating flood extent, flow velocity and rise velocity. Since creating and validating composite hydrographs is time-consuming, only a discrete set of flood maps was created (e.g., 1, 2, 5, 10, 25, 50, 100, 250 years for the Dender catchment). If more historical data are available, flood maps for even longer return periods can be calculated.

4.2.2 Damage Calculations

In this step, land use information and socio-economic data are used to produce a maximum damage map. This maximum damage map contains the potential damage value per surface area, where maximal damage can occur from a hazardous event. Put differently, this map indicates the cost value for a virtual scenario in which everything is destroyed by a (flood) event. By combining the maximum damage map with the flood maps, expected damage for a given inundation can be calculated.

4.2.2.1 Different Types of Damage

Numerous definitions of damage can be found in the disaster literature (e.g., Cochrane 2004). However, a number of distinctions are common with regard to flooding (De Maeyer et al. 2003). Financially, damage can be split into monetary (tangible) and non-monetary (intangible – including emotional) damage. A second classification can be made between internal and external damage. Internal damage is damage caused in the inundated zone itself, external damage occurs outside the inundated area. An example of the latter is production loss due to economic dependence on customers and/or suppliers located in the flooded area. A third classification is between direct and indirect damage. The first refers to damage affecting buildings, furniture, stocks, crops, and the like while the second refers to production losses and clean-up costs.

The risk methodology used here only considers monetary, internal, and direct/indirect damage. Although several authors have performed flood risk assessment including non-monetary (Yates 1992; Lekuthai and Vongvisessomjai 2001; Simonovic and Carson 2003) and external damage (Penning-Rowsell et al. 2003; Van der Veen and Logtmeijer 2005), these criteria were beyond the scope of this study.

4.2.2.2 Maximum Damage Map

Different land use categories have different potential maximum damage values. Damage values for completely destroyed cropland are less when compared to the total destruction of a factory. Therefore, land use information is needed to create a maximum damage map. Two major resources were used to create an overall land use map of Flanders: CORINE Land Cover (a classified land use map that covers all European member states) and the Small Scale Land Use map of Flanders and Brussels.[2] The combination of these data makes it possible to classify land use into different categories such as built-up areas, industrial grounds, crop lands, pastures, transport infrastructure and airports (Vanneuville et al. 2003). Both CORINE Land Cover and the Small Scale Land Use Map are based on LANDSAT images with a resolution of 30 m per pixel. As this resolution was insufficient to fulfill all needs, vector-based land use information such as road and railroad networks, and locations of highly valued buildings (e.g., hospitals, fire stations, schools, churches, electricity and communication infrastructure) was added to the database.

Once land use information is available, the maximum damage values have to be linked to the land use categories. To perform this task, socio-economic data is gathered. As it is difficult[3] to incorporate the individual value of each household, factory

[2]Both land use maps are included for two reasons: (i) the combination provides additional land use information unavailable when using only one data source, and (ii) each data set has a different renewal period, so the most recent land use map can be used when required.

[3]Insurance companies possess information on the monetary value of individual households, but are generally unwilling to disclose such private information. For croplands, another problem arises

or cropland, aggregated spatial data was used (e.g., mean housing value per statistical area, average value of crops per agricultural area, average value of factories per industrial sector). This approach causes every house in a particular statistical area to have the identical maximum damage value, but homes in residential areas will have higher values than those found in areas that are economically disadvantaged. Similarly, croplands in agricultural areas where fruits and vegetables are most important will carry a higher maximum damage value than croplands in agricultural areas where potatoes and cereals are more common. Data was gathered and grouped for each land use category (for a detailed description, see Vanneuville et al. 2003). After combining the land use map with the damage values, a maximum damage map can be produced.

4.2.2.3 Calculating Damage Maps

The next step combines the maximum damage map with the different flood maps to create maps of real flood damage suffered during each return period. Floods rarely lead to total destruction. The extent of damage depends on water depth because all land use categories have different relationships between the amount of damage that occurs and water depth. These relationships are defined by damage functions or α-factors (Penning-Rowsell et al. 2003). To illustrate, five different damage functions are shown in Fig. 4.4. The quantitative relationship reflected in these functions

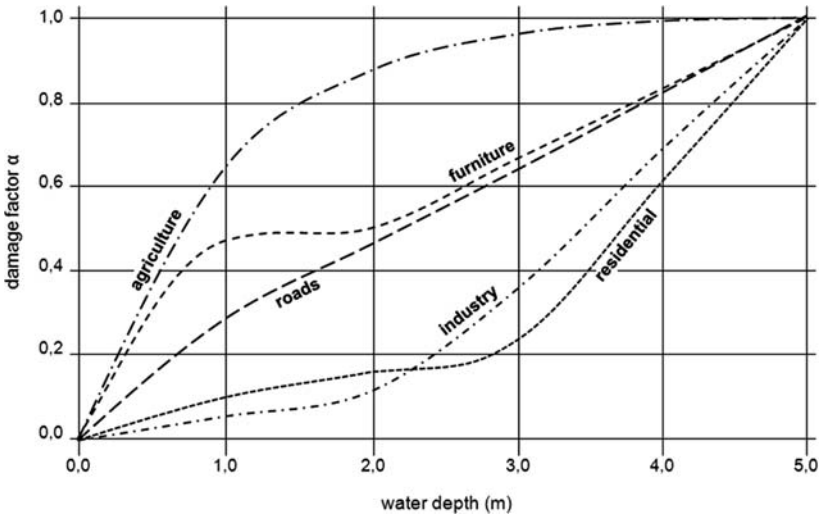

Fig. 4.4 Damage functions: real damage as a function of water depth

because of regular shifts in cultivation. For example, one year potatoes may be cultivated and the next corn; the gathering of such information is very intensive, time-consuming and sometimes impossible (due to privacy reasons).

are based on Van de Sande and Corné (2001) and Vanneuville et al. (2003). Each damage function represents a relationship between a given water depth (X-axis) and the dependent damage factor (Y-axis) that can be expected for that land use category. For example, a water depth of 3 m equals a damage factor of approximately 0.36 (36%) for industry. The same water depth causes nearly 100% damage to agriculture. The odd shape of the furniture curve is caused by the assumption that all homes and offices have a "ground floor" containing furniture and the slightest amount of water depth can cause substantial damage. A water depth of 2 m or higher corresponds to an increasing damage factor caused by the appearance of furniture installed on higher floors of a building.

Another important concept in our approach is the "doorstep level" (Vanneuville et al. 2003), or the height above ground level that defines the "zero" level for damage. For industry and housing the "doorstep level" is a physical reality; the concept is based on calibration methods performed in the Netherlands, by which people were asked to indicate the water height above their doorsteps (Vrisou Van Eck et al. 1999). Water levels were conservatively grouped into 25 cm increments, with all water levels in the flood map rounded to the next multiple of 25 cm. Below the "doorstep level", damage is set to zero. For housing, the doorstep level is 25 cm, whereas for roads and industry the doorstep is 50 cm (for roads, the assumption is that low water heights do not cause any damage in the short term). For all other classes of land use, the doorstep level is 0 cm, meaning that damage occurs the moment there is water.

In a flood zone the real damage caused by inundation at a certain water height can be calculated by summing all unique surface entities (i.e., discrete land use categories) and combining the water depth (translated to the corresponding α-factor, the parameter that is represented in Fig. 4.4) with the maximum damage of that land use category. Mathematically, this is described as:

$$S_w = \sum_{landusei} \alpha_i \times S_{i,\max} \tag{4.1}$$

Where

S_w : real damage in a zone
$S_{i,max}$: maximal damage in a land use class *i*
α_i : coefficient expressing the relationship between water depth and damage for land use class *i*

4.2.3 Risk Calculation

In the final step, the different damage maps for each return period are combined into one risk map. As stated above, risk is defined as the probability of a certain event multiplied by the damage caused by that event. The risk (expressed as the mean annual damage per surface unit per year) is then equal to the damage caused by

an event with a 1-year return period, plus half of the damage difference between a 2-year flood and a 1-year flood, plus one-third of the damage difference between a 3-year flood and a 2-year flood, and so forth. The mathematical explanation of this procedure is explained in Equations 4.2 and 4.3:

$$R = \sum_{i=1}^{n} \frac{1}{i}(S_i - S_{i-1}) \tag{4.2}$$

Or

$$R = \frac{1}{1}S_1 + \frac{1}{2}(S_2 - S_1) + \frac{1}{3}(S_3 - S_2) + ... + \frac{1}{n}(S_n - S_{n-1}) \tag{4.3}$$

Where

R risk
S_i the damages related to a flood with a return period of i years
n the highest return period

As explained above, the creation and validation of flood maps is time-consuming, so only a few have been created. To calculate risk in practice, it is assumed that linear interpolation of the flood damage between two return periods is valid, so the formula (in the case of return periods of 1, 2, 5, 10, 25, 50 and 100 years) can be simplified to (Vanneuville et al. 2003):

$$R = \frac{1}{1}S_1 + \frac{1}{2}(S_2 - S_1) + \frac{\frac{1}{3} + \frac{1}{4} + \frac{1}{5}}{5 - 2}(S_5 - S_2) + \frac{\frac{1}{6} + \frac{1}{7} + \frac{1}{8} + \frac{1}{9} + \frac{1}{10}}{10 - 5}(S_{10} - S_5) + ... \tag{4.4}$$

Equation 4.4 can be further simplified to:

$$\begin{aligned} R = {} & 0.5 \times S_1 + 0.2389 \times S_2 + 0.132 \times S_5 + 0.07 \times S_{10} + 0.0318 \\ & \times S_{25} + 0.0135 \times S_{50} + 0.0138 \times S_{100} \end{aligned} \tag{4.5}$$

4.3 Flow Velocity

Until recently, damage and risk calculations were performed only for flood events caused by the overflow of dikes, restricting the main cause of damage to water depth. However, overflow is not the only failure mechanism. Technical failures caused by dike/dune breaching may inflict damage to built-up areas that is much greater than that caused by overflow. In the vicinity of a breach, high flow velocities can even cause total collapse of buildings (Jonkman et al. 2008). Therefore, the potential for flow velocity damage needs to be incorporated into damage calculations based purely on depth. This additional damage cannot be greater than the difference

between maximum damage and damage caused by water depth. Based on Vrisou Van Eck et al. (1999), new damage functions were developed combining levels of water depth with flow velocity (Verwaest et al. 2008).

In cases of breaching, flow velocity at a certain location is a function of three parameters: (i) distance to the breach, (ii) bottom shear, and (iii) the presence of obstacles in the inundated area (e.g., a road above ground level). The approach differs depending on whether a 1-D or 2-D hydraulic model is available.

In cases where hydrodynamic boundary conditions are known only from a 1-D model, no detailed information on depth or velocity in the inundated area is available. This limitation necessitates a conceptual approach (Kellens and Vanneuville 2007), which is schematically depicted in Fig. 4.5 and which represents a dike breach along a river. Around the breach, three concentric zones (A, B, C) are defined according to expected amounts of property damage. In Zone A, closest to

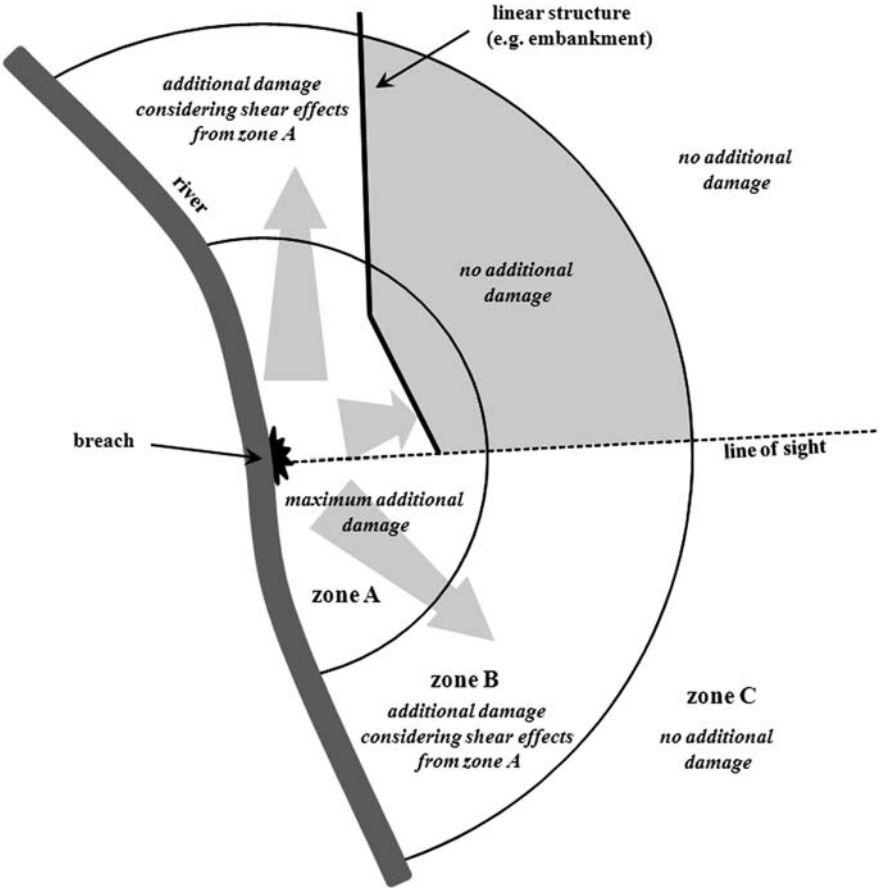

Fig. 4.5 Summary of the conceptual approach (Kellens and Vanneuville, 2007)

the breach, maximum additional loss is expected. Traveling away from the breach, flow velocities and damage decline because of shear and directional spreading of the water. The influence of shear depends on the land use in Zone A, as the water has to travel through this zone before it reaches Zone B; the influence of land use on flow resistance is based on Maijala (2001). The radii of Zones A and B are a function of the maximum discharge through the breach. The influence of barriers is also included; based on available vector data, possible obstructions for the traveling water are identified within the inundated area. Behind embankments no additional damage is expected provided there are no culverts or under-passes. The zone of influence of these barriers is determined by a line-of-sight analysis. Zone C sustains no additional damage.

In cases where water levels and velocity output are available from 2-D hydrodynamic models, Vrisou Van Eck et al. (1999) proposed combining flow velocity and water depth to determine maximum additional damage to construction due to breaching. Those authors considered a velocity of 3 m/s and a water depth of at least 0.5 m as necessary thresholds for buildings to collapse. For combinations of velocity and water depths lower than these values, continuous functions were constructed. The shape of the functions reflects the nature of the damage sustained: at low values for both parameters, losses are expected to be small. If either flow velocity or water depth increases, damage will increase dramatically until maximum additional losses occur.

4.4 Casualties

Besides material damage, floods cause human casualties due to the instability of people in rapidly flowing water and from building collapse (Jonkman et al. 2008). Although some have attempted to place a monetary value on human life (Card and Mooney 1977; Breyer and Felder 2005), a similar undertaking was not part of this study. Ramsbottom et al. (2003) and Jonkman and Vrijling (2008) denote the importance of water depth, rise velocity and flow velocity with regard to calculating loss of life caused by floods. The combination of great water depths and the rapid rise of water creates hazardous situations. People have limited time to reach higher floors or shelters and they may be trapped inside buildings. Consequently, the number of victims is calculated as the number of inhabitants multiplied by two proportionality factors, one for water depth and a second for rise velocity. Based on the findings of Jonkman et al. (2008), the model assumes 100% casualties if the water depth is higher than 6 m or if the rise velocity exceeds 3 m/h. For values lower than these thresholds, casualty functions were taken from Vrisou Van Eck et al. (1999).

An additional factor was added in the case of coastal inundations, where wave overtopping of coastal defense structures can create a substantial number of victims. Based on the work of Verhaeghe (2002) and Allsop (2005), an overtopping discharge of 0.095 l/m/s was set as the threshold value above which the maximum of casualties can be expected.

4.5 Implementation of the Methodology in a GIS

4.5.1 Early GIS-Model

The development of the risk-based methodology described above is insufficient, of itself, to perform risk analysis. The method needs to be translated into a useful model that executes all necessary steps in a pre-programmed chain of actions. Starting with land use maps and flood maps, all steps to create risk maps are separated into submodels based on a raster GIS approach. To determine whether to use raster or vector GIS, a preliminary study was performed (Vanneuville et al. 2003). While the tests did not produce large differences in precision nor accuracy, calculation times in raster GIS occur much more quickly than in vector GIS; 90% of the over 400 computations were more optimally performed in a raster-based GIS (Burrough and McDonnel 1998). One disadvantage of raster-based GIS is that the required storage capacities are much higher than for vector data; however, this is regarded as a minor issue (Eastman 2006).

The model was initially implemented in IDRISI® software (developed by Clark Labs, Clark University, Massachusetts) for raster GIS calculations. All operations were implemented using the software's model builder, which enables implementation of the different steps (as outlined above) within different submodels to reduce complexity. Unfortunately, the design of the software did not produce satisfactory results. As one example, it was necessary to perform time-consuming preprocessing of all necessary input layers and an intensive start-up procedure for each risk computation. The intensive start-up procedure made it difficult for other users in the organization who are unfamiliar with the methodology or IDRISI, to independently compute damage and risk maps.

Although the IDRISI model had possibilities (optimal computing capacities and built-in standard modules), its disadvantages led to the development of *LATIS*. *LATIS* is a GIS application that guides the user through each step of the different damage and risk calculations with a user-friendly interface.

4.5.2 Development of a Flood Risk Assessment Tool: LATIS

In 2007, Flanders Hydraulics Research, in cooperation with the Department of Geography at Ghent University developed a GIS tool named *LATIS* as a substitute for the model structure described above. One of the main prerequisites for the development of the tool was a user-friendly and easy accessible Graphical User Interface (GUI). Therefore, the GUI of *LATIS* (the "Client Application" in Fig. 4.6) is built in the C#.NET programming language. The interface of *LATIS* is a simple windows application, hiding the complexity of professional GIS software. The algorithms of the methodology are also implemented in C#.NET, but for the execution of the geospatial operations, *LATIS* still uses the optimal computing capacity and built-in standard modules (which perform the geospatial operations) of IDRISI. The .NET technology enables the use and execution (in the background)

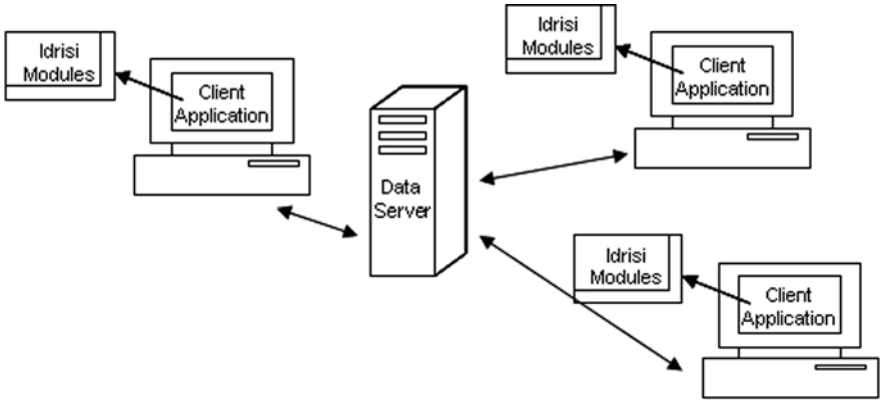

Fig. 4.6 Overview of the *LATIS* structure

of those IDRISI modules (Fig. 4.6, where the single-headed arrows represent the relationships between the client applications and the IDRISI modules), which are stand-alone executable files. The tool performs all necessary actions with the corresponding parameters in the background of the application so the user only has to input data that affect the risk calculations (i.e., the flood and land use maps and the socio-economic data).[4]

LATIS was also designed to address data management by developing a system that allows administrators to easily manage basic land use maps and socio-economic data. These maps and data are uniformly gathered for the extent of Flanders and are centrally managed on a data server. The manipulation of these base data is possible via the *LATIS* application of an administrator (shown in Fig. 4.6 by the arrows in the direction of the data server). When a user runs a damage and risk assessment, the application selects and extracts the necessary data (the standard is to select the most recent data) for the extent of a certain flooding scenario from the data server (shown in Fig. 4.6 by the arrows in the direction of the applications). Consequently, the application performs the preprocessing of land use and socio-economic data and the user only has to input the flood maps. The data management system also records what data is used in an assessment so a specific risk calculation can easily be repeated. Development of *LATIS* now allows damage and risk maps in Flanders to be calculated in an efficient, uniform, and reproducible manner.

4.6 LATIS in Action: Impact of Climate Change on Risk

The calculation of climate change scenarios in Flanders is one of the first projects for which the *LATIS* tool has been used. These climate change scenarios are based on regional climate models for different levels of CO_2 emissions. Based on potential

[4] *LATIS* is not an acronym – it is the Celtic goddess of water (and beer).

change in rainfall and evaporation rates, a high, mean and low scenario was defined for the summer and winter period in Flanders. In general, the potential for drought is expected to increase during the summer, while changes that may occur during the winter are highly uncertain (represented by a strong increase in flooding in the high scenario to a slight decrease in flooding in the low scenario).

The runs of the hydraulic model were executed based on the climate change scenarios and the available measurement series for water level, discharge and evaporation in order to derive catchment flood maps with different return periods. Both flood extent and water depth were used as the main factors influencing damage. Flood maps were used to recalculate damage and risk maps with the most recent socio-economic data available. These maps were used as references and compared with the flood risk maps produced under the climate change scenarios. For all four scenarios (current, low, mean and high), the flood risk is based on the same series of return periods as are used for flood map calculations (1, 50, 100 and 500 years).

A relatively small increase or decrease in water level can cause large differences in damage and risk. Vulnerable sites that are flooded once a century (on average) can be flooded more frequently, causing the risk to increase significantly. On the other hand, a large increase in water depth on agricultural land does not lead to a large increase in damage and risk because once crops are rotten, water depth is no longer important.

Economic damages are generally calculated for such features as housing, industry, and agricultural land. However, special attention is given to local features that are: (1) sensitive to extreme high damage values (e.g., power supply installations, museums), (2) important in case of an emergency (e.g., fire brigades, police stations) and (3) problematic due to evacuation reasons (e.g., hospitals, retirement homes).

Interpretation of the results of the damage and risk maps from the climate change scenarios is done (as for all flood risk assessments) in a relative manner. Because many generalizations are incorporated into the model, the risk values are not used as absolute stand-alone values – risk values of one scenario have to be compared with the risk values of other scenarios. Consequently, risk values between the scenarios are not compared on a pixel by pixel basis. Instead, the individual risk values in zones are grouped in order to evaluate scenarios. In the example of the Dender catchment (Table 4.1) the values are summarized in eight zones between two successive sluices and locks (Fig. 4.7).

As Table 4.1 indicates, the high scenario lead to a serious increase in monetary risk for the Dender catchment. In the master plan for this catchment – for which studies are already on-going – the location and dimensioning of the sluices will be evaluated and adapted. The proposed measures also have to be sustainable under conditions of climate change, so that the evaluated scenarios can be reused.

Figures 4.8 and 4.9 illustrate risk maps for part of the Dender catchment (the area covered by the rectangle in Fig. 4.7) representing the low (Fig. 4.8) and high (Fig. 4.9) climate change scenarios. These figures show a much larger spatial extent for risk in the high than the low scenario. For example, the factory at the south of the image is nearly 100% flooded in the high scenario compared to the low.

Table 4.1 Risk calculation for different climate change scenarios, Dender catchment (1000 euro/year)

Zone	Present	Low	Mean	High
1	806	148	445	1558
2	441	89	337	793
3	186	63	278	543
4	759	115	944	2426
5	257	126	320	1835
6	10	0	2	45
7	45	5086	5754	5933
8	720	276	374	423
Sum	3224	5902	8455	13,556

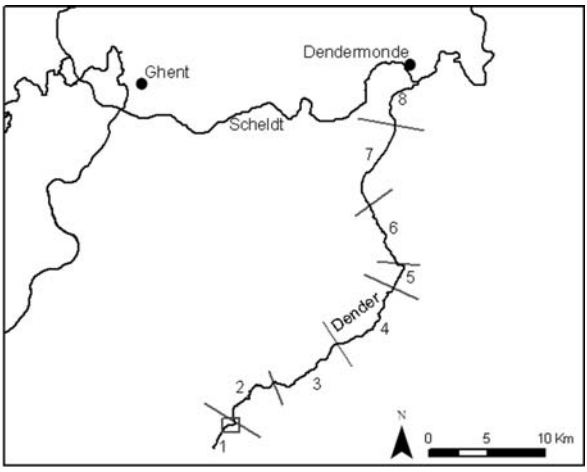

Fig. 4.7 Overview of the different zones in the Dender catchment (the *small rectangle* at the bottom of the figure indicates the location of the area shown in Figs. 4.8 and 4.9)
Source: Vectoriële versie van de "VHA-waterlopen & -zones", Vlaamse Milieumaatschappij – Afdeling Operationeel Waterbeheer (AGIV)

4.7 Conclusions and Further Developments

LATIS, a GIS application for assessing flood risk in Flanders, Belgium has been described, including an overview of the underlying risk methodology, which incorporates hydrologic and hydraulic models, land use information and socio-economic data. Presently, *LATIS* is being used as part of social cost-benefit analyses for estimating the effects of flood mitigation measures. These analyses are being performed in support of several riverine and coastal management plans, including studies on the widening and deepening of waterways, the construction of controlled flood zones, and proposed improvements in the coastal defense infrastructure. These plans not

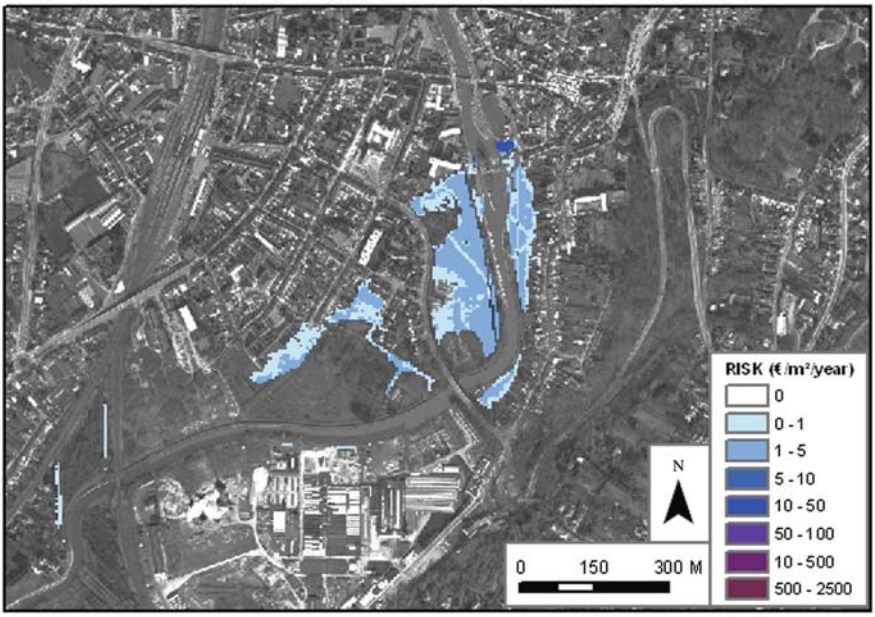

Fig. 4.8 Flood risk under the low climate change scenario in part of the Dender catchment Source of background map: Digitale versie van Orthofoto's, middenschalig, kleur, provincie Oost-Vlaanderen, AGIV en Provincie Oost-Vlaanderen, opname 2006 [GIS-Vlaanderen]

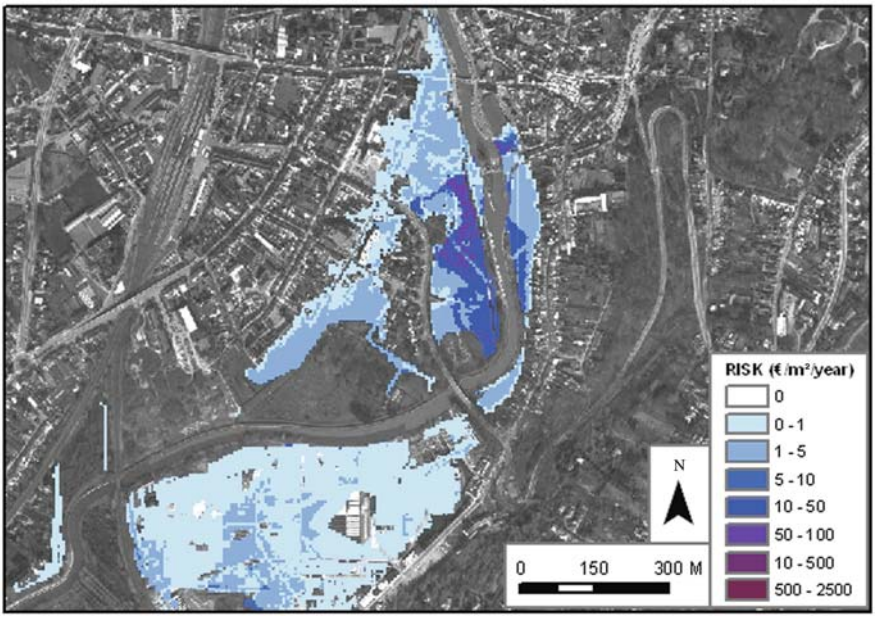

Fig. 4.9 Flood risk under the high climate change scenario in part of the Dender catchment Source of background map: Digitale versie van Orthofoto's, middenschalig, kleur, provincie Oost-Vlaanderen, AGIV en Provincie Oost-Vlaanderen, opname 2006 (GIS-Vlaanderen)

only seek to protect against current flood risk conditions but also to incorporate adjustments to deal with possible climate changes.

Currently, *LATIS* is limited to only four types of damage: monetary, internal, and direct/indirect. Future improvements to the methodology could include adding external and non-monetary damage to the model.

The model could be further improved with the use of more detailed base data. The main reason the current methodology uses aggregated data is pragmatic: data gathering is a time-consuming and costly job and processing time becomes longer with more detailed data. Therefore, the decision was made to work with generalized spatial data and to proceed gradually to more detailed data when more time and resources become available. This future work is important because estimating the number of people who could be afflicted directly impacts evacuation needs. Fortunately, although Flanders' flood plains are densely populated, it boasts a dense road network that is expected to support substantial evacuation numbers in the event of a calamity.

While flow velocity and the calculation of casualties due to floods were attempted, certain assumptions and simplifications were necessary for the present study. However, as these knowledge gaps are filled, more robust results could be produced. *LATIS* has proven its usefulness for calculating flood risk scenarios in Flanders. However, the real challenge lies in the near future, when European standards have to be met with respect to flood risk management. In 2007, the European Union released its European Flood Directive (2007/60/EC). In the next few years, all European member states have to comply with the demands described in that directive, most of which involve creating an inventory of objects in flood zones. Concurrent with that effort, potential flood damage and its likelihood will be evaluated, and necessary modifications made to improve the model. This on-going work will continue to strengthen *LATIS'* ability to function as an efficient data integration and data management system combined with a user friendly interface to improve flood risk management.

Acknowledgments The authors wish to acknowledge the financial support by the Flemish Government under contract WL16EB/06/07.

References

Ahola, T., Virrantaus, K., Krisp, J. M., Hunter, G. J. (2007). A spatio-temporal population model to support risk assessment and damage analysis for decision-making. *International Journal of Geographical Information Science*, 21(8), 935–953.

Allsop, N.W.H. (2005). D38: *Report on Hazard Analysis*. Report CLASH WP6, Coordinator HR Wallingford, 28p.

Breyer, F., Felder, S. (2005). *Mortality Risk and the Value of a Statistical Life: The Dead-Anyway Effect Revis(it)ed.* Geneva Risk and Insurance Review, 30(1), 41–55.

Burrough, P.A., McDonnel R.A. (1998). *Principles of Geographical Information Systems*, Oxford University Press, Oxford, p. 333.

Card W.I., Mooney G.H. (1977). What is the monetary value of a human life? *British Medical Journal*, 2, 1627–1629.

Cochrane, H.C. (2004). Indirect losses from natural disasters: measurement and myth. In: Okuyama, Y., Chang, S.E. (Eds.), *Modelling Spatial and Economic Impacts of Disasters*. Springer-Verlag, Berlin Heidelberg New York.

De Maeyer Ph., Vanneuville W., Maeghe K., Mostaert F. (2003). *Modélisation des effets de crue dans le bassin de la Dendre, basée sur une méthodologie de risqué* (Modelling the Effects of Flooding in the Dender Catchment based on a Risk Methodology), Le Geo Evenement, 4–6 march 2003, Paris, Actes des conférences sur Cd-rom, p. 7.

De Nocker, L., Broekx, S., Liekens, I. (2004). *Social Cost Benefit Analysis on Safety against Flooding in the River Scheldt Estuary – Conclusions on the Outlines*. VITO in cooperation with RA-IMDC, s.l., 92pp.

Eastman J.R. (2006). *Idrisi Andes, Guide to GIS and Image Processing*, Clark Labs – Clark University, Worchester, USA.

European Flood Directive. (2007). Directive 2007/60/EC of the European Parliament and of the Council, 23 October 2007. *Official Journal of the European Union*, L 288, 27–34.

Kellens, W., Vanneuville, W. (2007). *Damage and Risk Calculations, Report of Action 3b of the Interreg IIIB Project SAFECoast*, Ghent University and Flanders Hydraulics Research, Antwerp, Belgium, p. 41.

Jacobs, L., Worthley, R. (1999). A comparative study of risk appraisal: A new look at risk assessment in different countries. *Environmental Monitoring and Assessment*, 59(2), 225–247.

Jonkman, S. N., Vrijling, J. K. (2008). Loss of Life due to Floods. *Journal of Flood Risk Management*, 1(1), 43–56.

Jonkman, S.N., Vrijling, J.K., Vrouwenvelder, A.C.W.M. (2008). Methods for the estimation of loss of life due to floods: A literature review and a proposal for a new method. *Natural Hazards*, 46(3), 353–389.

Lekuthai, A., Vongvisessomjai, S. (2001). Intangible flood damage quantification. *Water Resources Management*, 15(5), 343–362.

Maijala M. (2001). *RESCDAM: Development of Rescue Actions Based on Dam-Break Flood Analysis.* Final Report June 1999–March 2001, p. 48.

Penning-Rowsell E., Johnson C., Tunstall S., Tapsell S., Morris J., Chatterton J., Coker A., Green C. (2003). *The Benefits of Flood and Coastal Defence: Techniques and Data for 2003*. Flood Hazard Research Centre, Middlesex University (book + CD-ROM with damage data).

Ramsbottom D., Floyd P., Penning-Rowsell E. (2003). *Flood Risks to People – Phase 1*. R&D Technical Report FD2317TR.

Simonovic, S.P., Carson, R.W. (2003). Flooding in the Red River Basin – Lessons from post flood activities. *Natural Hazards*, 28(2–3), 345–365.

Vaes, G., Willems P., Berlamont J. (2002). *Selectie en compositie van representatieve hydrogrammen voor riviermodellering.* Water, May 2002, p. 8.

Van de Sande, Corné (2001). *River Flood Damage Assessment using IKONOS Imagery*. In cooperation with the European Commission, Joint Research Centre, Space Applications Institute, EGEO Unit, Natural Hazards Project, Flood Damage and Flood Hazard assessment.

Van der Veen, A., Logtmeijer, C. (2005). Economic hotspots: Visualizing vulnerability to flooding. *Natural Hazards*, 36(1–2), 65–80.

Vanneuville W., De Maeyer Ph., Maeghe K., Mostaert F. (2003) Model the Effects of a Flood in the Dender Catchment, Based on a Risk Methodology. *Society of Cartography Bulletin*, 37(2), 59–64.

Vanneuville W., De Rouck K., Maeghe K., Deschamps M., De Maeyer Ph., Mostaert F. (2005). *Spatial Calculation of Flood Damage and Risk Ranking*, In: Conference Proceedings of Agile 2005, 8th Conference on Geographic Information Science, pp. 549–556.

Verhaeghe, H. (2002). *Toelaatbare Golfoverslag Over Zeeweringen: Literatuuroverzicht*. Universiteit Gent, vakgroep Civiele Techniek, Afdeling Weg- en Waterbouwkunde, intern rapport, p. 23.

Verwaest, T., Van Poucke, Ph., Reyns, J., Van der Biest, K., Vanderkimpen, P., Peeters, P., Kellens, W., Vanneuville, W (2008). *SAFECoast: Comparison Between Different Flood Risk Method-*

ologies: action 3B report, SAFECoast Interreg IIIb NorthSea project, Flanders Hydraulics Research, Belgium.

Vrisou Van Eck, N., Kok, M., Vrouwenvelder, A.C.W.M. (1999). *Standaardmethode Schade & Slachtoffers als gevolg van overstromingen – deel 2: Achtergronden*, HKV-Lijn in Water en TNO Bouw in opdracht van RWS-DWW.

Yates, S. (1992). Lay attributions about distress after a natural disaster. *Personality and Social Psychology Bulletin*, 18(2), 217–222.

Chapter 5
Using Geographic Information Science to Estimate Vulnerable Urban Populations for Flood Hazard and Risk Assessment in New York City

Juliana Maantay, Andrew Maroko, and Gretchen Culp

Abstract The research presented in this chapter seeks to demonstrate a new method to more accurately estimate populations vulnerable to hazards, especially in densely developed mega-cities, and to characterize at-risk populations based on measures of social, physical, and health vulnerability. Emergency management and disaster preparation, planning, mitigation, and recovery requires accurate estimation of potentially at-risk populations and sub-populations. Census data alone, however, cannot provide sufficiently detailed knowledge of population location and distribution, particularly in large, hyper-heterogeneous urban areas like New York City. Additionally, specific sub-populations (i.e., racial/ethnic minorities) may be at higher risk, yet under-counted by existing methods of calculating potentially exposed or impacted populations. We discuss two new inter-related methods that employ Geographic Information Science (GISc) to assess and quantify risk and vulnerability: the Cadastral-based Expert Dasymetric System (CEDS) and the New York City Hazard Vulnerability Index (NYCHVI). CEDS uses an expert system and dasymetric mapping to disaggregate population and sub-population data to the property tax lot level. The analysis shows that compared to CEDS, conventional areal weighting of census data and centroid-containment selection methods under count at-risk population for floods by 37 and 72%, respectively. We found that minorities and other vulnerable sub-populations are disproportionately underestimated using traditional methods, which impairs preparedness and relief efforts. NYCHVI provides a straightforward way of assigning a vulnerability rating to populations in potentially impacted areas, and incorporates locally significant factors that are not captured using national models. Used in tandem, CEDS and NYCHVI are effective in characterizing the vulnerable populations and areas subject to flooding and other hazards, enabling significant improvements in estimating vulnerability over prevailing methods.

J. Maantay (✉)
GISc Program and the Urban GISc Lab, Environmental, Geographic, and Geological Sciences Department, Lehman College, City University of New York, Bronx, NY 10468, USA
e-mail: juliana.maantay@lehman.cuny.edu

P.S. Showalter, Y. Lu (eds.), *Geospatial Techniques in Urban Hazard and Disaster Analysis*, Geotechnologies and the Environment 2, DOI 10.1007/978-90-481-2238-7_5,

Keywords Flood hazard · Dasymetric mapping · CEDS · Vulnerability · Cadastral · NYCHVI · HVA

5.1 Flood Hazard and Vulnerable Populations in New York City

Emergency management and disaster preparation, planning, mitigation, and recovery require accurate estimation of potentially at-risk populations and sub-populations, yet census data alone do not necessarily yield sufficiently detailed knowledge of population location and distribution, particularly in large, hyper-heterogeneous urban areas like New York City (NYC). Additionally, specific sub-populations (i.e., racial/ethnic minorities) may be at higher risk (Blaikie et al. 1994; Cutter 2006; Fielding and Burningham 2005; Fothergill et al. 1999; Mitchell 1999), yet minority sub-populations remain under-counted by existing methods of calculating potentially exposed or impacted populations. New York City, most of which is at or only slightly above sea-level, is at risk from flooding due to storm surge from hurricanes, "nor'easters," and the effects of sea-level rise from global warming, as well as from other natural and technological disasters (Bloomfield et al. 1999; Coch 1994; Gornitz et al. 2002).

This chapter demonstrates the benefits of developing new geomatic methods to more accurately estimate populations vulnerable to hazards, especially in densely developed mega-cities, and to characterize the at-risk populations based on measures of social, physical, and health vulnerability. Geomatics (geospatial technologies) is the discipline of gathering, storing, processing, and delivering of geographic information, or spatially referenced information, and it encompasses the tools and techniques used in land surveying, remote sensing, geographic information systems (GIS), photogrammetry, geodesy, global navigation satellite systems, and related forms of earth mapping. We introduce two new geomatic methods that employ Geographic Information Science (GISc) and models loosely-coupled with the GIS. These two methods, the Cadastral-based Expert Dasymetric System (CEDS) and the New York City Hazard Vulnerability Index (NYCHVI), represent inter-related ways to assess and quantify risk and vulnerability.

5.1.1 FEMA 100-Year Floodplain

Flooding has been, and continues to be, a concern not only in the New York City region, but across the country. Nationally, according to the United States Geological Survey, floods annually average 140 deaths and $6 billion in property damage.

A common way to delineate the extent of the flood hazard is with what is termed the "100-year floodplain." This designation represents areas with a 1-percent-annual-chance for flooding and was created as a standardized measure among federal, state, and local agencies involved with floodplain management. The Federal Emergency Management Agency (FEMA) estimates that nearly 150,000 square miles of the United States (over 4% of the total area) are within the 100-year

Fig. 5.1 FEMA Q3 100-year floodplain in New York City Source: FEMA 1996

floodplain (FEMA 1983). Approximately 15% of NYC's land area is within this floodplain. As one of the nation's most densely populated metropolitan regions susceptible to flood hazards, the City would be particularly difficult to evacuate because it is a city of islands surrounded by water – oceans, rivers, tidal straits, estuaries, and bays – with nearly 600 miles of coastline and numerous inland waterbodies (Bloomfield et al. 1999; Fig. 5.1).

Given the high density of NYC's built environment, encompassing both residential and commercial development, there is enormous potential for damage to life and property from flooding. New York City experiences frequent and destructive "nor'easters", and the occasional hurricane, and the storms' strength and potential for devastation are magnified by the unique configuration of Long Island's land mass in relation to the mainland – it sits at nearly a 90-degree angle to the eastern seaboard of the US. Hurricane experts state that even a Category 3 hurricane here could have devastating consequences (Coch 1994).

Further exacerbating the situation, it is predicted that global warming and accelerated sea level rise could greatly increase flood risk. Gornitz (2000) claims that the ". . .vulnerability of the Metropolitan East Coast Region to coastal hazards, such as more frequent storm flooding, beach erosion, submergence of coastal wetlands, and saltwater intrusion, will intensify as sea level rises" (p. 45) and that due to accelerated sea level rise ". . .the return period of the 100-year storm flood could be reduced to 19–68 years, on average, by the 2050s, and 4–60 years by the 2080s" (p. 61).

5.1.2 Vulnerable Populations

It is of particular importance in risk assessment of floods and other natural and technological disasters to determine what portion of the population is vulnerable, and

more specifically, the location of these potentially vulnerable populations. Vulnerability may be defined using several criteria, each of which serves as a "vulnerability indicator" that can contribute to a person's or a community's overall vulnerability potential.

Certain people may be disproportionately exposed to hazards not only due to physical factors (i.e., living in poor quality housing that inadequately withstands hazard events), but also due to lack of access to strong social, financial, or political support structures. Such individuals thus suffer greater relative loss and experience a longer recovery time after a disaster than those populations considered affluent, mainstream, or socially supported (Mitchell 1999; Marandola and Hogan 2007). Consequently, identical physical phenomena can have dramatically different impacts on those who are socially and economically vulnerable, and/or whose access to a social support structure is limited (Blaikie et al. 1994).

Previous research in the United States has demonstrated increased disaster risk and vulnerability for communities of color (Fothergill et al. 1999). Additional factors, such as an individual's health status, can also result in increased vulnerability. People with reduced mobility, or who suffer from conditions such as heart disease, emphysema, asthma, AIDS, or cancer, as well as those who are blind or deaf tend to be more vulnerable and at increased risk from flooding (Kilbourne 1997; Sanderson 1997; Etzel and French 1997). Young children and the elderly are also considered to be more vulnerable than other age cohorts (Noji 1997).

Negri et al. (2005) note that by,

> analyzing census data with GIS tools, we can identify specific areas where people are at risk for floods and landslides. Some factors further increase social vulnerability, such as limited access to political power and representation, lack of access to resources (including information and technology), lack of social capital (like social networks), and poor health. Beliefs and customs, and the age, type, and density of infrastructure, buildings, and lifelines are also factors that affect risk and potential losses (p. 1245)

Different populations represent differing demographics, socio-economic characteristics, and health conditions for those at risk from floods, and therefore may require different strategies and approaches to disaster preparedness, emergency response, and disaster relief. In order to design appropriate warning communications, mitigation, and recovery planning efforts for implementation prior to or in the aftermath of a flood, it is not only necessary to determine the size and location of potentially affected populations, but also to know exactly which members of those populations are most vulnerable to a major natural disaster.

5.2 GeoTechnical Contributions to Flood Hazard Assessment: CEDS and NYCHVI

Geographic Information Science is a discipline which employs geomatic technologies such as Geographic Information Systems (GIS), remote sensing, Global Positioning Systems (GPS), geo-statistical analysis, and environmental modeling, to

examine research issues. The technologies are used to assemble, create, store, display, analyze, edit, and map spatial and attribute data. GIS can convert "real world" information into constituent elements, creating data layers or themes, which can then be re-combined within the GIS to yield information that was unavailable when the data were separate. GIS, which combines specialized mapping software, spatial and attribute databases, is a powerful tool in the hands of the analyst/user who makes decisions about and interprets the datasets, the methodologies employed, the analyses, the output, and the results (Maantay and Ziegler 2006).

We developed two geographic information system tools to determine the "who" and "where" regarding the potentially most impacted and vulnerable populations. The first of the two tools is the Cadastral-based Expert Dasymetric System (CEDS), which is described in Section 5.2.1. The second tool is the New York City Hazard Vulnerability Index (NYCHVI) based on the Human Vulnerability Assessment (HVA) model, and is described in Section 5.2.2. Each data layer of vulnerability indicators can also be utilized independently of the compiled index, which can be very useful for many planning and management needs.

5.2.1 Disaggregating Population Data Using CEDS

The Cadastral-based Expert Dasymetric System (CEDS) is a model that uses both an expert system and dasymetric mapping to disaggregate population data (e.g., from the census) into much higher resolution data, giving a more realistic depiction of population locations and densities (Maantay et al. 2007). Dasymetric mapping uses ancillary datasets to refine and redistribute the locations of some phenomena (e.g., population) to reflect its distribution more accurately. CEDS, for instance, uses data sets that mask off the areas where people tend not to live (such as parks and waterbodies), then re-distributes the census populations throughout only the known inhabited areas, rather than throughout the entirety of the census unit area. CEDS then uses tax-lot (cadastral) data, which in NYC is on average 150 times finer resolution than the census block group data, to further disaggregate the census population data, as described below.

The expert system is a computerized decision-making program, which has been instructed to "decide", based on heuristic rules and expert judgment, which among several variables in the tax-lot data set to use for disaggregating the census data to calculate the optimally accurate tax-lot level population. Total populations, as well as sub-populations such as racial/ethnic groups, age cohorts, income/poverty status, and educational attainment levels, can be reliably disaggregated with CEDS.

5.2.1.1 Comparison of Three Methods: CEDS, FAW, and CCM

There are a few commonly-used methods to estimate at-risk populations. The Federal Emergency Management Agency (FEMA) uses a model called HAZUS (FEMA 2006). HAZUS employs the centroid containment method (CCM) to select only the

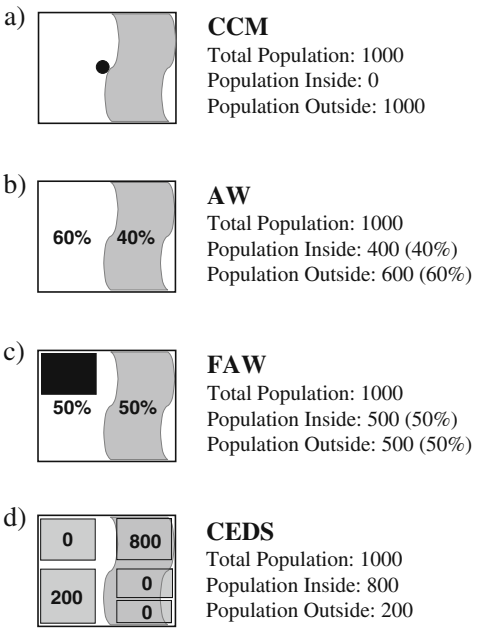

Fig. 5.2 Methodological differences and potential improvement of population estimation of the CEDS method (**d**), over the CCM – Centroid Containment method (**a**); AW – Areal Weighting (**b**); and FAW – Filtered Areal Weighting (**c**). Note that the *light grey* curved area represents a hazard area (e.g. floodplain) and the *black rectangle* in figure (**c**) represents an unpopulated area (e.g. park)

tract or block group polygons whose geometric centroids fall within the boundaries of interest, e.g., the floodplain (Fig. 5.2a).

Unfortunately, difficulties are encountered when trying to estimate population data within areas that do not coincide with the boundaries of census units. For instance, the boundaries of the floodplain are rarely, if ever, spatially coincident with the boundaries of census tracts, making it difficult to determine how many people are within the floodplain that intersects the census unit. This problem is commonly addressed by using areal weighting (AW), which is a spatial interpolation method that assumes a population is distributed homogeneously throughout a unit (Wu et al. 2005). This assumption also creates errors when trying to establish accurate counts for analyses that rely on a smaller, or different spatial unit of analysis than the original (Eicher and Brewer 2001; Holt et al. 2004).

With AW, if the boundaries of the phenomena of interest (e.g., floodplain) intersect a census unit a ratio based on areal proportions is applied to the population. If a quarter of an area is within the zone, one quarter of the population is assumed to be within the zone (Fig. 5.2b). Of course, in the real world, this assumption is a gross generalization and in hyper-heterogeneous urban areas like NYC can lead to incorrect estimation of the distribution of population in terms of both number and rate. Within census tracts and even block groups and blocks in NYC, there are very often enormous variations in land uses and population locations.

Areal weighting does not capture the nuances of complex urban areas. Filtered areal weighting (FAW) is an attempt to refine AW by using an ancillary data set to mask out uninhabited areas. The purpose is to redistribute the population only within

inhabited areas, but its accuracy is still insufficient for performing environmental, health, or risk analyses in a city such as NYC (Fig. 5.2c).

Due to the inexact results of the previous three approaches, we needed an improved method to estimate population within impact zones. CEDS has provided superior results by disaggregating data to the tax lot level (Fig. 5.2d). One of the main benefits of using CEDS is that it can estimate population data within areas that do not coincide with the boundaries of census units, for instance, floodplain boundaries. Figure 5.3 illustrates the necessity for a finer-grained method such as CEDS in a hyper-heterogeneous setting. The figure shows a typical New York City block, illustrating that even within the relatively small geographic unit of a census block there is considerable variation in population density and land use types (Fig. 5.3).

5.2.1.2 CEDS Methodology

The Cadastral-based Expert Dasymetric system relies primarily upon two proxies for population distribution – residential area (RA), which is the amount of square feet designated for residential use in the tax lot, and number of residential units (RU), which is the number of individual dwellings in the tax-lot (LotInfo 2003). Both of these are proxies for the population in each tax lot, and are therefore inexact. The tax lot data do not reveal how many people live within each lot or within each residential unit on the lot, nor how many square feet of residential area exist for each person, therefore one must estimate the population by disaggregating from the census data using RA or RU as proxies.

CEDS-derived population estimates were calculated in a two-step process, with each step occurring at different scales. Step 1, which informs the expert system, disaggregates the census tract population (from the US Bureau of the Census) to the tax-lot level based on either the ratio of RA in the tax lot versus the RA in the entire census tract or the ratio of the number of RU in the tax-lot versus the RU of the tract. Tax-lots that contain a greater proportion of proxy units are assumed to have an equally greater proportion of the population. The estimated tax-lot level populations are then re-aggregated up to the census block group level and compared with the block group population data as reported by the US Census Bureau. The absolute difference between the CEDS-estimated population, for both RA and RU, is then assessed and summed over each block group in the tract. The ancillary dataset that functioned better (i.e., lower absolute difference) is then chosen to be used as the proxy data for the geographic sub-groups contained within that particular census tract during Step 2. Step 1 was repeated for each of NYC's census tracts. These data not only inform the expert system but also act as validation by comparing its performance with data disaggregated by different, more common, techniques such as filtered areal weighting, as shown in Fig. 5.4a and b. The figures, which compare scatterplots of CEDS and FAW NYC block group population estimates, reveal that CEDS produces a superior output.

Step 2 calculates the final CEDS-derived population. Each census block group, rather than census tract, is disaggregated to the tax-lot level using the higher functioning proxy unit (RA or RU), as determined in Step 1 by the expert system. The

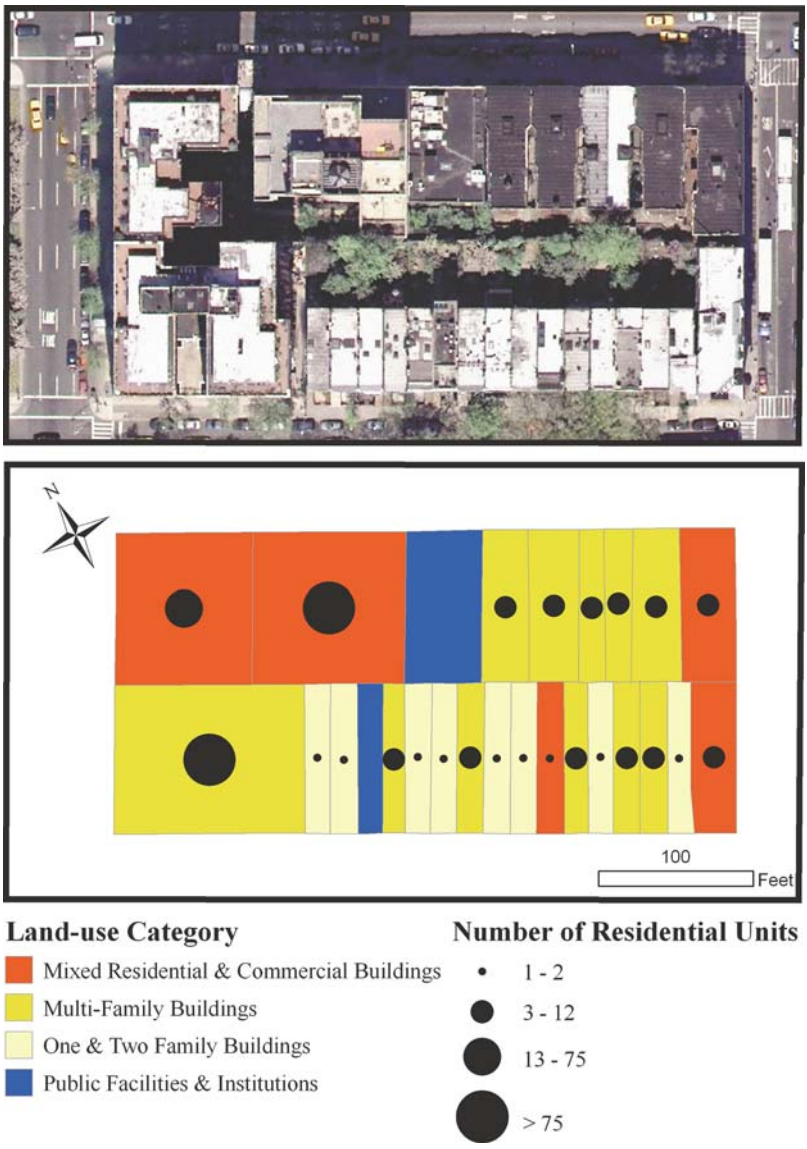

Fig. 5.3 Heterogeneity of a Manhattan city block. The orthophoto (*above*) and the cadastral map show the uneven distribution of land use categories and residential units at the tax-lot level even when examining only one city block. (There are, on average, more than 16 city blocks in a New York City census tract)
Source: NYCMap 2004; LotInfo 2003

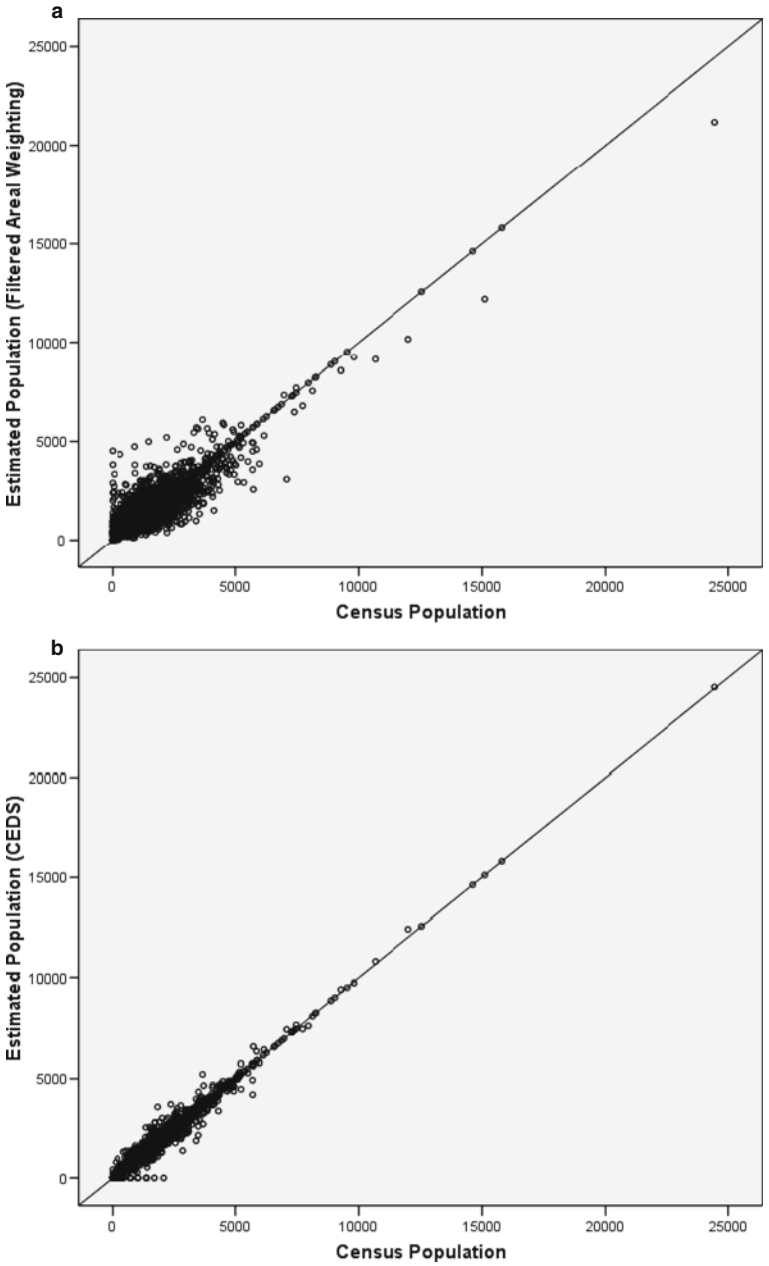

Fig. 5.4 Scatterplots of population estimations in New York City as compared to Census block group data using (**a**) Filtered Areal Weighting (FAW); and (**b**) CEDS

assumption is that when the source data is at a finer spatial resolution (census block groups are smaller than census tracts) there is less error in the system since CEDS is by nature a pycnophylactic process where mass is preserved (population numbers remain constant within the boundaries of each block group).

In this study, CEDS has been applied not only to the total population of NYC and specific racial and ethnic groups, but also to other census-based variables which are particularly important when assessing vulnerability, such as income (poverty status); educational attainment (persons 25 years and older without a high school diploma); age (persons 10 years and younger, and 65 and above); linguistic ability (persons 5 and older who speak English either 'not well' or 'not at all'); and disability (a self reported variable based on non-institutionalized individuals five years old and older). Although the sub-population estimations tend to be distributed similarly to the CEDS-derived total population, the expert system still functions independently for each variable. As such, the resulting estimates are distinct and vary in terms of redistribution ratios across the datasets. The census-based vulnerability variables have been disaggregated by CEDS, FAW, and CCM, and the resulting estimations of populations and sub-populations within the floodplain compared.

5.2.1.3 CEDS Results Versus Other Methods

In addition to total population numbers, ethnic and racial sub-populations were also spatially disaggregated to the property tax lot in this study to determine if there are any environmental justice impacts associated with flood risk in NYC (Fig. 5.4). Compared to the CEDS method, there are 37% (overall) fewer people estimated to be at risk from floods using the conventional areal weighting of census data and 72% fewer people at risk using the centroid containment selection method (Fig. 5.5). While minority populations city-wide do not disproportionately live within the floodplain, they are disproportionately undercounted by the traditional methods of population estimation. For example, in the floodplain, Non-Hispanic Blacks are undercounted at twice the rate of Non-Hispanic Whites.

The utility of CEDS for estimating potentially impacted vulnerable populations is illustrated by the case study of Brighton Beach, Brooklyn, New York. Brighton Beach is a community on the peninsula of Coney Island, which is joined by an isthmus to the rest of the borough of Brooklyn (Fig. 5.6). The community is a fairly dense residential neighborhood with a large population of immigrants and residents of Russian and Ukrainian descent. A considerable portion of Brighton Beach is also within the FEMA 100-year floodplain.

Population within the floodplain was estimated using the centroid containment method, filtered areal weighting, and CEDS (Fig. 5.7). Of the just over 35,000 residents in Brighton Beach, CCM estimates 4661 (13.2%) are in the floodplain, FAW estimates 9487 (26.9%) are in the floodplain, while CEDS estimates 11,798 (33.5%) are in the floodplain.

The markedly different estimates for this neighborhood indicate that the centroid containment method yields the least satisfactory results, FAW is an improvement, and CEDS provides the most precise estimates for total population as well as for

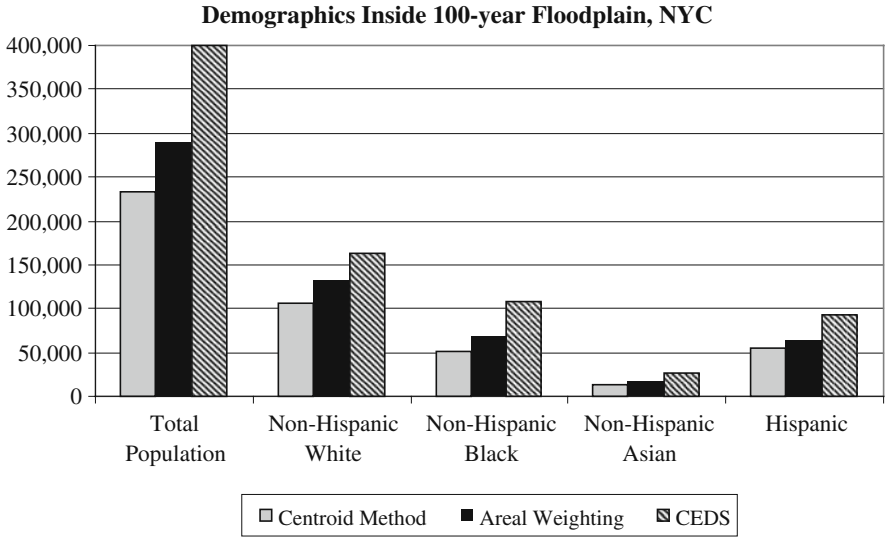

Fig. 5.5 Estimated populations and sub-populations within the 100-year floodplain in NYC comparing CEDS, FAW and CCM

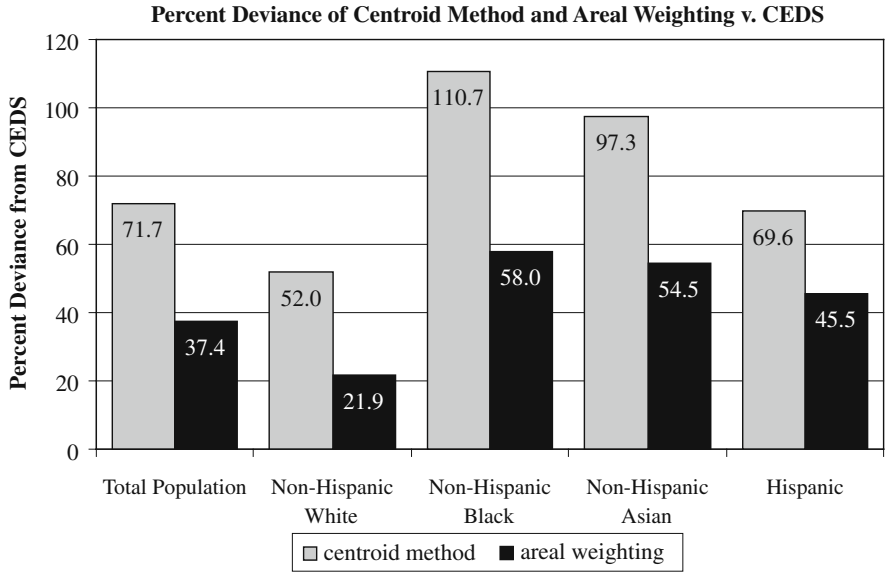

Fig. 5.6 Percent deviance of the Centroid Containment Method and AW vs. CEDS regarding undercounting of racial/ethnic groups

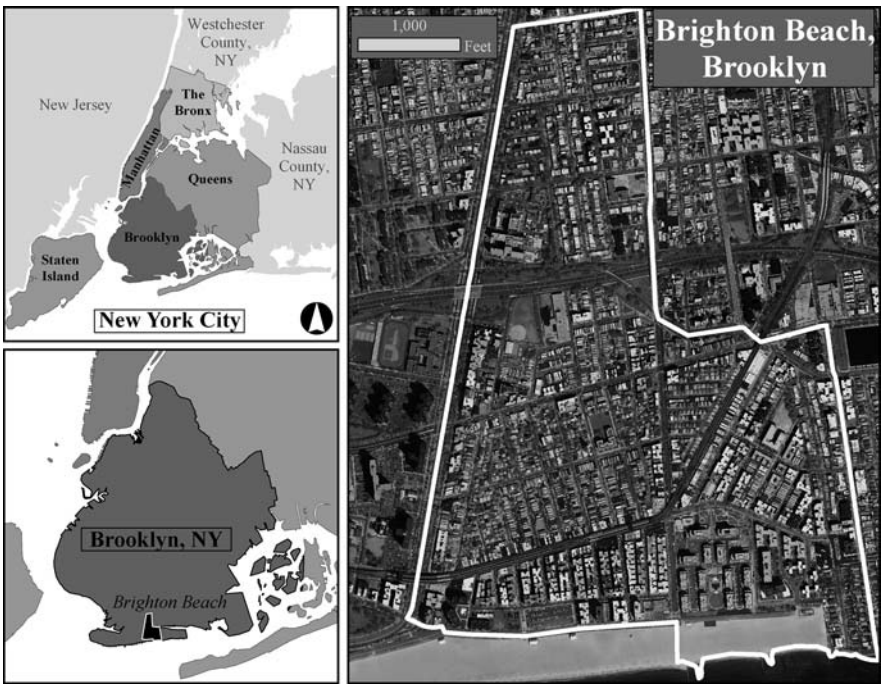

Fig. 5.7 Locator map of Brighton Beach community in Brooklyn, New York

all the sub-populations examined in the case study (Figs. 5.7, 5.8, and 5.9). Some populations estimated by the centroid containment method are undercounted by 200% or more (e.g., elderly 65 years and older; non-Hispanic black; and Hispanic) when compared against the estimates derived from CEDS. This undercounting of vulnerable populations can have serious ramifications for disaster planning, management, and mitigation.

5.2.2 New York City Human Vulnerability Index (NYCHVI) Model

The New York City Human Vulnerability Index (NYCHVI) is a user-driven hazard-of-place model based on the Human Vulnerability Assessment (HVA), a qualitative risk analysis tool created by the Geospatial Research, Analysis, and Services Program (GRASP) at the Centers for Disease Control and Prevention (CDC). The HVA is an application composed of an ArcObjects® MXD project, as well as data layers crafted from US Census and ESRI® Data and Maps (ESRI®, Inc.).

Conventionally, in times of disaster, attention was focused on property loss rather than estimation of human casualties (Cutter et al. 2000). Disaster epidemiologists, however, are tasked with measuring and describing adverse health effects, and factors contributing to those effects, that result from natural and human disasters in

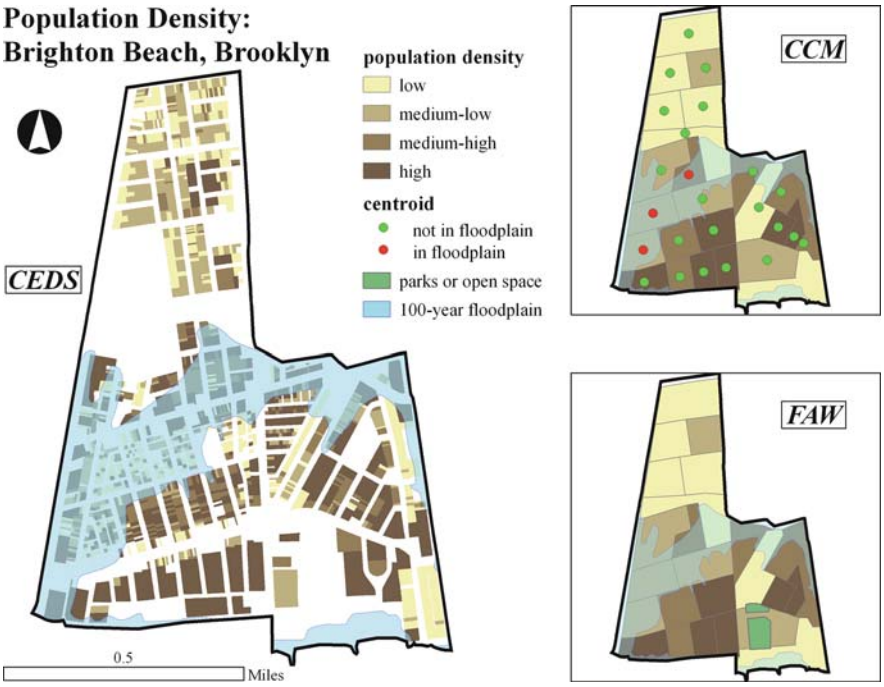

Fig. 5.8 Estimated total population densities in the case study area of Brighton Beach, Brooklyn, comparing CEDS, FAW and CCM. CEDS is aggregated to the tax lot, whereas FAW and CCM are at the census block group level. Population densities are shown in quartiles based on each dataset individually since the denominator (area) is not consistent across datasets (CEDS only accounts for the tax lot areas, whereas FAW and CCM utilize the entire census block group area)
Source: US Census 2000; LotInfo 2003; NYC Parks and Recreation Dept.; FEMA, Q3 2006

order to assess and meet the needs of disaster-affected populations. The HVA produces map-based reports "on-the-fly", allowing for the identification of populations potentially at risk of higher morbidity or mortality during a disaster. This model is intended to assist state and local decision-makers in targeting populations vulnerable to natural and man-made disasters. At this point in time, HVA is available only as a beta version, thus, its map reports may be subject to incompleteness or various inconsistencies.

5.2.2.1 Constructing the NYCHVI Model

In order to construct a locationally-relevant vulnerability index, it was necessary to modify and augment the national-level HVA by incorporating geographically specific datasets. The HVA model employs fifteen US Census variables at the census tract level. The model calculates the percentile rank of ninety or higher (PRC90) for each variable. If a variable is within the ninetieth percentile, it receives a PRC90 score of one. The overall vulnerability is determined by summing the

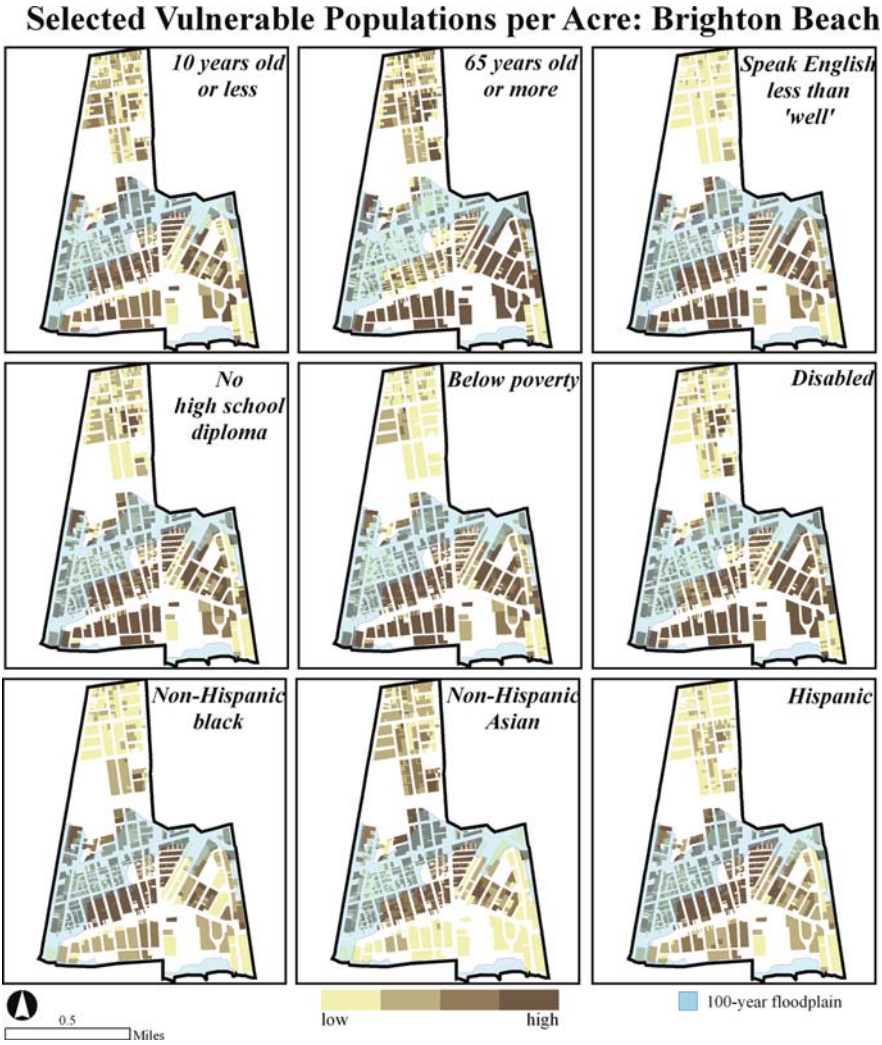

Fig. 5.9 Selected vulnerability variables – Persons per Acre. Each map represents a CEDS-derived variable at the tax lot level whose individual data range has been classified by quartiles
Source: US Census 2000; LotInfo 2003; NYC Parks and Recreation Dept.; FEMA, Q3 2006

PRC90 for all variables, which are not standardized and are weighted equally. The HVA overall vulnerability score can range from zero (very low vulnerability) to fifteen (extremely vulnerable). In addition, these fifteen variables can be organized into four indicator groups that measure the source of social vulnerability: *Socio-Economic* (income, poverty, employment, and education); *Household Structure and Disability* (age, dependency, disability, and single-parenting); *Race and Ethnicity* (minority status and non-English speaking); and *Housing and Transportation* (urban/rural housing, crowding, and transportation) (Table 5.1). These indicator

Table 5.1 HVA Variables (adapted from CDC 2008)

Variable	Data source*	Additional description
Group A. Socio-economic status		
1. Percent individuals below poverty	2000 US Census, Summary File 3, Population for Whom Poverty Status is Determined, Table P88. Ratio of Income in 1999 to Poverty Level	Individuals below poverty = "Under 0.50" + "0.50 to 0.74" + "0.75 to 0.99". Percent of persons below federally-defined poverty line, a threshold that varies by the size and age composition of the household. Denominator is total population where poverty status is checked.
2. Percent civilian unemployed	2000 US Census, Summary File 3, Population 16 years and Over, Table P43. Sex by Employment Status	Based on total population 16+. Civilian persons unemployed divided by total civilian population. Unemployed persons actively seeking work.
3. Per Capita Income in 1999	2000 US Census, Summary File 3, Total Population, Table P82. Per Capita Income in 1999	The mean income computed for every person in the census tract.
4. Percent persons with no high school diploma	2000 US Census, Summary File 3, Population 25 Years and Over, Table P37. Sex by Educational Attainment	Percent of persons 25 years of age and older, with less than a 12th grade education (including individuals with 12 grades but no diploma).
Group B. Household structure and disability		
5. Percent persons 65 years of age or older	2000 US Census, Summary File 3, Total Population, Table P8. Sex by Age	Percent persons 65 years of age or older.
6. Percent persons 17 years of age or younger	2000 US Census, Summary File 3, Total Population, Table P8. Sex by Age	Percent persons 17 years of age or younger.
7. Percent persons more than 5 years old with a disability	2000 US Census, Summary File 3, Civilian non Institutionalized Population 5 Years and Over, Table P42. Sex by Age by Disability Status by Employment Status	Percent civilian population not in an institution that are 5 years of age and older with a disability.
8. Percent male or fe-male householder, no spouse present, with children under 18	2000 US Census, Summary File 3, Households, Table P10. Household Size by Household Type by Presence of Own Children Under 18 Years	Other Family: Male Householder, no wife present, with own children under 18 years + Other Family: Female Householder, no husband present, with own children under 18 years.

Table 5.1 (continued)

Variable	Data source*	Additional description
Group C. Minority status and language		
9. Percent Minority	2000 US Census, Summary File 3, Total Population, Table P6. Race and Table P7. Hispanic or Latino by Race	Total of the following: "Black or African American alone" + "American Indian and Alaska Native alone" + "Asian alone" + "Native Hawaiian and Other Pacific Islander alone" + "Some Other race alone" + "Two or more races" + "Hispanic or Latino – White alone".
10. Percent persons 5 years of age or older who speak English less than "well"	2000 US Census, Summary File 3, Population 5 Years and Over, Table P19. Age by Language Spoken at Home by Ability to Speak English	For all age groups and all languages – the total of persons who speak English "not well" or "not at all".
Group D. Housing and transportation		
11. Percent multi-unit structure	2000 US Census, Summary File 3, Housing Units, Table H30. Units in Structure	Percent housing units with 10 or more units in structure
12. Crowding	2000 US Census, Summary File 3, Housing Units, Table H30. Units in Structure	At household level, more people than rooms. Percent total occupied housing units (i.e., households) with >1 person per room
13. No vehicle available	2000 US Census, Summary File 3, Occupied Housing Units, Table H44. Tenure by Vehicles Available	Percent households with no vehicle available.
14. Percent of persons in group quarters	2000 US Census, Summary File 3, Total Population, Table P9. Household Type by Relationship	Percent of persons who are in institutionalized group quarters (e.g., correctional institutions, nursing homes) and non-institutionalized group quarters (e.g., college dormitories, military quarters).
15. Percent mobile homes	2000 US Census, Summary File 3, Housing Units, Table H30. Units in Structure	Percent housing units which are mobile homes

*Beginning in 1790, the United States Census Bureau has conducted a decennial count of everyone living in the United States and its territories. In-depth population and housing data collected on a sample basis from the Census 2000 long form survey in addition to topics from the short form 100-percent data (age, race, sex, and vacancy status) are presented in Summary File 3. This includes population totals for ancestry groups as well as selected characteristics for a limited number of race and Hispanic or Latino categories. For more information on the United States Census, please refer to http://www.census.gov/.

groups are based on eleven factors devised by Cutter et al. (2003) to distinguish US counties according to level of social vulnerability in relation to environmental hazards. The HVA presents this information in a dynamic letter-sized cartographic report that includes six maps: one for each indicator group, an overall index and a reference map. The HVA model is national in scope and generates user-driven reports by county (e.g., Kings) or region (e.g., New York, NY – Northeastern New Jersey). This coarse scale may not provide adequate detail for local jurisdictions (CDC/ATSDR 2008). In addition, the HVA contains variables that are geared toward suburban or rural areas (number of mobile homes, for instance) and is therefore inappropriate for an urban hazard-of-place model.

The HVA variables are selected to serve as a broad overview and are considered a guide for potential indicators of vulnerability. A good vulnerability index emphasizes hazards that could potentially impact a community, indicates possible locations of hazard-related damage, and identifies those community elements that should be addressed to lessen exposure. NYCHVI (Table 5.2) is intended to enhance the HVA for New York City, not only by using locationally-specific data, but also by

Table 5.2 NYCHVI variables

Variable	Data source*	Additional description
Group A. Socio-economic status		
1. Percent individuals below poverty	Same as HVA (Table 5.1).	Same as HVA.
2. Percent civilian unemployed	Same as HVA.	Same as HVA.
3. Per Capita Income in 1999	Same as HVA.	Same as HVA.
4. Percent persons with no high school diploma	Same as HVA.	Same as HVA.
Group B. Household structure and disability		
5. Percent persons 65 years of age or older	Same as HVA.	Same as HVA.
6. Percent persons 10 years of age or younger	2000 US Census, Summary File 3, Total Population, Table P8. Sex by Age	Percent persons 10 years of age or younger
7. Percent persons more than 5 years old with a disability	Same as HVA.	Same as HVA.
8. Percent male or female house-holder, no spouse present, with children under 18	Same as HVA.	Same as HVA.
Group C. Minority status and language		
9. Percent Minority	Same as HVA.	Same as HVA.

Table 5.2 (continued)

Variable	Data source*	Additional description
10. Percent persons 5 years of age or older who speak English less than "well"	Same as HVA.	Same as HVA.
Group D. Housing and transportation		
11. Percent multi-unit structure	Same as HVA.	Same as HVA.
12. Crowding	Same as HVA.	Same as HVA.
13. No vehicle available	Same as HVA.	Same as HVA.
14. Percent of persons in group quarters	Same as HVA.	Same as HVA.
Group E. Public health		
15. AIDS	New York State Department of Health SPARCS – 2006 Persons, ICD-9: 042–044	Percent of population that underwent an AIDS-related hospitalization
16. Asthma	New York State Department of Health SPARCS – 2006 Persons, ICD-9: 493	Percent of population that underwent an asthma-related hospitalization
17. Cancer	New York State Department of Health SPARCS – 2006 Persons, ICD-9: 140–208	Percent of population that underwent a cancer-related hospitalization
18. Diabetes	New York State Department of Health SPARCS – 2006 Persons, ICD-9: 250	Percent of population that underwent a diabetes-related hospitalization
19. Heart Condition	New York State Department of Health SPARCS – 2006 Persons, ICD-9: 390–429	Percent of population that underwent a heart condition-related hospitalization

*Established in 1979, the Statewide Planning and Research Cooperative System (SPARCS), a comprehensive data reporting system, is the result of cooperation between the health care industry and government. While SPARCS was initially created to gather information on hospital discharges, it currently collects patient level data on patient characteristics, diagnoses and treatments, services, and charges for every hospital discharge, ambulatory surgery patient, and emergency department admission in New York State. The World Health Organization′s International Classification of Diseases Ninth Revision (ICD-9) is designed to facilitate international comparability in the collection, processing, classification, and presentation of mortality and morbidity statistics. In SPARCS, all hospital discharges are assigned an ICD-9 code based on the disease or condition associated with the hospitalization. For more information on the SPARCS dataset, please refer to http://www.health.state.ny.us/statistics/sparcs/.

expanding the model to take additional factors such as biophysical information into account – the HVA currently does not include a biophysical vulnerability component. Thorough vulnerability indices provide analysis of all critical public and private facilities and infrastructure (CDC/ATSDR 2008). For example, "special needs" facilities (i.e., health care facilities, schools, day care centers, and senior centers) are at higher risk because their occupants are dependent on others for their well being (Cutter et al. 2000). Proximity to "lifeline" resources including key infrastructure (e.g., public transit) and emergency response facilities (e.g., fire houses) may provide valuable information for mitigation planning. Capability of structures and lifeline systems to withstand past disasters is yet another consideration (Noji 1992). A comprehensive vulnerability index must also contain spatial information regarding areas prone to natural hazards (e.g., floodplain) (Cutter et al. 2000; Fedeski and Gwilliam 2007). Thus, important elements that (ideally) should be included in a hazard vulnerability index model include hazard-specific layers such as floodplain, hazardous waste facilities, building data, special needs facilities (e.g., hospitals, schools, eldercare centers), infrastructure (e.g., bridges, transportation, utilities), and public health data (e.g., hospitalization records regarding medically vulnerable individuals) other than the limited disability fields of the 2000 Census Survey (Table 5.3).

Elements should be symbolized employing a standard set of symbols developed for Emergency Management and First Responder agencies at the National, State, Local and Incident level that provide immediate and general understanding of the event (Homeland Security Working Group 2005).

The NYCHVI examines areas (ranging from borough to tax lot) within New York City's boundaries. This index can aid disaster preparation, management, mitigation, and recovery by identifying the locations of specific sub-populations that are at increased risk in a natural disaster.

5.2.2.2 NYCHVI Methods and Results

NYCHVI's (Table 5.2) variables for *Socio-economic Status* (Group A), and *Minority Status and Language* (Group C) are identical to those of HVA (Table 5.1). NYCHVI's *Household Structure and Disability* (Group B) category differs from that of HVA by the replacement of the original variable "Percent persons 17 years of age or younger" with "Percent persons 10 years of age or younger." Epidemiological literature suggests that younger children are more vulnerable to hazards than teenage adolescents and adults (Noji 1997). For the *Housing and Transportation* (Group D), the metric "Percent mobile homes" was removed because very few (~0.07%) of New Yorkers reside in mobile homes. NYCHVI's main departure from HVA is found with the addition of a new group of variables examining public health indicators (Group E). These data originated from New York State's Department of Health, Statewide Planning and Research Cooperative System (SPARCS), which estimates vulnerability based on pre-existing medical conditions (i.e., heart condition, AIDS, asthma, diabetes, and cancer).

Table 5.3 NYCHVI natural hazard and spatial layers

Spatial sector	Layer file	Source
Infrastructure	Subways	New York City Transit (NYCT)
	NYC streets (Linear Integrated Ordered Network – LION streets)	City of New York Department of City Planning (DCP)
	Property tax lot data – (Planning Primary Land Use Tax Lot Output – PLUTO)	City of New York Department of City Planning (DCP)
	Buildings footprints	New York City Department of Information Technology and Telecommunications (DoITT)
Biophysical	100-floodplain	Federal Emergency Management Agency (FEMA)
Lifeline	Police stations	City of New York Police Department (NYPD)
	Fire houses	New York City Fire Department (FDNY)
Special needs	Senior centers	New York City Department for the Aging (DFTA)
	Senior facilities	New York City Department for the Aging (DFTA)
	Charter schools	New York City Department of Education (DOE)
	Day care centers	City of New York Department of City Planning (DCP)
	Institutional housing	City of New York Department of City Planning (DCP)
	Hospitals	New York City Office of Emergency Management (OEM)
	Special education	New York City Department of Education (DOE)
	Regional schools	New York City Department of Education (DOE)

These pre-existing medical conditions are also used to create the New York City Department of Health and Mental Hygiene's Community Health Profiles, annual reports that address the health status and vulnerability of NYC neighborhoods (NYC-DOHMH 2006).

As with HVA, NYCHVI overall vulnerability is determined by summing the PRC90 for all variables featured in Table 5.2 (which are not standardized and are weighted equally), with an overall vulnerability score that can range from zero (very low vulnerability) to nineteen (extremely vulnerable). While HVA calculates the PRC90 on a national level, NYCHVI determines PRC90 on a city level. In other words, HVA compares a census tract to all other census tracts within the United States while NYCHVI compares a census tract to all other census tracts within

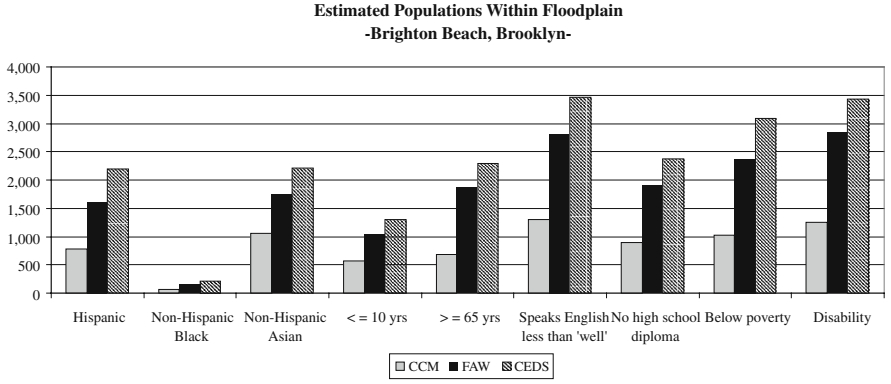

Fig. 5.10 Estimated total and sub-populations within the 100-year floodplain in the case study area of Brighton Beach, Brooklyn, comparing CEDS, FAW and CCM

New York City. A user-driven NYCHVI report for the Brooklyn neighborhood of Brighton Beach is shown in Fig. 5.10.

The "Special Needs" dataset (Table 5.3) was created to account for the facilities where particularly vulnerable populations gather, including hospitals, day care facilities, schools, institutions and senior housing. "Lifeline" and "Infrastructure" datasets incorporate data regarding transportation, residential (tax) lots, building footprints and emergency responder location (e.g., fire, police). Finally, a biophysical vulnerability component (FEMA's 100-year floodplain) was added. Where feasible, overlays were symbolized using the Homeland Security Emergency Management Symbol set. Figures 5.11 and 5.12 depict user-driven NYCHVI letter size (11″ X 8.5″) reports featuring a finely detailed map for the Brighton Beach area of Brooklyn (Please note, these reports are for illustrative purposes and have been reduced to fit the pages of this book). These figures depict neighborhood level maps of the same extent and are meant to be viewed as a set. Figure 5.11 plots the hazard vulnerability variables while Fig. 5.12 is a block level detail of Fig. 5.11 showing important features such as building level data as well as the floodplain.

5.3 Discussion

CEDS and NYCHVI can work in tandem, yet independently, as illustrated in Figs. 5.7, 5.8, 5.9, 5.10, 5.11, 5.12, and 5.13. As an example, we introduce the case study area of Brighton Beach, Brooklyn. NYCHVI can be used to quickly and efficiently disseminate crucial information to decision-makers and field personnel via an easily understood and interpreted dynamic user-driven and interactive cartographic product. For instance, the NYCHVI tool can be utilized to site critical care facilities (e.g., temporary housing, triage units, morgues) as well as expedite flexible

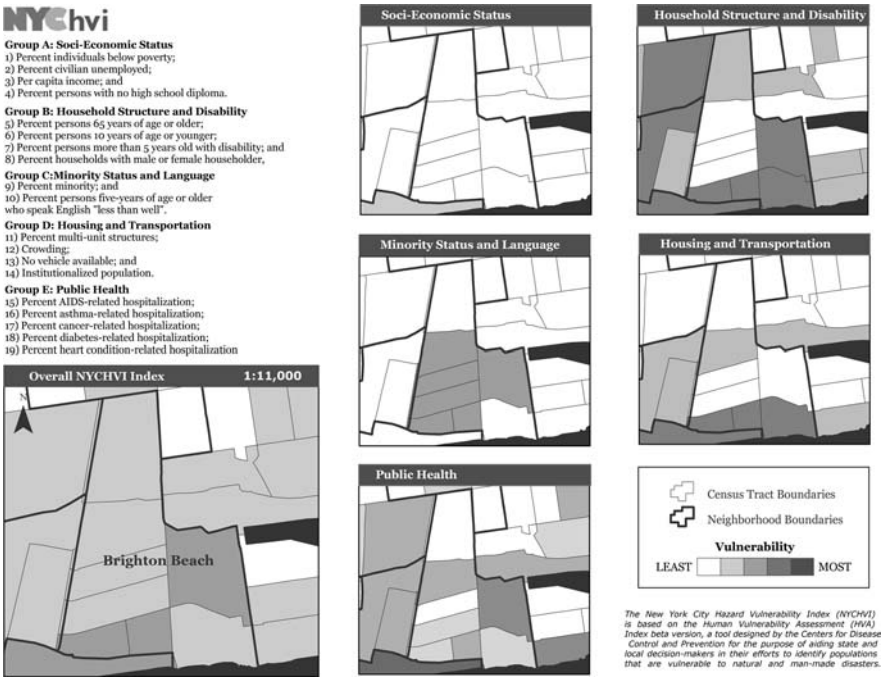

Fig. 5.11 NYCHVI print-out depicting five indicator groups and resulting overall index for the neighborhood of Brighton Beach, Brooklyn, NY at a scale of 1:40,000
Source: Tables 5.1, 5.2 and 5.3

planning for evacuation routes as information about the areal extent and magnitude of the disaster becomes available. For pre-disaster planning and mitigation, the NYCHVI model can be used to identify communities most vulnerable to flood hazards based on various socio-demographic factors. This ability enables more effective educational outreach, including the ability to create and distribute linguistically- and culturally-appropriate bulletins and publications. NYCHVI can also be employed to target specific at-risk communities for pre- and post-disaster resource allocation, based on socio-economic need and the particular health concerns of their residents.

Figure 5.11, for example, illustrates the potentially devastating effects of a flood on both special needs facilities and transportation systems. Several schools, childcare and eldercare institutions are either within the floodplain or are cut off from the main landmass by the floodplain's extent. The same situation holds true for the subway lines servicing the neighborhood as well as for a network of major and minor roadways. Figure 5.12 displays a specific grade school and neighboring residential buildings that are at risk of from the flood hazard.

CEDS provides more precise estimates of populations and sub-populations that could be directly affected by flooding, enabling efficient pre-disaster evacuation planning and allocation of post-disaster emergency resources. Used in tandem with

Fig. 5.12 NYCHVI user-driven report featuring overlay of lifeline and special needs facilities affected by a FEMA 100-year floodplain for the neighborhood of Brighton Beach, Brooklyn, NY at a scale of 1:10,000
Source: See Tables 5.1, 5.2 and 5.3

NYCHVI, the information is even more compelling. For instance, by examining the easternmost census tract in Brighton Beach (Fig. 5.10), NYCHVI reveals a comparatively high level of vulnerability mainly due to public health concerns, linguistically ability, and preponderance of specific age cohorts. Simultaneously, CEDS (Fig. 5.8) reinforces this impression by providing the absolute numbers and concentrations of vulnerable populations in categories such as disabled, elderly, children, limited English-speaking ability, lower-income, and racial/ethnic minorities.

5.4 Conclusion

The purpose of this chapter is to demonstrate the utility of two new complementary geomatic techniques: CEDS and NYCHVI. Using cadastral-based dasymetric disaggregation of census data, as well as the creation of vulnerability indices, more accurate and nuanced information is made available for emergency response and disaster planning.

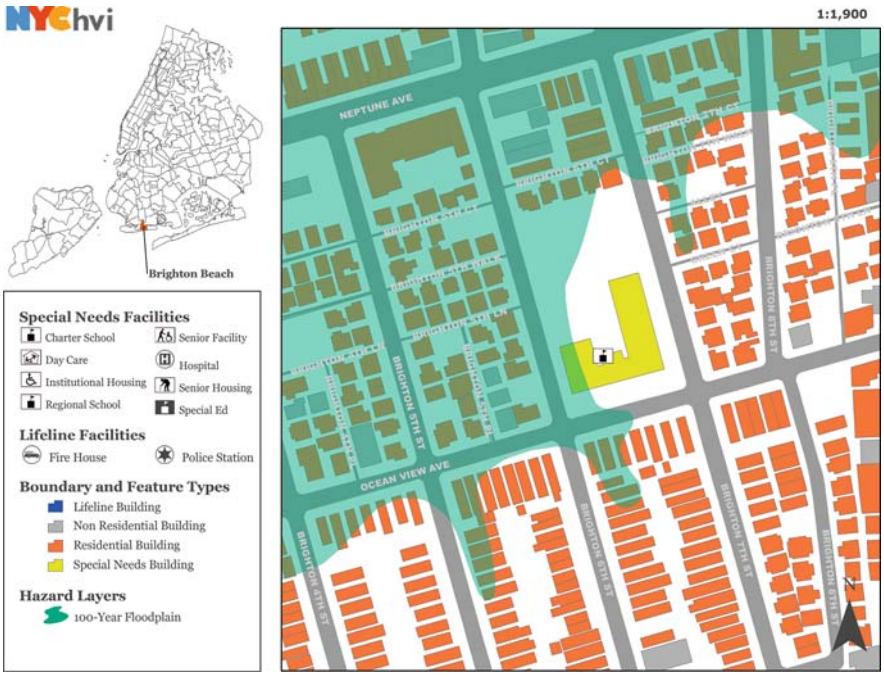

Fig. 5.13 NYCHVI user-driven report showing life line, special needs and residential buildings affected by FEMA 100-year floodplain for the neighborhood of Brighton Beach, Brooklyn, NY at a scale of 1:1900
Sources: Tables 5.1, 5.2 and 5.3

Both CEDS and NYCHVI enhance understanding of the geographic extent and magnitude of vulnerability to the flood hazard in New York City, providing significantly improved vulnerability estimates over previous methods. Through the addition of important elements, the manipulation of existing variables, and the incorporation of particularized spatial data layers and supplementary indicator data, the resulting NYCHVI is an overall vulnerability index based on potentially exposed population and population density, salient population indicators, and social and biophysical vulnerability. The disaggregation of census data with the CEDS technique results in a more precise way to delineate the boundaries containing populations potentially impacted by hazards.

The CEDS and NYCHVI methods are complementary but not duplicative, and each has specific purposes. CEDS provides general and sub-population density information revealing those who are especially vulnerable to hazards. NYCHVI examines relative quantities (e.g., rates, percentages) of vulnerable populations' potential exposure to flood risk in order to assist with resource allocation and plans for the provision of emergency services. Together, CEDS and NYCHVI provide a more comprehensive and accurate estimate than would be obtained using either method individually because they are taking into account different factors at different spatial scales.

While there is a benefit to examining vulnerability at different scales, inherent difficulties arise if one wishes to devise a single standard metric for a combined vulnerability index. NYCHVI works with census tract level data (e.g., health data), which is unlikely to be available at a finer resolution. CEDS performs at the tax lot level. While it might be possible to integrate CEDS and NYCHVI into a single index in the future, it currently seems more useful to retain them as separate indices since they are measuring different aspects of vulnerability.

There are substantial policy implications if CEDS and NYCHVI are used to estimate and identify populations at risk. These tools can more accurately determine the number of people at risk, as well as provide a more realistic indication of their socio-demographic characteristics. This knowledge can support planning efforts for emergency management, preparation, prevention, mitigation, and recovery planning, as well as encourage planning and response activities be crafted to address the specific needs of the populations involved. Culturally- and linguistically-appropriate materials can be developed to improve disaster preparation by better informing potentially affected communities, and also to better serve specific populations in a disaster's aftermath. Having precise knowledge of a at-risk populations' general health conditions (e.g., disabilities, mobility issues) that might complicate preparation or response activities (e.g., evacuation) could be critical in the event of a disaster. Such access also facilitates sending aid targeted to areas most in need of immediate help, for instance, areas with a high proportion of the elderly, disabled, or young. Since it has been shown that traditional methods of estimation significantly undercount populations of non-Hispanic Blacks, Hispanics, and those 65-years old or older that are located in NYC's flood hazard zones, these and similar populations will also benefit from these new models.

CEDS and NYCHVA can serve as a model to help other municipalities develop customized methods to estimate vulnerability to hazards, tailored to the specific conditions and characteristics of their locales. While this study focused on the flood threat, the models can estimate vulnerability and exposure to other types of hazards such as earthquakes, extreme weather events, and technological disasters (e.g., chemical spills, nuclear/toxic releases). By improving on past methods, CEDS and NYCHVA provide a robust visualization of biophysical and social vulnerability with more precise quantification of potential exposure.

Acknowledgments This research was partially supported by the National Oceanic and Atmospheric Administration's Cooperative Remote Sensing Science and Technology Center (NOAA-CREST) under NOAA grant number NA17AE162. The National Institute of Environmental Health Sciences of the National Institutes of Health also provided critical support for this project under NIEHS grant number 2 R25 ES01185-05. The statements contained within this paper are not the opinions of the funding agencies or the US government, but reflect the authors' opinions. This research was also supported by a Faculty Research Award from the Professional Staff Congress of the City University of New York (PSC-CUNY), Awards # 69372-0038, "Perfecting the Denominator: Developing a Cadastral-based Expert Dasymetric System in New York City."

List of Acronyms

ATSDR	Agency for Toxic Substances and Disease Registry
AW	Areal weighting
CCM	Centroid Containment Method
CDC	Centers for Disease Control and Prevention (US)
CEDS	Cadastral-based Dasymetric Expert System
FAW	Filtered Areal Weighting
FEMA	Federal Emergency Management Agency
GIS	Geographic Information System
GISc	Geographic Information Science
GPS	Global Positioning Systems
GRASP	Geospatial Research, Analysis, and Services Program
HAZUS	Hazards US
HVA	Human Vulnerability Assessment
NYC	New York City
NYCHVI	New York City Hazards Vulnerability Index
RA	Residential Area
RU	Residential Units
SPARCS	Statewide Planning and Research Cooperative System (New York State Department of Health)

References

Blaikie, P., Cannon, T., Davis, I., and Wisner, B. (1994). *At Risk: Natural Hazards, People's Vulnerability, and Disasters.* London, UK: Routledge.

Bloomfield, J., Smith, M., and Thompson, N. (1999). *Hot Nights in the City: Global Warming, Sea-Level Rise and the New York Metropolitan Region.* Washington, DC: Environmental Defense Fund.

Centers for Disease Control and Prevention/Agency for Toxic Substances and Disease Registry (CDC/ATSDR). (2008). *The CDC/ATSDR Public Health Vulnerability Mapping.*

Coch, N.K. (1994). Hurricane hazards in the Northeast US. *Journal of Coastal Research, Special Issue*, 12:115–147.

Cutter, S.L. (Ed.) (2006). *Hazards, Vulnerability and Environmental Justice.* London, UK: Earthscan.

Cutter S.L., Boruff B.J., and Shirley W.L. (2003). Social vulnerability to environmental hazards. *Social Science Quarterly*, 84(2):242–261.

Cutter, S.L., Mitchell, J.T., and Scott, M.S. (2000). Revealing the Vulnerability of People and Places: A Case Study of Georgetown County, South Carolina. *Annals of the Association of American Geographers*, 90(4):s713–737.

Eicher, C., and Brewer, C. (2001). Dasymetric mapping and areal interpolation: implementation and evaluation. *Cartography and Geographic Information Science*, 28:125–138.

Etzel, R.A., and French. J.G. (1997). Chapter 16: Air Pollution. In Noji, E.K. editor. *The Public Health Consequences of Disasters*. 1st ed. New York: Oxford University Press, pp. 336–353.

Federal Emergency Management Agency (FEMA) (1983). *The 100-year Base Flood Standard and the Floodplain Management Executive Order: A Review.* Prepared for the Office of Management and Budget. Washington DC: US Printing Office.

Federal Emergency Management Agency (FEMA) (2006). *HAZUS: FEMA's Software Program for Estimating Potential Losses from Disasters*, FAQ; www.fema.gov/plan/prevent/hazus/.

Fedeski, M., and Gwilliam, J. (2007). Urban Sustainability in the presence of flood and geological hazards: The development of a GIS-based vulnerability and risk assessment methodology. *Landscape and Urban Planning*, 83:50–61.

Fielding, J, and Burningham, K. (2005). Environmental inequality and flood hazard. *Local Environment*, 10(4):379–395.

Fothergill, A., Maestas, E.G.M., and Darlington, J. (1999). Race, ethnicity and disasters in the United States: A review of the literature. *Disasters*, 23(2):156–173.

Gornitz, V. (2000). *Climate Change and a Global City: An Assessment of the Metropolitan East Coast (MEC) Region Coastal Zone Sector Report: Sea Level Rise and Coastal Hazards*. (June 8, 2000). http://metroeast_climate.ciesin.columbia.edu/.

Gornitz, V., Couch, S., and Hartig, E. (2002). Impacts of sea level rise in the New York City metropolitan area. *Global and Planetary Changes*, 32:61–88.

Holt, J. B., Lo, C.P., and Hodler, T. W. (2004). Dasymetric estimation of population density and areal interpolation of census data. *Cartography and Geographic Information Science*, 31:103–121.

Homeland Security Working Group. (14 Sept. 2005). *Homeland Security Working Group Symbology Reference*. 28 Apr 2008 http://www.fgdc.gov/HSWG/index.html.

Kilbourne, E.M. (1997). Chapter 12: Heat waves and hot environments. In: Noji, E.K. (ed.) *The Public Health Consequences of Disasters*. 1st ed. New York: Oxford University Press, pp. 245–269.

LotInfo, LLC. (2003). *LotInfo*. SpaceTrack, Inc. 304 Park Ave, 11th Floor New York, NY 10010.

Maantay, J.A., Maroko, A., and Herrmann, C. (2007). Mapping population distribution in the urban environment: The cadastral-based expert dasymetric system (CEDS). *Cartography and Geographic Information Science*, 34(2):77–102.

Maantay, J.A., and Ziegler, J. (2006). *GIS for the Urban Environment*. Redlands, CA: Environmental Systems Research Institute (ESRI) Press.

Marandola Jr., E. and Hogan, D.J. (2007). Vulnerabilities and risks in population and environmental studies. *Population and Environment*, 28(2):83–112.

Mitchell, J.K. (1999). *Crucibles of Hazard: Megacities and Disasters in Transition*. Tokyo: United Nations University Press.

Negri, A., Burkardt, N., Golden, J., Halverson, J., Huffman, G., Larsen, M., McGinley, J., Updike, R., Verdin, J., and Wieczorek, G. (2005). The hurricane–flood–landslide continuum. *Bulletin of the American Meteorological Society*, 86(9):1241–1247.

New York Coty Department of Health and Mental Hygiene [DOHMH]. (2006). *Community Health Profiles: Southern Brooklyn.*

Noji, E.K. (1992). Disaster epidemiology: Challenges for public health action. *Journal of Public Health Policy*, 13(3):332–340.

Noji, E.K. (1997). Chapter 8: Earthquakes. In: Noji, E.K. (ed.) *The Public Health Consequences of Disasters*. 1st ed. New York: Oxford University Press, pp. 135–178.

Sanderson, L.M. (1997). Chapter 18: Fires. In Noji, E.K. editor. *The Public Health Consequences of Disasters*. 1st ed. New York: Oxford University Press, pp. 373–396.

Wu, S., Qiu, X., and Wang, L. (2005). Population estimation methods in GIS and remote sensing: A review. *GIScience and Remote Sensing*, 42(1):80–96.

Chapter 6
Geo-Information Technology for Infrastructural Flood Risk Analysis in Unplanned Settlements: A Case Study of Informal Settlement Flood Risk in the Nyabugogo Flood Plain, Kigali City, Rwanda

Jean Pierre Bizimana and Michele Schilling

Abstract The main objective of this research was to improve flood mitigation within Rwanda's rapidly growing Kigali City using Geo-Information Technology (GIT) to identify flood hazard zones, analyze flood exposure and vulnerability, and suggest planning interventions. Multiple sources of data and methods were utilized including a very high resolution Quickbird image, Global Positioning Systems, interviews and a survey that aided flood hazard zone delineation, flood depth interpolation and mapping. The flood exposure analysis incorporated vulnerable infrastructure, buildings, population and economic activities and revealed that 27% of buildings were located in flood prone areas. Additionally, two sensitive sectors of infrastructure, four sensitive economic sectors and approximately 500 people were identified as vulnerable. The results influenced policy because Kiruhura's major market was relocated to a new site and new urban developments were restricted from building within the flood way. The study developed a model for flood risk analysis adapted to the specificity of Kigali City, demonstrating the need to explicitly incorporate these risks into the recently developed Kigali City Master Plan. The research stresses the importance of the integration of flood risks (and natural risks, in general) into major national development strategies, policies and laws related to Rwanda's urbanization.

Keywords Rwanda · Flood modeling · Flood management · Developing country · Africa

---

J.P. Bizimana (✉)
Geography Department, Faculty of Sciences, National University of Rwanda,
Affiliated Researcher at CGIS-NUR Butare, Rwanda
e-mail: bizijp@yahoo.fr

At the time of writing, Dr. Michele A. Schilling was a Senior Lecturer in the Geography Department, Faculty of Sciences, and an Affiliated Researcher in the Geographic Information Systems and Remote Sensing Centre of the National University of Rwanda. As founder and Director of the Center (2001-2007), Schilling was instrumental in the development of a GISc-based Education and Research program at the University and in Rwanda.

P.S. Showalter, Y. Lu (eds.), *Geospatial Techniques in Urban Hazard and Disaster Analysis*,
Geotechnologies and the Environment 2, DOI 10.1007/978-90-481-2238-7_6,

6.1 Introduction

Urbanization in flood hazard zones creates a challenge as urban areas accommodate higher concentrations of people, buildings and infrastructure (Wamsler 2004). Despite increasing flood risk awareness, human settlements continue to develop in flood-prone areas due to the need for land, and poverty (Gupta 1994). These conditions reflect reality for the urban poor who are faced with little option other than to illegally occupy public land or purchase affordable land in hazard zones (Montoya 2006).

Recently, this general relationship between urbanisation and informal settlement growth in flood-prone areas has been observed in Kigali, capital of Rwanda (MINITERE/Rwanda 2004). Rwanda, known as the "Country of a Thousand Hills", has a topography characterized by steep hills and mountains. While these characteristics generate landscapes of exceptional beauty, they also pose serious challenges for urban planning in Kigali.

Kigali City, which is located on interlocking hills separated by valleys and swampy areas, has little land for urban development. According to the recent Kigali City Master Plan, most informal developments in the city are located in wetlands or on steep slopes where 12% of the built-up areas are already located on land unsuitable for development (MININFRA/Rwanda 2006). This situation is aggravated by cumbersome legal procedures that discourage access to land by the urban poor. As noted by Duran Lasserve (2005), the urban poor (such as those in Kigali) cannot comply with construction standards and regulations, so find themselves living in slums.

Recognition of the increased vulnerability of people and infrastructure to the threat of flood loss in Kigali stimulated the need for a robust assessment of risks in flood-exposed informal settlements, and the complexity of the problem called for the application and adaptation of contemporary Geo-Information Technologies (GIT). The research applied existing GIT-based approaches for flood risk analysis of rapidly growing and unplanned settlements in Kigali City to improve urban planning and policy formulation by decision makers. Table 6.1 provides the sub-objectives and research questions defined for the study.

Table 6.1 Objectives and research questions

Sub-objectives	Research questions
Identify the flood zones in the study area.	■ What locally measurable indicators can be used to identify flood hazards? ■ What is the extent of flood hazards in the study area?
Analyze flood exposure and identify elements that are highly exposed to flooding	■ What indicators can be used to analyze exposure to flooding? ■ What elements are exposed to flooding?
Analyse flood vulnerability	■ What are suitable indicators for identifying vulnerability to flooding? ■ What was the impact of the last flood event on buildings, infrastructure, population, and economy in the study area?

Table 6.1 (continued)

Sub-objectives	Research questions
Suggest effective planning strategies to mitigate the risks of flooding along the Nyabugogo River	■ What are the expected losses or damage to property when the next flood occurs? ■ What are the implications for future policy development for areas along the Nyabugogo River? ■ What policy is needed to prevent urban expansion in flood-prone areas along the Nyabugogo River?

6.2 Flood Risks

6.2.1 Urban Flooding: The Global Context

Dartmouth University's flood database reveals that flooding has killed about 300,000 people between 1985 and 2006. From January to October 2006 alone, more than 6790 people died while 17,336,000 people were displaced around the world due to floods (University of Dartmouth 2006). A single event, a tropical cyclone flood in 1991, killed 138,000 people in Bangladesh. In Africa, approximately 980 people died and more than 500,000 were displaced by floods in 2006 (University of Dartmouth 2006).

Asian countries are more affected by floods due to monsoonal rain, high population density in the cities, and lack of planning regulations and flood controls (Nelson 2006). However, the West is not immune to the problem, as was dramatically illustrated by the flooding of New Orleans in 2005 – 80% of the city was inundated, mainly due to the breaching of 53 different levees. And, in view of the recent damages caused by successive hurricanes worldwide in 2008, the threat of flooding seems to be on the increase (Dartmouth Flood Observatory).

In general, flood losses have greatly increased over the years due to land-use change, urbanization of flood-prone areas, sub-standard construction, and high population density (Guarin et al. 2004). Cities are more affected by floods than rural areas due to high population densities and concentration of economic activities (Merson et al. 2004; Montoya 2003). Urban floods are intensified by impermeable surfaces and runoff concentration, and by buildings that obstruct water flow. Mendel (2006) describes four types of urban flood: (1) localized – occurs many times a year especially due to increased runoff and poor drainage conditions; (2) small stream – water rises quickly with high flows that exceed drainage capacity if channels are not regularly maintained; (3) river – results from upstream land use change and engineering works when dams and levees break, leading to sudden flooding downstream (urbanization of flood plains also impacts the natural river overflow and increases the possibility of flooding); (4) seasonal – when rain and river water combine to elevate water levels at certain times of the year. Urban areas in developing countries are at greater risk due to high population growth and rapid urbanization caused by rural-

to-urban migration. Large numbers of urban immigrants find themselves in fragile economic circumstances, which lead to the creation/expansion of informal settlements in high risk zones. Therefore, urban flooding increases with urbanization in flood-prone areas (Alkema 2003).

Fortunately, the United Nations Development Program's global report (UNEP 2004) states that urbanization doe not necessarily have to lead to an increased disaster risk and can, if properly managed, contribute to disaster reduction. When urban growth in flood hazard-prone locations is accompanied by proper building standards and planning considerations, the flood risk can be managed or even reduced. However, the complexity of the flood risk in urban areas suggests that high resolution data collection systems are required in order to identify patterns of flood hazard, vulnerability and exposure. Where the required data and information are lacking, urban flood risk assessment and monitoring poses a wide range of conceptual, methodological, and implementation challenges. Such is the case in Rwanda, and especially in Kigali City, where rapid urban development spreads out on steep slopes and in flood-prone locations where flood information is not regularly recorded.

6.2.2 Kigali City: Urban Growth and Rainfall Exposure

Kigali is the only official city in Rwanda. It is located in the central part of the country (Fig. 6.1).

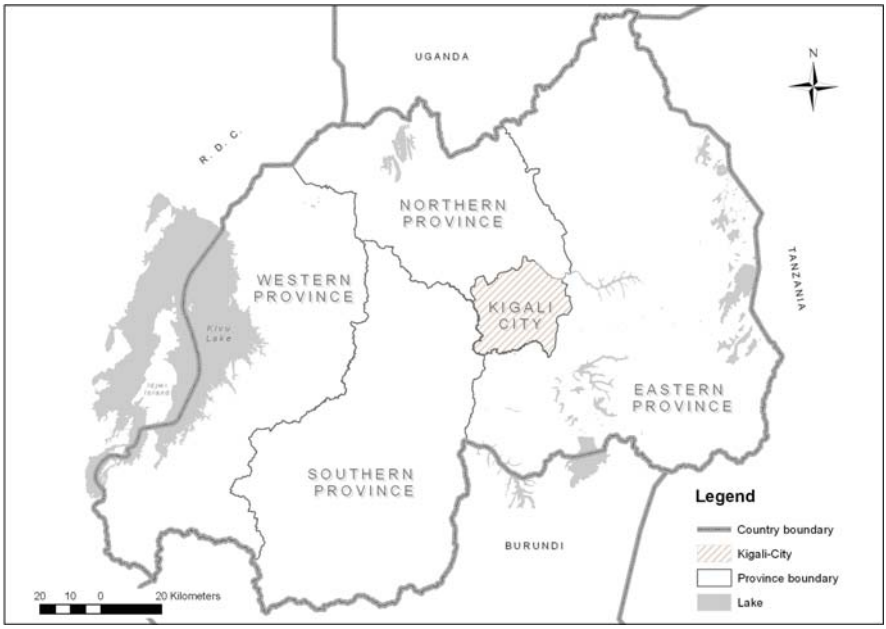

Fig. 6.1 Location of Kigali City in Rwanda.
Source: MINITRACO/CGIS-NUR, 2001 and NISR, 2006

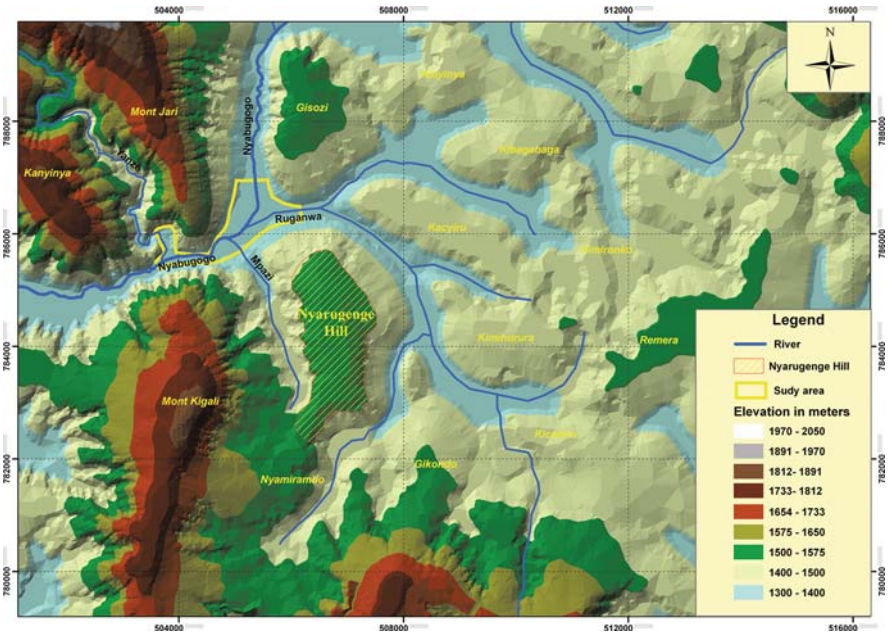

Fig. 6.2 Location of the study site
Source: Topographic map of Rwanda, 1988

The new administrative region of Kigali City is large and dominated by rural land use but also encompasses a mix of urbanized and urbanizing areas. The growth of Kigali City during the colonial period (from 1909 to 1962) was very slow and limited to the Nyarugenge hill (Fig. 6.2). Soon after independence, when all administrative functions were relocated to Kigali, the city extended beyond Nyarugenge hill to neighboring hills such as Nyamirambo, Gikondo, Kimihurura and Kacyiru (MININFRA 2006).

The study area (Fig. 6.2) lies near the original hill of Nyarugenge along Nyabugogo River, between the steep hills of Gisozi, Mont Jari and Kanyinya, Mont Kigali and Nyarugenge. Due to the steepness of relief and intense rainfall, the swampy valleys constitute hazardous locations for settlements and a drainage challenge, especially along Nyabugogo River.

From 1996 to 2002, Kigali City's population increased from 350,000 to 603,000, an increase of 42% (MINECOFIN 2002; MININFRAST 2004); the average annual growth rate is 2.6%. The current urban population is more than one million, located within a "built-up" area estimated to be 65.6 km^2 in size. Urban development is characterized by the coexistence of formal and informal growth, with the majority of people (83–85%) living in informal settlements (Aibinu 2001).

As Kigali City urbanized, people began occupying the Nyabugogo River's flood plains, raising the issue of flood exposure. Figure 6.3 illustrates this issue by showing the proximity of the Kiruhura Market to the river's waterway.

Fig. 6.3 Location of Kiruhura Market near Nyabugogo River Source: Photo Tordjeman, April 2003

Data from the closest weather stations to Kigali City show that the annual rainfall between 1992 and 2006 ranges from 900 to 1600 mm. The total annual rainfall within the city of Kigali averaged just over 900 mm (MININFRA 2006; MININFRAST 2004). Figure 6.4 illustrates that the western highlands and north-western parts of Kigali are receiving higher rainfall than regions further east. In the Nyabugogo River plain, the highest average annual rainfall varies from 1100 to 1600 mm.

The combination of intense rainfall, wetland areas, and steep slopes make the areas around Kigali City highly susceptible to risk of flooding.

6.2.3 Kigali: Recent Flood History

Due to the steepness of its terrain, intense rainfall (Sirven et al. 1974; Verdoodt 2003), and population pressure on land, many areas of Rwanda have been flooded in the last twenty years. In May 1988, a flood occurred in former Ruhengeri Province

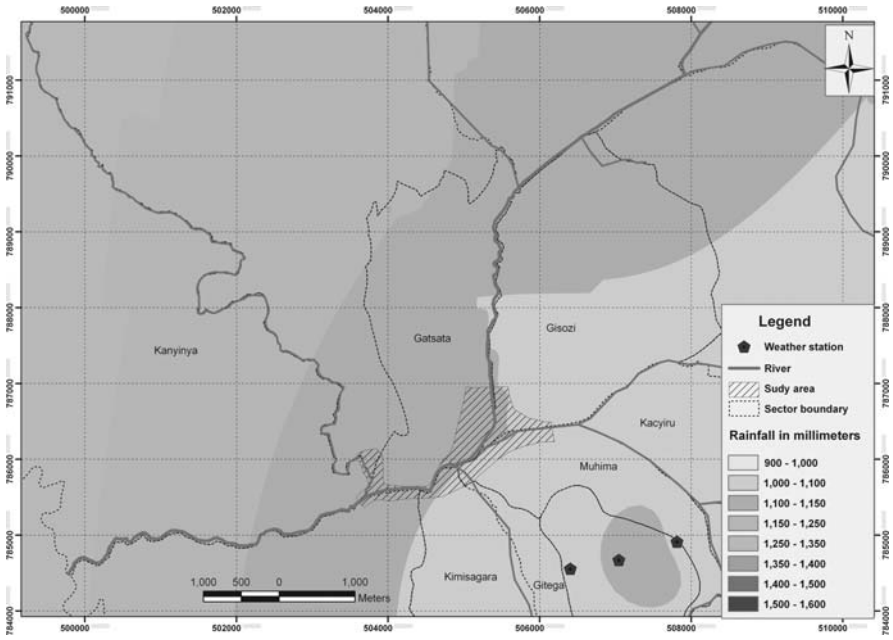

Fig. 6.4 Average rainfalls distribution for the study area from 1992 to 2006
Source: Rwanda Meteorological Services, MININFRA, 2006

(Byers 1992), during September and December 2001 floods damaged infrastructure and crops in west Rwanda (MININFRA/Rwanda 2004b) and another flood occurred that November in Kijote settlement (formerly Gisenyi Province) (University of Dartmouth 2006; USAID 2001). Recently, on 28 November 2006, 25 people died in Rulindo district when the Base River burst its banks and swamped a village. Similarly in Rubavu District (Western Province) during a flood in September 2007, houses were flooded and people died (New Times[1]).

In April 2002, the main road connecting traffic between Rwanda's two major cities (Kigali and Butare, now Huye) was cut off at Nyabarongo Bridge and became temporarily impassible. This situation created traffic congestion. More recently, a flood in April 2006 destroyed 40 houses and resulted in two deaths (New Times,10 April 2006). The Kiruhura market in the Nyabugogo River plain (Fig. 6.3) is located in a narrow valley between two steep mountainous areas and the river overflowed into the shops reaching 1.5 m in height. The 132 small shops had to be temporarily relocated upstream. In May 2006, the Kigali City council decided to relocate the market to a new site free of flood hazard risks. Similarly, the RWANTEXICO factory was flooded to 1.5 m and ceased functioning (Fig. 6.5).

The cases described above show that repeated flooding is becoming a serious problem and challenge for urban and regional planners in the City. The flood chal-

[1]New Times, Rwanda daily newspaper (www.newtimes.co.rw)

Fig. 6.5 Flood level observed in RWANTEXICO floods of April 2006
Source: Photo taken by Jean Pierre Bizimana, September 2006

lenge requires that new strategies and mitigation measures be implemented in areas identified as being at risk of floods.

6.3 Flood Risk Analysis: Conceptual Frame and Analytic Steps

6.3.1 Analytic Components of Flood Risk Analysis

The key concepts underpinning this research are flood hazard, flood exposure, flood vulnerability and flood risk. Although often used interchangeably, these terms have meanings that communicate slightly different ideas (Zeigler et al. 1983). The flood hazard denotes the probability and severity of occurrence of a flood of a certain magnitude (Alkema 2003). The flood exposure refers to the extent to which property, buildings, economic activities, infrastructure and population are located in relationship to a flood hazard (Barroca et al. 2006; McEwen et al. 2002). Flood vulnerability encompasses physical, social, economic and environmental factors which increase susceptibility to the flood hazard (UN/ISDR 2004a). Flood risk represents expected loss or damage to property, loss of human life, and interruption of economic activities due to flooding. Flood risk depends on flood hazard, exposure and vulnerability (Davidson 1997). For example, if buildings are located in a flood plain, both hazard and exposure are present, but if the buildings are perfectly resistant to floods, vulnerability is absent, so there is no flood risk. As another example, consider an empty plot of land within the flood plain – the hazard is present but both exposure and vulnerability are absent, so there is no flood risk for that property (Fedeski and Gwilliam 2007).

When analyzing flood risks, some basic questions flood analysts might ask are: What can go wrong in the case of flooding? How likely is it that it will happen? If it does happen, what may be the consequences? What can be done to eliminate flood occurrence or reduce the risk of flooding? (Zeigler et al. 1983). Geographers are interested in spatial questions such as: Where will the flood occur? How likely is it that a flood hazard will happen at this place? If it is flooding, what will be the event's geographical extent and impact? How can the space be managed to reduce flood risks? Answering these questions can help identify effective planning strategies to mitigate the risks of flooding.

Different frameworks have been developed to identify flood hazards and risks (Barredo et al. 2005; Davidson 1997). One such study used the flood hazard, exposure, vulnerability and capacity indicators to analyse the flood risk in the Volga River Basin, Russia (UNU-IEHS and NNSUACE 2006; Fig. 6.6). But this proposed framework does not contain suitable indicators for flood risk analysis in Kigali City. The capacity component can not be assessed for this research as the necessary data are lacking or difficult to acquire in the study area. Consequently, the framework has been altered, as shown in Fig. 6.7.

The framework in Fig. 6.7 is instructive but highly generalized. Therefore, a clearer explanation of flood risk indicators is necessary. The next section of this chapter discusses our attempt to identify indicators for each component and describes how these components can be analyzed.

6.3.2 Flood Hazard Identification and Mapping

Various definitions of flood hazard have been provided. According to Alkema (2003), flood hazard represents the probability of occurrence at a certain level

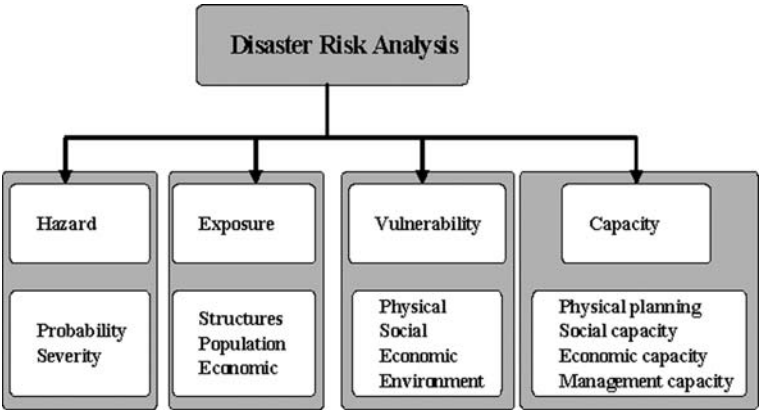

Fig. 6.6 Framework for flood risk analysis
Source: Modified from UNU-IEHS and NNSUACE, 2006

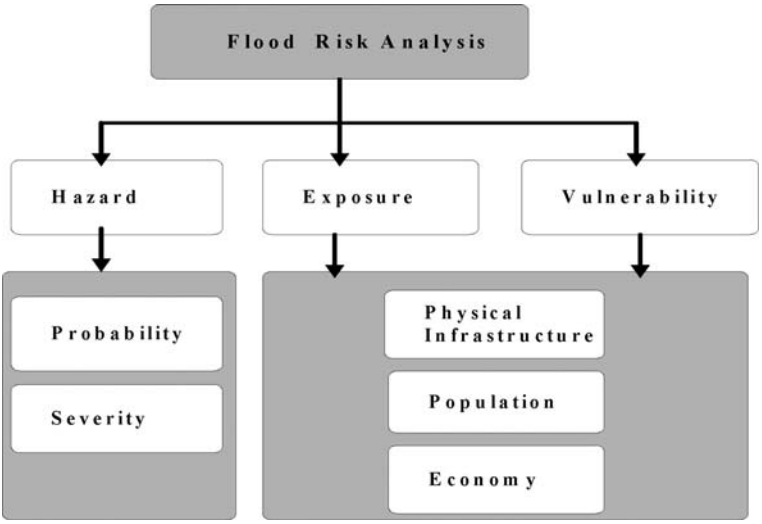

Fig. 6.7 Modified framework for flood risk analysis
Source: Modified from Davidson 1997 and UNU-IEHS/ NNSUACE, 2006

of severity. Flood severity is characterized by water level, flood duration and velocity, while probability refers to flood frequency (Alkema 2003; Barroca et al. 2006). Other authors add to the definition warning time, the rate at which the water rises, accessibility to flooded areas, and level of development (which may impede or improve access) to characterize flood hazards (New South Wales 2005). Similarly, the Disaster Management Programme of the United Nations Commission for Human Settlement has recommended consideration of the following indicators: flood rate, load sediments, volume of water, duration and area affected (UNCHS-Habitat 2001). As can be seen by the above, one approach to flood analysis is largely based on physical characteristics (depth, duration, velocity, frequency, extent, flood size, and load sediments), and another approach on response variables (warning time, readiness, rate of rise and access). This research emphasizes the physical characteristics with a focus on measurable indicators such as flood depth, frequency, and duration.

When a flood hazard is identified, the next step may be flood mapping. This step identifies and displays the spatial variation and extent of the flood (Noson 2002). To fulfill this step, one approach is based on historical records of flood characteristics where flood depth is the main indicator (Islam and Sado 2002). Sanyal and Lu (2005) argue that a higher flood depth is associated with a higher discharge of water which determines the extent of flood-induced flood damages. The flood level is defined as the highest level reached by water above the local height datum. The flood extent map defines how far a given water level will locally extend. Based on flood level, different methodologies have been developed to generate flood extent maps. MacKinnon (2004) derived flood extent from a digital elevation model (DEM) by separating pixel values into areas below and above the high

flood level, thereby delineating areas that would or would not be flooded. To assess potential flood damage, flood depth and extent were modeled by giving pixels at water level values of zero to enable pixels below water level to have positive values depending on their "depth". Then, using the flood extent map, the flood depth raster map was clipped to display flood depth values solely within the extent of the flood (MacKinnon 2004). Tennakoon (2004) reclassified the flood depth pixel values into different flood hazard zones, with 0.8 and 1.2 m representing the upper limits of low and medium flood, respectively. The present research is based on MacKinnon's and Tennakoon's approach.

While spatial extent and flood depth are commonly used for flood mapping, it is also quite useful to integrate flood duration and velocity (Tennakoon 2004) to help evaluate flood severity. However, duration has not been integrated into many flood hazard studies due to the data and expertise cost of its estimation (Tennakoon 2004), which requires hydrologic modeling. These constraints, as well as the lack of reliable hydrological records for the study area, preclude the use of flood duration data in this research.

When there are no flood records, remote sensing technology can be used to map flooded areas if satellite images have been acquired during the flood's peak (Prathumcha and Samarakoon 2005). While estimating flood depth from remote sensing images is very difficult, indirect methods based on the amount of energy reflected by water have been developed (Sanyal and Lu 2005). However, such estimates require advanced satellite image processing capability utilizing radar (e.g., Synthetic Aperture Radar). Although radar imagery can penetrate cloud cover, its use in developing countries such as Rwanda is constrained by its high price and limited spatial and temporal coverage due to the lack of ground receiving stations.

6.3.3 Flood Exposure

Flood exposure is the extent to which properties, houses, economic activities and infrastructure are geographically situated in flood-prone areas (Barroca et al. 2006; McEwen et al. 2002). Exposure relates the floodplain, people's location and closeness to the area of inundation, and housing/property characteristics to one another. The relationship between flood exposure and vulnerability of exposed elements is directly proportional: as exposure increases, vulnerability increases. Accordingly, there is no vulnerability to flooding where there is no flood and there is no vulnerability if no elements are exposed (Goosby et al. 2005).

Flood exposure analysis identifies flood-prone areas and the elements within them that are exposed to flooding. The physical characteristics of the flood are examined and information about exposed elements (proximity to river, location in or closeness to flood plain) provided. In urban areas, elements at risk may include properties, buildings, infrastructure, population, environment, cultural assets and economic activities (Messner and Meyer 2006). To document exposure requires knowledge about the number of people, buildings, critical facilities and infrastructure (e.g., roads, bridges), and land use types (e.g., residential, commercial, industrial, agricultural) within flood prone areas (Barredo et al. 2005).

6.3.4 Flood Vulnerability Assessment

There are three main approaches to assess flood vulnerability: physical, social context, and combined (or global). The physical approach focuses on human occupancy of flood zones, degree of loss, flood characteristics, and flood impacts (Messner and Meyer 2006). This approach determines how exposed people, physical objects and activities may be affected (Davidson 1997). Physical vulnerability can be assessed through examining infrastructure, housing, economic activities, geographic location and population density. Exposed elements (e.g., residential houses, infrastructure, industrial or commercial activity, health services) have different degrees of vulnerability when located in the same flood-prone area (Barroca et al. 2006). Some mechanisms such as location of structures, structure types, their ability to resist flood damage, and tendency to flood can turn a mundane flood into disaster by increasing physical vulnerability to the flood (Blaikie et al. 1994).

Social vulnerability approaches examine the social context of floods as it relates to the coping response of communities (Messner and Meyer 2006). In this context, flood vulnerability analysis examines how well prepared and equipped a community is to avoid or cope with floods (Etkin et al. 20043). Coping includes the adaptive capacity of a system or people to deal with floods or reduce flood risk. Another aspect relates to the knowledge of exposed people as is studied by examining awareness and perception. When aware of the flood risk, individuals or societies are able to adapt. They may modify urban development plans or change building techniques (Barroca et al. 2006). Flood vulnerability can also be assessed by documenting the lack of ability or unwillingness of planning authorities to reduce the flood risk (Messner and Meyer 2006).

The global approach combines the physical and social approaches by including physical, social, economic and environmental factors (UN/ISDR 2004a). According to Barroca et al. (2006), this approach is gaining increasing significance in scientific research. This research sees flood vulnerability as a combination of the characteristics and location of properties, buildings, housing, infrastructure, population, and economic activities in terms of their capacity to anticipate, cope with or resist floods. Identifying the strengths and weaknesses of the exposed elements and relevant stakeholders allows decision makers to effectively allocate limited resources to prevent or mitigate the effects of the floods (UN-Habitat and UNEP 2001).

6.3.5 Flood Risk Indicators

Following the above description of the main aspects in flood risk analysis, the analytical framework and the associated indicators for this urban flood research is presented in Fig. 6.8. This framework considers three main components of flood risks and corresponding indicators. If data are locally available, they can help identify flood-prone areas, determine exposed elements, and analyze vulnerability to flooding. Unfortunately, reliable, timely data are difficult to obtain in developing

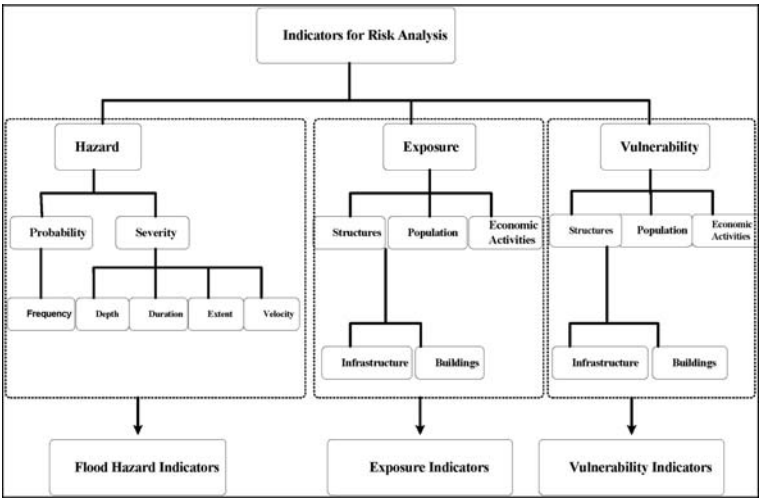

Fig. 6.8 Indicators for flood risk analysis
Source: Adapted from Davidson 1997 and UNU-IEHS and NNSUACE, 2006

countries; in some cases, the information may be known but not adequately communicated to, or perceived by decision makers (Bacic-Ivan et al. 2006) who seek to formulate flood risk reduction strategies. In this study, GIT is utilized as most of the data are spatial in nature (Beerens 2006; Montoya 2006). Using GIS and remote sensing to identify and help visualize flood risks can improve understanding and therefore help reduce the impact of flooding.

6.4 Research Methods and Findings

6.4.1 Data Collection

This research has been guided by an extensive literature review of research articles, government reports and policy documents analysis. Secondary data and primary data were both used. Secondary spatial datasets consist of a Quickbird multispectral satellite image acquired on 26 December 2004 with a resolution of 2.82 m (available from CGIS-NUR[2]), aerial photos taken in 2003 above Kiruhura market, existing spatial datasets (boundaries, roads network, river streams) derived from topographical maps of Rwanda (1:50,000 sheet, Kigali 1988), and meteorological data linked to the weather stations. Primary data consist of field observations, photography, interviews with urban planning authorities at sector, district and city levels and a household survey (including GPS location data of housing

[2] *Geographic Information Systems and Remote Sensing Training and Research Center of National University of Rwanda.*

units). This survey was conducted during September 2006 with 120 households. The survey sample was selected within or along the Nyabugogo flood plain in areas that experienced the April 2006 flooding and within a distance of 20 m from the flood plain (the distance was chosen because construction is not allowed in closer proximity to the floodplain) (Primature-Rwanda 2005). Sampling was based on proximity to the riverbank or flood plain, experience with floods, and occupation by infrastructure, properties, housing or settlements. In collaboration with community leaders, flooded areas were delineated using the Quickbird satellite image aided by local knowledge about flood extent in the study area. To generate building footprints and other critical land uses in the study area, the Quickbird image was georeferenced and digitized on a computer screen using ArcGIS® 9.2 software.

6.5 Flood Risk Analysis: Identifying and Mapping Flood Hazard-Prone Areas

As discussed earlier, the flood hazard consists of probability and severity. Because of data limitation, the analysis focused on severity. Flood severity was assessed using flood depth and flood extent. To identify the flood hazard areas, the flowchart in Fig. 6.9 illustrates the methodology used to generate the flood map. The input data were contour lines, the Quickbird image, and flood depth information from the household surveys. The flood hazard map was generated through the delineation of the flood plain extent using information from local experts at the district level, Digital Elevation Model (DEM) quality improvement, extraction of elevation information at the houses (point location of flood depth), subdivision of the study area into two zones, flood depth interpolation and flood depth mapping based on average house elevation in each zone.

6.5.1 Data Quality Control and Preparation

As the study area occupies a narrow valley between two highlands, the lowest elevation was not shown by the lowest contour line of 1375 m. However, most of the household samples were located below 1375 m. Therefore, an alternative approach was needed to improve the low resolution DEM. Based on methodology developed by Hengl et al. (2004), the resolution was improved by digitizing a supplementary contour line and interpolating other intermediate contour lines that indicate small morphologies not indicated on the topographic map. The new value of the digitized contour line was assigned using spot height values of the river in the topographic map. The final DEM was generated using an Inverse Distance Weighted Interpolation technique that calculates height value for any point that falls between two contour lines. The result is an improved DEM with new elevation contour lines in the flood plain, providing more topographical information regarding variation in elevation.

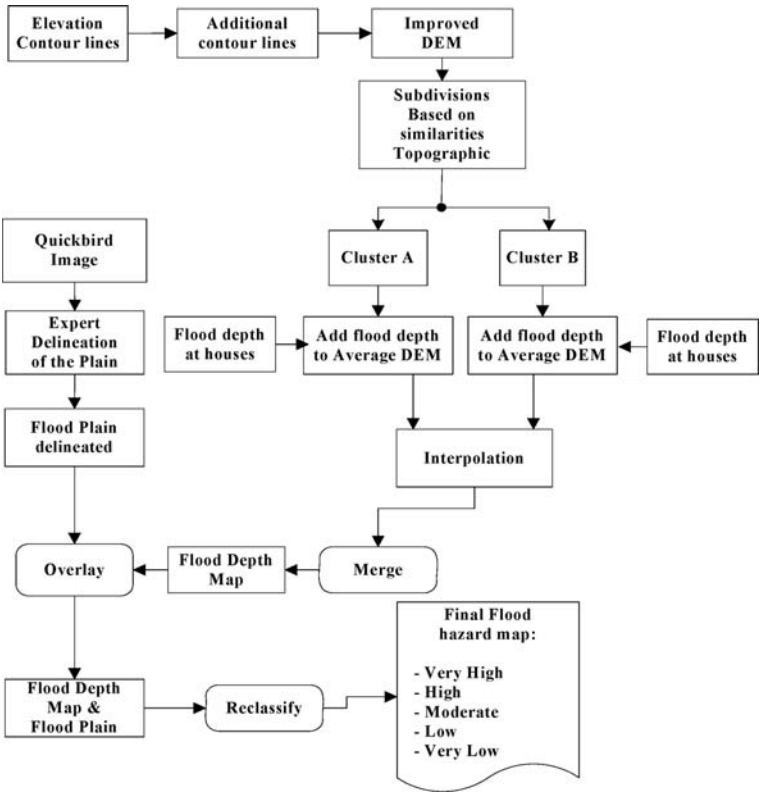

Fig. 6.9 Flowchart process for flood hazard mapping

Once the DEM was improved, a triangulated irregular network (TIN) was generated at 10 m pixel size. The 10 m pixel size was chosen because it illustrates more details in the valley. To obtain topographic information at each house, the household sample points digitized from the Quickbird image were superimposed on the TIN and elevation was extracted for each house's location (Fig. 6.10). This way, the resolution of the DEM was improved to help extract topographic information needed for flood hazard mapping.

6.5.2 Mapping Flood Extent and Depth

The data used for flood extent mapping were obtained from official interviews at the district level. To identify the flood extent, the flood plain was delineated by local experts and digitized from the Quickbird image. The flood depth from household surveys was estimated based on watermarks found on the houses with reference to the ground. To obtain data of flood depth, the observed flood depth at a house

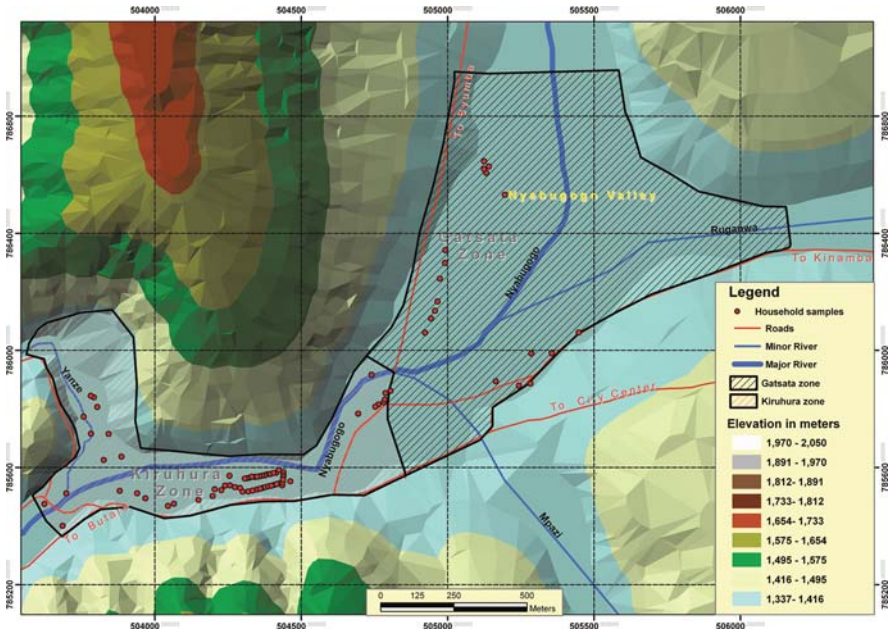

Fig. 6.10 Topography and location of surveyed houses
Source: Topographic map of Rwanda, 1988

location was first added to the corresponding elevation value from the DEM; interpolation was then conducted to generate a flood depth surface. However, the elevation of the study area varied greatly (from 1368 to 1377 m) within a very small area and flooding is strongly influenced by flatness or steepness of topography. For example, different houses experienced the same degree of flooding (1.00 m of flood depth) while being located in areas of great difference in elevation (4 m of elevation difference). Thus, interpolating flood depth based on elevation would not produce an accurate result. To solve this issue, it was decided to analyze flood depth extent in two subdivisions based on the topographic similarities of the house samples (zones with almost the same altitudes and slopes). Figure 6.10 illustrates that the two flood zones are largely separated by the paved road to Byumba.

Data for a runoff flood were not integrated because that type of flood is very localized. The flood map was generated by interpolating flood elevation values based on average elevation of flooded houses and presents the spatial distribution of flood level, from a very low to a very high flood. The corresponding flood class values are listed as: very low (0−0.30 m), low (0.30−0.60 m), moderate (0.60−0.90 m), high (0.90−1.20 m) and very high (1.20−1.50 m). Based on flood depth distribution, three high flood zones are distinguished (Fig. 6.11). The first zone in the southwest lies near the confluence of the Yanze and Nyabugogo Rivers. The second zone is located near the Kiruhura market where buildings obstruct the flood ways and delay or hold back water flow. The third zone (northeast) is on very flat

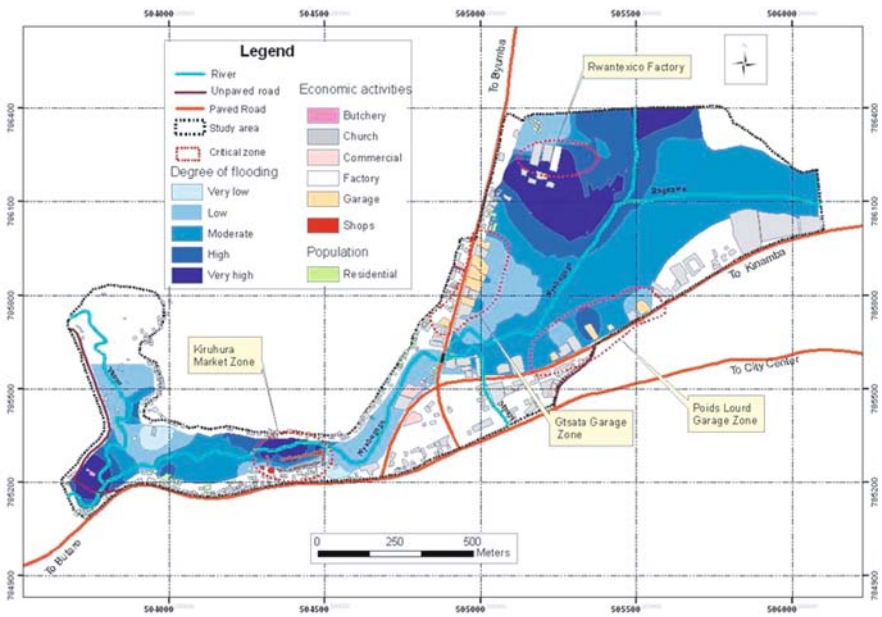

Fig. 6.11 Flood exposed economic activities in Nyabugogo valley

terrain where Nyabugogo valley is located. This zone is swampy and acts to store large amounts of water during the rainy season. Interestingly, a runoff flood was located in the Gatsata zone caused by poor drainage infrastructure (an inadequate bridge and closed culverts). Nevertheless, this finding was not incorporated into the analysis because it is much localized and strongly dependent on topography and/or drainage infrastructure.

6.6 Flood Risk Analysis: Analyzing Flood Exposure

After mapping the flood depth, information about elements at risk (e.g., buildings, roads, bridges, water supply, population, economic activities) were overlaid on the flood zones. Figure 6.12 presents a flowchart that describes the methodology used to estimate the exposed elements in each flood zone.

The flood exposure analysis was performed by locating exposed elements in relation to flooding. The result of the analysis revealed that 27% of buildings were located in flood prone areas in addition to two sensitive zones of infrastructure, and approximately 500 people. Four sensitive economic zones were also identified as exposed: Kiruhura Market, Gatsata Garage, Poids Lourd Garage and Rwantexico factory (Fig. 6.12). The Kiruhura market is located in a high flood zone, in the flood way of Nyabugogo valley. The market's location makes it prone to seasonal river flooding. Moreover, the concentrations of buildings (mainly shops) are not only

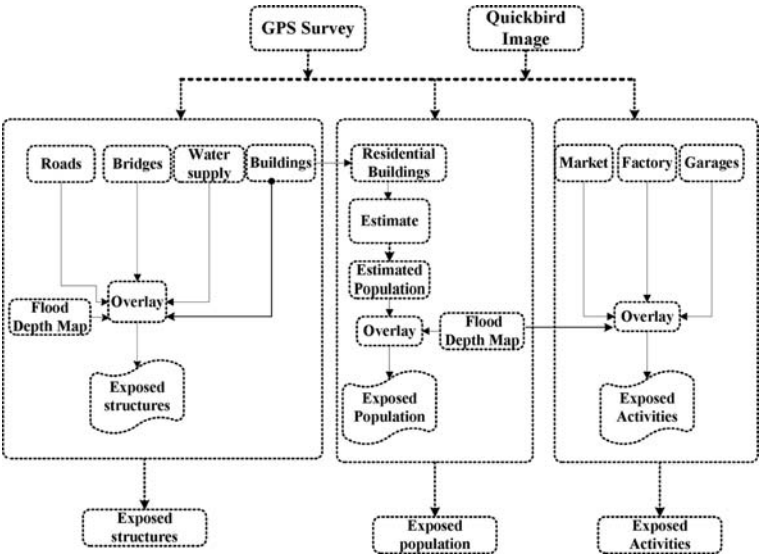

Fig. 6.12 Flowchart process for flood exposure analysis

exposed to flood, but also contribute to flooding by blocking water flow. In the Gatsata and Poids Lourd Garage zones, the flood exposure is related to their location in flood storage areas. Some buildings are located in a swamp so they are exposed to seasonal floods and groundwater movements. Finally, the Rwantexico factory zone is located in a high flood risk zone within the Nyabugogo floodplain. Due to the flooding, this factory stops functioning during rainy season.

It was not feasible, within the scope of this research, to conduct an analysis for every type of infrastructure. Therefore, the analysis focused on those parts of the physical infrastructures considered important by local authorities at the district and sector levels. These types of infrastructure include roads, bridges and water supply lines. Bridges and water supply lines were visited and located using GPS during field observation, while roads were digitized from the Quickbird image. Subsequently, the roads, bridges, water supply lines, and buildings were overlaid on the flood hazard zone map for exposure analysis. The flood depth values used in this analysis are based on watermarks left on houses after the flood of April 2006.

Figure 6.13 displays the distribution of exposed infrastructure relative to the flood zone. For example, in the southwest, the Yanze Bridge is located in a high flood zone near the confluence of the Yanze and Nyabugogo Rivers. At this location, a bridge and a water supply line for Kigali City are regularly swept away by overflows during the rainy season. The heavy load of sediment carried by flash floods from mountainous areas cut the water supply lines resulting in drinking water contamination (MININFRA/Rwanda 2006). In the central part of the study area, the Nyabugogo Bridge on the Kigali-Gatuna asphalt road is a piece of critical infrastructure that, even though located outside the high flood zone, is affected by overflow at the

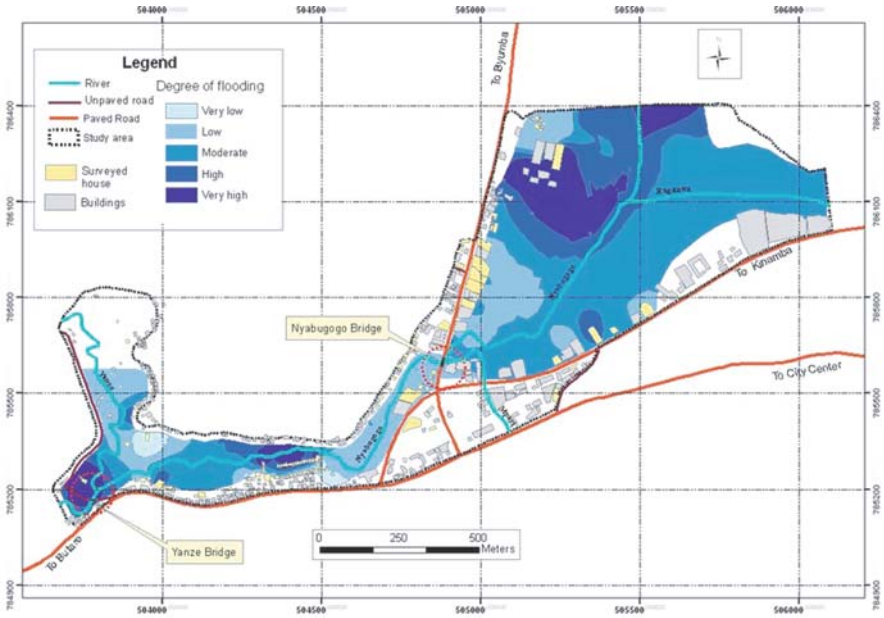

Fig. 6.13 Buildings and infrastructures in flood-prone areas

confluence of Nyabugogo and Mpazi Rivers. The problem is aggravated by the fact that the natural flow of the river was changed to create plots for new houses. The road and bridge are being eroded by water from the Nyabugogo River, which has been redirected from its natural flow.

6.7 Flood Risk Analysis: Analyzing Flood Vulnerability

Figure 6.14 summarizes the framework used for flood vulnerability analysis in the study area. Housing vulnerability was estimated by recording three variables: type of wall material, foundation, and vulnerability of the water supply line. Analysis of population vulnerability was based on the level of flood protection and flood mitigation activities. Lastly, vulnerability of critical economic activities (e.g., market, factory) located in the flood prone areas were estimated.

The general trend shows a higher proportion of collapsed buildings in the high flood zone (62.5%) than in the low flood zone (37.5%). Figure 6.15 shows the vulnerability of buildings by virtue of their location.

Masonry and wood houses constituted 31% of the total sample of visited houses (120). Of the masonry houses, severe building damage was observed in 87% of the cases while only 13% of the wood houses suffered the same level of damage. The three types of foundation found in the study area were stone in mortar (57%), stone

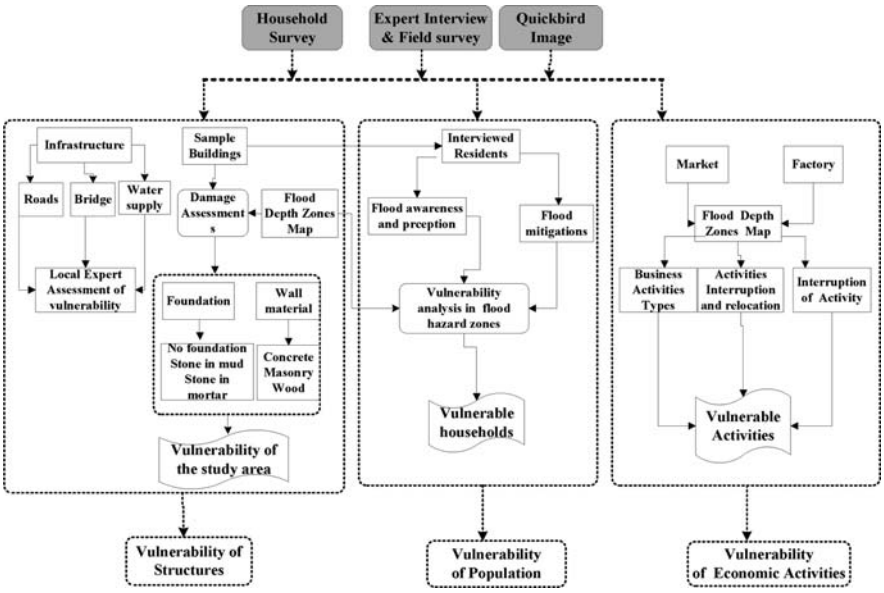

Fig. 6.14 Flowchart process for flood vulnerability analysis

Fig. 6.15 Vulnerability of housing by location. Collapsed house in swampy area; A house near the river stream
Source: Photo taken by Bizimana, September 2006

in mud (21%), and buildings without a foundation (22%). Interestingly, the quality of foundation did not reveal a clear difference as related to flood damages.

As for the recovery of the buildings following the flood, few buildings (16%) were repaired. The main reasons people did not pursue repairs were regulatory constraints from district authorities and the ongoing relocation process.

Fig. 6.16 Inadequate flood protection measure
Source: Photo taken by Jean Pierre Bizimana, September 2006

Unfortunately, damaged buildings that remain un-repaired are more vulnerable to the next flood.

Flood protection measures (as applied by respondents) were also examined in an effort to better understand vulnerability. Sixty percent of the respondents did not attempt to implement flood protection measures (e.g., open up drainages, raising the parcel's elevation, water proofing, sandbags, relocation). Some measures (e.g., sand bagging) cannot efficiently deal with the magnitude of flooding (Fig. 6.16). Due to poverty, many owners can only use sandbags in an attempt to prevent water from entering their houses. The fact that houses occupy the flood zone implies inadequate flood mitigation planning to protect vulnerable groups in the Nyabugogo flood plains within Kigali City.

Another situation that exacerbates flooding is the poor drainage system. Figure 6.17 shows efforts to open closed culverts on the former drainage channel of Mpazi River before its confluence with Nyabugogo River. Simultaneously, other people were attempting to excavate the river stream by removing solid wastes dumped into the river near the Gatsata garage zone. These local initiatives to improve the drainage conditions are having limited success, however, because other people continue to dump solid wastes into the river stream, even though such activity is strictly forbidden by existing environmental law. Therefore, to improve flood protection measures, assistance is needed for environmental law enforcement at the neighborhood level.

Fig. 6.17 Local initiatives to improve drainage conditions: (**a**) opening up of closed culvert; (**b**) excavation of Nyabugogo River
Source: Photo taken by Bizimana, September 2006

6.8 Flood Risk Management and its Implications for Kigali City Planning

The research performed in this study indicates a direct correlation between risk of flooding and inadequate planning and control. Most of the recently constructed buildings have no building permit or land registration ownership; some (especially the garage and shops) were officially located in the swamp lands by municipal planning authorities.[3] The location of the Kiruhura Market, started in 1998 by shoe traders on a small scale, was purposely chosen in the flood plain because there the traders were less likely to be forcefully evicted by authorities.[4] Over time, the market attracted more and more people who then settled in the nearby flood-prone areas and on steep slopes. The new settlements and mixed shops increase the flood risk along the Nyabugogo River, and the situation is aggravated by illegal dumping of solid waste in the river (Primature-Rwanda 2005).

Planning interventions within Kigali City suffer from inadequate legislative sanctions on those who illegally occupy the flood plain and a lack of planning capacity to cope with rapid urban growth (Aibinu 2001). As a consequence, local authorities are now facing the challenge of demolition, relocation, and resettlement of exposed households and properties to reduce the risk of flooding. Future plans should include the prohibition of new urban developments in high flood-prone areas and the relocation of the buildings within highly flooded zones (approximately 110 buildings).

[3]Interview with local authority at sector level.

[4]Interview with traders in the former Kiruhura market.

6.9 Conclusion

The main objective of this research was to develop a GIT-based approach using locally available data to identify flood hazard zones, analyze flood exposure and vulnerability, and use the findings to suggest possible strategies for flood mitigation in unplanned settlements along the Nyabugogo River in Kigali City, Rwanda. GI Technology proves to be a necessary tool to locate the household samples and calibrate the flood depth by interpolation and delineate the flood plain extent. Associated with local perceptions about floods and very high resolution satellite imagery, the flood zone and exposure maps were produced.

While the research confirms the usefulness of GIT for flood risk analysis, it also reveals constraints associated with the availability of base data (e.g., topographic information). Very high resolution satellite imagery combined with GPS field survey data can be utilized for delineating flood plains and analysing flood risk for properties and infrastructure in a developing-world urban setting when other data are not readily available. Participatory GIS could also be explored as a method to improve flood vulnerability assessments by incorporating local population's knowledge into the database and, hence into flood risk models.

For planning and decision making purposes, this research revealed a number of constraints that increase the vulnerability of properties along the Nyabugogo River that are in need of adequate flood migration measures. First, the lack of reliable flood records makes it difficult to prevent urban development in flood risk zones. Second, there is a lack of awareness about construction techniques that can improve housing resistance to floods. Third, the majority of the residents are not using any flood protection measures. Fourth, there is inadequate intervention by urban authorities to improve and regularly maintain drainage along the Nyabugogo River, where most of the urban development is informal.

As an immediate strategy to reduce the risk of flooding within the Nyabugogo flood plain, Kigali City Planning needs to improve the poor drainage infrastructure which has been identified as the main cause of flooding. As mid- and long-term strategies, proper construction standards should be carefully designed and implemented and guidance provided regarding where urban development takes place and levels of infrastructure needed to reduce the impact of future floods. Such initiatives require a level of land use management that influences land availability and encourages those struggling with poverty to avoid living in hazardous locations. Finally, to minimize financial loss and to avoid the situation of having to relocate or resettle those living in the flood plain, a technical flood risk assessment should first be required during the land allocation process. Ultimately, this study highlights the need to further explore the potential of GIT to assist urban planners and decision-makers with formulating appropriate planning and policy strategies in order to limit flood losses in developing countries.

References

Aibinu, A., 2001. GIS Application in Urban Planning and Urban Management: Utilizing GIS in Kigali Urban Planning and City Management, CORP 2001, Vienna University of Technology.

Alkema, D., 2003. Flood risk assessment for EIA: Environmental impact assessment, an example of a motorway near Trento, Italy. In: Studi Trentini di Scienze Naturali: Acta Geologica, 78: 147–154.

Bacic-Ivan, L.Z., Rossiter, D.G. and Bregt, A.K., 2006. Using spatial information to improve collective understanding of shared environmental problems at watershed level. Landscape and Urban Planning, 77: 54–66.

Barredo, J.I., Lavalle, C. and Ad De Roo, 2005. European flood risk mapping; EC DG JRC – Weather Driven Natural Hazards, Joint Research Center, European Commussion.

Barroca, B., Bernardara, P., Mouchel, J.M. and Hubert, G., 2006. Indicators for identification of urban flood vulnerability. Natural Hazards and Earth System Sciences, 6: 553–561.

Beerens, S.J.J., 2006. Facing disasters with geo-information and earth observation: the UNU – ITC programme for disaster geo-information management: Keynote. Presented at ICAST 2006: 17th International Conference on Advances in Space Technologies, 2–3 September 2006 Islamabad, Pakistan, P. 7.

Blaikie, P., Cannon, T., Davis, I. and Wisner, B., 1994. At Risk, Natural Hazards, People's Vulnerability, and Disasters. Routledge, London.

Byers, A.C., 1992. Soil loss and sediment transport during the storms and landslides of May 1988 in Ruhengeri prefecture. Rwanda Natural Hazards, 5(3): 279–292.

Davidson, R., 1997. A multidisciplinary urban earthquake disaster risk index: EERI annual student paper award. Earthquake Spectra, 13(2): 211–223.

Duran Lasserve, A., 2005. Dealing with market eviction processes in the context of developing cities, Third World Bank Urban Research Symposium on Land Development, Urban Policy and Poverty Reduction, Brasilia, April 2005.

Etkin, D., Haque, E., Bellisario, L. and Burton, I., 2004. An Assessment of Natural Hazards and Disasters in Canada: A Report for Decision-Makers and Practitioners. The Canadian Natural Hazards Assessment Project.

Fedeski, M., and Gwilliam, J., 2007, Urban sustainability in the presence of flood and geological hazards: The development of a GIS-based vulnerability and risk assessment methodology. Landscape and Urban Planning, 83: 50–61.

Goosby, S., Chiesa, C., Mielbrecht, S. and Bosse, T., 2005. Assessing and reducing the impacts of disasters in the Asia Pacific Region, Pacific Disaster Center, First International Conference on Urban Disaster Reduction, Kobe, Japan.

Guarin, G.P., Westen, C.J. and Montoya, L., 2004. Community-Based Flood Risk Assessment Using GIS for the Town of San Sebastián, Guatemala. International Institute for Geo-information Science and Earth Observation (ITC).

Gupta, T.N., 1994. Vulnerability of Houses in hazard Prone Areas, The World Conference on the International Decade for Natural Disaster Reduction (IDNDR), Yokohama, Japan; May 23–27, 1994.

Hengl, T., Gruber, S. and Shrestha, D.P., 2004. Reduction of error in digital terrain parameters used in soil-landscape modelling. International Journal of Applied Earth Observation and Geoinformation, 5: 97–112.

Islam, M.M. and Sado, K., 2002. Development priority map for flood countermeasures by remote sensing data with geographic information system. Journal of Hydrologic Engineering, 7(5): 346–355.

MacKinnon, E., 2004. Three Dimensional Flood Modeling with High Resolution LIDAR; Applied Geomatics Research Group/Center of Geographic Sciences. Nova Scotia Community College (NSCC), Middleton, NS.

McEwen, L., Hall, T., Hunt, J., Dempsey, M. and Harrison, M., 2002. Flood warning, warning response and planning control issues associated with caravan parks: the April 1998 floods on the lower Avon floodplain, Midlands region, UK. Applied Geography, 22: 271–305.

Mendel, G., 2006. Climate Change, Urban Flooding and the Rights of the Urban Poor in Africa: Key Findings from Six African Cities, Action Aid International, London -Johannesburg.

Merson, M.E., Montoya, L. and Paresi, C., 2004. Manage data – manage hazards: development of urban hazard information infrastructure for the city of Windhoek Namibia. Management of Environmental Quality: An International Journal, 15(3): 276–293.

Messner, F. and Meyer, V., 2006. Flood damage, vulnerability and risk perception-challenges of damage research. In: Schanze, J., Zeman, E. and Marsalek, J. (Editors), Flood Risk Management-Hazards Vulnerability and Mitigation Measures, Leipzig.

MINECOFIN, 2002. The 3rd General Census of Population and Housing in Rwanda, Kigali.

MININFRA, 2006. Document de politique nationale d'urbanisation, Kigali, Rwanda.

MININFRA/Rwanda, 2004b. Generation and Application of Climate Information, Products and Services for Disaster Preparedness and Sustainable Development in Rwanda; Ministry of Infrastructure. Rwanda Meteorological Service.

MININFRA/Rwanda, 2006. Kigali City Master Plan: Existing Condition Analysis; Prepared by the Master Plan Team for the Ministry of Infrastructure; Kigali.

MININFRAST, 2004. National Human Settlement Policy in Rwanda, Ministry of Infrastructure, Kigali.

MINITERE/Rwanda, 2004. Sectorial Policy on Water and Sanitation; Ministry of Lands, Environment, Forestry, Water and Mines; Kigali.

Montoya, A., 2003. Geo-data acquisition through mobile GIS and digital video: an urban disaster management perspective. Environmental Modeling & Software, 18: 869–876.

Montoya, L., 2006. Disaster Management. In: Hofstee;P (ed.), GIS for urban planning in developing world, International Institute for Geo-Information Science for Earth Observation (ITC), Enschede, Lecture Note.

Nelson, S.A., 2006. River Systems and Causes of Flooding. http://www.tulane.edu/˜sanelson/geol204/riversystems.pdf.Last updated on 27 March 2006.

Noson, L., 2002. Hazard mapping and risk assessment, Regional Workshop on Best Practices in Disaster Mitigation, Bali, Indonesia; 24–26 September 2002.

Prathumcha, K. and Samarakoon, L., 2005. Application of Remote Sensing and GIS Techniques for Flood Vulnerability and Mitigation Planning in Munshiganj District of Bangladesh. www.geoinfo.ait.ac.th/publications/ACRS2005_Prathumchai_K.pdf

Primature-Rwanda, 2005. Organic law determining the modalities of protection, conservation and promotion of environment in Rwanda. Official gazette of the Republic of Rwanda, 44(9): 22–42.

Sanyal, J. and Lu, X.X., 2005. Remote sensing and GIS-based flood vulnerability assessment of human settlement, A case study of Gangetic West Bengal, India. Hydrological Processes, 19(18): 3699–3716.

Sirven, P., Gotanegre, J.F. and Prioul, C., 1974. Geographie du Rwanda, Editions A. De Boeck., Bruxelles.

Tennakoon, K.B.M., 2004. Parameterization of 2D Hydrodynamic Models and Flood Hazard Mapping for Naga City, Philippines, ITC, Enschede, 101pp.

UN-Habitat and UNEP, 2001. Vulnerability Assessment: Tools to Support Participatory Urban Decision Making Process. United Nations Human Settlements Programme and United Nations Environment Programme.

UN/ISDR, 2004a. Terminology: Basic terms for disaster risk reduction. United Nations International Strategy for Disaster Reduction (UN/ISDR), Palais des Nations, Switzerland. http://www.unisdr.org/eng/library/lib-terminology-eng%20home.htm.Updated 31 March 2004.

UNCHS-Habitat, 2001. Assessment of vulnerability to flood impacts and damages, Disaster Management Programme, Nairobi, Kenya.

University of Dartmouth, 2006. Global Active Archive of Large Flood Events, Dartmouth Flood Observatory.

UNEP, 2004, Reducing Disaster Risk: A Challenge for Development, United Nations Development Programme, Bureau for Crisis Prevention and Recovery, New York, NY 10017, USA www.undp.org/bcpr.

UNU-IEHS and NNSUACE, 2006. Indicator design for flood vulnerability assessment; United Nations University-Institute for Environment and Human Security, Germany/Nizhny Novgorod State University of Architecture and Civil Engineering, Russia. http://www.cabri-volga.org/DOC/D3 CaseStudies/CaseStudyIndicatorDesign.doc. Last accessed 23 January 2007.

USAID, 2001. Monthly Report on Food Security in Rwanda; PASAR-SISA Project, Agricultural Engineering Department of MINAGRI, Famine Early Warning System Network, November 7, 2001.

Verdoodt, A., 2003. Elaboration and Application of an Adjusted Agricultural Land Evaluation Model for Rwanda, PhD Thesis, University of Gent, Belgium.

Wamsler, C., 2004. Managing Urban Risk: Perceptions of Housing and Planning as a Tool for Reducing Disaster Risk. GBER, 4(2): 11–28.

Zeigler, D.J., Jonhson, J.H. and Brunn, S.D. 1983. Technological Hazards. Association of American Geographers; Washington, D.C.

Part II
Metropolitan Case Studies

Chapter 7
A Respiratory Riskscape for Texas Cities: A Spatial Analysis of Air Pollution, Demographic Attributes and Deaths from 2000 Through 2004

Susan M. Macey

Abstract This study utilizes readily available criteria air pollution data from federal government sources to determine the spatial pattern of urban air pollutants. Using both geographic information systems spatial processing functions and statistical analysis, these data are then combined with respiratory and nonrespiratory decedents' demographic characteristics (including age, race/ethnicity, and gender). Respiratory diseases, including asthma, chronic bronchitis and emphysema, are a leading cause of illness and death in the United States. The areas studied include the major Texas cities of Austin, Dallas-Fort Worth, El Paso, Houston and San Antonio. The purpose of this research is to develop a "respiratory riskscape" in two steps. First, a spatial model of air pollutants for major urban areas in Texas is created. Second, the spatial pattern revealed by that model is analyzed for any significant relationships between specific pollutant sources/emissions and decedent's demographic characteristics, and mortality rates where respiratory disease is a primary or contributing cause of death. Results show variations among urban areas, and a complex interaction between pollution data and mortality rates based on demographic attributes.

Keywords Air pollution · Respiratory disease · Public health · Mortality rates · Texas

7.1 Introduction

Air pollution is a leading urban hazard. The highly variable nature of this hazard along with its numerous origins makes its study a major challenge. While air quality has improved, concerns for human health, particularly among more susceptible subgroups, remains (US Environmental Protection Agency 2006). Geospatial

S.M. Macey (✉)
James and Marilyn Lovell Center for Environmental Geography and Hazards Research, Department of Geography, Texas State University-San Marcos, San Marcos, TX, USA
e-mail: sm07@txstate.edu

P.S. Showalter, Y. Lu (eds.), *Geospatial Techniques in Urban Hazard and Disaster Analysis*, Geotechnologies and the Environment 2, DOI 10.1007/978-90-481-2238-7_7,

information technologies have great potential to aid in identifying areas most at risk and to evaluate the potential impact of this hazard on populations residing in those areas.

Studies dating back to the mid-1980s have linked air pollution, a common technological hazard in urban areas, with negative health consequences (Goldberg et al. 2001; Kim et al. 2004; Schwartz 1991a, b; Schwartz and Dockery 1992a, b), and it is generally agreed that long term health risks from exposure to outdoor air pollution are likely underestimated (Adgate et al. 2004). Numerous epidemiological studies have documented consistent associations between specific ambient air pollution components, specifically the criteria air pollutants (CAPs) including carbon monoxide (CO), nitrous oxide (NO_x), particulate matter (PM_{10} and $PM_{2.5}$), sulfur dioxide (SO_2), and volatile organic compounds (VOC), with various adverse health conditions. These studies have found significant negative impacts on health at levels below the national air quality standards set by the 1990 Clean Air Act. While emissions have been reduced, concern remains as studies continue to show adverse health impacts.

This study utilizes criteria air pollution data from several public sources to determine the spatial pattern of urban air pollutants in the major urban areas of Texas for the period 2000–2004. These data are then combined with the demographic characteristics of the proximate population and data regarding respiratory deaths, most notably chronic obstructive pulmonary diseases (COPD). As defined by the American Thoracic Society (1995), COPD is a disease that is characterized by decreased expiratory flow in the airways of the lungs. COPD consists of three related diseases: asthma, chronic bronchitis and emphysema. As one of the leading causes of illness and death in the United States, COPD causes a substantial economic burden on individuals and society. The purpose of this research is twofold: (1) to create a spatial model of air pollutants for the major urban areas in Texas, and (2) to analyze the spatial pattern for any significant relationships between specific pollutants and pollution levels, decedent's demographic characteristics (including age, race/ethnicity, and gender), and mortality rates where respiratory disease is a primary or contributing cause of death. The goal of the research is to develop a respiratory riskscape for Texas' urban areas.

7.2 Literature Review

Studies dating back to the mid-1980s have linked air pollution with negative consequences for children's health (Erbas et al. 2005; Kim et al. 2004; Lin et al. 2002; Norris et al. 1999; Pouliou et al. 2008; Schenker et al. 1986). Asthma is a chronic condition that occurs when the main air passages of the lungs become inflamed and narrowed and breathing becomes difficult; it is one of the most frequent reasons for hospital admissions among children. Children are particularly susceptible to air pollution related attacks (Erbas et al. 2005). Daily ambient exposure to CAPs has been implicated in increased attacks or worsening of

the condition. In part, the problem has been linked to a larger deficit in lung function growth rate for children exposed to outdoor nitrogen dioxide (NO_2), $PM_{2.5}$, and PM_{10}(Gauderman et al. 2000, 2002). A recent study by Islam et al. (2007) noted that exposure to high levels of $PM_{2.5}$ attenuated the effect of better lung function against new onset asthma. Karr et al. (2007) suggest that infant bronchiolitis may be added to the list of adverse effects of $PM_{2.5}$ exposure. Several studies have also linked childhood asthma exacerbation to levels of ozone (Gent et al. 2003; McConnell et al. 2002; Thurston et al. 1997). Ozone was implicated in hospitalization for acute respiratory diseases for children under two years of age in a study by Burnett et al. (2001). Particulate matter in the form of PM_{10}(Timonen and Pekkanen 1997; Tolbert et al. 2000) or PM_{10} in combination with ozone (Gielen et al. 1997), and $PM_{2.5}$ have also been implicated even when levels were below annual National Ambient Air Quality Standard (NAAQS) levels (Norris et al. 1999). Indeed, recent studies suggest that the role of such pollutants as organic carbon and NO_2 as potential causes of chronic symptoms of bronchitis, decreased lung function and asthma in children may have been underestimated (Gauderman et al. 2002, 2004; McConnell et al. 2003). The prevalence of asthma among children under 18 years has increased from 3.6% of all children in 1980 to 8.9% in 2005 (Mitka 2008). Nitrogen oxides and VOCs, two major power plant emissions, are precursors of ozone.

The probability of asthma occurrence is also generally greater among minority children (Evans 1992). Elevated asthma levels for Hispanic children, especially those of Cuban and Puerto Rican extraction have been noted in several recent studies (Davis et al. 2006; Delfino et al. 2003a). Metzer and Delgado (1995) suggest that higher risk for Hispanic and other minority groups may be partly related to their disproportionate representation in areas failing to meet one or more National Ambient Air Quality Standards (NAAQS). While an early study of children with asthma in the vicinity of coal-fired power stations found occurrence of symptoms not to be associated with measurements of SO_2 and NO_x (Henry et al. 1991), recent studies have provided convincing evidence of an association even at distances of over 60 miles (Levy et al. 2002). Chestnut and Mills (2005) conclude that human health would benefit from further reductions in SO_2 and NO_x emissions from power plants beyond those currently required by Title IV, and that such reductions are clearly warranted.

Outdoor air pollution studies have also linked increased mortality rates, especially among infants, to CAP levels. For example, two studies have shown evidence of a link between sudden infant death syndrome (SIDS) with increases in levels of NO_2 (Ritz et al. 2006) and PM (Glinianaia et al. 2004). Kaiser et al. (2004) have called for further studies to quantify the relationship between infant mortality and air pollution. Other studies indicating a spatial connection between demographics and air pollution have found links with educational level (Levy et al. 2002), and income (O'Neill et al. 2003).

Traffic emissions have been a particular focus of study throughout the last 20 years (Tonne et al. 2007; Watson et al. 1988). Pollutants from traffic exposure have been associated with childhood asthma by several authors

(Gauderman et al. 2005; Kim et al. 2004; Lin et al. 2002). Some recent articles have focused on the use of geographic information systems (GIS) to analyze the distribution and impact of air pollution. Jerrett et al. (2001) compared the relative value of several criteria in modeling the relationship between socioeconomic status and exposure to suspended particles in the air. Chakraborty (2001) analyzed exposure of school children to accidental releases of hazardous substances.

While fewer studies have been published on the impact of air pollution on older persons' health, the heightened susceptibility of the elderly subpopulation along with their growing numbers warrants increased investigation. In the early and mid 1990s, studies by Schwartz and his colleagues (Schwartz and Dockery 1992a, b; Schwartz and Morris 1994; Schwartz and Morris 1995) found increases in ischemic heart disease among the elderly population associated with PM_{10} exposure. More recently, several studies have found a significant association between elderly health problems and levels of air pollution (Tonn et al. 2001), particularly particulate matter (Dominici et al. 2006; Hartog et al. 2003; Pope et al. 2004; Schwartz 1994a, b, c; Williams et al. 2000a, b; Zanobetti et al. 2000). Filleul et al. (2004) found a significant relationship between air pollution levels and elderly respiratory mortality. Just as asthmatic children have been found to be particularly vulnerable to ozone, adult asthma symptoms have also been associated with this pollutant (Eiswerth et al. 2005), and both respiratory and coronary deaths among the elderly population have been associated with ozone (Goldberg et al. 2001). Of particular note is the national study by Samet et al. (2000) which found an association between hospitalization, pneumonia and COPD, and PM_{10} for those 65 years and older.

The impact of air pollution on cardiovascular disease represents a further serious public health problem. Mann et al. (2002) found hospital admissions for ischemic heart disease were associated with levels of CO and NO_2. Creason et al. (2001) linked $PM_{2.5}$with heart rate variability in elderly individuals. Pope et al. (2006) also found short term exposure to ambient $PM_{2.5}$ to be associated with ischemic heart disease. Brook et al. (2004) noted a consistent increased risk for cardiovascular events in relation to present-day concentrations of ambient PM, particularly in certain at-risk subsets of the population. Hospital admissions for cardiovascular and respiratory diseases have also been linked to $PM_{2.5}$ Medicare patients (Peng et al. 2008). As in studies on children, this increased risk has been noted even when levels are within current air quality standards (Peters et al. 2001; Pope et al. 2002).

In sum, numerous studies have found significant negative health impacts of air pollutants even at levels below the NAAQS set by the 1990 Clean Air Act (Peters et al. 2001; Pope et al. 2002; Schwartz 1993). While emissions have been reduced, concern remains as studies continue to show adverse health impacts. Respiratory morbidity and mortality show consistent links to emission levels of CAPs. In light of these findings, this study evaluates the spatial aspects of the emission of criteria air pollutants (CAPs) from various sources and respiratory mortality in five major Texas urban areas.

7.3 Methodology

7.3.1 Study Area, CAP Emissions, and Demographic Data

Chronic obstructive pulmonary disease (COPD) was one of the ten most frequent causes of hospitalizations in Texas (Texas Department of State Health Services 2006), accounting for approximately 33,000 hospitalizations in 2002 (Texas Health Care Information Council 2005). Sixteen of the state's 254 counties had risk-adjusted admission rates for this indicator that were more than twice the state average, with one-third of these being in the eastern part of the state. Pediatric asthma hospitalizations were more significant in southern and western counties with 31 counties reporting significantly higher admission rates than the state average.

In Texas, nearly 51% of the state's population lives in counties that do not meet federal ozone standards (US Environmental Protection Agency 2006). The worst areas are coincident with major urban areas found around Austin, Dallas-Fort Worth, Houston, El Paso, and San Antonio (Fig. 7.1).

These five urban areas form the basis for this study. Houston, the largest city, lies adjacent to the Gulf of Mexico. There is a major industrial and port area in the southeastern sector of the city which contributes to Houston ranking first in emissions from all sources (Table 7.1). As may be expected from the size and spatial extent of the Dallas-Fort Worth metroplex, this conurbation ranks second in mobile pollution sources, but ranks third overall behind San Antonio where utility power plants contribute a greater share of the emissions. Austin, where the state's capital

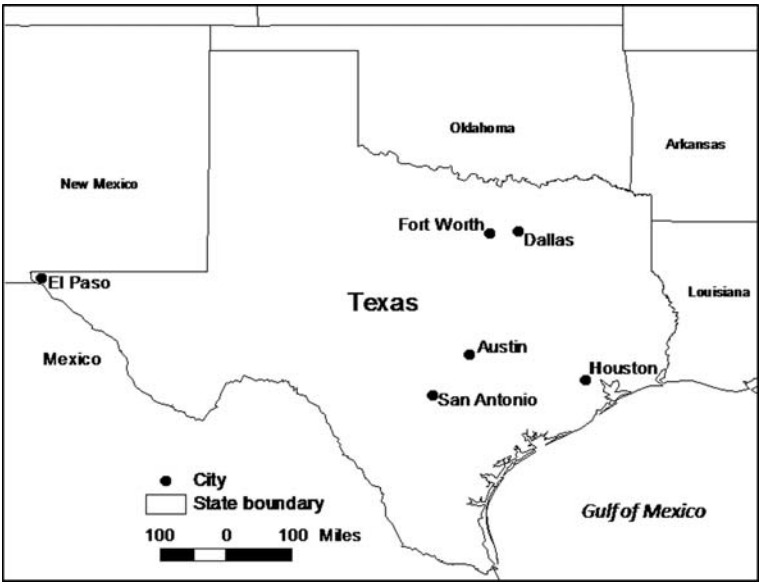

Fig. 7.1 Study area showing city locations

Table 7.1 Urban area rank* for criteria air pollutants by pollution source

	Austin	Dallas-Fort Worth	El Paso	Houston	San Antonio
Utility power plant	4	3	5	1	2
Nonpoint source	2	3	5	1	4
Nonroad mobile	4	2	5	1	3
Onroad mobile	4	2	5	1	3
Area source	4	3	5	1	2
Nonutility point source	3	4	2	1	5
Total – all sources	4	3	5	1	2

*Rank: 1 highest.

is located, ranks fourth, while El Paso, a much smaller city than the other four, consistently ranks lowest in emissions.

In Texas, electric utilities are the leaders in the volume of CAP emissions produced, including carbon monoxide (CO), nitrous oxide (NO_x), particulate matter (PM_{10} and $PM_{2.5}$), sulfur dioxide (SO_2), and volatile organic compounds (VOC). This situation is due in large part to the fact that two-thirds of the electric power plants were built or were under construction before 1971 and are therefore exempt from the tougher clean air standards and permit requirements of the Clean Air Act. Despite additional state legislation in 1999 aimed specifically at reducing emissions from these "grandfathered" electric generating facilities, problems persist. The Voluntary Emissions Reduction Permit (VERP) program under then Governor Bush was a failure – only one plant applied. One significant exempted facility emitted approximately 35% of the total air emissions in Texas in 1999 (Huston et al. 2001). In 1998, Texas led the nation in nitrous oxide production and was second nationally in releases of carbon monoxide and volatile organic compounds (US Energy Information Administration 2003). The state also led the nation in carbon dioxide emissions from electric power plants in 2001. Smog reduction is characteristically focused on three primary sources – automobiles, heavy industry, and power plants. Grandfathered industries and power plants produced as much nitrous oxides in 1997 as 18 million automobiles (US Environmental Protection Agency 1997) making these facilities prime targets for study.

Coal (bituminous, lignite, sub-bituminous, and petroleum coke), biomass and wood products are more commonly used as utility energy sources in Texas. The Texas Natural Resource Conservation Commission's 1997 Emissions Inventory confirmed the extent of the contribution of these facilities by documenting that grandfathered plants accounted for 900,000 tons of pollution annually – 36% of the state total (Huston et al. 2001). One response to these emissions was Bernsen's amendment to state HB 2912 (introduced at the end of 2001) that requires all grandfathered facilities in Texas to apply for permits by September 1, 2003 if the facility is located in East Texas, and by September 1, 2004 if located in West Texas. Grandfathered facilities have been ordered to comply with all conditions of the permits, including installation of emissions controls or reductions of emissions of air

contaminants, by March 1, 2007 for facilities in the East of the state and by March 1, 2008 in the West.

The Clear Skies Act of 2003 set a new emissions reduction goal of 40% less SO_2 for Texas (US Environmental Protection Agency 2006). A reduction in NO_x of 22% is also expected by 2020, with associated reductions in premature deaths, hospitalizations/emergency room visits for asthma and chronic bronchitis, and fewer nonfatal heart attacks. Since their introduction over the last 18 years existing Clean Air Act regulations have resulted in CAP level reductions. The primary focus of the Clear Skies Act is to further reduce power plant emissions, including those from 13 units spread throughout Texas. In all, 27% of Texas' facilities would install Selective Catalytic Reduction (SCR) devices while 24% of plants would install scrubbers.

The two demographic groups considered most at risk from CAPs are the young and the elderly population. Consequently, Texas' demographic composition makes it a good candidate for study because 28% of the population is under 18 years of age and approximately 10% is aged 65 years or older (Table 7.2) (US Bureau of the Census 2000). The proportion of senior citizens is also growing, particularly with the influx of 'snowbirds' (elderly, seasonal inmigrants) to southern parts of the state. In terms of other demographic variables, Texas has a large and growing Hispanic population, currently comprising approximately one-third of the state's total population. Blacks represent a smaller proportion of the total mix (approximately 12%) having higher representation in the northern and eastern counties. In the five study cities, the populations in Austin and El Paso are slightly younger than those of the others. Houston and Dallas-Fort Worth have a higher proportional representation of Blacks while San Antonio and El Paso outrank the others in the proportions of Hispanics, where they comprise more than half of the total population.

Table 7.2 Demographic characteristics of Texas and the five urban study areas

	Texas	Austin	Dallas-Fort Worth	El Paso	Houston	San Antonio
Total population	20,851,820	901,920	4,145,659	674,801	3,822,509	1,327,554
Median age (years)	32.3	30.1	31.7	30.0	31.4	32.0
Percent < 18 years	28.2	24.9	28.1	32.0	29.2	28.4
Percent 18–64 years	61.9	69.0	64.2	58.2	63.5	61.2
Percent 65 and older	9.9	6.1	7.8	9.8	7.3	10.4
Percent White	71.0	69.3	65.5	73.5	59.1	68.5
Percent Black	11.5	9.0	15.9	3.0	18.2	7.5
Percent Hispanic	32.0	26.8	24.0	78.8	31.6	54.5
Percent male	49.6	51.0	49.8	48.2	49.8	48.5

Source: US Bureau of the Census (2000)

7.3.2 Data Sources and Analysis Techniques

To meet the objective of creating a respiratory riskscape for the five major urban areas in Texas, the best available public data on the sources and types of air pollution emissions was used. Specific air pollutants studied here are those designated as criteria air pollutants (CAPs), and include carbon monoxide, nitrogen oxides, particulate matter (PM_{10} and $PM_{2.5}$), sulfur dioxide, and volatile organic compounds recorded in the National Emissions Inventory (NEI) database. As discussed above, these pollutants have been repeatedly implicated in studies of respiratory illnesses. Data on air pollution sources and emissions for Texas were downloaded from two existing Environmental Protection Agency (EPA) databases and served as the environmental predictors in this study.

The NEI data for CAPs in 2002 breaks sources down by nonpoint, area, non-road and on-road mobile sources, and nonutility point sources including heavy industry (US Environmental Protection Agency 2008b). NEI 'onroad mobile', 'nonroad mobile', 'nonpoint' and 'area' source data are only available at the county level. Studies have shown traffic related emissions to be a factor in childhood asthma hospitalization up to 200 or 300 m from the source (Hoffman et al. 2007; Lin et al. 2002; Kim et al. 2004). Therefore, in order to provide a more realistic view of their potential impact, a 250 m buffer was created around major roadways and onroad sources. County information was subsequently attached to these buffers. County-level values for nonroad mobile emissions were also attached to their potential sources (e.g., airports, railroads) to derive a potentially more accurate definition for such emissions. Each of these features was extracted from the ESRI® data sets provided with the software and a 500 m buffer attached to each feature to account for the potential extent of exposure from each source.

Nonpoint and area sources are more problematic as they may include any source that individually does not produce sufficient emissions to qualify as a point source, but collectively may be significant (US Environmental Protection Agency 2008b). These sources may range from home or office buildings to diffuse stationary sources such as agricultural tilling and wildfires. Therefore, the data on specific pollutants for these county based sources were first joined into one table. Then the county value was assigned to tracts so that a composite total emission value was calculable. Unfortunately, the county level nature of the emission information remains a primary limitation when examining contribution from nonpoint and area sources.

These data were supplemented with the location of electric power plants and their emission data for four pollutants: nitrous oxide, ozone, sulfur dioxide and carbon dioxide emissions using the EPA's emission and generation resource integrated database (e-GRID) (US Environmental Protection Agency 2008a). These emissions are all listed in the NAAQS as CAPs. The eGRID database is a comprehensive source of data on the environmental characteristics of all electric power generated in the United States from 1997 through 2002. The database's attributes include primary fuel type, plant age and the last year the plant added production capacity, plant efficiency, production, air pollutant emissions, allowances, resource mix for

individual plants, and the compliance methods employed by the plants (US Environmental Protection Agency 2008a).

In order to evaluate the health impacts of the pollutants emanating from these sources, mortality data from the individual mortality files compiled by the Texas Department of State Health Services (2006) were downloaded for the years 2000–2004, the latest year currently available. Additional attributes were created to separate cases where deaths associated with COPD were listed as the primary cause of death or as a contributing cause under the International Classification of Diseases (ICD-10) (such causes include bronchitis, emphysema, chronic obstructive pulmonary disease and asthma, using codes J40–J47).

Finally, demographic tract level data from the US 2000 Census (US Bureau of the Census 2000) for the attributes of age, race/ethnicity and gender were extracted for the five major urban areas. Tract level data were used because block group number of deaths were too low to allow meaningful rates to be calculated for each demographic category. The 2000 Census was selected as more closely correlated to the years available for the mortality data being studied (2000–2004), as well as the time frame for which the pollution data were available. The mortality records were aggregated to the tract level and these data were then combined with the census data to calculate mortality rates for respiratory disease as the primary or contributing cause of death. Nonrespiratory-related death rates were also calculated to serve as a benchmark against which to compare the respiratory death rates.

ArcView® GIS 3.3, a desktop GIS software package, was used to create the GIS layers for the spatial dimensions of the respiratory riskscape in this research. Preliminary processing of the emissions data included matching the NEI power plant data with the corresponding plants in eGRID to produce a composite layer with both plant and emission characteristics for each of the datasets. As studies have shown adverse health effects from exposure to air pollutants at a variety of distances from utility sources including from 6 to 60 miles from power plants (Henry et al. 1991; Levy et al. 2002; Levy et al. 2003), a conservative buffer corresponding to a distance of 6 miles from each plant was created to serve as the basis for analyzing the effect of their impact on death rates over space. Nonutility point sources can be anything from a recycling facility or a dry cleaning shop to a chemical plant. The disparate nature of these points precludes their being considered as part of a surface where pollution values might be interpolated. Therefore, they were retained as points to maintain their integrity.

Several GIS functions were then used to create a composite layer containing source emissions and demographic attributes. Emissions for the point and mobile sources were combined with the buffered features that represent their spatial location. Census areas within the urban area boundary for the cities included in the study were then extracted and the emissions data were combined with the census data. Point locations of decedents from the Texas DSHS were joined to the emissions and census data to identify corresponding attributes in the latter for the residence location of each decedent. Mortality rates were calculated by summing the number of individual decedents in each census tract; rates per 1000 population were then

calculated. This level of specificity was necessitated by the low frequency of cases in each block group making rates at a finer spatial resolution meaningless. Maximum emission levels for each pollutant from all sources found in each tract were also calculated.

Following the spatial processing of the data, statistical analysis was undertaken using the Statistical Package for the Social Sciences (SPSS) software. First, cases were examined for annual and seasonal trends. Then a comparison of decedent characteristics was made among the five urban areas. Decedent's demographic characteristics (age, race, ethnicity, gender) were evaluated in relationship to respiratory disease being listed as a primary or contributing cause of death. Nonrespiratory decedent characteristics were also examined for comparative purposes. Finally, death rates were calculated at the tract level and these rates were evaluated for their association with specific sources and types of pollutants. Nonparametric tests including Spearman's rank order correlation and chi-square statistics were used to test for associations or differences. As the number of cases was large, a more conservative probability level of 0.01 was set as the minimum level for significance throughout the analysis.

7.4 Discussion of Results

7.4.1 Spatial Pattern of Air Pollution Sources

The spatial pattern of urban air pollutant sources detailed below identifies the areas of greatest potential respiratory health risk within each of the major urban areas. As noted above, Houston consistently had the highest levels of emissions for all sources among all urban areas studied (Table 7.1). Six electric power plants are inside the urban boundary while five impinge on the southern and eastern sides of the city (Fig. 7.2). The map of the Houston urban area shows radial and radiating sources of nonroad and onroad mobile sources, plus numerous nonutility point sources which tend to coincide with transportation routes particularly on the eastern side of the city.

The Dallas-Fort Worth metroplex also presents a tangle of onroad and nonroad sources (Fig. 7.3), and ranks second for emissions from both these sources (Table 7.1). Eight electric power plants are within the urban area while the six mile buffer for three more overlap parts on the northern side of the metroplex. Dallas-Fort Worth ranks third behind San Antonio in electric power plant and area emissions, and third behind Austin for nonpoint source emissions. While dotted with nonutility point sources, emissions from these sources contributed the least to air pollution in the Dallas-Fort Worth area.

Taking all sources into consideration, emissions in San Antonio elevate this urban area to the second highest ranking in terms of total amount of pollution. While fewer in number than in Houston and Dallas-Fort Worth, electric power plants, along with area sources contribute more than other sources for this city (Fig. 7.4).

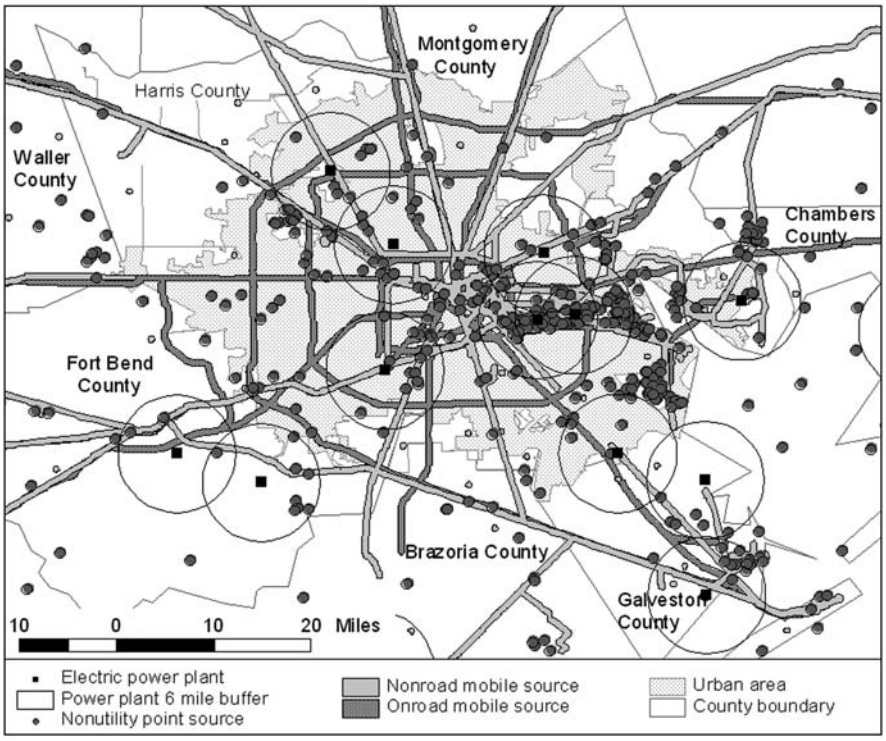

Fig. 7.2 Houston urban area air pollution sources

Nonutility point sources are also fewer in the Austin urban area. Austin's emissions ranked fourth overall and for most of the emission sources. Only three electric power plants are located in the city, which also has far fewer nonutility point sources listed (Fig. 7.5).

El Paso ranked consistently lowest for all but nonutility point sources. The city has only one electric power plant within the urban area and one whose buffer overlaps a northern section of the urban area (Fig. 7.6). One caveat regarding the accuracy of observations for El Paso is that it lies adjacent to the Mexican border. No data on emissions from the adjacent area in Mexico that could potentially contribute to air pollution levels in the El Paso area is available. However, it is suspected that air pollution from south of the border confounds the situation.

By far the largest quantity of emissions was recorded for carbon monoxide (Fig. 7.7) followed by PM_{10}, NO_x, SO_2 and VOC (US Environmental Protection Agency 2008b). Nitrous oxides noted in several studies (Chestnut and Mills 2005; Gauderman et al. 2000, 2002; Henry et al. 1991; Mann et al. 2002) came from a variety of sources including (in order of importance) onroad mobile, nonroad mobile, electric utility plants and nonutility point sources. The largest contribution of PM_{10}, cited as having a negative impact on health in numerous studies (Dominici et al.

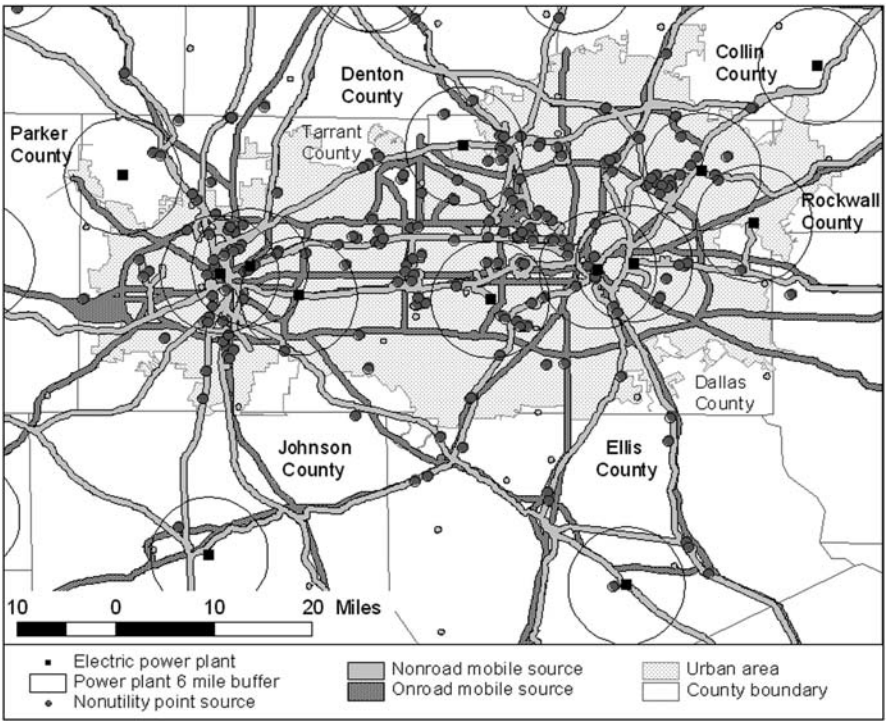

Fig. 7.3 Dallas-Fort Worth urban area air pollution sources

2006; Hartog et al. 2003; Pope et al. 2004; Samet et al. 2000; Schwartz 1994a, b, c; Williams et al. 2000a, b; Zanobetti et al. 2000) came predominantly from area sources. $PM_{2.5}$ which has received much attention in recent years (Islam et al. 2007; Karr et al. 2007; Peng et al. 2008) was present in the lowest levels and also came mainly from area sources. The makeup of sources and their contribution for VOC particularly linked to asthma in children (Delfino 2003b) reflected those of NO_x, though area sources contributed more to VOC.

The largest proportion of emissions came from onroad mobile sources which in addition to their large emission of CO, added to the levels of NO_x and VOC (Fig. 7.8) (US Environmental Protection Agency 2008b). Area sources, the greatest source of PM_{10}, contributed the second largest amount of pollutants, primarily being the major source of PM_{10} and $PM_{2.5}$, as well as a primary source of VOC. Nonroad mobile sources such as airports and railroad lines are notable for their CO, and to a lesser extent, NO_x and VOC contributions. Point sources, both from electric utility power plants and nonutility point sources add a lesser amount of air pollution than the other four sources noted, but combined contribute the most SO_2 which has been cited in studies by Chestnut and Mills (2005), Henry et al. (1991), and Levy et al. (2002). Carbon dioxide and ozone data were only available for electric utility power plants and are therefore not shown. The average level of power plant CO_2 emissions

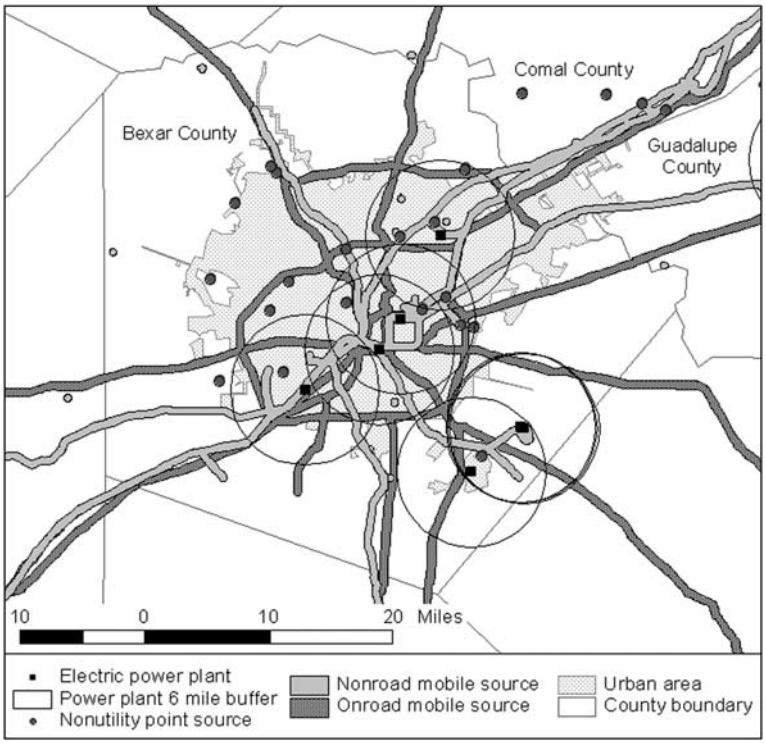

Fig. 7.4 San Antonio urban area air pollution sources

recorded was five times that for CO from onroad mobile sources while mean levels of ozone ranked between power plant emissions of NO_x and SO_2. Ozone has been implicated as a factor contributing to asthma in children by a number of studies (Burnett et al. 2001; Eiswerth et al. 2005; Gent et al. 2003). It must be remembered that NO_x and VOC are precursors of ozone and therefore, while ozone is not specifically recorded for all sources, any source of these pollutants could contribute to the problem.

7.4.2 Decedent Attributes

Turning to the cause of death, cases were first examined to establish the relative proportion of deaths where respiratory disease was listed as the primary cause or a contributing cause. Respiratory causes include bronchitis, emphysema, chronic obstructive pulmonary disease and asthma and are denoted by the ICD-10 codes, J40–J47. Where respiratory disease was listed as a contributing cause of death, the major primary causes noted here were chronic ischemic heart disease (ICD-10 code I25) listed for 23.2%, lung cancer (ICD-10 code C34) at 15.2%, heart failure

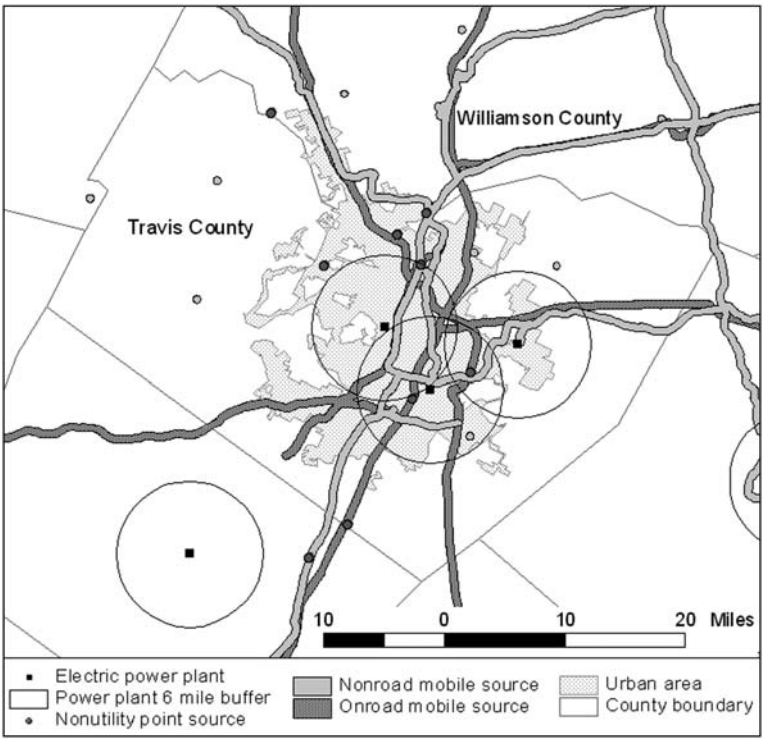

Fig. 7.5 Austin urban area air pollution sources

(ICD-10 code I50) in 3.9%, and stroke (ICD-10 code I64) for 2.1% of cases. The breakdown of deaths in each category by urban area is listed in Table 7.3.

By far the greatest proportion of respiratory deaths was cited as COPD, accounting for nearly 80% or more of all primary respiratory deaths for each area. The highest level was observed in San Antonio (85.3% of all respiratory primary cause deaths) and the lowest one in Houston (78.1%). Emphysema was the second highest proportion in all areas with the largest percent being recorded in Houston (16.0% of primary causes) and the lowest in San Antonio (9.6%), the reverse of the COPD pattern. Asthma shows much lower fatality proportions, accounting for between 2.9% at the low end for Austin to a high of 3.8% for Houston. In all instances, the percentages for respiratory disease as a contributing cause of death were slightly higher than those for primary cause percentages ranging from 4.2% for Houston to 5.5% for El Paso.

An examination of the characteristics of decedents in each respiratory category gives a more complete view of the relative contribution of respiratory disease versus nonrespiratory related causes for mortality. Minority group status, especially Hispanic ethnicity has been evaluated as a risk factor with studies particularly focusing on Hispanic children (Evans 1992; Davis et al. 2006; Delfino et al. 2003a; Metzer and Delgado 1995). The proportion of respiratory related deaths (primary

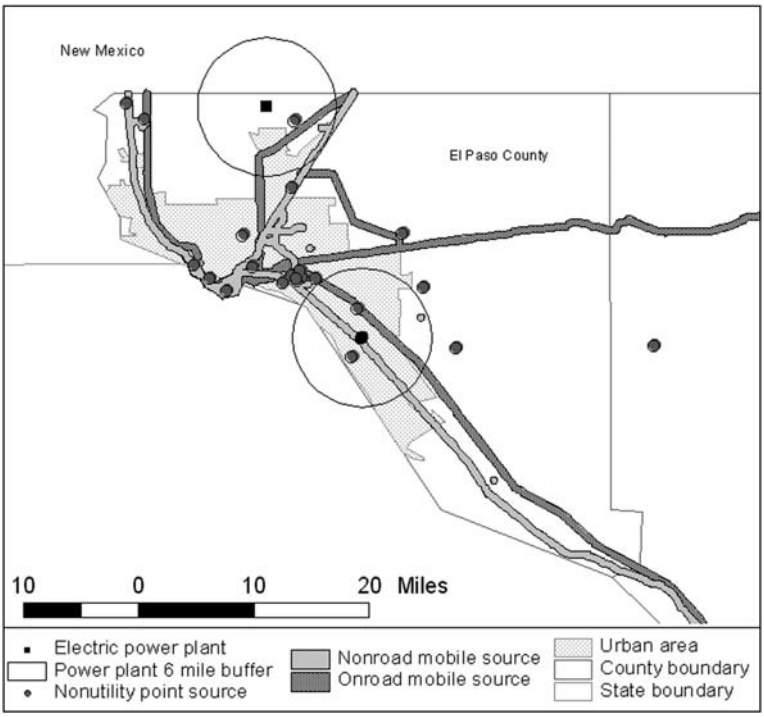

Fig. 7.6 El Paso urban area air pollution sources

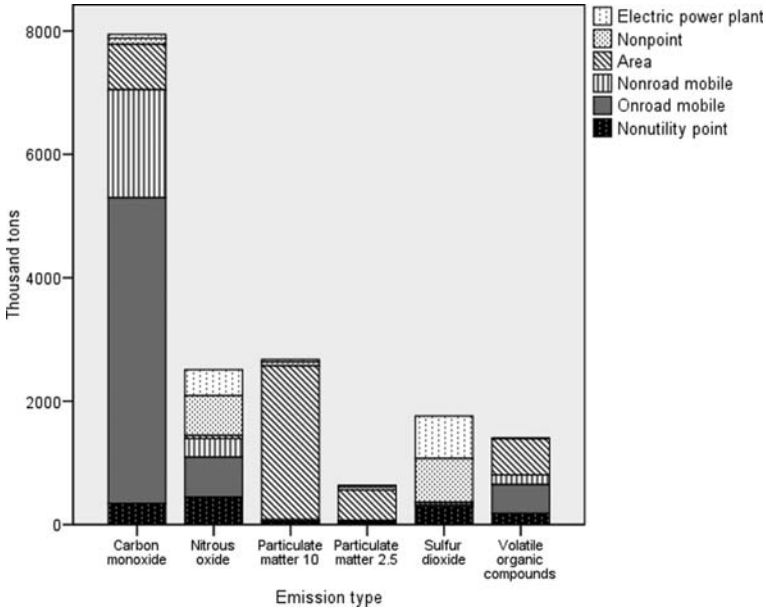

Fig. 7.7 Air pollution emission type by source

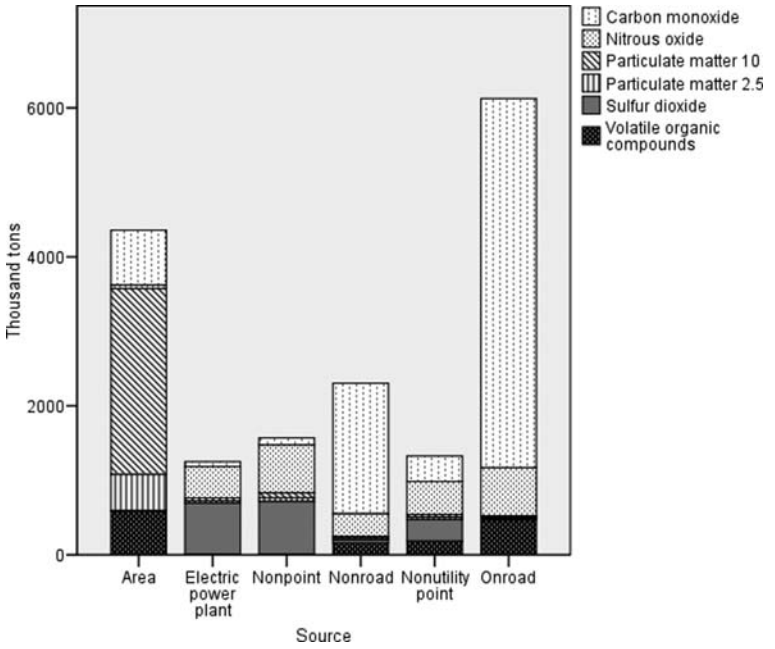

Fig. 7.8 Air pollution source contributions to emission total

and contributing) for Hispanics was highest in El Paso and San Antonio (Table 7.4), though the percentage was lower than for Hispanic nonrespiratory caused deaths. Black proportions were highest in the largest urban areas, Houston and Dallas-Fort Worth and again were lower than percentages for nonrespiratory deaths. The percentage of male respiratory decedents was highest in El Paso (51.8%) and lowest in Austin (42.7%). This pattern reflects that for nonrespiratory decedents more closely than for any other demographic category. While mean age in years shows little variation among urban areas, respiratory (both as a primary and contributing cause) decedents were older than nonrespiratory decedents. In order to examine the two primary respiratory risk groups based on age noted in the literature, children (Adgate et al. 2004; Gauderman et al. 2000, 2002; Pouliou et al. 2008) and the elderly population (Filleul et al. 2004; Goldberg et al. 2001; Samet et al. 2000; Tonn et al. 2001), those less than 18 years of age were grouped to represent children in the mortality data, and those 65 years and older were grouped to represent elderly decedents. The percentage of children dying from respiratory related diseases or having one as a contributing cause was very low across all locations and was considerably lower than nonrespiratory percentages. The situation for elderly decedents showed the reverse pattern with the respiratory primary and contributing cause categories being 15–20 percentage points higher than for nonrespiratory deaths.

These results support findings in previous studies. Elderly individuals have been cited as being at greater risk in numerous studies (Dominici et al. 2006; Hartog

Table 7.3 Cause of death for urban areas

	All areas	Austin	Dallas-Fort Worth	El Paso	Houston	San Antonio
Respiratory primary cause						
Number of cases	12,654	769	5609	772	3539	1965
Percent for urban area						
Bronchitis	0.4	0.5	0.4	0.4	0.5	0.4
Chronic bronchitis	0.4	0.5	0.4	0.6	0.4	0.5
Emphysema	14.3	14.3	14.9	14.0	16.0	9.6
COPD	80.2	79.2	79.7	80.6	78.1	85.3
Asthma	3.5	2.9	3.5	3.0	3.8	3.1
Status asthmaticus	0.4	1.2	0.3	1.2	0.5	0.1
Bronchiectasis	0.8	1.4	0.7	.3	0.8	1.2
Percent of primary cause deaths by area	100	6.1	44.3	6.1	28.0	15.5
Respiratory contributing cause						
Number of cases	14,399	754	6224	983	4117	2321
Percent of contributing cause deaths by area	100	5.2	43.2	6.8	28.6	16.1
Nonrespiratory cause						
Number of cases	270,837	15,735	106,126	16,166	90,714	42,096
Percent of nonrespiratory deaths by area	100	5.8	39.2	6.0	33.5	15.1
All cases						
Percent						
Respiratory primary	4.2	4.5	4.8	4.3	3.6	4.2
Respiratory contributing	4.8	4.4	5.3	5.5	4.2	5.0
Nonrespiratory	90.9	91.2	90.0	90.2	92.2	90.8

et al. 2003; Pope et al. 2004; Schwartz 1994a, b, c; Tonn et al. 2001; Williams et al. 2000a, b; Zanobetti et al. 2000). They need to be considered as at higher risk as their representation in both respiratory primary and contributing cause categories are almost uniformly 20 percentage points above their proportional representation in the nonrespiratory deaths category. Those individuals with heart conditions need to be particularly vigilant as they comprise the largest group (approximately 25%) of the contributing cause category, and the association between respiratory and cardiovascular disease is well documented (Schwartz and Dockery 1992a, b; Schwartz and Morris 1994, 1995) especially for elderly individuals (Creason et al. 2001; Hartog et al. 2003; Pope et al. 2004). The under-18 years of age category shows the reverse pattern in all areas, perhaps reflecting the low respiratory mortality versus morbidity for children. Several studies have addressed childhood morbidity, especially related to asthma (Burnett et al. 2001; Delfino et al. 2003a; Erbas et al. 2005; Gauderman et al. 2000 and 2002; Gent et al. 2003; Lin et al. 2002).

Table 7.4 Urban area decedent demographic characteristics by cause of death

	All areas	Austin	Dallas-Fort Worth	El Paso	Houston	San Antonio
Respiratory primary cause						
Number of cases	12,654	769	5609	772	3539	1965
Mean age (years)	76.0	76.5	75.6	78.2	75.5	77.5
Percent < 18 years	0.3	0.4	0.4	0.4	0.3	0.2
Percent 18–64 years	13.7	12.6	15.1	9.2	14.7	10.6
Percent 65 and older	85.9	87.4	84.5	90.4	85.0	89.2
Percent White	80.3	87.9	86.5	59.8	77.2	73.3
Percent Black	10.7	7.5	10.3	2.2	16.1	6.6
Percent Hispanic	8.0	3.6	2.4	37.0	5.3	19.5
Percent male	46.6	42.7	45.7	51.8	47.6	46.9
Respiratory contributing cause						
Number of cases	14,399	754	6224	983	4117	2321
Mean age (years)	75.6	77.5	74.7	78.8	74.6	77.7
Percent < 18 years	0.3	0.0	0.3	0.2	0.2	0.2
Percent 18–64 years	16.4	11.4	18.5	8.2	18.9	11.6
Percent 65 and older	83.3	88.6	81.2	91.6	80.9	88.2
Percent White	75.6	83.8	82.1	54.9	75.2	65.1
Percent Black	13.1	9.3	14.5	2.2	16.9	13.1
Percent Hispanic	10.4	6.2	2.8	41.8	6.2	26.3
Percent male	52.4	48.5	51.0	52.2	54.0	54.8
Nonrespiratory cause						
Number of cases	270,837	15,735	106,126	16,166	90,714	42,096
Mean age (years)	68.4	68.9	68.3	70.6	67.0	70.5
Percent < 18 years	3.2	3.3	3.4	2.6	3.4	2.7
Percent 18–64 years	32.2	31.7	32.3	26.9	35.1	30.0
Percent 65 and older	64.6	65.0	64.3	70.5	61.5	69.4
Percent White	59.6	69.1	69.2	32.8	56.8	48.2
Percent Black	18.5	13.9	19.6	2.8	25.6	8.5
Percent Hispanic	20.0	15.7	9.4	63.7	14.9	42.9
Percent male	49.8	49.3	49.1	50.8	50.7	49.6

7.4.3 Association of Mortality Rates with Air Pollution Sources and Types

While the number and percentage of deaths is instructive in terms of the absolute magnitude of the potential problem, in order to discern any disproportional risk, rates must be evaluated. The mortality records were aggregated to census tract level. Rates per thousand were then calculated using census tract values for each demographic attribute. For the under-18 year old age category, values were too low to be meaningful, and so this category was dropped from further analysis. The mean rates for all other demographic attributes under study are displayed in Table 7.5.

Table 7.5 Average death rates per thousand at the tract level by urban area

	Austin	Dallas-Fort Worth	El Paso	Houston	San Antonio
Respiratory primary cause rate					
All case**	4.75	7.28	6.43	12.71	7.41
Aged 65 years or older*	2.87	1.88	0.78	1.20	1.88
White**	5.83	10.18	5.47	6.92	7.72
Black[1]	2.96	3.16	4.21	3.44	5.14
Hispanic**	0.73	0.68	2.68	0.95	2.15
Male**	4.15	6.94	7.01	4.99	6.92
Female**	5.38	7.64	5.91	5.30	7.86
Respiratory contributing cause rate					
All case**	4.59	8.22	7.94	6.25	9.11
Aged 65 years or older[1]	1.52	1.62	2.64	1.18	1.19
White**	5.59	10.75	6.28	8.12	8.59
Black*	2.91	5.38	4.81	3.86	8.32
Hispanic**	1.13	1.12	3.83	1.13	3.68
Male**	4.42	8.65	8.76	6.86	10.04
Female**	4.78	7.85	7.19	5.58	8.24
Nonrespiratory cause rate					
All case**	103.48	160.75	138.56	155.86	171.46
Aged 65 years or older**	35.71	29.79	22.50	22.59	25.60
White**	99.80	153.50	69.21	133.27	116.75
Black*	112.10	132.19	126.21	140.61	158.30
Hispanic**	50.17	55.89	103.55	61.61	107.91
Male**	101.43	147.35	146.81	145.61	176.46
Female**	105.86	145.17	131.37	135.93	162.69

[1]Difference among areas not significant
*Difference significant at $p < 0.01$
**Difference significant at $p < 0.001$

In the case of respiratory as primary cause deaths, Houston topped the list when all cases were considered together and the rate exceeded those for all other urban areas by nearly two to one over Dallas-Fort Worth, El Paso, and San Antonio, or more in the case of Austin (Table 7.5). This result could be expected given that Houston ranked first for all air pollution sources (Table 7.1). The overall rates for the other urban areas also reflect their overall air pollution ranking. All group rates except for Black decedents also showed significant differences among urban areas. White rates were highest in Dallas-Fort Worth, Black rates highest in San Antonio, and Hispanic rates higher in El Paso and San Antonio than in the other three areas. In all cases, rates for Whites were higher than for Blacks, with Hispanics exhibiting the lowest rates. In the case of gender, male and female rates differed among the urban areas. El Paso, Dallas-Fort Worth and San Antonio exhibit higher values than Houston and Austin for both genders. San Antonio has the highest female rates and El Paso the highest male rates. Female rates exceeded male rates in all cities

except El Paso. The single category where Austin exceeded all other areas was for individuals aged 65 years and older. In general, elderly rates were lower than for all other categories except Hispanics who had the lowest respiratory-related death rates of all race/ethnicity groups in this study. The latter finding somewhat contradicts the literature which suggests that Hispanics are at higher risk than other racial or ethnic groups (Davis et al. 2006; Delfino et al. 2003a; Metzer and Delgado 1995). However, these previous studies examined morbidity rather than mortality. Thus, while Hispanics comprise a larger proportion of the population than Blacks in Texas, Blacks experience a higher death rate suggesting the need for further research. The higher rates for White decedents may reflect the influence of economic status whereby access to health professionals improves the accuracy of information found on death certificates while the Hispanic death rate may be underreported due to the opposite.

Where respiratory disease was a contributing cause, the differences among group rates generally reflect those for primary cause with three exceptions: the variation in the rate for Blacks was significantly different among urban areas while the rate for the elderly group was not. San Antonio rates for all cases also exceeded those for the other urban areas, and for males as well as Blacks. For nonrespiratory cases, rates differed on all attributes among the urban areas. Unlike the comparable rates for respiratory-primary and respiratory-contributing related deaths, rates for Blacks exceeded those for Whites, and, with the exception of EI Paso where the White rate was lower than that for Hispanics, rates for Hispanics were the lowest in all categories except for elderly deaths.

When mortality rates were tested for association with pollution emission levels for all urban tracts, only weak relationships were observed (all Spearman rank order correlation values were below 0.23.). All cause categories were positively associated with emissions from electric utility power plants, nonpoint, and nonroad mobile sources (Table 7.6), with the strength of correlations for electric power plants being the highest. As noted above, pollution from power plants in Texas has long been a source of contention. The findings here reinforce the greater contribution of this source to mortality not just for respiratory but also for nonrespiratory causes.

No association was noted between primary or contributing rates and onroad source emissions. Area sources did not register as significant in overall respiratory rates, though three of the pollutants from this source (CO, NO_x and VOC) were positively associated with contributing rates. When the total from all sources was examined, the same three pollutants showed a positive association with both primary and contributing rates, while total emissions of $PM_{2.5}$ also showed a positive association with contributing rates. The overall lack of association between total emissions for particulate matter pollutants and primary rates suggests that studies that focus solely on these pollutants, while valuable in establishing specific levels for PM, may miss the broader sweep of the influence of complex pollution mixes.

When race rates were considered, power plant and nonpoint source pollutants were associated with death rates for all groups, though the associations were weak (Table 7.7). The Black primary and contributing rates were also associated with nonroad and onroad mobile sources. White contributing rates also showed a weak association with onroad sources, while Hispanic rates showed no association with any of these sources. Respiratory as the primary cause and nonrespiratory rates for

Table 7.6 Death rates by source and type of pollution

	Respiratory primary cause rate	Respiratory contributing cause rate	Nonrespiratory cause rate
Electric power plant			
Nitrous oxide	0.15*	0.20*	0.23*
Ozone	0.15*	0.20*	0.23*
Sulfur dioxide	0.13*	0.19*	0.20*
Carbon dioxide	0.13*	0.19*	0.21*
Nonpoint source			
Carbon monoxide	0.09**	0.15**	0.12**
Nitrous oxide	0.10**	0.15**	0.13**
Particulate matter 10	0.08**	0.14**	0.12**
Particulate matter 2.5	0.08**	0.14**	0.11**
Sulfur dioxide	0.07**	0.13**	0.11**
Volatile organic compounds	0.09**	0.15**	0.12**
Area source			
Carbon monoxide	ns	0.06*	0.17**
Nitrous oxide	ns	0.07**	0.15**
Particulate matter 10	ns	ns	0.14**
Particulate matter 2.5	ns	ns	0.15**
Sulfur dioxide	ns	ns	0.11**
Volatile organic compounds	ns	0.07**	0.18**
Nonroad mobile source			
Carbon monoxide	0.07*	0.07*	0.13**
Nitrous oxide	0.07*	0.07*	0.13**
Particulate matter 10	0.07*	0.07*	0.13**
Particulate matter 2.5	0.07*	0.07*	0.13**
Sulfur dioxide	0.06*	0.06*	0.13**
Volatile organic compounds	0.07*	0.07*	0.13**
Onroad mobile source			
Carbon monoxide	ns	ns	0.09**
Nitrous oxide	ns	ns	0.09**
Particulate matter 10	ns	ns	0.09**
Particulate matter 2.5	ns	ns	0.09**
Sulfur dioxide	ns	ns	0.09**
Volatile organic compounds	ns	ns	0.09**
Nonutility point source			
Carbon monoxide	−0.08**	ns	−0.06*
Nitrous oxide	−0.08**	ns	−0.06*
Particulate matter 10	−0.08**	ns	−0.06*
Particulate matter 2.5	−0.07**	ns	−0.06*
Sulfur dioxide	−0.09**	ns	−0.07**
Volatile organic compounds	−0.06*	ns	ns
Total – all sources			
Carbon monoxide	0.07**	0.09**	0.16**
Nitrous oxide	0.08**	0.09**	0.16**
Particulate matter 10	ns	ns	0.16**
Particulate matter 2.5	ns	ns	0.16**
Sulfur dioxide	ns	0.09**	0.20**
Volatile organic compounds	0.09**	0.11**	0.19**

ns Difference among areas not significant
*Significant at $p < 0.01$
**Significant at $p < 0.001$

Table 7.7 Race/ethnicity death rates by source and type of pollution*

	Respiratory primary cause rate			Respiratory contributing cause rate			Nonrespiratory cause rate		
	White	Black	Hispanic	White	Black	Hispanic	White	Black	Hispanic
Electric power plant									
Nitrous oxide	0.11	0.11	0.14	0.15	0.13	0.16	0.14	0.20	0.17
Ozone	0.11	0.11	0.14	0.15	0.13	0.16	0.15	0.20	0.16
Sulfur dioxide	0.10	0.10	0.13	0.14	0.13	0.14	0.13	0.19	0.15
Carbon dioxide	0.10	0.10	0.12	0.15	0.12	0.15	0.14	0.19	0.15
Nonpoint source									
Carbon monoxide	0.08	0.07	0.07	0.11	0.10	0.10	0.08	0.10	0.09
Nitrous oxide	0.09	0.07	0.07	0.12	0.10	0.11	0.09	0.11	0.10
Particulate matter 10	0.07	0.07	0.08	0.10	0.10	0.11	0.07	0.10	0.10
Particulate matter 2.5	0.07	0.07	0.08	0.10	0.10	0.11	0.07	0.10	0.10
Sulfur dioxide	0.07	0.06	0.06	0.10	0.09	0.10	0.08	0.09	0.08
Volatile organic compounds	0.10	0.08	ns	0.13	0.12	0.07	0.11	0.11	0.06
Area source									
Carbon monoxide	ns	0.08	ns	0.06	ns	ns	0.14	0.12	0.13
Nitrous oxide	0.09	0.11	−0.12	0.11	0.07	−0.09	0.22	0.15	ns
Particulate matter 10	ns	0.08	ns	ns	ns	0.06	0.10	0.12	0.13
Particulate matter 2.5	0.06	0.10	−0.08	0.08	0.06	ns	0.19	0.15	0.06
Sulfur dioxide	ns	ns	0.15	ns	ns	0.19	ns	0.07	0.19
Volatile organic compounds	ns	0.09	ns	0.06	ns	0.07	0.13	0.14	0.15
Nonroad mobile source									
Carbon monoxide	ns	0.10	ns	ns	0.10	ns	ns	0.15	0.08
Nitrous oxide	ns	0.09	ns	ns	0.10	ns	ns	0.15	0.08
Particulate matter 10	ns	0.09	ns	ns	0.10	ns	ns	0.15	0.07
Particulate matter 2.5	ns	0.09	ns	ns	0.10	ns	ns	0.15	0.07
Sulfur dioxide	ns	0.09	ns	ns	0.10	ns	ns	0.15	0.07
Volatile organic compounds	ns	0.10	ns	ns	0.10	ns	ns	0.15	0.07

Table 7.7 (continued)

	Respiratory primary cause rate			Respiratory contributing cause rate			Nonrespiratory cause rate		
	White	Black	Hispanic	White	Black	Hispanic	White	Black	Hispanic
Onroad mobile source									
Carbon monoxide	ns	0.09	ns	0.06	0.09	ns	0.06	0.12	0.04
Nitrous oxide	ns	0.09	ns	0.07	0.09	ns	0.09	0.12	ns
Particulate matter 10	ns	0.09	ns	0.07	0.09	ns	0.08	0.12	ns
Particulate matter 2.5	ns	0.09	ns	0.07	0.09	ns	0.08	0.12	ns
Sulfur dioxide	ns	0.09	ns	0.07	0.09	ns	0.09	0.12	ns
Volatile organic compounds	ns	0.09	ns	0.07	0.09	ns	0.09	0.12	ns
Nonutility point source									
Carbon monoxide	−0.06	ns	ns	ns	ns	ns	−0.06	ns	ns
Nitrous oxide	−0.06	ns	ns	ns	ns	ns	−0.06	ns	ns
Particulate matter 10	ns	ns	ns	ns	ns	ns	−0.06	ns	ns
Particulate matter 2.5	ns	ns	ns	ns	ns	ns	−0.06	ns	ns
Sulfur dioxide	−0.07	ns	ns	ns	ns	ns	−0.07	ns	−0.06
Volatile organic compounds	ns	ns	ns	ns	ns	ns	−0.06	ns	ns
Total – all sources									
Carbon monoxide	0.08	0.12	ns	0.09	0.12	ns	0.12	0.17	0.07
Nitrous oxide	0.09	0.13	ns	0.10	0.12	ns	0.15	0.18	ns
Particulate matter 10	ns	0.10	0.07	ns	0.07	0.10	0.11	0.16	0.17
Particulate matter 2.5	ns	0.11	ns	0.07	0.08	ns	0.16	0.17	0.08
Sulfur dioxide	ns	0.11	ns	0.07	0.08	ns	0.16	0.17	0.08
Volatile organic compounds	0.10	0.13	ns	0.11	0.11	ns	0.16	0.18	0.10

ns Difference among areas not significant
* Significant at $p < 0.01$

Whites were negatively associated with nonutility point source emissions. As these sources vary greatly in type, ranging from dry cleaning stores to chemical plants, it was not possible to capture the spatial extent of each facility's potential influence. However, the negative association may reflect the "not-in-my-backyard" effect of the more visible sources, such that the residents try to avoid proximity to such facilities.

7.5 Conclusion

While air pollution emissions have been reduced across the United States, concern for public health remains as studies continue to show the negative impact of emissions at levels below those set by national air quality standards. This study sought to evaluate the spatial aspects of the emission of criteria air pollutants from various sources on respiratory mortality in the five major Texas urban areas of Austin, Dallas-Fort Worth, El Paso, Houston and San Antonio. Using GIS spatial processing functions, a spatial picture of air pollution sources was created and joined to individual level mortality data to allow a comparison of the association of pollution sources and types with deaths where respiratory disease was listed as either the primary or as a contributing cause. It is clear from this analysis that the urban areas differ not only in pollution sources and levels, but also in the composition of the population affected as characterized by age, race/ethnicity and gender. As would be expected, Houston has both the highest rank for emissions, and the highest rate of respiratory primary cause mortality. Race/ethnicity appears to be a more defining attribute than gender or age in identifying the subgroup in the population with the highest risk. While Hispanics have been the focus of much research, findings here show that White and Black primary and contributing rates were higher for the five urban areas in this study. The respiratory related rate of mortality for those aged 65 years or older did not show elevated levels when compared to the elderly group's nonrespiratory rate.

The associations between pollution sources and mortality rates examined here showed only weak positive associations overall. The weak strength of these associations may reflect methodological limitations, as this study sought to use readily available government pollution data that were largely limited in spatial resolution, the complex nature of exposure, and factors that predispose individuals to be at risk for respiratory diseases. In addition, the decedent's work location and mode of transportation for any work commute was not available. Therefore, only residential exposure was able to be identified. Similarly, the emission data only represent outdoor exposure. However, because several studies have found indoor and outdoor pollution concentrations to be associated, this limitation was not deemed to be major (Delfino 2002; Koenig et al. 2005; Rodes et al. 2001; Rojas-Bracho et al. 2000; Williams et al. 2000a).

However, two findings stand out as noteworthy. First, electric power plant pollutants showed the strongest association with all mortality rates, while nonutility point source pollution exhibited negative relationships with all rates. In the case of the former, there has been considerable public pressure resulting in policy that should

reduce future power plant emissions. It is suggested that the negative association for rates and nonutility point sources may reflect the effectiveness of public avoidance of the larger facilities in this category. Second, the complex variation in associations between the different pollution sources and types and the demographic attributes suggest that additional evaluation is needed to find specific reasons for such variations. Overall, this research provides a benchmark for further air quality investigations related to emissions reduction from specific sources. As such, the work may facilitate future efforts to spatially evaluate the impact of facilities that produce air pollution, leading to the improvement of public health and resulting in measurable health benefits.

References

Adgate, J. L., Church, T. R., Ryan, A. D., Ramachandran, G., Fredrickson, A. L., Stock, T. H., Morandi, M. T., and Sexton, K. (2004). Outdoor, indoor, and personal exposure to VOCs in children. *Environmental Health Perspectives, 112*(14), 1386–1392.

American Thoracic Society. (1995). Standards for the diagnosis and care of patients with chronic obstructive pulmonary disease. *American Journal of Respiratory and Critical Care Medicine, 152*(5), S77–S121.

Brook, R. D., Franklin, B., Cascio, W., Hong, Y., Howard, G., Lipsett, M., Luepker, R., Mittleman, M., Samet, J., Smith, S. C., Jr, and Tager, I. (2004). Air pollution and cardiovascular disease: a statement for healthcare professionals from the expert panel on population and prevention science of the American heart association. *Circulation, 109*(21), 2655–2671.

Burnett, R. T., Smith-Doiron, M., Stieb, D., Raizenne, M. E., Brook, J. R., Dales, R. E., Leech, J. A., Cakmak, S., and Krewski, D. (2001). Association between ozone and hospitalization for acute respiratory diseases in children less than 2 years of age. *American Journal of Epidemiology, 153*(5), 444–452.

Chakraborty, J. (2001). Analyzing exposure of school children to accidental releases of hazardous substances. *Journal of Exposure Analysis and Environmental Epidemiology, 11*(4), 269–278.

Chestnut, L. G., and Mills, D. M. (2005). A fresh look at the benefits and costs of the US acid rain program. *Journal of Environmental Management, 77*(3), 252–266.

Creason, J., Neas, L., Walsh, D., Williams, R., Sheldon, L., Liao, D., and Shy, C. (2001). Particulate matter and heart rate variability among elderly retirees: the Baltimore 1998 PM study. *Journal of Exposure Analysis and Environmental Epidemiology, 11*, 116–122.

Davis, A. M., Kreutzer, R., Lipsett, M., King, G., and Shaikh, N. (2006). Asthma prevalence in Hispanic and Asian American ethnic subgroups: ressults from the California Healthy Kids Survey. *Pediatrics, 118*(2), 363–370.

Delfino, R. J. (2002). Epidemiologic evidence for asthma and exposure to air toxics: Linkages between occupational, indoor, and community air pollution research. *Environmental Health Perspectives, 110*(Supplement 4), 573–589.

Delfino, R. J., Gong Jr., H., Linn, W. S., Pellizzari, E. D., and Hu, Y. (2003a). Asthma symptoms in Hispanic children and daily ambient exposures to toxic and criteria air pollutants. *Environmental Health Perspectives, 111*(4), 647–656.

Delfino, R. J., Gong, H., Linn, W. S., Hu, Y., and Pellizzari, E. D. (2003b). Respiratory symptoms and peak expiratory flow in children with asthma in relation to volatile organic compounds in exhaled breath and ambient air. *Journal of Exposure Analysis & Environmental Epidemiology, 13*(5), 348–363.

Dominici, F., Peng, R. D., Bell, M. L., Pham, L., McDermott, A., Zeger, S. L., and Samet, J. M. (2006). Fine particulate air pollution and hospital admission for cardiovascular and respiratory diseases. *Journal of the American Medical Association, 295*(10), 1127–1134.

Eiswerth, M. E., Shaw, W. D., and Yen, S. T. (2005). Impacts of ozone on the activities of asthmatics: revisiting the data. *Journal of Environmental Management, 77*(1), 56–63.

Erbas, B., Kelly, A.-M., Physick, B., Code, C., and Edwards, M. (2005). Air pollution and childhood asthma emergency hospital admissions: Estimating intra-city regional variations. *International Journal of Environmental Health Research, 15*(1), 11–20.

Evans, R. (1992). Asthma among minority children: a growing problem. *Chest, 101*(6), 368S–371S.

Filleul, L., Tertre, A. L., Baldi, I., and Tessier, J.-F. (2004). Difference in the relation between daily mortality and air pollution among elderly and all-ages populations in southwestern France. *Environmental Research, 94*(3), 249–253.

Gauderman, W. J., McConnell, R., Gilliland, F., London, S., Thomas, D., Avol, E., Vora, H., Berhane, K., Rappaport, E. B., Lurmann, F., Margolis, H. G., and Peters, J. (2000). Association between air pollution and lung function growth in southern California children. *American Journal of Respiratory and Critical Care Medicine, 162*, 1383–90.

Gauderman, W. J., Gilliland, G. F., Vora, H., Avol, E., Stram, D., McConnell, R., Thomas, D., Lurmann, F., Margolis, H. G., Rappaport, E. B., Berhane, K., and Peters, J. M. (2002). Association between air pollution and lung function growth in southern California children: results from a second cohort. *American Journal of Respiratory and Critical Care Medicine, 166*, 76–84.

Gauderman, W. J., Avol, E., Gilliland, F., Vora, H., Thomas, D., Berhane, K., McConnell, R., Kuenzli, N., Lurmann, F., Rappaport, E., Margolis, H., Bates, D., and Peters, J. (2004). The effect of air pollution on lung development from 10 to 18 years of age. *The New England Journal of Medicine, 351*(11), 1057–1067.

Gauderman, W. J., Avol, E., Lurmann, F., Kuenzli, N., Gilliland, F., Peters, J., and McConnell, R. (2005). Childhood asthma and exposure to traffic and nitrogen dioxide. *Epidemiology, 16*(6), 737–743.

Gent, J. F., Triche, E. W., Holford, T. R., Belanger, K., Bracken, M. B., Beckett, W. S., and Leaderer, B. P. (2003). Association of low-level ozone and fine particles with respiratory symptoms in children with asthma. *Journal of the American Medical Association, 290*(14), 1859–1867.

Gielen, M. H., van der Zee, S. C., van Wijnen, J. H., and van Steen, C. J. (1997). Acute effects of summer air pollution on respiratory health of asthmatic children. *American Journal of Respiratory and Critical Care Medicine, 155*, 2105–2108.

Glinianaia, S. V., Rankin, J., Bell, R., Pless-Mulloli, T., and Howel, D. (2004). Does particulate air pollution contribute to infant death? A systematic review. *Environmental Health Perspectives, 112*(14), 1365–1370.

Goldberg, M. S., Burnett, R. T., Brook, J., III, J. C. B., Valois, M.-F., and Vincent, R. (2001). Associations between daily cause-specific mortality and concentrations of ground-level ozone in Montreal, Quebec. *American Journal of Epidemiology, 154*(9), 817–826.

Hartog, J. J. d., Hoek, G., Peters, A., Timonen, K. L., Ibald-Mulli, A., Brunekreef, B., Heinrich, J., Tiittanen, P., Wijnen, J. H. v., Kreyling, W., Kulmala, M., and Pekkanen, J. (2003). Effects of fine and ultrafine particles on cardiorespiratory symptoms in elderly subjects with coronary heart disease: the ULTRA Study. *American Journal of Epidemiology, 157*(7), 613–623.

Henry, R. L., Bridgman, H. A., Wlodarczyk, J., Abramson, R., Adler, J. A., and Hensley, M. J. (1991). Asthma in the vicinity of power stations: II. Outdoor air quality and symptoms. *Pediatric Pulmonology, 11*, 134–140.

Hoffmann, B., Moebus, S., Mohlenkamp, S., Stang, A., Lehmann, N., Dragano, N., Schmermund, A., Memmesheimer, M., Mann, K., Erbel, R., Jockel, K.-H., and for the Heinz Nixdorf Recall Study Investigative Group. (2007). Residential exposure to traffic is associated with coronary atherosclerosis. *Circulation, 116*(5), 489–496.

Huston, R. J., Marquez, R. B. R., Baker, J. M., and Saitas, J. A. (2001). *Grandfathered Facilities Report* (SFR-071). Austin: Office of Permitting, Remediation and Registration Texas Natural Resource Conservation Commission.

Islam, T., Gauderman, W. J., Berhane, K., McConnell, R., Avol, E., Peters, J. M., and Gilliland, F. D. (2007). Relationship between air pollution, lung function and asthma in adolescents. *Thorax, 62*(11), 957–963.

Jerrett, M., Burnett, R. T., Kanaroglou, P., Eyles, J., Finkelstein, N., Giovis, C., and Brook, J. R. (2001). A GIS – environmental justice analysis of particulate air pollution in Hamilton, Canada. *Environment and Planning A, 33*(6), 955–973.

Kaiser, R., Romieu, I., Medina, S., Schwartz, J., Krzyzanowski, M., and Künzli, N. (2004). Air pollution attributable postneonatal infant mortality in US metropolitan areas: a risk assessment study. *Environmental Health: A Global Access Science Source, 3*(1), 1–6.

Karr, C., Lumley, T., Schreuder, A., Davis, R., Larson, T., Ritz, B., and Kaufman, J. (2007). Effects of subchronic and chronic exposure to ambient air pollutants on infant bronchiolitis. *American Journal of Epidemiology, 165*(5), 553–560.

Kim, J. J., Smorodinsky, S., Lipsett, M., Singer, B. C., Hodgson, A. T., and Ostro, B. (2004). Traffic-related air pollution near busy roads. *American Journal of Respiratory and Critical Care Medicine, 170*(5), 520–526.

Koenig, J. Q., Mar, T. F., Allen, R. W., Jansen, K., Lumley, T., Sullivan, J. H., Trenga, C. A., Larson, T. V., and Liu, L.-J. S. (2005). Pulmonary Effects of Indoor– and Outdoor-Generated Particles in Children with Asthma. *Environmental Health Perspectives, 113*(4), 499–503.

Levy, J. I., Greco, S. L., and Spengler, J. D. (2002). The importance of population susceptibility for air pollution risk assessment: a case study of power plants near Washington, DC. *Environmental Health Perspectives, 110*(12), 1253–1260.

Levy, J. I., Wilson, A. M., Evans, J. S., and Spengler, J. D. (2003). Estimation of primary and secondary particulate matter intake fractions for power plants in Georgia. *Environmental Science and Technology, 37*(24), 5528–5536.

Lin, S., Munsie, J. P., Hwang, S.-A., Fitzgerald, E., and Cayo, M. R. (2002). Childhood asthma hospitalization and residential exposure to state route traffic. *Environmental Research Section A, 88*(2), 73–81.

Mann, J. K., Tager, I. B., Lurmann, F., Segal, M., Queensberry, C. P., Lugg, M. M., Shan, J., and Van Eeden, S. K. (2002). Air pollution and hospital admissions for ischemic heart disease in persons with congestive heart failure or arrhythmia. *Environmental Health Perspectives, 110*(12), 1247.

McConnell, R., Berhane, K., Gilliland, F., London, S. J., Islam, T., Gauderman, W. J., Avol, E., Margoli, H. G., and Peters, J. M. (2002). Asthma in exercising children exposed to ozone: a cohort study. *The Lancet, 359*, 386–391.

McConnell, R., Berhane, K., Gilliland, F., Molitor, J., Thomas, D., Lurmann, F., Avol, E., Gauderman, W. J., and Peters, J. M. (2003). Prospective study of air pollution and bronchitic symptoms in children with asthma. *American Journal of Respiratory and Critical Care Medicine, 168*, 790–97.

Metzer, R., and Delgado, J. L. (1995). Environmental health and Hispanic children. *Environmental Health Perspectives Supplements, 103*(Supplement 6), 25–32.

Mitka, M. (2008). New evidence-based guidelines focus on treatment of children with asthma. *Journal of the American Medical Association, 299*(10), 1122–1123.

Norris, G., YoungPong, S. N., Koenig, J. Q., Larson, T. V., Sheppard, L., and Stout, J. W. (1999). An association between fine particles and asthma emergency department visits for children in Seattle. *Environmental Health Perspectives, 107*(6), 489–493.

O'Neill, M. S., Jerrett, M., Kawachi, I., Levy, J. I., Cohen, A. J., Gouveia, N., Wilkinson, P., Fletcher, T., Cifuentes, L., and Schwartz, J. (2003). Health, wealth, and air pollution: advancing theory and methods. *Environmental Health Perspectives, 111*(16), 1861–1870.

Peng, R. D., Chang, H. H., Bell, M. L., McDermott, A., Zeger, S. L., Samet, J. M., and Dominici, F. (2008). Coarse particulate matter air pollution and hospital admissions for cardiovascular and respiratory diseases among medicare patients. *Journal of the American Medical Association, 299*(18), 2172–2179.

Peters, A., Dockery, D. W., Muller, J. E., and Mittleman, M. A. (2001). Increased particulate air pollution and the triggering of myocardial infarction. *Circulation, 103*(23), 2810–2815.

Pope III, C. A., Burnett, R. T., Thun, M. J., Calle, E. E., Krewski, D., Ito, K., and Thurston, G. D. (2002). Lung cancer, cardiopulmonary mortality, and long-term exposure to fine particulate air pollution. *Journal of the American Medical Association, 287*(9), 1132–1141.

Pope III, C. A., Hansen, M. L., Long, R. W., Nielsen, K. R., Eatough, N. L., Wilson, W. E., and Eatough, D. J. (2004). Ambient particulate air pollution, heart rate variability, and blood markers of inflammation in a panel of elderly subjects. *Environmental Health Perspectives, 112*(3), 339–345.

Pope III, C. A., Muhlestein, J. B., May, H. T., Renlund, D. G., Anderson, J. L., and Horne, B. D. (2006). Ischemic heart disease events triggered by short-term exposure to fine particulate air pollution. *Circulation, 114*(23), 2443–2448.

Pouliou, T., Kanaroglou, P. S., Elliott, S. J., and Pengelly, L. D. (2008). Assessing the health impacts of air pollution: a re-analysis of the Hamilton children′s cohort data using a spatial analytic approach. *International Journal of Environmental Health Research, 18*(1), 17–35.

Ritz, B., Wilhelm, M., and Zhao, Y. (2006). Air pollution and infant death in Southern California, 1989–2000. *Pediatrics, 118*(2), 493–502.

Rodes, C. E., Lawless, P. A., Evans, G. F., Sheldon, L. S., Williams, R. W., Vette, A. F., Creason, J. P., and Walsh, D. (2001). The relationships between personal PM exposures for elderly populations and indoor and outdoor concentrations for three retirement center scenarios. *Journal of Exposure Analysis & Environmental Epidemiology, 11*(2), 103–115.

Rojas-Bracho, L., Suh, H. H., and Koutrakis, P. (2000). Relationships among personal, indoor, and outdoor fine and coarse particle concentrations for individuals with COPD. *Journal of Exposure Analysis and Environmental Epidemiology, 10*(3), 294–306.

Samet, J. M., Dominici, F., Curriero, F. C., Coursac, I., and Zeger, S. L. (2000). Fine particulate air pollution and mortality in 20 US cities 1987–1994. *The New England Journal of Medicine, 343*(24), 1742–1749.

Schenker, M. B., Vedal, S., Batterman, S., Samet, J., and Speizer, F. E. (1986). Health effects of air pollution due to coal combustion in the Chestnut Ridge region of Pennsylvania: cross-section survey of children. *Archives of Environmental Health, 41*(2), 104–108.

Schwartz, J. (1991a). Particulate air pollution and daily mortality: a synthesis. *Public Health Review, 19*, 39–60.

Schwartz, J. (1991b). Particulate air pollution and daily mortality in Detroit. *Environmental Research, 56*, 204–213.

Schwartz, J. (1993). Air pollution and daily mortality in Birmingham, Alabama. *American Journal of Epidemiology, 137*(10), 1136–47.

Schwartz, J. (1994a). Air pollution and daily mortality: a review and meta-analysis. *Environmental Research, 64*, 36–52.

Schwartz, J. (1994b). Air pollution and hospital admissions for the elderly in Birmingham, Alabama. *American Journal of Epidemiology, 139*(6), 589–598.

Schwartz, J. (1994c). What are people dying of on high air pollution days? *Environmental Research, 64*, 26–35.

Schwartz, J., and Dockery, D. W. (1992a). Increased mortality in Philadelphia associated with daily air pollution concentrations. *American Review of Respiratory Disease, 145*, 600–604.

Schwartz, J., and Dockery, D. W. (1992b). Particulate air pollution and daily mortality in Steubenville, Ohio. *American Journal of Epidemiology, 135*(1), 12–19.

Schwartz, J., and Morris, R. (1994). Air pollution and hospital admissions for the elderly in Detroit, Michigan. *American Journal of Respiratory and Critical Care Medicine, 150*, 648–655.

Schwartz, J., and Morris, R. (1995). Air pollution and hospital admissions for cardiovascular disease in Detroit, Michigan. *American Journal of Epidemiology, 142*(1), 23–35.

Texas Department of State Health Services. (2006). *2002 Health Facts for Texas*. Texas Department of State Health Services. Available: http://www.dshs.state.tx.us/chs/cfs/cshdpa02.shtm [December 9].

Texas Health Care Information Council. (2005). *Preventable Hospitalizations, 2002*. Texas Department of State Health Services. Available: http://www.dshs.state.tx.us/THCIC/Publications/Hospitals/PQIReport2002/PreventableHospitalizations2002.shtm [2008, April 22].

Thurston, G. D., Lippmann, M., Scott, M. B., and Fine, J. M. (1997). Summertime haze air pollution and children with asthma. *American Journal of Respiratory and Critical Care Medicine, 155*, 654–660.

Timonen, K. L., and Pekkanen, J. (1997). Air pollution and respiratory health among children with asthmatic or cough symptoms. *American Journal of Respiratory and Critical Care Medicine, 156*(2), 546–552.

Tolbert, P. E., Mulholland, J. A., MacIntosh, D. L., Xu, F., Daniels, D., Devine, O. J., Carlin, B. P., Klein, M., Dorley, J., Butler, A. J., Nordenberg, D. F., Frumkin, H., Ryan, P. B., and White, M. C. (2000). Air quality and pediatric emergency room visits for asthma in Atlanta, Georgia, USA. *American Journal of Epidemiology, 151*(8), 798–810.

Tonn, B. E., Waidley, G., and Petrich, C. (2001). The ageing US population and environmental policy. *Journal of Environmental Planning and Management, 44*(6), 851–876.

Tonne, C., Melly, S., Mittleman, M., Coull, B., Goldberg, R., and Schwartz, J. (2007). A case–control analysis of exposure to traffic and acute myocardial infarction. *Environmental Health Perspectives, 115*(1), 53–57.

US Bureau of the Census. (2000). *Census of Population and Housing, Summary Tape File 3a*. Washington, DC: Department of Commerce.

US Energy Information Administration. (2003). *State Electricity Profiles* (DOE/EIA-0348(01)/2). Washington, DC: US Department of Energy.

US Environmental Protection Agency. (1997). *National Air Quality and Emissions Trends Report, 1997*. Available: http://www.epa.gov/air/ airtrends/aqtrnd97/ [2008, April 22].

US Environmental Protection Agency. (2006). *Clear Skies in Texas*. Available: http://www.epa.gov/air/clearskies/state/tx.html [2008, April 22].

US Environmental Protection Agency. (2008a). *eGRID 2002 Archive*. Available: http://www.epa.gov/cleanenergy/energy-resources/egrid/archive.html [2008, April 22].

US Environmental Protection Agency. (2008b). *National Emissions Inventories for the US*. US Environmental Protection Agency. Available: http://www.epa.gov/ttn/chief/net/ [2008, April 22].

Watson, A. Y., Bates, R. R., and Kennedy, D. (1988). *Air Pollution, the Automobile, and Public Health*. Washington, DC: National Academies Press.

Williams, R., Suggs, J., Zweidinger, R., Evans, G., Creason, J., Kwok, R., Rodes, C., Lawless, P., and Sheldon, L. (2000a). The 1998 Baltimore particulate matter epidemiology–exposure study: part 1. Comparison of ambient, residential outdoor, indoor and apartment particulate matter monitoring. *Journal of Exposure Analysis and Environmental Epidemiology, 10*(6), 518–532.

Williams, R., Suggs, J., Creason, J., Rodes, C., Lawless, P., Kwok, R., Zweidinger, R., and Sheldon, L. (2000b). The 1998 Baltimore particulate matter epidemiology–exposure study: part 2. Personal exposure assessment associated with an elderly study population. *Journal of Exposure Analysis and Environmental Epidemiology, 10*(6), 533–543.

Zanobetti, A., Schwartz, J., and Gold, D. (2000). Are there sensitive subgroups for the effects of airborne particles? *Environmental Health Perspectives, 108*(9), 841–845.

Chapter 8
Spatial Distribution of Toxic Release Inventory Sites in Chicago Area: Is There Environmental Inequity?

Fahui Wang and Yvette C. Feliberty

Abstract The purpose of this study is to determine if "environmental inequity" can be associated with the spatial distribution of Toxic Release Inventory (TRI) facilities in the Chicago area. The chapter examines whether neighborhoods with minority concentrations or lower-income residents experience disproportionate exposure to facilities that release toxic emissions into the environment. Demographic information is extracted from 2000 Census data, and facility data are based on the 2004 Environmental Protection Agency's Toxic Release Inventory. Geographic Information Systems (GIS) is used to create "buffers" of various spatial extent around the facilities. Statistical analysis (including *t*-tests and regressions) is conducted to examine whether areas within the buffers are significantly more likely to consist of minority and low-income residents and households than areas outside the buffers. Results indicate that at both the census tract and block group levels, Hispanic and non-white classes as well as low-income residents are more likely to be located within the buffers. Therefore, this study corroborates earlier research findings that minority and low-income groups are disproportionately exposed to environmental hazards.

Keywords GIS · Toxic Release Inventory (TRI) sites · *t*-Test · Environmental inequity · Chicago area · Minority

8.1 Introduction

Since the early 1980s, there has been mounting interest in *environmental equity* in relation to the distribution of environmental hazards in neighborhoods predominantly inhabited by low-income residents and/or minority background. This interest was codified in July 1990 by the Environmental Protection Agency's (EPA)

F. Wang (✉)
Department of Geography and Anthropology, Louisiana State University, Baton Rouge, LA 70803, USA
e-mail: fwang@lsu.edu

P.S. Showalter, Y. Lu (eds.), *Geospatial Techniques in Urban Hazard and Disaster Analysis*, Geotechnologies and the Environment 2, DOI 10.1007/978-90-481-2238-7_8,

Environmental Equity Workgroup, which began to examine (and, ultimately confirmed in 1992) the allegation that racial minorities and low-income populations were at higher environmental risk than others (EPA 2008a). Within their definition of "environmental justice", the EPA states that, "Fair Treatment means that no group of people, including racial, ethnic, or socioeconomic groups, should bear a disproportionate share of the negative environmental consequences resulting from industrial, municipal, and commercial operations ..." (EPA 2008b). Examples of such operations include polluting industries, landfills, incinerators, and illegal dumps (Pellow 2004).

In many studies, environmental equity has been treated as a "chicken and egg" situation due to the question of what came first, the residents or the facility. Essentially, those engaged in answering these questions seek to ascertain whether the residents of a particular area are exposed to environmental hazards due to circumstance (i.e., they moved into an area where environmental hazards pre-existed), or because environmentally hazardous facilities have been purposely located in areas largely occupied by low-income and/or minority residents. If the former is the case, the issue is one of housing availability or housing choice. Either there is a lack of affordable housing elsewhere, or people are making a conscious choice to expose themselves to environmental risk so they can reside in a more convenient location and/or enjoy better housing amenities (Pastor et al. 2001). The policy implication under such circumstances is to address issues pertaining to discrimination in the housing and/or job markets. If the latter is the case, "unfair treatment," and therefore environmental inequity, can be alleged. However, even in cases where environmental inequity seems evident, claims of discrimination cannot automatically be inferred due to community growth and change as well as the complex public processes governing the placement of industrial sites. Consequently, causal statements trying to establish environmental inequity are not fully warranted on scientific grounds (Bowen and Wells 2002).

This study examines possible environmental inequity in the spatial distribution of Toxic Release Inventory (TRI) facilities in the Chicago area, specifically Cook County, Illinois. Cook County is an appropriate study area for several reasons. First, the county is predominantly urban (it includes the City of Chicago), containing large populations of various racial/ethnic and economic backgrounds. Second, the county contains a large number of TRI facilities. Third, the time required to geocode the TRI facilities (a significant number of which required manual geocoding) was offset by the large sample size available for use. Finally, our understanding of the study area's historical development, acquired via an extensive literature review, raises our confidence in the interpretation of our findings.

This study examines whether the neighborhoods containing minority concentrations or low-income residents experience disproportionate exposure to facilities releasing toxic emissions into the environment. Demographic information is extracted from 2000 Census data at two data aggregation levels (census tract and block group). The EPA's 2004 TRI provides the location data for environmentally hazardous sites. Statistical analyses, including regressions and *t*-tests, examine whether residents within specified distances from the facilities have significantly

higher ratios of minorities or lower income residents than areas at further distances. If proximity to hazardous sites by disadvantaged population groups is confirmed, policy implications arise in terms of the vulnerability of such residents to disaster events (whether natural or technological in nature) that could cause releases impacting those neighborhoods.

The remainder of this chapter is organized as follows. Section 8.2 provides a literature review of environmental justice and a brief history of Cook County, Illinois. Section 8.3 explains the data used in this study. Section 8.4 addresses the methodological process employed. Section 8.5 presents and discusses the study results. And, Section 8.6 provides concluding comments on the study's major findings and limitations.

8.2 Background and Literature Review

8.2.1 The Environmental Justice Movement

The Environmental Justice Movement rose to prominence in the early 1980s in response to the growing awareness of the unequal distribution of waste sites, other hazards, and overall environmental degradation prominent in many minority and low-income communities throughout the country. Cole and Foster (2001) identified six major benchmarks in the environmental justice movement that helped shape the future of those involved and of the movement itself: civil rights; grassroots anti-toxics movements; academics; labor movements, such as the farm worker movement of the 1960s; traditional environmentalism; and finally, the struggles of indigenous groups across the United States. Together, these causes helped create a unified front struggling for social justice with regard to the physical environment where low-income and minority groups lived and raised their families.

The First National People of Color Environmental Leadership Summit in Washington, DC, held in 1991, is considered the most important event in the movement's history. The summit broadened the movement's goals beyond that of focusing on anti-toxics to include issues such as public health, worker safety, land use, transportation, housing, resource allocation, and community empowerment (Bullard and Johnson 2000). The movement led to important public policy initiatives such as the 1994 Executive Order 12898 (Federal Actions to Address Environmental Justice in Minority Populations and Low-Income Populations) and the subsequent founding of the EPA's National Environmental Justice Advisory Council (NEJAC) (Bolin et al. 2000; Faber and McCarthy 2001).

8.2.2 Studies on Environmental Justice

Most studies on environmental equity have concluded that minorities and the poor are disproportionately exposed to various types of waste sites in the United States (e.g., Bowen et al. 1995; Pinderhughes, 1996; Towers 2000). Five major works are

credited with publicizing environmental equity issues (Hunter 2000; Pellow et al. 2001). The first was by the US General Accounting Office (USGAO 1983), and revealed that three out of four commercial hazardous waste landfills were located in predominantly African American communities. Another prominent work by the United Church of Christ Commission for Racial Justice (UCCCRJ 1987) found that there were a disproportionate number of waste facilities situated in areas with high rates of poverty and minority habitation throughout the United States. Bullard (1990) compiled a series of case studies that documented methods of resistance to waste sites in the communities of color along with issues regarding environmental racism. Lavelle and Coyle (1992) discussed the roles that government and private corporations played in environmental inequities against minorities of all economic backgrounds. And finally, the Committee on Environmental Justice at the Institute of Medicine (CEJ 1999) concluded that the fields of medicine and science must concentrate on the problems and concerns of non-white communities with regard to environmental health.

Research closely related to our work is a study by Baden and Coursey (2002) on the City of Chicago. Using 1960 and 1990 census data, they performed various regressions at the census tract level to test whether the distribution of waste sites was correlated to populations of minorities and the poor and whether there was any historical pattern to that distribution. They concluded that in 1960 more waste sites were located in poor, non-African American neighborhoods, and that in 1990 Hispanic but not African American neighborhoods were disproportionately represented. They also found that, historically, Hispanics were disproportionately exposed to waste sites. Our study builds on their work by using newer data, an expanded study area, multiple geographic levels and a series of distance ranges from waste sites to revisit the issues they identified, with the goal of obtaining more robust results.

8.2.3 Causes for Environmental Inequity

As explained earlier, an important aspect regarding the discourse in relation to environmental justice is the "chicken and egg" dilemma. In addition, researchers disagree about whether the occupancy of residences close to waste sites is voluntary or forced. Some studies support the idea that poor and minority residents often have environmental disamenities thrust upon them. Hite (2000) posits that personal choice is a key factor in the decision-making process to reside in proximity to a waste site. This selective behavior may cause a person to trade the environmental quality of a neighborhood for other housing desires (e.g., number of rooms) and/or location characteristics (e.g., school districts, or accessible transportation) that are personally appealing. Other studies have concentrated on the powerlessness of poor and minority communities in contending with environmental inequity issues. Glasmeier and Farrigan (2003, 132) state that poor communities are often located in unacceptable areas due to "economic forces" (e.g., more affordable housing prices in undesirable areas).

Others contend that people living in these areas have not been made aware of the consequences and dangers of living in neighborhoods blighted by waste sites (Baden and Coursey 2002). Hunter's (2000) study analyzed the dissemination of information throughout a community from the perspective of linguistic isolation in immigrant households. This "environmental unawareness" causes a lack of public participation in the decision-making process of the community (Laurian 2003). Participation of citizens and community-based organizations in the policy process rests upon equitable access to agency-generated environmental information and effective use of that information by citizens (Kellogg and Mathur 2003). Without adequate knowledge and awareness of issues surrounding proposed planning objectives, residents tend not to engage themselves in public discourse because they are not fully aware of the gravity of the situation (Rast 2006; Ross and Leigh 2000). Public disclosure of information can help stimulate effective and informed participation, and can increase pressure on facilities to reduce their impact on the environment (Arora and Cason 1999). Other researchers (Boone and Modarres 1999; Hunter 2000; Talih and Fricker 2002) find that the poor and minority groups are taken advantage of and deprived of appropriate access to resources.

Zoning laws are often cited as the foundation for the disproportionate distribution of toxic sites in poor and minority neighborhoods (Boone and Modarres 1999; Fricker and Hengartner 2001; Ross and Leigh 2000). The purpose of zoning is to restrict the entry of industrial facilities into residential areas, thereby protecting neighborhoods from the detrimental effects of such facilities. However, some believe that some zoning ordinances (labeled "expulsive zoning") are written as a mechanism to use minority neighborhoods as dumping sites for landfills or other unwanted residential uses (Ross and Leigh 2000).

8.2.4 Brief History of Cook County

Knowledge of the demographic, economic, environmental, and industrial history of the study area allows us to fully understand the "chicken and egg" dilemma surrounding environmental justice discourse. In other words, it is important to know whether the residents or the hazardous sites were the first occupants of an area.

Cook County, comprised of the City of Chicago and its suburbs, is the hub of all major economic activities in Illinois. Located along the western banks of Lake Michigan, Chicago has historically been a key port city, providing explorers and merchants with access to the central United States. The city gained this reputation in the middle of the 19th century when it became a hub for "trade, transportation, and the processing of raw materials from the Midwest" (Baden and Coursey 2002: 65). At this time, businesses were developed along the banks of the rivers stretching out of the lake, such as the Chicago River. Such businesses included "a tannery, a meat packing plant, a soap factory, and a brick yard . . . mainly on the North Side" of the city (Hoyt 1933: 19). The West Side saw the advent of lumberyards, breweries, woodworking shops, foundries, and metal-smithing firms (Baden and Coursey 2002). As industry boomed throughout the city, pollution and waste increased. Lake

Michigan, the Chicago River, Lake Calumet, and other waterways were used as dumping grounds for the waste created, and dumping into these Chicago waterways stretched well into the 20th century. Waste dredged from the Calumet and Chicago Rivers was also dumped into Lake Michigan until these actions were banned by the federal government in 1967 (Colten 1985). In fact, the river flows were reversed to limit the inflows of pollution into the lake.

The construction of the first railroads during the late 1800s provided another mode of transportation and opened up many more opportunities for the expansion of industry further into the state and away from waterways. As Cronon (1991: 74) states, the railroad "would rapidly emerge as the chief link connecting Chicago with the towns and rural lands around it, so the city came finally to seem like an artificial spider suspended at the center of a great steel web." After World War II, it was the advent of the highway system that further changed the methods used in siting industrial and commercial businesses and that introduced commercial and industrial decentralization into the suburbs surrounding the city. As the population living in the city increased, so did the amount of household waste. In the late 1940s, residents of the city began utilizing city dumps, or city-owned sanitary landfills, for the majority of their waste although private lots and dumps continued receiving refuse after this time. Following the Solid Waste Disposal Act of 1965, open dumping and burning was prohibited by city officials (Colten 1985).

Race has also played an integral role in shaping the history of Chicago and the Cook County area. Historically, Hispanics and African Americans have been the two most significant ethnic groups in Chicago. The African American population was typically concentrated in urban ghettoes. The practice of "redlining", which began with the National Housing Act of 1934, prohibited many minority neighborhoods from receiving housing loans. The subsidization of suburbanization during the New Deal era further diverted attention from minority neighborhoods. The Urban Renewal era (1950–1970) produced high-rise public housing buildings within urban ghettoes that further isolated low income, minority residents from surrounding areas. Hispanic residents of Chicago have also faced isolation, although not as much as African Americans. Most residents who identify themselves as Hispanic are first, second, or third generation immigrants from Mexico or Puerto Rico. Mexican migrants began settling in Chicago in 1910, with a significant increase between 1960 and 1980 (Baden and Coursey 2002). Puerto Ricans entered the city after World War II, and their numbers increased from 32,371 in 1960 to 112,074 in 1980 (Black et al. 1983). Both ethnic groups migrated to Chicago in search of work in the unskilled labor sector, and have settled in a few highly concentrated areas such as Humboldt Park, West Town, and Logan Square.

To summarize this section, the environmental justice movement grew out of a joint effort by different parties. Their goal was the same, however, to educate the public about environmental inequality issues and thus begin bringing about change. Many studies, including Baden and Coursey's (2002) on the City of Chicago, generated evidence that minorities and the poor are disproportionately exposed to waste facilities. A common dilemma is determining whether residents or waste facilities occupied an area first. Several theories propose reasons for the cause of such

environmental inequity including a lack of public participation, lack of information, language barriers, zoning laws, and the powerlessness of disadvantaged groups. Cook County has been shaped mostly by its location on the banks of Lake Michigan where the Chicago and Calumet Rivers once flowed. This location provided many with access to the interior of the country as well as with a location for depositing refuse. Railroad construction improved communications and increased the area allotted for industry and commerce. And, as in many US cities, Hispanics and African Americans have historically been segregated and isolated in Chicago, a circumstance that spurs concern whether environmental inequality is disproportionately present in the areas in which they reside.

8.3 Data Sources

Toxic Release Inventory (TRI) data are extracted from the *TRI Explorer*, a database provided by EPA (EPA 2008c). This data became available under the Emergency Planning and Community Right-to-Know Act of 1986 and was later expanded under the Pollution Prevention Act of 1990. Information listed in the TRI database is publicly available and contains data on toxic chemical releases and other waste management activities reported annually by certain covered industry groups as well as federal facilities. Covered industry groups are those facilities with ten or more full-time employees that process 25,000 pounds or more or use 10,000 pounds or more of any one specific TRI chemical (Dolinoy and Miranda 2004). The TRI facility data used in this study were for the year 2004, the most current TRI information available at the time this research began.

The TRI facilities analyzed in this study include all listed TRI facilities for Cook County for the year 2004, and we encountered several issues when using these data. First, the data are self-reported emissions estimates, not actual measures of release (Pastor et al. 2004). Second, some of the geographic coordinates provided by the TRI database were incorrect or missing – we found 122 facilities with missing coordinates. Consequently, verification of coordinate locations is necessary when working with EPA databases, as the data are self-reported to state agencies by the facilities and later passed on to the EPA (Scott et al. 1997). The problem was resolved by cross-referencing the TRI data with the EPA's Resource Conservation and Recovery Act list and correcting any coordinate discrepancies. Based on the addresses provided by the EPA, we used a web-based service provided by Steve Morse (stevemorse.org/jcal/latlon.php) to manually geocode the facilities one by one. Third, the TRI data do not include releases from mobile sources and smaller emissions facilities, both of which are known to contribute to pollution levels and health risks (Pastor et al. 2004). Ultimately, a total of 428 TRI facilities were accessible for use in this study.

In an effort to address the *modifiable areal unit problem* (MAUP; Fotheringham and Wong 1991; Anderton et al. 1994; Bolin et al. 2000; Mennis 2002), this study performs analysis at the census tract and block group levels to determine whether the results are consistent across differently sized units of analysis. Block groups are

the smallest unit for which the Census Bureau ordinarily reports economic information pertinent for the study (Harner et al. 2002). Census tract and block group level data were retrieved from the US Census Bureau website for the year 2000 (US Census Bureau 2008b). The following variables summarize the racial and ethnic composition of the geographic areas involved in this study: White, African American, Hispanic, Native American, Asian, Hawaiian/Pacific Islander, and Other. Additional variables include total population and median income.

It is important to note that these categories of race and ethnicity underwent a revision since the previous census. In 1977, the Office of Management and Budget (OMB) issued Statistical Policy Directive Number 15, "Race and Ethnic Standards for Federal Statistics and Administrative Reporting" (US Census Bureau 2008a). This directive established four main racial categories: American Indian or Alaskan Native, Asian or Pacific Islander, African American, and White. It also established two ethnic categories: Hispanic and Non-Hispanic. Due to the changing racial and ethnic structure of the country since 1977, the Census Bureau determined that these classifications were no longer accurate. Therefore, in 1997, the OMB revealed its new racial and ethnic categories, which include: American Indian or Alaska Native, Asian, African American, Native Hawaiian or Other Pacific Islander, and White. It also includes the category Some Other Race, which is intended to capture ethnicities such as Mulatto, Mestizo, and Creole.

Figure 8.1 illustrates the locations of the 428 facilities throughout Cook County with census tracts as the background. The majority of the facilities are located in the central portion of the county, with many other facilities spreading out towards the northwestern and southern suburbs. The spread may be a result of the post-war decentralization of commerce and industry.

8.3.1 Analysis Methods

The purpose of this study is to determine whether there is evidence of environmental inequity for different racial/ethnic and income groups in Cook County. Environmental inequity will be measured based on whether there is a disproportionate distribution of TRI facilities in areas inhabited by minority groups or residents with low median incomes throughout the county. Mapping the distribution of TRI sites against demographic and socioeconomic backgrounds gives us a visual representation of the relationship. However, statistical analysis is needed to rigorously test the hypothesis.

8.3.1.1 Data Preparation and Mapping

Two aggregation levels of data were used in this study, census tracts, and block groups. Table 8.1 presents the basic statistics for various racial/ethnic group ratios in Cook County at both levels. This study considers four minority groups – African American, Hispanic, Asian and Other – comprising an average of more than four percent of population across census tracts or block groups in the study area.

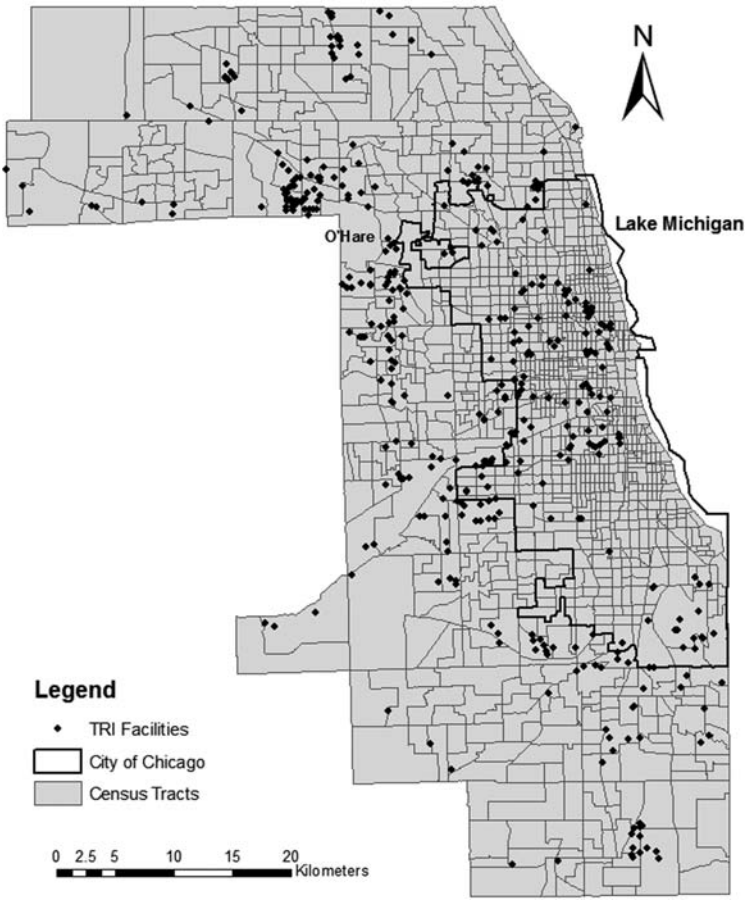

Fig. 8.1 Toxic release inventory (TRI) sites in cook county, 2004

American Indians/Eskimo and Hawaiian/Pacific Islanders are not included because their percentages are considered too low to be significant for this study.

Three distances – 500, 1000 and 1500 m – were used to define proximity to the TRI facilities. Glickman (2004) points out that in urban areas, neighborhoods (and any hazards present within them) typically do not extend further than a mile. If the centroid of a tract or block group falls within one of the aforementioned distances from any TRI facility, it is grouped as "within the proximity," otherwise it is grouped as "outside". A binary variable is created to flag whether a tract or block group is within (=1) or outside (=0) proximity to a TRI site in each of the three distance scenarios. A tract (block group) may be partially within and partially outside the distance described. One may use a spatial interpolation method to allocate population between the split portions. However, by assuming a uniform distribution of attributes within an areal unit, it would create two samples with identical attributes

Table 8.1 Basic statistics for proportions of racial/ethnic groups in cook county 2000

	Census tracts (n = 1337)			Census block groups (n = 4219)		
Variable	Mean	Std dev	Max*	Mean	Std dev	Max*
African Am.	0.33	0.40	1	0.31	0.40	1
Hispanic	0.19	0.25	0.97	0.18	0.25	1
White	0.51	0.35	1	0.54	0.36	1
Am. Indian/Esk.	0.003	0.004	0.05	0.002	0.01	0.57
Asian	0.04	0.08	0.86	0.04	0.08	0.90
Hawaiian/P.I.	0.0005	0.001	0.01	0	0.001	0.05
Other	0.09	0.15	0.68	0.09	0.14	0.74

Note: * Minimum value in all cases is 0.

(i.e., ethnic group ratios or income): one inside and another outside of the range. This does not contribute to the statistical test power. Some population assignment methods using additional information (e.g., Wu 2006) may be also used. Given time constraints and data availability, such approaches were not feasible for this study.

A series of maps were created to examine the relationship between TRI sites and demographic (income) distributions, three of which are included, here. Figures 8.2 and 8.3 illustrate the distribution of African American and Hispanic populations respectively. In Fig. 8.2, African Americans were mainly concentrated in the south of Cook County (where some TRI sites can be found), in another area at the southwest corner, and in the middle of the county, but very few in the area near downtown Chicago. In Fig. 8.3, one cluster of Hispanic population was on the north side by the lake, one was to the southwest of the downtown area, and another band around O'Hare International Airport. All three areas indicate the presence of TRI sites.

Figure 8.4 illustrates the geographic pattern of median income in the study area. The greatest concentration of the highest median income bracket is seen in the northwestern and southwestern suburbs of the county. There are also areas of high median income located within the Loop area of Chicago extending north along the coast of Lake Michigan. One can also see a general absence/lack of TRI facilities in these high income areas, with the exception of a few located near the north and southwestern suburbs.

8.3.1.2 Pooled *t*-Test

Evidence of disproportionate exposure throughout minority areas is supported when the values of the ethnicity ratio of the tracts within the specified distance are larger than the values of the tracts found outside the distance. Given the nature of aggregated data from the census, our hypothesis for testing environmental justice with regard to racial/ethnic groups is structured as:

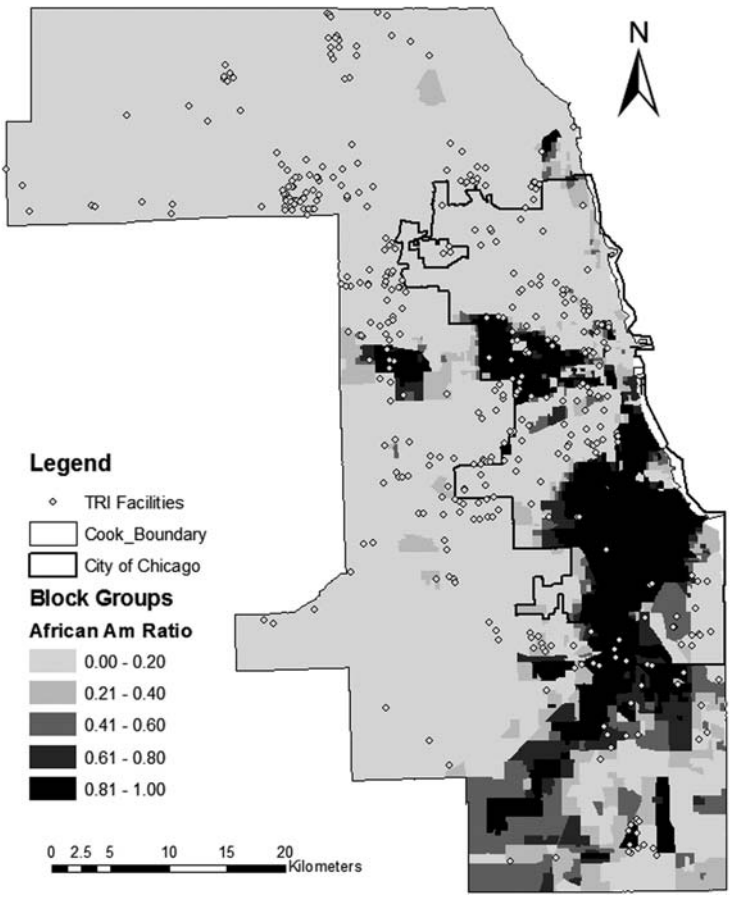

Fig. 8.2 African American population ratios across block groups in cook county, 2000

H_0 (null hypothesis): the ratios of a minority in areas within the proximity of TRI facilities are not different from those outside.

Evidence of disproportionate exposure determined by median income is supported when the values of the median income of the tracts within the specified distance are less than that of the tracts found outside of the distance. Our hypothesis for testing environmental justice with regard to income distribution is:

H_0 (null hypothesis): median incomes in areas within proximity of TRI facilities are not different from those outside.

A pooled *t*-test was used to compare the sample mean of those tracts (block groups) within a specified distance from a TRI facility and the sample mean of those located outside the distance. In this study, Statistical Analysis Software (SAS®; specifically, the "TTEST" procedure) was used to implement the *t*-test.

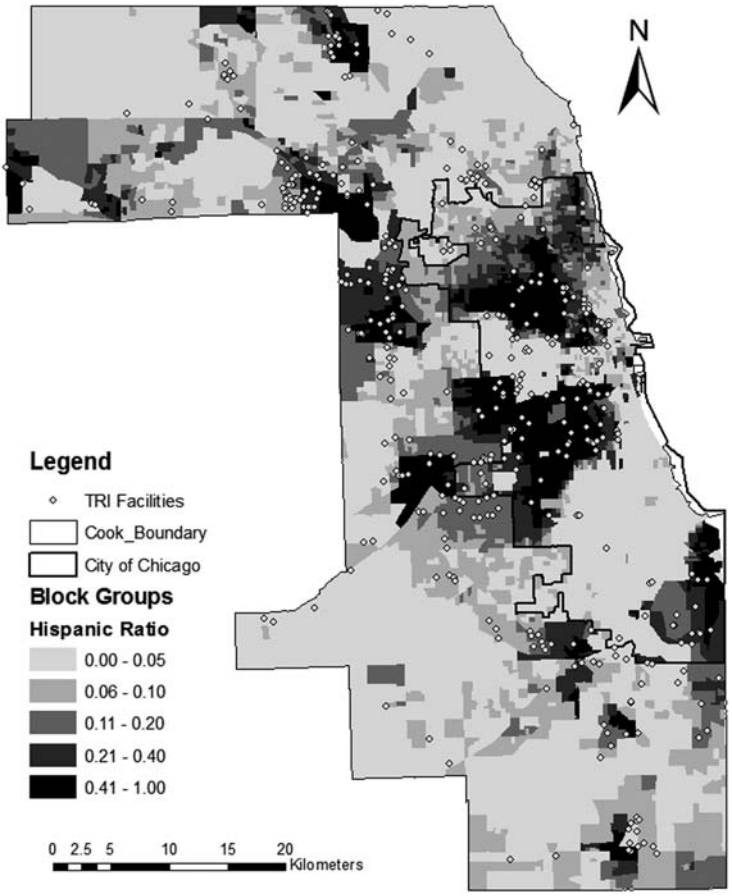

Fig. 8.3 Hispanic population ratios across block groups in cook county, 2000

Table 8.2 presents the results of the *t*-test on Hispanic ratios at the census tract level in Cook County. The sample mean of Hispanic ratios in 979 tracts within 1500 m was 0.2349, and the sample mean of the Hispanic ratios in 358 tracts outside 1500 m was 0.0647. On average, Hispanic ratios within the proximity of TRI sites were 0.1702 higher than outside of the range. Given the sample sizes, means and standard deviations, the t-statistic was calculated to be 11.42, much larger than the critical value of 3.29 at the 0.001 (two-tailed test) level. The hypothesis of no difference in Hispanic ratios between tracts within and outside the proximity of TRI sites is rejected. Similar conclusions can be drawn from Table 8.2 based on the distance ranges of 1000 and 500 m.

Regression with a binary independent variable The pooled *t*-test can be also implemented in a commonly-used regression model. From the above example, the regression model is constructed as

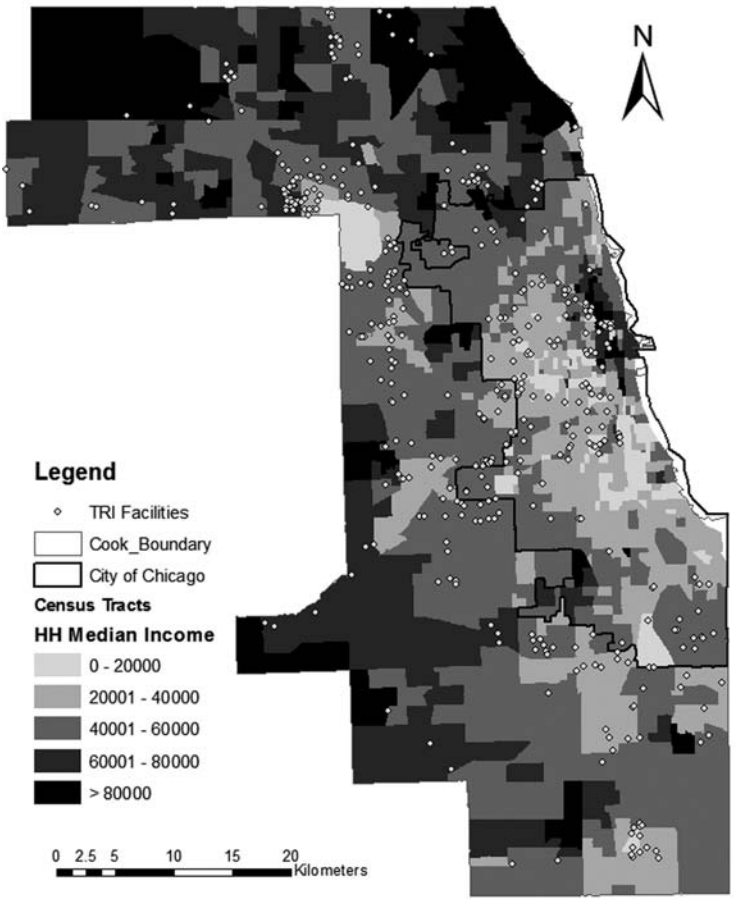

Fig. 8.4 Household median income across census tracts in cook county, 2000

$$Y = a + b * Flag \tag{8.1}$$

where the dependent variable Y is Hispanic ratios in various census tracts, the independent variable *Flag* is a binary dummy variable coded to identify whether a tract was within the proximity of any TRI facilities (=0) or outside (=1), and a and b are parameters to be estimated.

For instance, using 1500 m as the distance range at the census tract level, the regression result for Hispanics (see Table 8.3) is

$$Y = 0.2349 - 0.1702\, Flag$$
$$(30.47)\ (-11.42)$$

Table 8.2 Pooled *t*-Test for Hispanics in census tracts in cook county

	n	Mean	Standard deviation	t-value
All	1337	0.1893	0.2527	
Within 1500 m	979	0.2349	0.2744	11.42
Outside of 1500 m	358	0.0647	0.1065	
Within 1000 m	793	0.2600	0.2877	13.11
Outside of 1000 m	544	0.0864	0.1356	
Within 500 m	552	0.2835	0.2966	12.03
Outside of 500 m	785	0.1231	0.1906	

Table 8.3 Regression results on ethnicity ratios across cook county census tracts (n = 1337)

Minority group	Distance	Variable	Parameter	Std. error	*t* value
Afr. American	1500 m	*a*	0.2836	0.0127	22.42
		b	0.1743	0.0244	7.13
	1000 m	*a*	0.2611	0.0140	18.64
		b	0.1700	0.0220	7.74
	500 m	*a*	0.2323	0.0168	13.83
		b	0.1668	0.0219	7.61
Hispanic	1500 m	*a*	0.2349	0.0077	30.47
		b	−0.1702	0.0149	−11.42
	1000 m	*a*	0.2600	0.0085	30.77
		b	−0.1736	0.0132	−13.11
	500 m	*a*	0.2835	0.0102	27.75
		b	−0.1604	0.0133	−12.03
Asian	1500 m	*a*	0.0445	0.0026	17.45
		b	−0.0054	0.0049	−1.10
	1000 m	*a*	0.0438	0.0028	15.47
		b	−0.0019	0.0044	−0.43
	500 m	*a*	0.0430	0.0034	12.66
		b	0.0001	0.0044	0.02
Other	1500 m	*a*	0.1192	0.0045	26.46
		b	−0.0922	0.0087	−10.58
	1000 m	*a*	0.1333	0.0049	26.98
		b	−0.0952	0.0077	−12.30
	500 m	*a*	0.1462	0.0060	24.49
		b	−0.0879	0.0078	−11.29

The corresponding t values for the intercept a and slope b are in parentheses underneath the equation. Based on the regression result, if $Flag = 0$, then $Y = 0.2349$, which is the intercept, i.e., the sample mean of Hispanic ratios for tracts *within* the distance range (1500 m) from the TRI sites. If $Flag = 1$, then $Y = 0.2349 - 0.1702 = 0.0647$, which is the sample mean of Hispanic ratios for tracts *outside* the distance range. The slope $b = -0.1702$ indicating the difference between

the two sample means, and its corresponding t value (-11.42) is the same as the t value in the pooled-t test (the negative sign indicating a lower sample mean for tracts identified by $Flag = 1$).

In summary, the regression is completely equivalent to the pooled-t test. In the next section, only the regression results are presented. Our primary interest from the regression is on the t value for the slope b, indicating whether and how statistically significant the difference is between the two samples. Since the model is not designed to explain the variation of Y by explanatory variables, the R^2 value, which can be derived from the t value in any bivariate regression (as is the case here), is redundant and thus not presented.

8.4 Results and Discussion

8.4.1 Analyzing Race and Ethnicity

Table 8.3 presents regression results for four racial/ethnic minority groups in Cook County at the census tract level. Table 8.4 shows the results at the block group level. In the tables, the intercept a represents the average ratio of a minority group in tracts within the given distance, and the slope b is the difference of the ratios between those tracts within and outside the distance. A *positive b* indicates a higher average minority ratio *outside than inside* the distance range from TRI sites; and a negative b indicates otherwise. Whether the difference is statistically significant is reflected by the corresponding t value (as well as by the significance level Pr>| t |).

The regression results in Tables 8.3 and 8.4 suggest evidence of environmental inequity for the Hispanic population and those classified as "Other" at each of the three distances (500, 1000, and 1500 m). For Hispanics, as illustrated in the previous section, the average percentage across census tracts inside the given distances from the TRI sites was 23−28% in contrast to 6−12% outside the distance ranges. For "Other", the difference in percentages was about 9%. All are highly significant statistically. However, the results also show that the percentage of African American population living within proximity to TRI facilities was *lower* than those outside, and the difference was statistically significant. This result is surprising because it was expected that the African American population would exhibit some sign of being disproportionately exposed to these facilities. At the census tract level, the percentage of African Americans outside the distance ranges was about 17% higher than the percentage inside the ranges; and at the block group level, the difference was also above 10%. The difference for Asian Americans was not statistically significant.

For comparison, we also tested the model on the white population at both geographic levels and found no evidence of environmental inequity with respect to proximity to TRI facilities. Although there is no evidence of disproportionate exposure with respect to the White population, it must be noted that income plays a role in environmental justice discourse. Because the White population is not devoid of

Table 8.4 Regression results on ethnicity ratios across cook county block groups (n = 4219)

Minority Group	Distance	Variable	Parameter	Std. error	*t* value
Afr. American	1500 m	*a*	0.2666	0.0076	34.88
		b	0.1143	0.0128	8.92
	1000 m	*a*	0.2544	0.0088	28.70
		b	0.1016	0.0123	8.27
	500 m	*a*	0.229	0.0118	19.42
		b	0.1074	0.0138	7.77
Hispanic	1500 m	*a*	0.2383	0.0045	52.93
		b	−0.1617	0.0075	−21.42
	1000 m	*a*	0.2626	0.0052	50.43
		b	−0.1573	0.0072	−21.79
	500 m	*a*	0.2836	0.0070	40.17
		b	−0.1412	0.0082	−17.07
Asian	1500 m	*a*	0.0428	0.0014	28.94
		b	−0.0035	0.0024	−1.41
	1000 m	*a*	0.0426	0.0017	24.89
		b	−0.0020	0.0023	−0.88
	500 m	*a*	0.0419	0.0022	18.42
		b	−0.0005	0.0026	−0.21
Other	1500 m	*a*	0.1199	0.0026	45.78
		b	−0.0873	0.0043	−19.90
	1000 m	*a*	0.1338	0.0030	44.27
		b	−0.0866	0.0041	−20.66
	500 m	*a*	0.1439	0.0041	35.10
		b	−0.0756	0.0048	−15.75

low-income residents, those in the white population that do not have high median incomes may also be affected by disproportionate exposure to TRI facilities and other environmental hazards. This issue will be analyzed in the next subsection.

A census tract covers a larger area, and is made up of a number of block groups, and therefore contains generalized information that may not clearly capture the differences in its resident population. Therefore, block groups are more likely to exhibit variations in data across the study area. The statistics displayed in Tables 8.3 and 8.4 are highly consistent, indicating the robustness of the results and therefore providing little evidence of the Modifiable Area Unit Problem (MAUP).

8.4.2 Analyzing Income Distribution

Median income was only available at the census tract level, therefore the analysis is limited to that level. As described earlier, the regression model in Equation (8.1) is used, with Y as income, to examine the difference in median income between the census tracts inside and outside the distance ranges. Table 8.5 presents the regression results. In the tracts inside 1500 m from the TRI facilities, the average median

income was $44,135. In tracts outside the range, the average median income was $3298 higher. The difference was statistically significant at the 0.05 level. When the distance range is defined as 1000 m, the result is similar with a higher statistical significance (i.e., at the 0.01 level). The difference is no longer significant when using the 500 m distance range. In other words, there is evidence that residents closer to the TRI sites had lower median income than those farther away. The only exception is when using a short distance such as 500 m to define proximity. Note that census tracts are much larger than block groups. By representing an area by its centroid, the result from census tracts is not as reliable as that from block groups; therefore the results obtained at a shorter distance are less reliable than a longer distance.

Table 8.5 Regression results on median income across cook county census tracts (n = 1337)

Distance	Variable	Parameter	Std. error	*t* value
1500 m	*a*	44,135.00	733.85	60.14
	b	3298.24	1419.90	2.32
1000 m	*a*	43,378.00	813.41	53.33
	b	4040.03	1277.35	3.16
500 m	*a*	43,895.00	978.79	44.85
	b	1910.36	1277.47	1.50

8.5 Concluding Comments

The purpose of this study is to determine if there is disproportionate exposure to environmental hazards in areas occupied predominantly by minority groups or those of low median incomes. Three characteristics differentiate this study from previous work on environmental justice research, particularly the one by Baden and Coursey (2002) that is closely related to ours. First, GIS techniques are used in this study in order to determine the proximity of the nearest TRI facility to a census tract or block group more accurately. Second, geocoding the TRI data set with a combination of automatic and manual procedures ensures a maximum matching ratio. Therefore, nearly all the TRI sites are included in the study. Third, data analysis at different aggregation levels helps determine the effects of the Modifiable Area Unit Problem in the study. Consistent results across different areal units demonstrate the robustness of the conclusions drawn from the analysis.

Environmental inequity is a complicated situation that has affected many minority and low-income residents throughout the United States. Cook County, which contains the City of Chicago, has long been highly industrialized and those industrial activities play an integral role in determining who has been exposed to industrial waste products. Some studies find that race is often a better predictor of exposure to environmental hazards than income (e.g., Cole and Foster 2001). The results of the study suggest that both race and income seem to be relevant to

the environmental inequity issue. Evidence of environmental inequity was found for the Hispanic population and those classified as "Other", but not for Asian Americans. As discussed earlier, this finding does not necessarily suggest that TRI facilities were purposely sited where there were higher concentrations of Hispanics or other minorities. Because the Hispanic population developed relatively recently, it is likely that they moved close to industrial areas where many could find jobs and where housing was relatively inexpensive. The surprising result is that the percentage of the African American population living within proximity to TRI facilities was *lower* than those outside, and that the difference was statistically significant. Finally, there is evidence that residents closer to TRI sites have lower median income than those farther away.

Several limitations of the data used in this study need to be pointed out. The data set only contains those facilities listed on the EPA's Toxic Release Inventory Site and does not include those that may not meet the requirements for federally mandated reporting of the facility. The data also exclude noxious facilities such as landfills, underground storage tanks, brownfield areas, or other areas that pose environmental risks and hazards for those living in their proximity. Another aspect of these hazardous sites that was not examined in this study is the type of toxins released, their mode of release (i.e., air, ground, water), and the amounts released. These three characteristics also play a role in determining the level of risk and method of transmission to those residing near release sites. Toxins released by air may travel further and at a different rate than those that are waterborne. Once released from confinement, their chemical structure may be altered when combined with the chemical structure of molecules found in the air, land, and water. All are important issues that may be addressed in future research when better data become available. In terms of methodology, two directions may be pursued to expand or improve the study. This study considers race and income separately. However, the two factors can be correlated with each other as well as other socioeconomic variables, such as poverty levels, ownership status of the residence, and owner and rental cost characteristics. Future work may consolidate these variables into a compound factor (for instance, labeled as "concentrated disadvantages") using factor analysis. Another minor issue is the so-called "edge effect". Residents near the border of the county may be also exposed to TRI facilities of adjacent counties. Inclusion of those TRI facilities within a buffer distance from the county boundary will enhance the value of the work. Finally, this study uses aggregated demographic data at the block group and census tract levels from the census. The analysis is generally adequate for public policy purposes within regulatory agencies, but is not appropriate for environmental epidemiology studies.

References

Anderton, D.L., Anderson, A.B., Oakes, J.M., and Fraser, M.R. (1994). Environmental equity: The demographics of dumping. *Demography 31*: 229–248.

Arora, S. and Cason, N. (1999). Do community characteristics influence environmental outcomes? Evidence from the toxics release inventory. *Southern Economic Journal 65*: 691–716.

Baden, B.M., and Coursey, D.L. (2002). The locality of waste sites within the City of Chicago: A demographic, social, and economic analysis. *Resource and Energy Economics 24*: 53–93.

Black, S.A., Eichenthal, D.R., Espinosa, R., Heidinger, T.E., Hogan III, W.C., Levin, M.R., Maude, J.L., Niemi, P., O'Donnell, M., and Wolfberg, M.L. (1983). *Latinos in Metropolitan Chicago: A Study of Housing and Employment*. Chicago: Latino Institute.

Bolin, B, Matranga, E., Hackett, E.J. Sadalla, E.K., Pijawka, K.D., Brewer, D., and Sicotte, D. (2000). Environmental equity in a sunbelt city: The spatial distribution of toxic hazards in Phoenix, Arizona. *Environmental Hazards 2*: 11–24.

Boone, C.G. and Modarres, A. (1999). Creating a toxic neighborhood in Los Angeles county: A historical examination of environmental inequity. *Urban Affairs Review 35*: 163–187.

Bowen, W.A., Salling, M.J., Haynes, K.E. and Cyran, EJ. (1995). Toward environmental justice: Spatial equity in Ohio and Cleveland. *Annals of the Association of American Geographers 85*: 641–663.

Bowen, W.M. and Wells, M.V. (2002). The politics and reality of environmental justice: A history and considerations for public administrators and policy makers. *Public Administration Review*: *62*: 688–698.

Bullard, R.D. (1990). *Dumping in Dixie: Race, Class, and Environmental Quality.* Boulder, Co: Westview Press.

Bullard, R.D. and Johnson, G.S. (2000). Environmental justice: Grassroots activism and its impact on public policy decision making. *Journal of Social Issues*, *56*: 555–578.

Cole, L.W. and Foster, S.R. (2001). *From the Ground Up: Environmental Racism and the Rise of the Environmental Justice Movement.* New York: New York University Press.

Colten, C.E. (1985). *Industrial wastes in the Calumet area, 1869 – 1970: An historical geography*. Champaign, IL: Hazardous Waste Research and Information Center.

Committee on Environmental Justice, Institute of Medicine (CEJ). (1999). *Toward Environmental Justice: Research, Education, and Health Policy Needs*. Washington, DC: National Academy Press.

Cronon, W. (1991). *Nature's metropolis: Chicago and the Great West*. New York: W.W. Norton and Company.

Dolinoy, D.C. and Miranda, M.L. (2004). GIS modeling of air toxics releases from TRI reporting and non-TRI-reporting facilities: Impacts for environmental justice. *Environmental Health Perspectives 112*: 1717–1724.

Environmental Protection Agency (EPA) 2008a. "What is the Origin of Environmental Justice at EPA?" Environmental Justice: Frequently Asked Questions, http://www.epa.gov/compliance/resources/faqs/ej/index.html, last updated February 5. Accessed September 6, 2008.

Environmental Protection Agency (EPA) 2008b. "How Does EPA Define Environmental Justice?" Environmental Justice: Frequently Asked Questions, http://www.epa.gov/compliance/resources/faqs/ej/index.html, last updated February 5. Accessed September 6, 2008.

Environmental Protection Agency (EPA) 2008c. TRI Explorer. Chemical Report. http://www.epa.gov/triexplorer/, last updated July 23. Accessed September 6, 2008.

Faber, D. and McCarthy, D. (2001). The evolving structure of the environmental justice movement in the United States: New models for democratic decision-making. *Social Justice Research 14*: 405–421.

Fotheringham, A.S. and Wong, D.W.S. (1991). The modifiable areal unit problem in multivariate statistical analysis. *Environment and Planning A 23*: 1025–1044.

Fricker, Jr., R.D. and Hengartner, N.W. (2001). Environmental equity and the distribution of toxic release inventory and other environmentally undesirable sites in metropolitan New York City. *Environmental and Ecological Statistics 8*: 33–52.

Glasmeier, A.K. and Farrigan, T.L. (November 2003). Poverty, sustainability, and the culture of despair: Can sustainable development strategies support poverty alleviation in America's most environmentally challenged communities? *The Annals of the American Academy of Political and Social Science 590*: 131–149.

Glickman, T.S. (2004). *Evaluating equity in Alleghany County*. New York: Program for the Human Environment, Rockefeller University. Available at http://phe.rockefeller.edu/comm_risk/commrsk3.html [accessed May 2, 2007]

Harner, J., Warner, K., Pierce, J., and Huber, T. (2002). Urban environmental justice indices. *The Professional Geographer 54*: 318–331.

Hite, D. (2000). A random utility model of environmental equity. *Growth and Change 31*: 40–58.

Hoyt, H. (1933). *One Hundred Years of Land Values in Chicago*. Chicago: University of Chicago Press.

Hunter, L.M. (2000). The spatial association between US immigrant residential concentration and environmental hazards. *International Migration Review 34*: 460–488.

Kellogg, W.A. and Mathur, A. (2003). Environmental justice and information technologies: Overcoming the information-access paradox in urban communities. *Public Administration Review 63*: 573–585.

Lavelle, M. and Coyle, M. (1992). Unequal protection: The racial divide in environmental law. *National Law Journal 15*: S1–S12.

Laurian, L. (2003). A prerequisite for participation: Environmental knowledge and what residents know about local toxic sites. *Journal of Planning Education and Research 22*: 257–269.

Mennis, J. (2002). Using geographic information systems to create and analyze statistical surfaces of population and risk for environmental justice analysis. *Social Science Quarterly 83*: 281–297.

Pastor, Jr., M., Sadd, J., and Hipp, J. (2001). Which came first? Toxic facilities, minority move-in, and environmental justice. *Journal of Urban Affairs 23*: 1–21.

Pastor, Jr., M., Sadd, J.L., and Morello-Frosch, R. (2004). Waiting to exhale: The demographics of toxic air release facilities in 21st century California. *Social Science Quarterly 85*: 420–440.

Pellow, D.N. (2004). The politics of illegal dumping: An environmental justice framework. *Qualitative Sociology 27*: 511–525.

Pellow, D.N., Weinberg, A., and Schnaiberg, A. (2001). The environmental justice movement: Equitable allocation of the costs and benefits of environmental management outcomes. *Social Justice Research 14*: 423–439.

Pinderhughes, R. (1996). The Impact of Race on Environmental Quality: An Empirical and Theoretical Discussion. *Sociological Perspectives 39*: 231–248.

Rast, J. (2006). Environmental justice and the new regionalism. *Journal of Planning Education and Research 25*: 249–263.

Ross, C.L. and Leigh, N.G. (2000). Planning, urban revitalization, and the inner city: An exploration of structural racism. *Journal of Planning Literature 14*: 367–380.

Scott, M., Cutter, S.L., Menzel, C., and Ji, M. (1997). Spatial accuracy of the EPA's environmental hazards databases and their use in environmental equity analysis. *Applied Geographic Studies 1*: 45–61.

Talih, M. and Fricker, Jr., R.D. (2002). Effects of neighborhood demographic shifts on findings of environmental injustice: A New York City case study. *Journal of the Royal Statistical Society: Series A (Statistics in Society) 165*: 375–397.

Towers, G. (2000). Applying the political geography of scale: Grassroots strategies and environmental justice. *Professional Geographer 52*: 23–36.

United Church of Christ Commission for Racial Justice (UCCCRJ). (1987). *Toxic Wastes and Race in the United States: A National Report on the Racial and Socio-Economic Characteristics of Communities with Hazardous Waste Sites.* New York: United Church of Christ.

US Census Bureau (2008a). Race Data. *Recommendations from the Interagency Committee for the Review of the Racial and Ethnic Standards to the Office of Management and Budget Concerning Changes to the Standards for the Classification of Federal Data on Race and Ethnicity*. http://www.census.gov/population/www/socdemo/race/Directive_15.html last updated April 10. Accessed March 24, 2008.

US Census Bureau (2008b). United States Census 2000. *Your Gateway to Census 2000*. http://www.census.gov/main/www/cen2000.html, last updated April 24. Accessed September 6, 2008.

US General Accounting Office (USGAO). (1983). *Siting of Hazardous Waste Landfills and Their Correlation with Racial and Economic Status of Surrounding Communities*. Washington, DC: GAO/RCED.

Wu, S-S. 2006. *Incorporating GIS and Remote Sensing for Census Population Disaggregation*. ETD Collection for Texas State University. Paper AAI3221522. http://ecommons.txstate.edu/dissertations/AAI3221522

Chapter 9
Risk and Exposure to Extreme Heat in Microclimates of Phoenix, AZ

Darren M. Ruddell, Sharon L. Harlan, Susanne Grossman-Clarke, and Alexander Buyantuyev

Abstract As rapid urban development continues, the impacts of temperature extremes on human health and comfort are expected to increase as threshold temperatures of human tolerance are crossed more frequently and for longer periods of time. This study examined extreme heat as an urban hazard throughout the Phoenix (Arizona, USA) metropolitan area during a four-day 2005 summer heat wave. Utilizing the Weather Research and Forecasting (WRF) model to simulate 2 m air temperature variability throughout the region, the distribution of threshold temperatures and heat exposure was examined in 40 diverse neighborhoods. Neighborhood residents also responded to a social survey about perceived temperatures and heat-related health problems during the summer of 2005.

Results indicated that extreme heat was variably distributed throughout the neighborhoods; residents' perceptions of temperature and self-reported experiences with heat-related illnesses were related to environmental conditions; the highest risk of exposure to extreme heat was among elderly, minority, and low-income residents; and land use/cover characteristics exhibited strong relationships with local threshold temperatures. Research contributions include the development of a geotechnical analysis method that could help cities to prepare for and respond to the most vulnerable residents during periods of extreme heat as well as the interrelation of regional atmospheric model results with socio-economic data.

Keywords Climate · Hazard · GIS · Environmental justice · Urban heat island · Weather-forecasting

9.1 Introduction

Cities in most types of climate regimes are becoming warmer over time and, consequently, urban populations are increasingly vulnerable to the hazards of summertime heat. In cities, the effect of rising global temperatures is compounded by regional

D.M. Ruddell (✉)
School of Geographical Sciences, Arizona State University, Tempe, AZ 85287-0104, USA
e-mail: darren.ruddell@asu.edu

P.S. Showalter, Y. Lu (eds.), *Geospatial Techniques in Urban Hazard and Disaster Analysis*, Geotechnologies and the Environment 2, DOI 10.1007/978-90-481-2238-7_9,

climate change caused by large-scale, rapid urbanization. The global average temperature has risen 0.5°C since the 1970s (McMichael et al. 2006) but in roughly the same period, differences between temperatures in the city compared to surrounding rural areas have been measured ranging from 1 to 12°C (Aniello et al. 1995; Brazel et al. 2000; Voogt 2002). One study found that US cities, on average, experience 10 more hot summer nights than they did 40 years ago (DeGaetano and Allen 2002).

Urbanization affects physical processes that alter the surface energy balance, and therefore, near-surface air temperatures (Arnfield 2003; Oke 1982). For example, surface cooling is inhibited by reduced outgoing long-wave thermal radiation due to the vertical structure of buildings, and sources of anthropogenic heat (e.g., vehicles, air conditioners, and industry) exhaust heat into the air near the urban surface (Grossman-Clarke et al. 2005). High heat capacity and thermal conductivity of building materials lead to greater storage of heat in the city compared to the natural land covers and agricultural land uses that preceded urbanization. These changes produce what has been described as the urban heat island (UHI) effect, where cities experience higher nighttime temperatures and generally higher but more variable daytime temperatures than the surrounding less built-up areas (Lowry 1967; Oke 1997; Voogt 2002). However, data acquired through remote sensing, surface weather stations, and regional atmospheric modeling also indicate significant temperature variability within urban areas (Arnfield 2003; Voogt and Oke 2003; Grimmond 2005). It is likely that urban vegetation serves as a mitigating factor against warm temperatures for some areas of the city while exacerbating high temperatures for other areas (Stabler et al. 2005; Jenerette et al. 2007). Much of the intra-urban temperature variation is, therefore, driven by human decisions and resources that determine residential land use/land cover (LULC) within the urbanized region.

Not only are cities experiencing chronic temperature increases, but global warming and UHIs are jointly responsible for causing more extreme heat events in cities. Extreme (acute) heat events, defined as sustained high temperatures exceeding the normal range of temperature variability, occur throughout the world and are projected to become more intense, more frequent and longer lasting over the next century (IPCC 2007; Meehl and Tebaldi 2004).

There is ample evidence that prolonged exposure to excessively warm weather is a major human health hazard, especially at junctures when critical temperature thresholds in cities are abruptly crossed (Sheridan and Kalkstein 2004). Temperature-mortality relationships are evident in temperate as well as warmer climate regimes (Patz et al. 2005). More people die in the US from extreme heat than any other weather-related phenomenon (CDC 2006) and very hot weather increases mortality rates as well as hospital admissions for cardiovascular, respiratory, and other pre-existing illnesses (Semenza et al. 1999). The 1995 Chicago heat wave, for instance, claimed over 700 lives (Semenza et al. 1996). Between 22,000 and 52,000 Europeans died during the 2003 heat wave, many of them in large cities (Larson 2006). Less publicized cases of heat waves in India and other Asian cities also report high excess death rates (e.g., Choi et al. 2005). As rapid

urban development continues, the impacts of heat-related hazards on human health and comfort are also expected to increase as the threshold of human tolerance to rising temperatures are crossed more frequently and for longer periods of time (Kalkstein and Greene 1997). The Intergovernmental Panel on Climate Change (IPCC) projects with "medium confidence" a future increase in heat wave-related deaths worldwide (Confalonieri et al. 2007). The number of heat-related fatalities could double in the near future (Larson 2006 citing the World Meteorological Association).

Almost all epidemiological studies treat the city as a single entity in tallying the temperature-related mortality during and immediately after heat events (Braga et al. 2002; Curriero et al. 2002; Michelozzi et al. 2006; Smoyer et al. 2000). Recently, heat watch-warning systems have been developed to mitigate the health impacts of sudden heat events by providing advance notification of dangerously warm weather. The warning systems are sensitive to local synoptic weather variables that vary from city to city, but they rely on data from a single, centrally-located weather station in each city and the warnings are broadly applied to entire urban areas (Sheridan and Kalkstein 2004; Smoyer-Tomic and Rainham 2001). Thus, current heat watch-warning systems lack sensitivity to intra-urban microclimate variation and the precise locations where heat hazards are the greatest.

Heat-health studies often find that advanced age and some types of chronic illnesses and disabilities are associated with higher morbidity rates attributable to extremely hot weather (McGeehin and Mirabelli 2001; Kilbourne 2002). These variables are treated as individual characteristics that predispose people to physiological weaknesses which, in turn, increase their vulnerability to heat. Other high risk populations, such as racial minorities and people living in poverty, often have poorer general health and lack access to air conditioning and critical socioeconomic resources (O'Neill et al. 2003; Naughton et al. 2002). Klinenberg's (2002) study of the 1995 Chicago heat wave disaster found that deaths among the elderly were most numerous in a few neighborhoods with high concentrations of minority residents who lacked strong social networks and support systems. The associations between characteristics of urban residents and risk of heat-related health problems can also be caused by environmental conditions in the places where they live. In one study, affluent whites lived in neighborhoods that were several degrees cooler in the summer of 2003 than low-income and Latinos neighborhoods (Harlan et al. 2006, 2008; Jenerette et al. 2007). Residents in the warmest neighborhoods spent 20% of the entire summer in conditions that exceeded the "danger" threshold on a heat stress index.

9.2 The Study

One of the most effective ways to reduce the impacts of disasters that cause large scale environmental health problems is to obtain "accurate exposure assessments" (Patz 2005). Recent advances in the accuracy, resolution, and sensitivity of geospatial tools and weather simulation models have enhanced our ability to

identify the locations of the places and people that are most vulnerable to extreme heat within cities.

This study examined the spatial distribution of air temperature during an extreme heat event and the exposure of people to threshold temperatures (defined in Section 2.2.1) at a very fine spatial resolution in the Phoenix (Arizona, USA) metropolitan area. By means of combining remote sensing and GIS techniques, regional atmospheric modeling, and socioeconomic data, we developed a geospatial tool to analyze heat hazards for Phoenix. We applied the Weather Research and Forecasting (WRF) model developed by the National Center for Atmospheric Research (Shamrock et al. 2005) to simulate 2 m air temperatures in the Phoenix metropolitan area during a four-day heat event in July 2005 and subsequently to quantify the heat hazard by hours of human exposure to threshold air temperatures for 40 diverse neighborhoods throughout the urban region. The model showed marked contrasts in temperature across neighborhoods.

Social survey data on residents' perceptions of temperature and experiences with illnesses caused by heat stress were related to the results of the weather simulation model. To assess human risk, WRF model output was compared to US Census block group population characteristics, which showed how exposure to extreme temperature varied by socioeconomic status (household income), ethnicity, and age composition of the neighborhood. As far as we are aware this was the first time that socioeconomic data have been interrelated with output from a regional atmospheric model. Finally, the association of air temperature with LULC was examined to better understand the mitigating influence of landscapes on local microclimate variability.

The variable temperatures and landscapes within the Phoenix UHI create a thermal "riskscape" of heat hazards that are distributed unevenly over the city and impact people differently. During a period of elevated temperature (i.e., heat wave), the places inhabited by populations that were least likely to have key economic and natural resources were more exposed to hazardous conditions. This study provides information that may help to prevent health disasters related to extreme heat in cities by answering three important research questions: *(1) How are heat hazards distributed among places in the Phoenix metropolitan area? (2) How closely do residents' perceptions of temperature and experience with heat-related illnesses align with simulated air temperatures in their neighborhoods? (3) Within the study area, what types of residents were most at risk and can certain types of local landscape serve as mitigating influences on temperature?*

9.2.1 Research Methods

For the investigation of heat-related hazards in urban areas there is clearly a need to better understand the distribution of air temperatures in relation to residents' means to cope with extreme heat within a regional study area. Using a multi-method approach, we examine data on threshold temperatures, analyze the spatial distribution of the data, and interpret the results.

9.2.2 Study Area

Located in the Sonoran Desert of the southwestern United States, the Phoenix metropolitan area is an ideal setting for studying human vulnerability to high temperatures (Fig. 9.1). Encompassing over 1800 square miles in Central Arizona, metropolitan Phoenix is home to over 65% of the state's 6.1 million residents (Census Bureau 2006). The city has a naturally warm climate and over the past 50 years of population growth, the average daily temperature has increased by more than 3°C (Brazel et al. 2000). The 2005 summer season which began June 21st and ended September 22nd, witnessed record (16 records tied or broken) high temperatures in the day as well as the evening. The Center for Disease Control (CDC 2005) recently reported that Arizona led the nation in heat-related deaths from 1993–2002. Although Phoenix has experienced a steady rise in average daily temperature, human exposure to high temperatures varies widely throughout this region. For example, Hedquist and Brazel (2004) measured average nighttime maximum temperature variation on a rural to urban gradient equal to 7.3°C in 2001.

Within the metropolitan area, the present study concentrates on 40 diverse neighborhoods under study as part of the 2006 Phoenix Area Social Survey (PASS) project. These neighborhoods offer insight into the spatial distribution of temperature variability throughout the region during a summer heat event, in addition

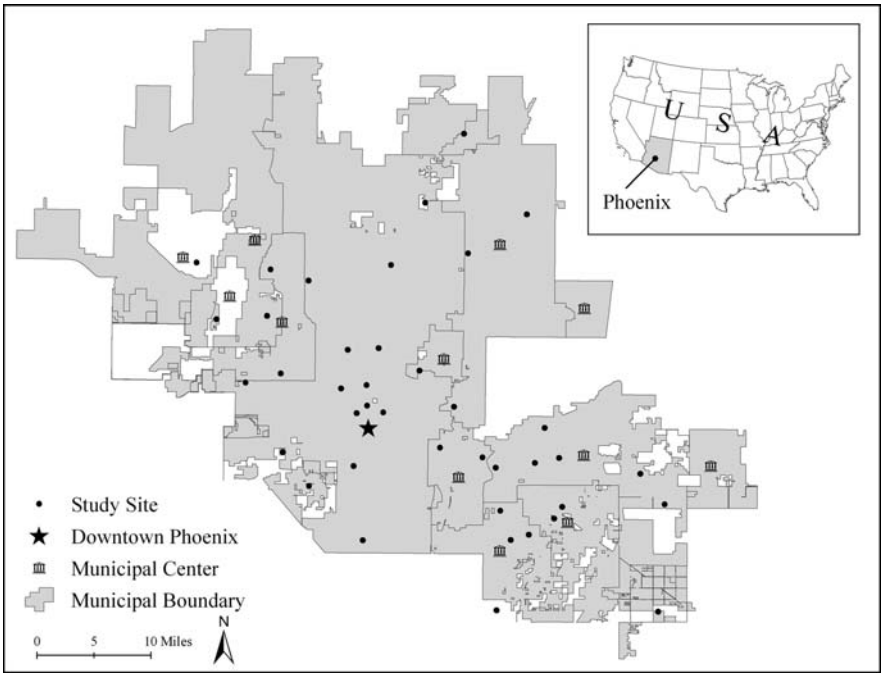

Fig. 9.1 Map of metropolitan Phoenix, Arizona

to a survey of residents' perceptions of and experiences with extreme heat. PASS employed a two-stage research design (Harlan et al. 2007). First, a systematic sample of 40 neighborhoods was selected from the 94 urban sites that are monitored by the Central Arizona-Project Long-Term Ecological Research CAP LTER project (Grimm and Redman 2004). Census data by block group were assembled for all 94 sites and classified by location (urban core, suburban, and fringe), median income, and ethnic composition. All types of neighborhoods in the Phoenix area were represented among the sample of 40. Second, a random sample of households within each neighborhood was selected to participate in a social survey, which is described in more detail below.

9.2.3 Extreme Heat Event Period

Following criteria used by Meehl and Tebaldi (2004), periods of extreme heat were identified in a three-step process. The first step was to examine National Oceanic and Atmospheric Administration (NOAA) temperature readings for Phoenix, AZ's Sky Harbor International Airport weather station, which is commonly used in climate studies (Brazel et al. 2000). This data set was used to determine normal historical (1961–1990) temperature variability in comparison to present day (2005) conditions. Second, using observed temperature readings, we calculated the distribution in percentiles for normal and present day summer temperatures. The third and final step to identify period(s) of extreme heat for the summer of 2005 was to compare the normal and present day conditions based on the three criteria of threshold temperatures (Threshold 1 [T1]: the 97.5 percentile of the observed distribution; and T2: the 81 percentile) identified by Meehl and Tebaldi (2004). Temporal periods satisfying all three of the following conditions are considered to be extreme heat events: (1) daily maximum temperature must be above T1 for at least three days; (2) average daily maximum temperature must be above T1 for the entire period; and (3) daily maximum temperature must be above T2 for the entire period.

After completing this process, the local threshold temperatures, based on normal conditions, were: T1 = 45°C (113°F); and T2 = 42°C (108°F). Comparing 2005 temperatures readings to normal conditions, there were three distinct heat events in the Phoenix metropolitan area on June 6–9; July 15–19; and August 1–3. The temporal period examined in this study is the four-day heat event from July 15–19, 2005, which represents the longest and most intense heat event during the year. The WRF model, described in the next section, was applied to simulate 2 m air temperature variability and exposure to threshold temperatures throughout the 40 neighborhoods.

9.2.4 WRF Modeling of Heat Event

An important step in the analysis of heat hazards in relation to human exposure is quantifying air temperature, usually at a height of 2 m, at appropriate spatial and

temporal scales. The spatial variability of temperatures in urban regions is more complex than a linear gradient from urban core to fringe, and an emerging theme of research on urban climate is to determine the factors that are associated with temperature variation. Current techniques to quantify air temperatures include measurements from weather stations and spatial information tools such as remote sensing or atmospheric models that simulate air temperature. Existing methods to quantify air temperature all possess various strengths and weaknesses. Surface meteorological stations, for example, offer precise information on air temperature changes over time at discrete sites in the urban area, but usually lack dense spatial coverage. Alternatively, remote sensing provides detailed spatially and temporally consistent information on surface temperature variability within urban areas, but it is limited to discrete temporal "snapshots" and surface temperatures are not necessarily an indicator of the magnitude of air temperature.

Modeling and simulation techniques continue to gain traction within the scientific community by offering new ways to study interactions of physical and social processes in urban areas where most humans live. The term model, as used in the context of meteorology and climate, refers to a complex computer code that numerically solves a set of differential equations that govern the evolution of the state of the atmosphere in space and time in terms of air temperature, pressure, specific humidity and wind speed. The evolution is determined in part through the interaction between the model variables, but also through external forcing (e.g. solar radiation) and interactions with the earth's surface through fluxes of heat, moisture and momentum. Physical properties of the earth's surface that influence the exchange with the atmosphere depend on land use/cover characteristics. The accurate characterization of LULC and corresponding physical properties therefore is an important input variable for meteorological models. The output of a global atmospheric model together with observations of the atmosphere are generally used to quantify initial and boundary conditions for the fine resolution regional model to determine atmospheric features that cannot be captured by the physical processes included in the regional model. Other methods for determining air temperature within urban areas are limited by the accuracy of regional atmospheric models that depend, among other factors, on limited knowledge of physical processes in the atmosphere and their mathematical description, as well as uncertainties in initial and boundary conditions as supplied by the global model.

Relatively recent developments in geocomputation have enabled advances in regional atmospheric models to resolve heterogeneity within urban areas, which, in turn, have inspired the development of model approaches that describe the energy exchange between the urban surface and the atmosphere by the climate community (Brown 2000; Masson 2006; Martilli 2007). The application of such schemes within atmospheric models have greatly improved the accuracy of urban air temperature simulations over the past 10 years, and today such models are widely employed to enhance scientific understanding of processes related to neighborhood scale climate and air quality (Taha 1997a, b; Civerolo et al. 2000; Seaman 2000; Lin et al. 2008).

This study combined WRF version 2 (Shamrock et al. 2005) together with the urban surface energy balance model by Kusaka and Kimura (2004) to simulate

2 m air temperatures for the period July 15–19, 2005. The model's spatial resolution of 1 km for horizontal model grid cells corresponds well with neighborhood block group data obtained from the Census. Since the average urban block group is about ¼ square mile, the model's spatial resolution of 1 km (or 0.39 square miles) roughly covers the same area. Grossman-Clarke et al. (2005, 2008) demonstrated that a well-tested mesoscale model is suited to simulate air temperature variability in the Phoenix metropolitan region.

The model run was started at 00 Coordinate Universal Time (1700 Local Standard Time, LST). Nested simulations with four domains and resolutions of 27 km (size east-west 3294 km; north-south 2700 km), 9 km (size east-west 1350 km; north-south 1080 km), 3 km (size east-west 594 km; north-south 414 km) and 1 km (size east-west 212 km; north-south 132 km), respectively and 51 vertical layers were performed with WRF. The innermost domain included the Phoenix metropolitan area, surrounding desert and agricultural land. Initial and boundary conditions were provided by the National Center for Environmental Prediction (NCEP) ETA grid 212 (40 km resolution) analysis. Every 6 hours the lateral boundary conditions were updated from the ETA analysis and NCEP/NCAR Reanalysis. Planetary boundary layer processes were included via the non-local closure Medium Range Forecast scheme (Hong and Pan 1996) in the version by Liu et al. (2006).

In order to evaluate the WRF model performance we compared National Weather Service temperature readings for 2 m air temperatures with the simulated data at Phoenix Sky Harbor Airport (Fig. 9.2). Generally the simulations are in close agreement with the measurements, although the simulated temperatures over-predict the peak measured observations for each day of the heat event by about 2°C. A complete agreement between observed and simulated air temperatures cannot be expected because of the complexity of the system, but also because the air temperature recorded at a weather station is a point measurement and is, therefore, conceptually different from the simulated air temperature that is the model grid cell

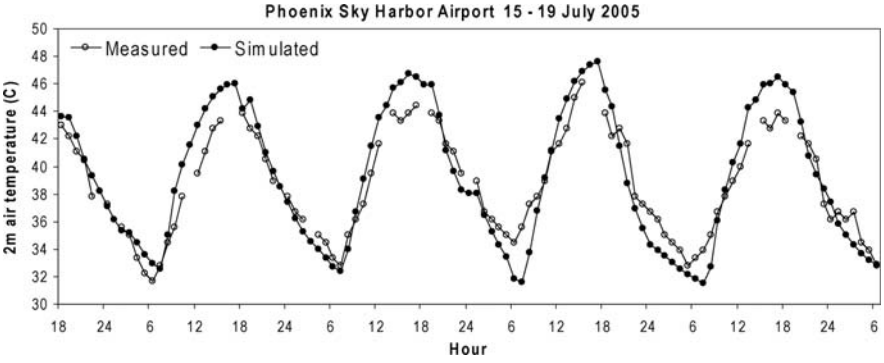

Fig. 9.2 Simulated and measured 2 m air temperature at the National Weather Service station at Sky Harbor Airport in the center of the Phoenix metropolitan region for the time period 15–19 July 2005

average temperature. The two are comparable if the station is placed in an extended homogeneous environment which is rare to find in an urban setting. Other possible reasons for the differences are an inaccurate assessment of the large scale synoptic weather conditions that are influencing the regional simulations through model boundary and initial conditions as provided from a global atmospheric model. These conditions hold true for all sites in the urban area and we assume, therefore, that the model captures differences between neighborhoods satisfactorily.

9.2.5 Land Use/Land Cover Classification System

The 24-category US Geological Survey (USGS) LULC system (Anderson et al. 1976) is the standard input for running WRF. Since the extent and heterogeneity of urban land use of the Phoenix metropolitan area are underrepresented in this dataset (Grossman-Clarke et al. 2005), we chose to use the 2005 12-category LULC classification available for Phoenix at the spatial resolution of 30 m, which is briefly described below.

The general reference LULC classification is based on the expert classification system (Stefanov et al. 2001) originally developed for use with Landsat Thematic Mapper (TM) data to monitor land cover changes in this rapidly expanding urban area. The system performs a posteriori sorting of classes initially derived using the supervised Maximum Likelihood classification. Such reclassification is implemented in the hypothesis-testing framework whereby all initially classified pixels are evaluated using sets of rules and by overlaying with co-registered auxiliary data layers. These layers originate from different sources or are computed directly from a Landsat image and include the county land-use map, image variance texture, water rights database, city boundaries, and Native American reservation boundaries.

The cloud-free Landsat TM image (path 37/row 37) used in the current classification was acquired on March 8, 2005. It was georeferenced and geometrically rectified using high resolution true color aerial photomosaic as a reference source. Raw digital numbers of image bands were converted into true surface reflectance values by applying an atmospheric correction. The final classification has a reported overall accuracy of 83% which is generally acceptable and common for Landsat-derived urban classification level of accuracy. User's accuracy for individual classes varies from 71 to 100% with the exception of commercial/industrial class (51%).

As described in detail in Grossman-Clarke et al. (2005), the derived 12-category LULC map was used to assign land cover class for each WRF 30-second grid cell by using majority rule to determine the highest associated fraction of land cover. We then used the revised land use/cover classifications as input into WRF, and coded the 30-second grid cells as one of the following categories: urban (commercial/industrial); xeric (urban residential draught resistant landscaping); desert (undisturbed natural land); or mesic (urban residential predominantly grass). The categories differed mainly by their type of vegetation and irrigation method (urban and desert – no irrigation; xeric – drought adapted vegetation with drip irrigation; mesic – well watered flood or overhead irrigated). The urban

(commercial/industrial) category was composed entirely of man-made surfaces with no significant vegetation or bare soil, while in the xeric and mesic residential categories, the fractional surface covers were, respectively, man-made (0.73/0.60), vegetation (0.10/0.23), and soil (0.17/0.17). Some peripheral neighborhoods, however, were located in undisturbed desert areas, so we also used the surface characteristics of this fourth classification to drive the model.

9.2.6 Household Survey on Sensitivity to Heat

One way to assess how well WRF simulations relate to human experience is to compare the WRF temperature output to the self-reports of 2006 Phoenix Area Social Survey (PASS) respondents about perceived temperatures and heat-related health problems in the summer of 2005. A comparison of model simulations with residents' reports has not been done before, probably because of the lack of social survey data that spatially corresponds to the model grids. In each of the 40 PASS neighborhoods, described above, 40 randomly selected households were recruited for participation in PASS until a minimum 50% response rate was achieved in each neighborhood. Overall survey response rate was 51% ($n = 808$). Data from the 2000 Census indicate variable numbers of dwelling units per neighborhood (minimum: 82; maximum: 3833; mean: 888). The percentage of households surveyed per neighborhood also varied from a minimum of 0.6 to a maximum of 24.4, with a mean of 4.4. Surveys were collected using a multi-modal approach (online, telephone, or personal interview), and the respondent who was 18 years or older with the most recent birthday was selected to participate in the study. The survey was administered by the Institute for Social Science Research (ISSR) at Arizona State University from April 29 through September 27, 2006.

As part of PASS, respondents answered the following two questions to gauge their sensitivity to heat: (1) During the summer of 2005, do you think your neighborhood was a lot cooler, a little cooler, a little hotter, or a lot hotter than most other neighborhoods in the Valley or do you think it was about the same temperature as other neighborhoods? (2) During last summer, did you or anyone else in your household have symptoms related to heat or high temperatures such as leg cramps, dry mouth, dizziness, fatigue, fainting, rapid heart beat or hallucinations? (Yes; No).

9.2.7 Neighborhood Demographics

The 2000 US Census Summary Files 1 and 3 for the sample neighborhoods were used to identify the following block group variables for comparisons: population per square mile, median income (US dollars), poverty rate (percent of population below the US government federal poverty guideline), ethnicity (percent minority), and age (median age and ages 65 and older). These variables were used in the analysis to show how different population groups experienced the heat event simulated by WRF.

9.3 Data Analysis

To investigate intra-urban variation in threshold temperatures, the data were analyzed in three phases. The first phase of analysis involved simulating threshold temperatures with the WRF model for the four-day (96 hours) heat event that occurred between July 15 and 19, 2005. Once the temperatures were simulated, GIS was used to map temperature variability for each study site throughout the area and neighborhoods' exposure to extreme heat was quantified. The severity of the heat hazard was calculated by determining the number of exposure hours for each study site to threshold temperatures at or above the 97.5 percentile for the heat event (Fig. 9.3). Exposure to threshold temperatures was then used to create three categories, herein referred to as Heat Intensity Classes. The Heat Intensity Classes were determined by calculating the mean hours of exposure for all 40 neighborhoods and using the difference of one standard deviation to establish each class (Table 9.1). The three levels of heat intensity are: low (less than 9 hours of exposure to temperatures at or above the 97.5 percentile for the 4-day heat event); medium (9–17 hours of exposure); and high (greater than 17 hours).

The final phase of analysis involved comparing the Heat Intensity Classes to household surveys, neighborhood demographics, and LULC types. We analyzed

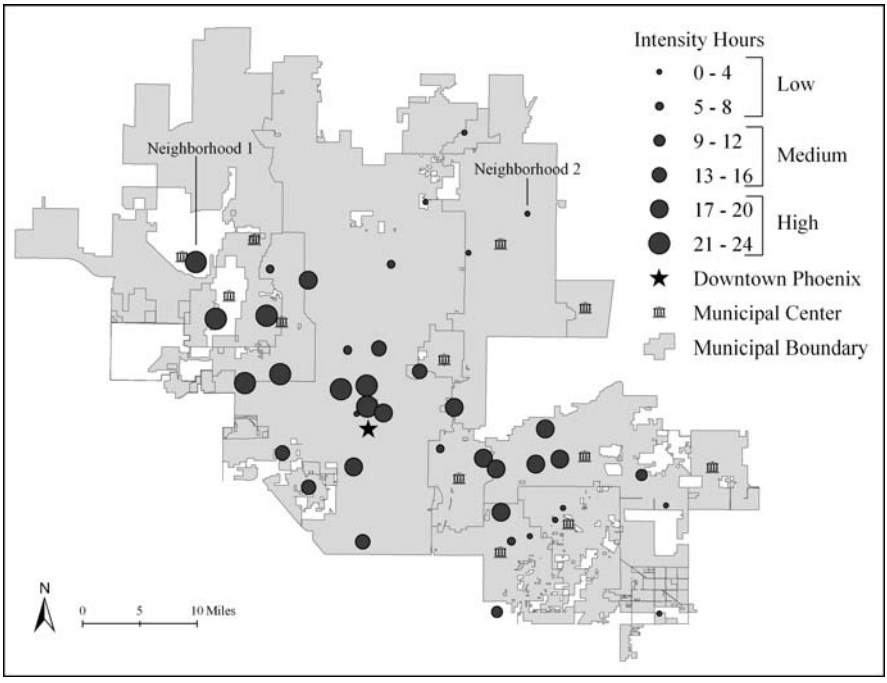

Fig. 9.3 Hours of Exposure to Threshold Temperatures at or above the 97.5 percentile from July 15–19, 2005 by Neighborhood

Table 9.1 Calculation of heat intensity classes based on hours of neighborhood exposure to threshold temperature

	Hours of exposure			Heat intensity classes		
Threshold temp	Range	Mean	SD	Low	Medium	High
97.5 percentile	24	12.6	7.9	<9 hours	9–17 hours	>17 hours

residents' perceptions of and experiences with extreme heat by conducting tests of significance on two measures of heat sensitivity, which serves as a validation of the WRF model. We also examined Census and LULC characteristics by Heat Intensity Class to better understand who is most vulnerable to extreme heat and what role vegetation may play in mitigating neighborhood exposure to threshold temperatures.

9.3.1 Results

9.3.1.1 Distribution of Heat Exposure Time

Tests for spatial autocorrelation presented in Table 9.2 report varying levels of statistical significance. Spatial autocorrelation permits statistical tests (e.g., Moran's *I*, Geary's *c*, Getis-Ord) which investigate spatial patterns by considering the presence of an attribute in space. Tests are based on correlation to neighbors whereby the pattern of a map is such that an area is similar (positive; aggregation) or dissimilar (negative; segregation) to adjacent areas (Burt and Barber 1996). The test both describes the structure of a spatial pattern and is also capable of detecting the presence of directional components (Legendre and Fortin 1989). Moran's *I* analyses on the distribution of simulated temperatures indicate that temperatures are not evenly distributed throughout the study area. While the mean four-day temperature reports modest temperature variation among the 40 neighborhoods (mean: 38.3°C; range: 4.9), hours of exposure to extreme temperatures varies significantly throughout the study area. Exposure to threshold temperatures at or above the 97.5 percentile, for instance, is significantly different among the 40 neighborhoods (mean: 12.6 hours;

Table 9.2 Spatial autocorrelation results for temperature simulations on the 40 neighborhoods

	Spatial autocorrelation			
Temperature simulations	Mean (sd)	Moran's *I*	Z-score	Significance
Mean four-day Temp ℃	38.3 (1.1)	0.03	1.73	0.10
Hours exposure: 81st percentile	29.4 (6.1)	0.04	2.37	0.05
Hours exposure: 97.5th percentile	12.6 (7.9)	0.08	3.1	0.01

range: 24). Results, therefore, indicate strong positive spatial patterns where adjacent neighborhoods in some areas are exposed to hazardous temperatures significantly more than other areas.

Figure 9.3 illustrates the varying levels of exposure to threshold temperatures throughout the 40 study sites. The circles represent the number of hours each neighborhood was exposed to threshold temperatures equal to or above the 97.5 percentile. The larger the circles, the greater the exposure to extreme conditions. Generally, the calculations exhibit the UHI pattern where neighborhoods near downtown centers are warmer with higher levels of exposure to threshold temperatures while neighborhoods on the fringe are cooler and have lower levels of exposure to threshold temperatures. However, the pattern of temperature gradients is more complex.

Physical and social processes may help to explain some of the variance in the distribution of air temperatures throughout the study area. Grossman-Clarke et al. (2005), for example, identified strong relationships between temperature and LULC, particularly the abundance of vegetation. In neighborhoods, residential landscapes are managed according to human preferences and availability of resources to cultivate vegetation (Larsen and Harlan 2006; Martin et al. 2004). Additionally, the Phoenix metropolitan region has an elevation gradient with increasing elevation to the north-east which causes differences in air temperature among neighborhoods with comparable land use. Air-flow patterns are influenced by the presence of mountains that typically cause upslope flows during the daytime towards the north and northeast. Downslope flow occurs during the night and is associated with cold advection that reaches various parts of the Phoenix metropolitan area at different times (Brazel et al. 2005). Depending on the location of a neighborhood, cooler or warmer air from areas with different land use/cover in the vicinity might occur. Finally, the current WRF version considers only four urban land use/cover classes and the predominant LULC type is assigned to a model grid cell but might not always be accurately representative, such as for mixed used areas.

Table 9.3 Neighborhood exposure to mean and threshold temperatures (Celsius) by heat intensity class

	Heat intensity class		
Temperature simulations	Low	Medium	High
N neighborhoods	15	10	15
Four-day heat event: Temp °C			
Mean average (sd)	37.2 (1)	38.5 (0.3)	39.2 (0.2)
Mean high (sd)	44.7 (0.9)	45.9 (0.2)	46.5 (0.2)
Mean low (sd)	29.8 (1.2)	30.9 (0.7)	31.8 (0.2)
Four-day heat event: Hours			
81st percentile (sd)	23.8 (6.9)	31.1 (0.9)	33.7 (0.9)
97.5th percentile (sd)	3.3 (2.5)	14.5 (2.6)	20.7 (1.9)

Note: A difference in 1°C = 1.8°F

Exposure to mean and threshold temperatures by Heat Intensity Class presented in Table 9.3 follow two distinct patterns. When considering mean temperatures (high, low, and average), there is a general positive linear relationship where temperatures increase modestly moving from low to high Heat Intensity Classes. Mean average temperature for the four-day heat event, for instance, increases from 37.2°C (Low) to 38.5°C (Medium) to 39.2°C (High), representing an increase of 2°C from the low to high classes. Exposure to threshold temperatures, however, reflects more pronounced differences among the three intensity classes. On average, neighborhoods in the high Heat Intensity Class were exposed to over six times the number of threshold hours that low intensity neighborhoods experienced during the four-day heat event. Among individual observations, three neighborhoods recorded zero hours of exposure to threshold temperatures in contrast to two neighborhoods that were exposed to twenty-four hours at or above threshold temperatures.

An analysis of the hourly temperature for the four-day heat event confirms variable levels of exposure to threshold temperatures among neighborhoods in the study area. Figure 9.4 presents the average temperature for all neighborhoods in addition to the temperature distribution of two particular neighborhoods. *Neighborhood 1* reported the warmest temperatures of the sample while *Neighborhood 2* reported the coolest temperatures. While the average temperature reached or exceeded the 97.5 percentile (45°C) each day during the heat event, Neighborhood 1 was exposed to considerably higher temperatures in the afternoon as well as the evening and early morning hours. Alternatively, Neighborhood 2 reported significantly cooler temperatures while remaining under 45°C for the duration of the four-day period.

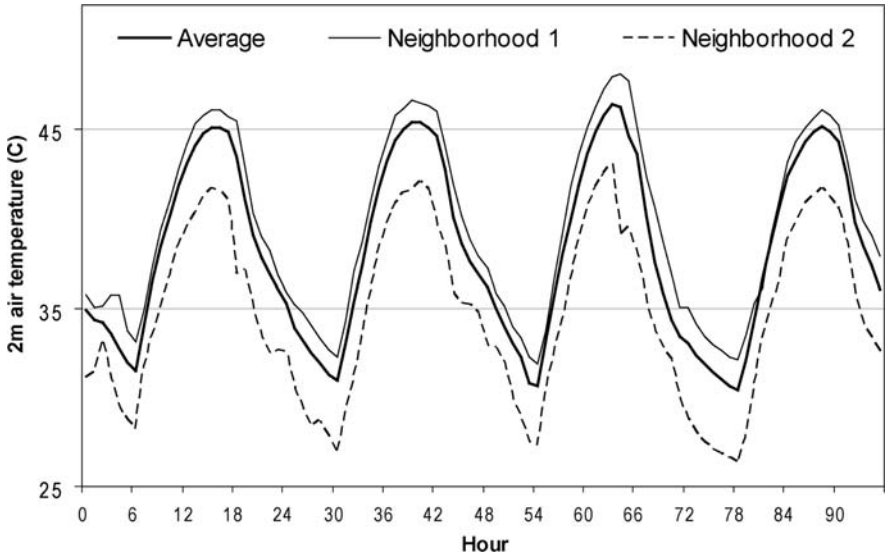

Fig. 9.4 Hourly Neighborhood Temperature (Celsius) Distribution for July 15–19, 2005 (45°C represents the 97.5 percentile)

The 65th hour of the four-day heat event produced the highest simulated temperatures. The temperatures ranged from 46.4°C (Average); 48.2°C (Neighborhood 1); to 43.1°C (Neighborhood 2), representing a difference of 5.1°C (or 9.2°F) between the warmest and coolest neighborhoods in the sample. Hourly neighborhood temperature, therefore, verifies significant variation in levels of exposure to extreme temperatures among the 40 neighborhoods.

9.3.1.2 Perceptions of and Experiences with Extreme Heat

Tests for global spatial autocorrelation analyses indicate the frequency and distribution of two social survey measures for residents' sensitivity to extreme heat are not statistically significant (Table 9.4). In other words, there is not a marked spatial pattern between location and residents' perceptions of and experiences with extreme heat. One explanation for this distribution is the fact that the survey responses reflect the average of 20 unique responses for each location. For instance, *Illness* was determined by coding individual survey responses (No heat-related household illness = 0; Yes = 1), and then we compared average scores at the neighborhood level. The aggregation of perceptions by neighborhood is subject to many influences which may explain the random distribution of the spatial autocorrelation analyses. In contrast to social perceptions, the 40 neighborhoods are variably exposed to threshold temperatures throughout the study area. In some cases, high intensity neighborhoods are adjacent to low intensity neighborhoods in both the urban core as well as residential suburban areas. Other considerations that could explain the spatial distribution of respondents' views include age and other demographics, housing quality, residential landscaping characteristics, and the availability of other resources that may influence individual residents' perceptions and experiences with extreme heat. Moreover, the question did not ask respondents where the heat incidents occurred, leaving open the possibility that incidents occurred outside their residential neighborhoods.

Analyses of local spatial autocorrelation, however, indicate that perception of risk and illness exhibit spatial clustering in some parts of the study area among adjacent

Table 9.4 Global spatial autocorrelation results for survey responses

	Global spatial autocorrelation		
Survey questions	Moran's *I*	Z-score	Significance
Perception of risk			
The temperature of your neighborhood compared to other neighborhoods for summer 2005	–0.05	−0.5	Random
Illness			
Experienced heat-related symptoms in household in summer 2005	−0.04	−0.2	Random

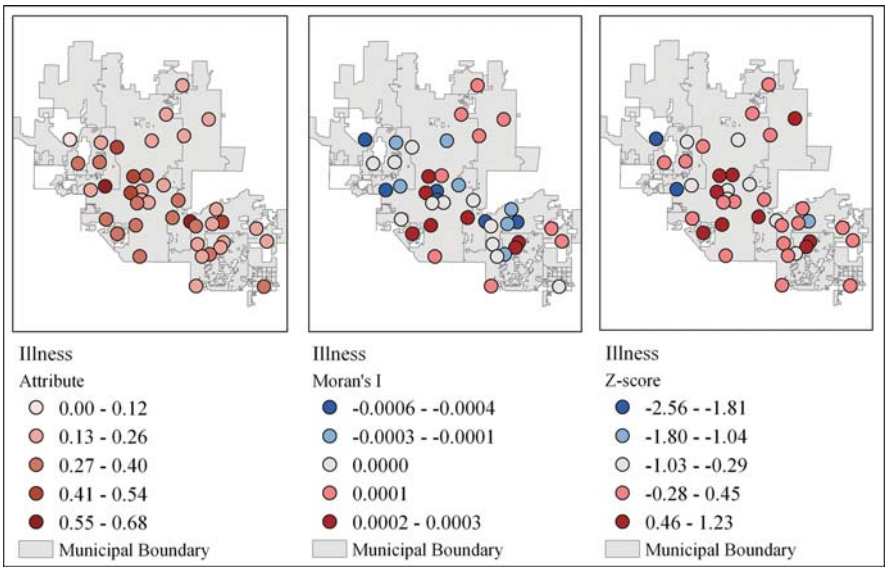

Fig. 9.5 Local spatial autocorrelation results for illness

neighborhoods. Aneslin's Local Index of Spatial Association (LISA) (Anselin 1995) for Moran's *I*, offers empirical insight into a spatial scale by measuring the similarity of an attribute and its spatial configuration to its neighbors. Figure 9.5 , for example, presents three maps illustrating the spatial distribution of self-reported illnesses associated with extreme heat. The first map shows the distribution of the attribute throughout the study area where lower attribute scores reflect fewer heat-related illnesses in the household while higher scores reflect a greater number of heat-related illnesses. The second map shows the distribution of the local Moran's *I* statistic which reports on similarity (low values reflect dissimilar neighbors and high values reflect similar neighbors). The third map presents Z-scores for each neighborhood where the dark red circles represent clustering 'hot spots' of statistically high morbidity (at the 95% confidence level) while the dark blue circles represent clusters of low morbidity. Notice LISA reports significant clustering of illness associated with extreme heat in neighborhoods in Central South Phoenix.

Organized by Heat Intensity Classes, Table 9.5 illustrates differences among residents' perceptions of and experiences with extreme heat. When considering perception of temperature, significantly more respondents in the high Heat Intensity Class reported that the temperature in their neighborhood was "hotter" compared to other Phoenix area neighborhoods for the summer of 2005. Likewise, illness, the second sensitivity measure, shows that almost 31% of respondents in the high Heat Intensity Class reported that someone in their household experienced a heat-related illness for the summer of 2005 in contrast to 24.1% and 24.2% for the low and medium Heat Intensity Classes, respectively. Although the distribution for illness is just outside the 0.10 significance level, results show variation among

Table 9.5 Perceptions of heat stress by heat intensity class

	Heat intensity class		
Survey questions	Low	Medium	High
N Neighborhoods	15	10	15
Perception of temperature			
Temperature in neighborhood compared to others: hotter*	19.0%	22.2%	30.6%
Illness			
Experienced heat-related symptoms: yes	24.1%	24.2%	30.9%

Chi-Square Test (2-sided): *p<0.01
Total number of respondents for Perception of Temperature n = 767; Illness n = 763.

residents' experiences with threshold temperatures. Respondents in high heat intensity neighborhoods, therefore, perceive and experience heat stress more than respondents in neighborhoods of medium and low Heat Intensity Class.

9.3.1.3 Neighborhood Demographics

The first two phases of the analysis found that threshold temperatures and residents' sensitivity to extreme heat are variably distributed throughout the 40 neighborhoods. This phase of analysis explored the types of people who live in the places that are most vulnerable to the exposure of extreme heat. Table 9.6 shows Census block group population characteristics for the following variables: density, income, ethnicity, and age. These variables are all highly related to Heat Intensity Class. Population per square mile, for instance, is roughly twice as high in the high Heat Intensity Class when compared to low and medium intensity classes. Median household

Table 9.6 Population characteristics of neighborhoods by heat intensity class

	Heat intensity class		
Demographics	Low	Medium	High
N neighborhoods	15	10	15
Density			
Population per sq mi	3569	3757	7550
Socioeconomic status			
Household income	$71,903	$62,669	$38,621
% in poverty	5.6	8.3	15.5
Ethnicity			
% minority	20.7	25.9	44.7
Age			
Median age	36.3	40.9	36.6
% ages 65 and over	9.8	20.4	17.5

Source: 2000 US Census, Summary Files 1 and 3

income for the high Heat Intensity Class was just over half the income of the low intensity class, and the percentage of minorities in the high intensity class was more than two times greater than the low class. Interestingly, neighborhoods in the high and medium Heat Intensity Classes had larger percentages of elderly residents, which is cause for concern because the elderly are one of the most vulnerable groups to extreme temperatures. Block groups in low heat intensity neighborhoods are characterized by low population density, higher income, and a relatively low presence of minorities or elderly. We expect that the people in these environments are the least vulnerable to extreme heat because they are likely to have more economic resources to buffer their exposure to threshold temperatures, which are the lowest and of shortest duration in these neighborhoods. Alternatively, high heat intensity class neighborhoods, in general, have high population densities, high percentage of minorities and elderly, and relatively low median household income. We expect that these people have fewer economic resources to buffer their exposure to many more hours of extremely high temperatures. Analyses, therefore, indicate that the urban residents most vulnerable to the risk of heat exposure live in the most hazardous environments.

9.3.1.4 LULC Characteristics

Tables 9.7 and 9.8 present results on the final phase of analysis which examines the relationship between local LULC characteristics, threshold temperatures, and Heat Intensity Classes. Table 9.7 shows that all six neighborhoods classified as urban are located in the high Heat Intensity Class while the eight mesic neighborhoods are all located in the low Heat Intensity Class. Of the 19 xeric neighborhoods, 3 are in the low Heat Intensity Class followed by 7 in the medium and 9 in the high Heat Intensity Class. Table 9.7 is consistent with previous research in showing that land-use patterns and land cover are significant drivers of air temperature differences within the urban area under conditions with weak synoptic forcing (Harlan et al. 2006; Stabler et al. 2005).

There are also some distinct patterns between LULC and simulated temperatures. One particular pattern is a bimodal trend where mesic and desert LULC classes report cooler temperatures when compared to the warmer xeric and urban classes

Table 9.7 Neighborhood LULC categories by heat intensity class

	Heat intensity class		
LULC	Low	Medium	High
N neighborhoods	15	10	15
LULC			
Urban	0	0	6
Xeric	3	7	9
Desert	4	3	0
Mesic	8	0	0

Table 9.8 Neighborhood exposure to threshold temperatures by LULC

	LULC class			
Temperature simulations	Urban	Xeric	Desert	Mesic
N neighborhoods	6	19	7	8
Four-day heat event: Temp °C				
Mean average (sd)	39.4 (0.2)	38.7 (0.5)	36.9 (1.3)	37.5 (0.6)
Mean high (sd)	46.6 (0.2)	46.0 (0.5)	44.6 (1.3)	44.9 (0.5)
Mean low (sd)	31.8 (0.2)	31.4 (0.4)	29.0 (1.1)	30.3 (0.6)
Four-day heat event: Hours				
81st percentile (sd)	33.8 (0.7)	31.5 (2.8)	22.4 (10)	26.9 (2.3)
97.5th percentile (sd)	21.8 (2.1)	15.8 (5.8)	6.0 (5.8)	4.1 (2.2)

(Table 9.8). The mean high, low, and average temperature of the xeric and urban classes all reported differences in temperature greater than 1°C when compared to mesic and desert classes. The hours at or above threshold temperatures reflect significant differences between the four LULC classes. Neighborhoods in the mesic class, for example, averaged 4.1 hours during the four-day heat event while urban and xeric neighborhoods averaged 21.8 and 15.8 hours at or above threshold temperatures, respectively. These analyses show that urban and xeric neighborhoods are exposed to warmer temperatures for much longer periods of time compared to mesic and desert neighborhoods. Thus, people who live in mesic neighborhoods or near natural desert landscapes have more natural resources in the form of vegetation that helps to lower the ambient temperature and thereby mitigate the impact of heat waves on people.

It is imperative to point out that WRF considers various physical processes in the governing temperature equation to calculate near-surface air temperature. Those physical processes include the strongly land use dependent vertical transport of heat between the atmosphere and the land surface as well as horizontal and vertical advection, horizontal diffusion, net radiative flux convergence and divergence, phase changes of water during fog and cloud formation, adiabatic warming and anthropogenic heating. While a relationship between land use characteristics and air temperature as mediated through vertical turbulent transport of heat can be expected, the strength depends on the synoptic conditions and the time of day and the other physical processes that might dominate temperature tendency near the surface. Using WRF's predecessor, MM5 (Mesoscale Meteorological Model), Grossman-Clarke et al. (2005) investigated the contribution of the different physical processes on the near-surface air temperature under typical summer conditions in Phoenix. Findings indicated that cooling through radiation fluxes accounted for the most significant contribution to changes in air temperature at night and that cooling is enhanced between sunset and midnight by horizontal advection while vertical turbulent transport of heat dominates the temperature tendency for most of the day leading to the reported relationship between land use characteristics and air temperature.

9.4 Discussion

This study offers three contributions to urban hazards and disaster analysis research. Unlike other studies that examine heat-related health disasters for entire cities, this study finds significant intra-urban variability for air temperature, exposure to threshold temperatures, human perceptions, and self-reported illnesses associated with extreme heat. Our first contribution, therefore, is to show that reliance on one climate station as a regional barometer to assess exposure to extreme heat will obscure significant climatic variation within a given urban area and, therefore, the locations and types of individuals who are most at risk from heat hazards.

A second contribution is the development of a methodology for simulating temperature variability for a given study area. Despite some limitations of climate models, which we discussed, we have established a baseline for modeling temperature variability which can be applied to any location. The methodological approach presented in this paper offers the ability to identify high risk urban areas, the areas that will be hit harder, earlier, quicker, and for longer periods of time during an extreme heat event when compared to other places within the same region. Identifying these places helps to enable efforts toward illness prevention and response.

Through the development of this methodology, a third contribution could be the application of this information via a disaster mitigation and response system. The large-scale health disasters caused by recent heat waves have prompted many cities to develop warning systems that alert people to the likely onset of dangerous weather conditions so that adaptive responses are possible. These systems are based on synoptic methods that use local weather data from a central location – such as the city airport – to record relevant variables, relate weather conditions to excess mortality, and create a synoptic analysis that forecasts dangerous heat conditions for a particular city (Kalkstein and Davis 1989; Kalkstein et al. 1996; Sheridan and Kalkstein 2004). While useful for anticipating an upcoming extreme heat event, current systems lack the spatial component reflecting which locations are the most vulnerable. The system developed in our study identifies spatially sensitive degrees of risk to threshold temperatures, based on historical records, to assist disaster efforts prior to a heat event. Benefits of this system are threefold: (1) to inform aid workers where to locate response units prior to the outset of a heat event; (2) to ensure staff and supplies are readily available to aid anyone requiring assistance during a heat event; and (3) to direct policy that may help reduce factors contributing to threshold temperatures (e.g., LULC, building codes) in high risk areas.

9.5 Conclusion

This study employs geospatial methods to investigate extreme heat as a human hazard in the Phoenix metropolitan area. Motivation for this study is to help prevent and reduce heat-induced illnesses, such as heat stroke, exhaustion, dehydration, cardiovascular, and respiratory problems, which strike suddenly and acutely during the warmest times of the year (ICLEI 1998; Semenza et al. 1999). Utilizing both

physical and social data, research findings indicate: (1) Exposure to threshold temperatures is variably distributed among places and people throughout the Phoenix metropolitan area; (2) Residents' perceptions of and experiences with extreme heat parallel simulated air temperatures; (3) The types of people most vulnerable to risk of exposure to extreme temperatures are minorities, elderly, and low income residents. (4) Neighborhoods with mesic landscaping or natural desert surroundings are significantly cooler than neighborhoods with urban or xeric yards. Public expenditures aimed at increasing outdoor amenities (e.g., vegetation, shade, public parks) would provide resources for people to cope during a heat wave event, while helping mitigate human exposure to threshold temperatures.

Simulations from the WRF climate model produced varying levels of mean temperature throughout the Phoenix region in general, and significantly distinct levels of exposure to threshold temperatures across the 40 neighborhoods in particular. While regional atmospheric modeling is currently the best available tool to assess air temperature variability within urban areas, there are limitations to the accuracy of the model output that must be considered when interpreting results. For instance, WRF only employed the predominant neighborhood LULC type as an input variable, which is not always representative in cases of mixed-use areas. Landscape classifications could be further improved in future modeling.

As extreme heat events are expected to increase in intensity, frequency, and duration throughout the world over the next century, monitoring regional weather stations is an insufficient system to mitigate human hazards to heat events. This study illustrates that temperatures vary significantly within the same urban area, and that some residents are at significantly greater risk of exposure to threshold temperatures than others. We applied advanced geotechnical methods to study extreme heat as an urban hazard, the results yielded theoretical, methodological, and practical contributions to disaster analysis research.

Acknowledgments This material is based upon work supported by the National Science Foundation under Grant Nos. DEB-0423704, ATM-0710631, and GEO-0816168. Any opinions, findings and conclusions or recommendation expressed in this material are those of the author(s) and do not necessarily reflect the views of the National Science Foundation (NSF). The authors would like to thank Drs. Pamela S. Showalter and Yongmei Lu for organizing this special issue, and the three anonymous reviewers for their constructive criticism.

References

Anderson, J. R., Hardy, E. E., Roach, J. T., Witmer, R. E., et al. 1976. A Land Use and Cover Classification System for Use with Remote Sensor Data. United States Geological Survey Professional Paper, 964, 36.

Aniello, C., Morgan, K., Busbey, A., Newland, L. et al. 1995. Mapping micro-urban heat islands using Landsat TM and a GIS. *Computer Geosciences*, 21, 965–969.

Anselin, L. 1995. Local Indicators of Spatial Association—LISA. *Geographical Analysis*, 27(2), 93–115.

Arnfield, A. J. 2003. Two decades of urban climate research: a review of turbulence, exchanges of energy and water, and the urban heat island. *International Journal of Climatology*, 23, 1–26.

Braga, A. L. F., Zanobetti, A., Schwartz, J., et al. 2002. The effect of weather on respiratory and cardiovascular deaths in 12 US cities. *Environmental Health Perspectives*, 110, 859–863.

Brazel, A. J., Selover, N., Vose, R., Heisler, G., et al. 2000. A tale of two climates—Baltimore and Phoenix urban LTER sites. *Climate Research*, 15, 123–135.

Brazel, A. J., Fernando H. J. S., Hunt, J. C. R., Selover, N., Hedquist, B. C., Pardviak, E., et al. 2005. Evening transition observations in Phoenix, Arizona. *Journal of Applied Meteorology*, 44(1), 99–112.

Brown, M. 2000. Urban parameterizations for mesoscale meteorological models. In Z. Boybeyi (Ed.), *Mesoscale atmospheric dispersion* (pp. 193–255). Southampton, UK: WIT Press.

Burt, J. E., and Barber, G. M. 1996. *Elementary statistics for geographers*. New York: The Guilford Press.

Census Bureau 2006. 2006 American Community Survey. www.census.gov; accessed October 26, 2008.

(CDC) Centers for Disease Control and Prevention 2005. Heat-related mortality – Arizona,1993–2002 and United States, 1979–2002. *Morbidity & Mortality Weekly Report*, 54 (25):628–630.

(CDC) Centers for Disease Control and Prevention 2006. Extreme heat: a prevention guide to promote your health and safety. http://www.bt.cdc.gov/disasters/extremeheat/heat_guide.asp; accessed 4/29/08.

Choi, G. Y., Choi, J. N., Kwon, H. J., et al. 2005. The impact of high apparent temperature on the increase of summertime disease-related mortality in Seoul: 1991–2000. *Journal of Preventive Medicine and Public Health*, 38, 283–290.

Civerolo, K. L., Sistla, G., Rao, S. T., Nowak, D. J., et al. 2000. The effects of land cover in meteorological modeling: implications for assessment of future air quality scenarios. *Atmospheric Environment*, 34, 1615–1621.

Confalonieri, U., Menne, B., Akhtar, R., Ebi, K. L., Hauengue, R. S., Kovate, B., Woodward, A., et al. 2007. Human Health. In M. L. Parry, O. F. Canziani, J. P. Palutikof, P. J. van der Linden and C. E. Hanson (Eds), *Climate Change 2007: Impacts, Adaptation and Vulnerability.* Contribution of Working Group II to the Fourth Assessment Report of the Intergovernmental Panel on Climate Change. Cambridge, UK: Cambridge University Press.

Curriero, F. C., Heiner, K. S., Samet, J. M., Zeger, S. L., Strug, L., Patz, J. A., et al. 2002. Temperature and mortality in 11 Cities of the eastern United States. *American Journal of Epidemiology*, 155, 80–87.

DeGaetano, A. T. and Allen, R. J. 2002. Trends in twentieth-century temperature extremes across the United States. *Journal of Climate*, 115, 3188–3205.

Grimm, N. B. and Redman, C. L. 2004. Approaches to the study of urban ecosystems: the case of Central Arizona – Phoenix. *Urban Ecosystems*, 7, 199–213.

Grimmond, C. S. B. 2005. Progress in measuring and observing the urban atmosphere. *Theoretical and Applied Climatology*. doi: 10.1007/s00704-00005-00140-00705.

Grossman-Clarke, S., Zehnder, J. A., Stefanov, W. L., Liu, Y., Zoldak, M. A. 2005. Urban modifications in a mesoscale meteorological model and the effects on near surface variables in an arid metropolitan region. *Journal of Applied Meteorology*, 44, 1281–1297.

Grossman-Clarke, S., Liu, Y., Zehnder, J. A., Fast, J. D., et al. 2008. Simulation of the Urban Planetary Boundary Layer in an arid metropolitan Area. *Journal of Applied Meteorology and Climatology*, 47(3), 752–768.

Harlan, S. L., Brazel, A. J., Prashad, L., Stefanov, W. L., Larsen, L., et al. 2006. Neighborhood microclimates and vulnerability to heat stress. *Social Science & Medicine*, 63, 2847–2863.

Harlan, S. L., Budruk, M., Gustafson, A., Larson, K., Ruddell, D., Smith, V. K., Yabiku, S. T., Wutich, A., et al. 2007. Phoenix Area Social Survey 2006 Highlights: Community and Environment in a Desert Metropolis. Central Arizona – Phoenix Long-Term Ecological Research Project, Contribution No. 4. Global Institute of Sustainability, Arizona State University.

Harlan, S. L., Brazel, A. J., Jenerette, G. D., Larsen, L., Jones, N. S., Prashad, L., Stefanov, W. L., et al. 2008. Made in the shade: The inequitable distribution of the urban heat island. *Research in Social Problems and Public Policy*, 15, 173–202.

Hedquist, B. C., and Brazel, A. J. 2004. Urban heat island (UHI) measures for the S.E. metropolitan area of the CAP LTER: transects versus fixed stations. Presented at the 6th Annual CAP LTER Poster Symposium, Tempe, AZ.

Hong, S. Y., and Pan, H. L. 1996. Nonlocal boundary layer vertical diffusion in a medium-range forecast model. *Monthly Weather Review*, 124, 2322–2339.

(ICLEI) International Council for Local Environmental Initiatives 1998. Cities at risk: assessing the vulnerability of United States cities to climate change. Toronto, Canada.

(IPCC) Intergovernmental Panel on Climate Change 2007. Climate Change 2007: Synthesis Report. http://www.ipcc.ch/pdf/assessment-report/ar4/syr/ar4_syr.pdf; accessed 4/29/08.

Jenerette, G. D., Harlan, S. L., Brazel, A. J., Jones, N., Larsen, L., Stefanov, W. L., et al. 2007. Regional relationships between vegetation, surface temperature, and human settlement in a rapidly urbanizing ecosystem. *Landscape Ecology*, 22, 353–365.

Kalkstein, L. S., and Davis, R. E. 1989. Weather and human mortality: an evaluation of demographic and inter-regional responses in the United States. *Annals of the Association of American Geographers*, 79, 44–64.

Kalkstein, L. S., and Greene, J. 1997. An evaluation of climate/mortality relationships in large US cities and the possible impact of a climate change. *Environmental Health Perspectives*, 105(1), 84–93.

Kalkstein, L. S., Jamason, P. P., Greene, J. S., Libby, J. Robinson, L., et al. 1996. The Philadelphia hot weather-health watch warning system: development and application, summer 1995. *Bulletin of the American Meteorological Society*, 77, 1519–1528.

Kilbourne, E. M. 2002. Heat-related illness: current status of prevention efforts. *American Journal of Preventive Medicine*, 22, 328–329.

Klinenberg, E. 2002. *Heat wave: A social autopsy of disaster in Chicago*. Chicago: University of Chicago Press.

Kusaka, H., and Kimura, F. 2004. Coupling a single-layer urban canopy model with a simple atmospheric model: impact on urban heat island simulation for an idealized case. *Journal of the Meteorological Society of Japan*, 82, 67–80.

Larsen, L., and Harlan, S. L. 2006. Desert dreamscapes: residential landscape preference and behavior. *Landscape and Urban Planning*, 78, 85–100.

Larson, J. 2006. Setting the record straight: more than 52,000 Europeans died from heat in summer 2003. *Earth Policy Institute*. Available at: http://www.earth-policy.org/Updates/2006/Update56.htm. Accessed October 19, 2007.

Legendre, P., and Fortin, M. J. F. 1989. Spatial pattern and ecological analysis. *Vegetation*, 80, 107–138.

Lin, C.-Y., Chen, F., Huang, J. C., Chen, W-C., Liou, Y.-A., Chen, W.-N., Liu, S-C., et al. 2008. Urban heat island effect and its impact on boundary layer development and land-sea circulation over northern Taiwan. *Atmospheric Environment*, 42, 5635–5649.

Liu, Y., Chen, F., Warner, T., Basara, J., et al. 2006. Verification of a Mesoscale Data-Assimilation and Forecasting System for the Oklahoma City Area During the Joint Urban 2003 Field Project. *Journal of Applied Meteorology*, 45, 912–929.

Lowry, W. 1967. The climate of cities. *Scientific American*, 217, 15–23.

Martilli, A. 2007. Current research and future challenges in urban mesoscale modeling. *International Journal of Climatology*, 27(14), 1909–1918.

Martin, C. A., Warren, P. S., Kinzig, A. P., et al. 2004. Neighborhood socioeconomic status is a useful predictor of perennial landscape vegetation in residential neighborhoods and embedded small parks of Phoenix, Arizona. *Landscape and Urban Planning*, 69, 355–368.

Masson, V. 2006. Urban surface modeling and the meso-scale impact of cities. *Theoretical and Applied Climatology*, 84(1), 35–45.

McGeehin, M. and Mirabelli, M. C. 2001. The potential impacts of climate variability and changer on temperature-related morbidity and mortality in the United States. *Environmental Health Perspectives*, 109, 185–189.

McMichael, A. J., Woodruff, R. E., Hales, S., et al. 2006. Climate change and human health: present and future risks. *Lancet*, 367, 859–869.

Meehl, G. A., and Tebaldi, C. 2004. More intense, more frequent, and longer lasting heat waves in the 21st century. *Science*, 305, 994–997.

Michelozzi, P., DeSario, M., Accetta, G., De'Donato, F., Kirchmayer, U., D'Ovidio, M., Perucci, C., et al. 2006. Temperature and summer mortality: geographical and temporal variations in four Italian cities. *Journal of Epidemiology and Community Health*, 60, 417–423.

Naughton, M. P., Henderson, A., Mirabelli, M. C. et al. 2002. Heat-related mortality during a 1999 heat wave in Chicago. *American Journal of Preventive Medicine*, 22, 221–227.

Oke, T. R. 1982. The energetic basis of the urban heat island. *Quarterly Journal of the Royal Meteorological Society*, 108, 1–24.

Oke, T. R. 1997. Part 4: The changing climatic environments: urban climates and global environmental change. In R. D. Thompson and A. Perry (eds.), *Applied Climatology Principals and Practice* (pp. 273–287). London: Routledge.

O'Neill, M. S., Jarrett, M., Kawachi, I., Levy, J. I., Cohen, A. J., Gouveia, N., Wilkinson, P., Fletcher, T., Cifuentes, L., Schwartz, J., et al. 2003. Health, wealth, and air pollution: advancing theory and methods. *Environmental Health Perspectives*, 111, 1861–1870.

Patz, J. 2005. Guest editorial: satellite remote sensing can improve chances of achieving sustainable health. *Environmental Health Perspectives*, 113, A84–85.

Patz, J., Campbell-Lendrum, D., Holloway, T., Foley, J. A., et al. 2005. Impact of regional climate change on human health. *Nature*, 438, 310–317.

Seaman, N. L. 2000. Meteorological modeling for air-quality assessments. *Atmospheric Environment*, 34, 2231–2259.

Semenza, J. C., Rubin, C. H., Falter, K. H., Selanikio, J. D., Flanders, W. D., How, H. L., Wilhelm, J. L., et al. 1996. Heat-related deaths during the July 1995 heat wave in Chicago. *American Journal of Preventive Medicine*, 16(4), 269–277.

Semenza, J. C., McCullough, J. E., Flanders, W. D., McGeehin, M., Lumpkin, J. R. et al. 1999. Excess hospital admissions during the July 1995 heat wave in Chicago. *American Journal of Preventive Medicine*, 16(4), 269–277.

Shamrock, W. C., Klemp, J. B., Dudhia, J., Gill, D. O., Barker, D. M., Wang, W., Powers, J. G., et al. 2005. A Description of the Advanced Research WRF Version 2. NCAR Technical Note.

Sheridan, S. C. and Kalkstein, L. S. 2004. Progress in heat watch-warning system technology. *Bulletin of the American Meteorological Society*, 85, 1931–1941.

Smoyer-Tomic, K. E., and Rainham, D. G. C. 2001. Beating the heat: Development and evaluation of a Canadian hot weather health-response plan. *Environmental Health Perspectives*, 109, 1241–1248.

Smoyer, K. E., Rainham, D. G., Hewko, J. N., et al. 2000. Heat-related stress mortality in five cities in southern Ontario: 1980–1996. *Institutional Journal of Meteorology*, 44(1809), 190–197.

Stabler, L. B., Martin, C. A., Brazel, A. J., et al. 2005. Microclimates in a desert city were related to land use and vegetation index. *Urban Forestry and Urban Greening*, 3, 137–147.

Stefanov, W. L., Ramsey, M. S., Christensen, P. R., et al. 2001. Monitoring urban land cover change: an expert system approach to land cover classification of semiarid to arid urban centers. *Remote Sensing of Environment,* 77, 173–185.

Taha, H. 1997a. Modeling the impacts of large scale albedo changes on ozone air quality in the south coast air basin. *Atmospheric Environment*, 31, 1667–1676.

Taha, H. 1997b. Urban climates and heat islands: albedo, evapotranspiration, and anthropogenic heat. *Energy and Buildings, 25*, 99–103.

Voogt, J. A. 2002. Urban Heat Island. In I. Douglas (ed.), *Encyclopedia of global environmental change* (pp. 660–666). Chichester: John Wiley and Sons.

Voogt, J. A., and Oke, T. R. 2003. Thermal remote sensing of urban climates. *Remote Sensing of Environment*, 86, 284–370.

Chapter 10
Wildfire Risk Analysis at the Wildland Urban Interface in Travis County, Texas

Yongmei Lu, Lori Carter, and Pamela S. Showalter

Abstract The term, "wildland urban interface" (WUI) refers to the area where structures and other human development meet or intermingle with undeveloped wildland or vegetative fuel. When development encroaches into wildland – areas that have been minimally impacted by human activities – the wildfire threat to life and property increases. A wildfire risk profile for the WUI in Travis County, Texas was created using a geographic information system (GIS). Historic wildfire records were linked to land cover types to identify the empirical relationship between fuels and ground cover. Topographical characteristics, land cover types, and housing density were combined to estimate wildfire risk. Risk levels for communities within and outside the WUI were compared. Analyses also compared wildfire risk levels for different types of WUI areas, which are distinguished based on vegetation coverage percentages and housing density. Findings indicate that in Travis County, TX, the wildfire risk is highest in high-density WUI areas, pointing to an urgent need for special fire control and fire regulations in this development zone. Vacant lands, which are likely future development sites, could be used by land managers to reduce wildfire risk if they can be managed as natural fire breaks or fuel free zones.

Keywords Wildland Urban Interface · Wildfire · Risk analysis · GIS · Texas

10.1 Introduction

The term "wildfire" refers to any unplanned or unwanted fire burning in forests, shrub lands, woodlands, or grasslands. Wildfire is one of the most destructive natural forces known to humanity. History is replete with episodes of notorious wildfires: the Miramichi fire in New Brunswick killed 160 people and burned three million acres (12,000 km^2) in 1825. The Peshitigo fire in 1872 killed over 1000 people

Y. Lu (✉)
Department of Geography, Texas State University-San Marcos, San Marcos TX 78666, USA,
e-mail: yl10@txstate.edu

P.S. Showalter, Y. Lu (eds.), *Geospatial Techniques in Urban Hazard and Disaster Analysis*,
Geotechnologies and the Environment 2, DOI 10.1007/978-90-481-2238-7_10,

in Wisconsin. California's 1991 Oakland Firestorm killed 25 people and destroyed 3469 homes and apartments. British Columbia's 2003 Okanogan Mountain Park Fire displaced 45,000 inhabitants, destroyed 239 homes, and threatened part of the City of Kelowna. That same year, San Diego County in Southern California suffered from a fire that took 15 lives and destroyed 2232 homes – that year California's total loss from wildfires neared $2 billion.[1]

Although most wildfires in Texas are of smaller scale, damages can be significant. For example, the Texas–Oklahoma wildfires of 2005–2006 caused enough damage to qualify for federal disaster relief funding. Higher than average precipitation rates during 2005 encouraged abundant vegetation growth. Subsequently, a period of extended drought with record high temperatures and high winds transformed the vegetation to dry fuel which, once ignited, sustained and spread the wildfire. In Texas, eleven people were killed and eight towns evacuated in early March of 2006. From late December 2005 until early April 2006, approximately five million acres (nearly 20,000 km^2) were burned and 423 homes destroyed (Lindley et al. 2007).

As pointed out by Dennison et al. (2007), fire presents the greatest hazard to land and life in the areas where humans and fire-prone vegetation meet. While vegetation fuel supply and weather conditions are major contributing factors to wildfire, continuing residential development in the wildland urban interface (WUI) – where structures and other human development meet or intermingle with undeveloped wildland or vegetative fuel (Cortner et al. 1990; Ewert 1993) – increases the possible occurrence of and subsequent damage from wildfires. Wildfires are often caused by human activities (Cardille et al. 2001; NIFC 2006). At the WUI, human activities occur where there are adequate fuel supplies, making it difficult to protect structures from wildfires (Cohen 2000; Winter and Fried 2001). The result: wildfire damage (as measured by both life and property loss) at the WUI tends to be greater than in other geographic locations.

The purpose of this study is to improve wildfire risk management by using a Geographic Information System (GIS) to perform wildfire risk analysis for one of the nation's fastest growing regions – Travis County, Texas (Fig. 10.1). Urban encroachment into wildland areas in the county has created a variety of "WUI communities"; the analyses reported in this paper took into account all of these communities. Spatial variation of vegetative fuel, county topography, and historic wildfire occurrences recorded by the Texas Forest Service were incorporated into the analysis. Using these criteria, statistical differences between the level of wildfire risk faced by each type of community were examined. Furthermore, because urban development is likely to move into vacant lands (which may, or may not, be within the WUI), the analysis also incorporated data regarding the county's vacant lands.

[1]More information about these and other notorious North American wildfires can be found at: http://en.wikipedia.org/wiki/List_of_wildfires

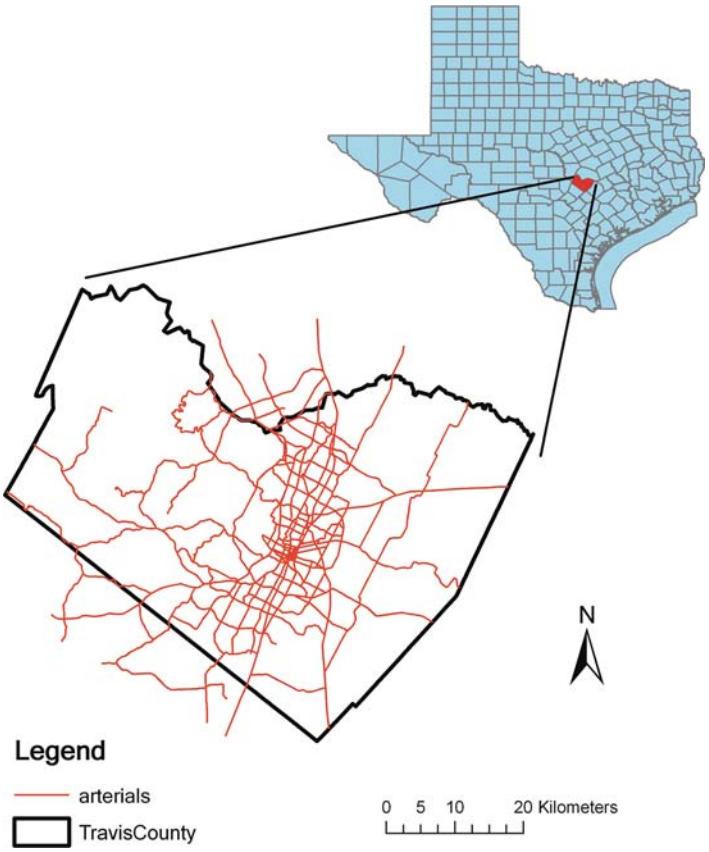

Fig. 10.1 Travis County, Texas

10.2 Risk Analysis and Wildfires

The concept of "risk" is as intriguing as it is multifaceted. Risk can be commonly accepted (e.g., driving a car), sought out (e.g., bungee-jumping from a bridge), or purposely avoided (e.g., refusing to fly). People perform "risk analysis" constantly as they go about their daily activities, while universities, companies, and governments study risk formally using scientific methods to better understand the dangers present in any given situation and how they can be effectively managed. Risk assessment requires both good science and good judgment (Keeney 1995) and can be either quantitative or qualitative. A risk assessment usually examines three items: hazard probability, expected loss, and loss mitigation (preparedness) (Finney 2005; Smith 2004). The risk assessment of wildfires in this study focuses on the first two items – probability and expected loss. The probability of wildfires is estimated by considering various factors that can contribute to the occurrence and sustenance of

wildfires throughout Travis County. These factors include vegetative fuel, topography, and the frequency with which different types of land cover have wildfires (as derived from historic fire records). The expected loss from wildfires in the WUI is determined by considering the size and density of population and housing units.

10.2.1 Natural Factors

Topography, weather conditions, and vegetative fuel loading play major roles in wildfire combustion potential (Cova et al. 2004). Fires that occur on larger slopes carry increased capacity to ignite fuels upslope (Thompson et al. 2000). Convective heat uplift from the fires down-slope (Pyne 2001) and longer flame lengths preheat vegetation above (Christiansen 2005; Davis 1990). On steep slopes, ignited materials can roll downhill with greater ease, spreading embers and flames. Aspect, or the direction that a slope faces, is also a significant factor. Slopes facing south and west in the northern hemisphere, patches of flat land, and very dry ridge tops have increased fire ignition potential because vegetative and soil moisture content decreases throughout the day due to longer exposure to solar radiation (Cova et al. 2004; Christiansen 2005; Johnson 2008; Perestrello de Vasconcelos et al. 2001; Thompson et al. 2000).

Climate and wind behavior can also contribute to the wildfire risk. Areas with temperate, moist climates have lower fuel ignition rates due to high retention of water within both vegetation and soil (Carapella 1996; Cardille et al. 2001). Areas subject to seasonal variations in moisture, such as much of the American West, Southwest, and Central Plains, have periods throughout the year when vegetative moisture retention is low. The low moisture retention is due to extended periods of lower than average rainfall coupled with higher than average temperature (Lawrimore 2005). The variables of high evaporation, low vegetation/soil moisture, and high vegetation density combine to create conditions most prone to wildfire ignition and spread. Under drier climatic conditions, areas with higher densities of vegetation are likely to have larger and more intense wildfires because of the increased fuel load. Without fuel breaks, wildfires can spread more rapidly and can be longer lived. Wind behavior further contributes to the wildfire risk because high wind speeds can carry firebrands or sparking embers of vegetation great distances[2] (Manzello 2007; Radeloff et al. 2005; Trembath 2005) while accelerating the drying process. Prolonged wind events can also "feed" existing fires by introducing more oxygen into the fire system (CSFS 2007).

[2]The California Forest Alliance estimates that firebrands from forest fires can be carried by winds or convective uplift for distances of up to 2.4 km (Radeloff et al. 2005).

10.2.2 Housing Density

Radeloff et al. (2005) considered housing density, vegetation type and density, and proximity to that vegetation as important variables for understanding wildfire risk. Other researchers have found that as the number of structures increases, the likelihood of anthropogenically-caused fire increases (Cardille et al. 2001; NIFC 2006; Perestrello de Vasconcelos et al. 2001; TFS 2007). Not surprisingly, denser residential developments tend to have greater loss of structures from wildfires (Trembath 2005) than those that are less dense. Communities that lack dense vegetation but are within reach of firebrands (Radeloff et al. 2005), overhanging branches, and contiguous grasslands (Trembath 2005) may be as vulnerable to wildfire as those with dense vegetation. In fact, the Texas Forest Service (TFS) recommends that structures be built more than 200 m from dense vegetation to prevent structural ignition from branch overhangs and grass fires (Cohen 2000; TFS 2007).

In conjunction with the wildfire problem faced by high density WUI areas, low density lands (including vacant lots) are commonly given insufficient attention when considering measures to reduce the wildfire threat. Given that urban growth commonly moves onto vacant lands, there are two important reasons for including these areas in wildfire risk analysis: (1) they represent future "built-up" areas, and (2) depending on how they are managed prior to development, they could serve as fire breaks, green buffers, or home ignition prevention zones (Cohen 2000; Ingalsbee 2003; IDL 2006); in short, they can behave either as a fire retardant or an accelerant, depending on how they are managed.

10.3 The Study Area

Located in Central Texas, Travis County is at the convergence of several distinct bioregions: the Edwards Plateau in the west, the Blackland Prairies toward the east and southeast, and the Cross-timbers and Prairies region toward the north (Travis County 2004). The county's varied topographical structure supports diverse vegetative communities. The Edwards Plateau's karst topography is characterized by plateaus and steep slopes dissected by waterways and supporting vegetation such as Ashe Juniper, Oak varieties and Mesquite. The Blackland Prairies region, whose deep rich soils are ideal for vegetative growth, supports agricultural endeavors and is experiencing considerable subdivision development. The Cross-timbers and Prairies region is characterized by rolling woodland savannah. At the southern tip of the Plains region, vegetation is characteristically grassy and interspersed with oak.

Occupying a transition zone between subtropical subhumid and subtropical humid climates, the County's average annual precipitation varies from 30 inches (71.2 cm) in the west to 36 inches (91.4 cm) in the east. Temperature range between an average January low of 39°F (3.89°C) and an average July high of 95°F (35°C). Major climatic hazards include straight line winds, lightning, flash floods, severe

heat, drought, and wildfires (Larkin and Bomar 1983). The County has recorded periods of extreme and prolonged rainfall followed by extended drought which has allowed wildfire fuel loads to collect and desiccate; towards the west, increased elevation and steep hill-slopes further exacerbate the risk of wildfire.

Travis County is one of the most rapidly growing counties in the US (TSDC/OSD 2006). Between 2002 and 2005, the population increased from 830,649 to 866,349 (TCHHS 2006), and by 2040 the population is projected to reach about 2 million (Travis County 2007). This growth is likely to increase the breadth of the WUI by converting lands that were formerly rural to those characterized by higher density development.

10.4 Data Utilized

To perform a wildfire risk assessment of Travis County, we combined vector data sets illustrating historic wildfires, ignition potential, and vacant lands in the study area with raster data sets containing information about elevation, slope, aspect, and vegetation/land cover at various resolutions. After identifying the related datasets, data extraction was performed followed by data cleaning, geocoding, registration, and other pre-processing where needed.

The Fire Reporting Database maintained by the Texas Forest Service Fire Department provided the data for wildfires occurring between January 1, 2005 and January 31, 2008 (for ease of discussion, referred to hereafter as between 2005 and 2007). After extracting, mapping, and cleaning the data, a total of 315 wildfires were identified (Fig. 10.2). Spatial distribution of the wildfires was used as a surrogate indicator of wildfire-prone areas, forming the foundation for further estimation of wildfire risk based upon historic records. Figure 10.2 displays the locations of these wildfires across Travis County, and reveals a clear association between the fires and urban areas. The term, “urban” in this paper follows the definition of the US Census Bureau. For Census 2000, “urban area” refers to all territory, population, and housing units located within an urbanized area or an urban cluster, which consists of core census block groups or blocks that have a population density of at least 1000 people per square mile and surrounding census blocks that have an overall density of at least 500 people per square mile.

Although Travis County’s annual precipitation varies spatially by about 6 inches (15.2 cm), for purposes of the study this variation was not included when modeling ignition potential. Spatial variation in temperature and moisture conditions for soil and vegetation was modeled by calculating surface exposure to solar radiation across the County. As wind pattern/wind speed data were unavailable for this study, the effect of wind for wildfire was not directly incorporated into the study. Rather, considering that wind tends to speed up as slope increases (Bradstock et al. 2002), relatively high wildfire potential was assigned to steeper slopes.

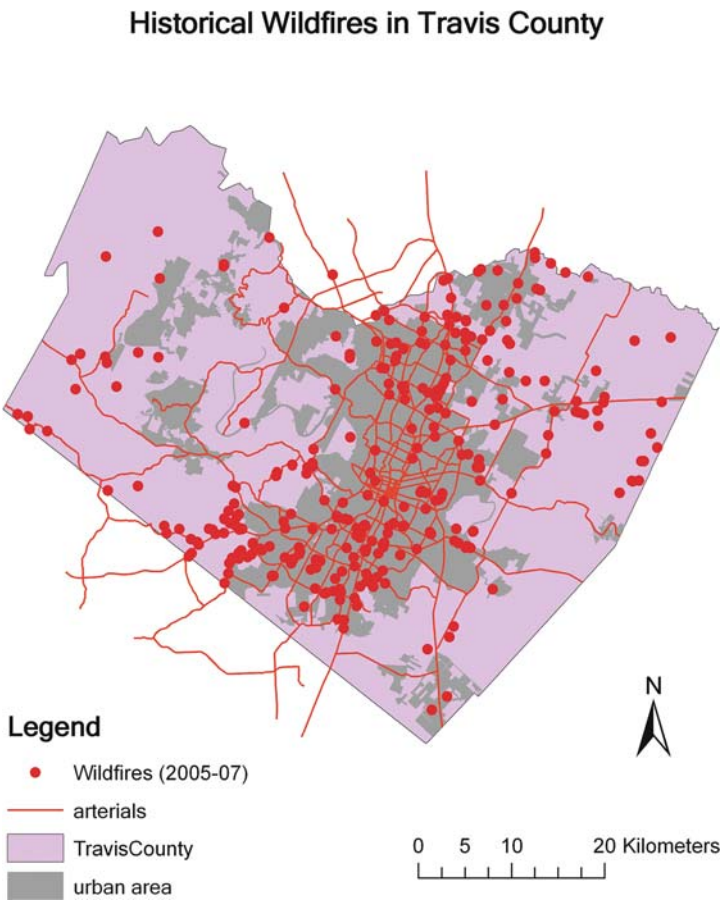

Fig. 10.2 Locations of Travis County wildfires between Jan. 1, 2005 and Jan. 31, 2008

Vacant land data were obtained from the Vacant Land Inventory (VLI) data set available from the Capital Area Council of Government (CAPCOG) Information Clearinghouse (CAPCOG 2008). The VLI was developed by CAPCOG to represent vacant lands identified through analysis of 2005 parcel and tax role information. These lands are normally five acres or lager in size and have improved value of $0.05 per square foot or less. Figure 10.3 displays the location of the 2005–2007 wildfires in relationship to vacant land in the County, and confirms the impression given by Fig. 10.2, that fewer fires occurred in or near vacant lands compared to "urban" areas.

The spatial extent of the WUI was defined by considering the spatial proximity of housing density and vegetation coverage. Travis County's WUI was defined

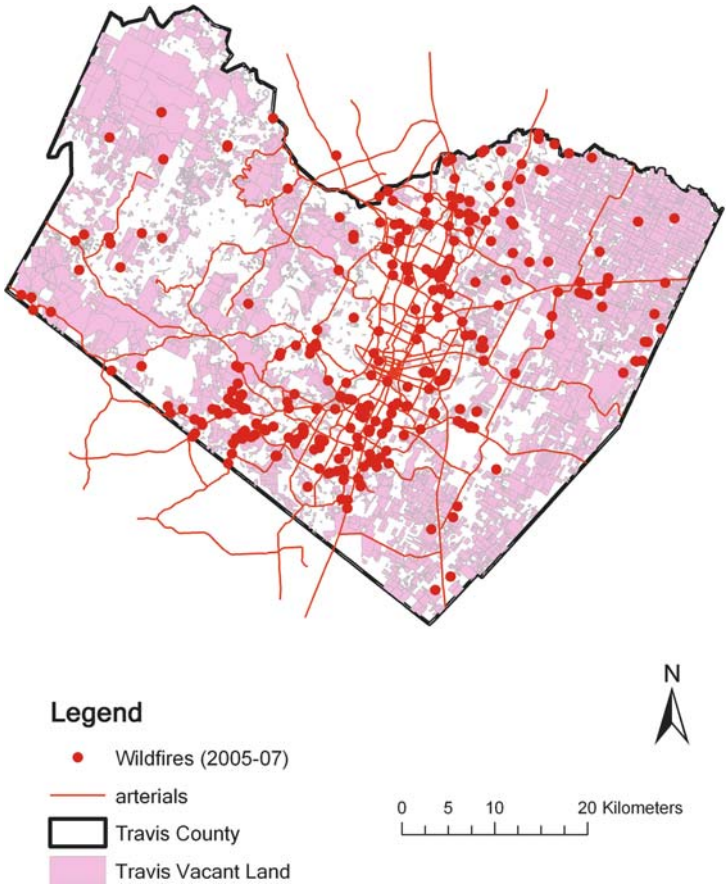

Fig. 10.3 Locations of the 2005–2007 wildfires in relation to Travis County's vacant land

following Radeloff et al. (2005) and Stewart et al. (2007). When vegetation covers over 50% of the land area, *High Density Intermix* refers to the blocks where housing density is higher than 741.3 housing units per km^2, *Medium Density Intermix* exists where housing density is between 49.2 and 741.3 units per km^2, and *Low Density Intermix* exists where housing density is between 6.2 and 49.2 units per km^2. In areas where vegetation covers less than 50% of the land but is within 2.4 km^2 of an area with 75% or more vegetation coverage, *High Density Interface* exists if the housing density is higher than 741.3 units per km^2, *Medium Density Interface* exists if the housing density is between 49.2 and 741.3 units per km^2, and *Low Density Interface* exists if the housing density is between 6.2 and 49.2 units per km^2(see Radeloff et al. [2005] for additional details). The WUI data set for Travis County was downloaded from Silvis Lab's webpage at the University of Wisconsin – Madison (Radeloff et al. 2005; Silvis Lab no date). Figure 10.4 displays

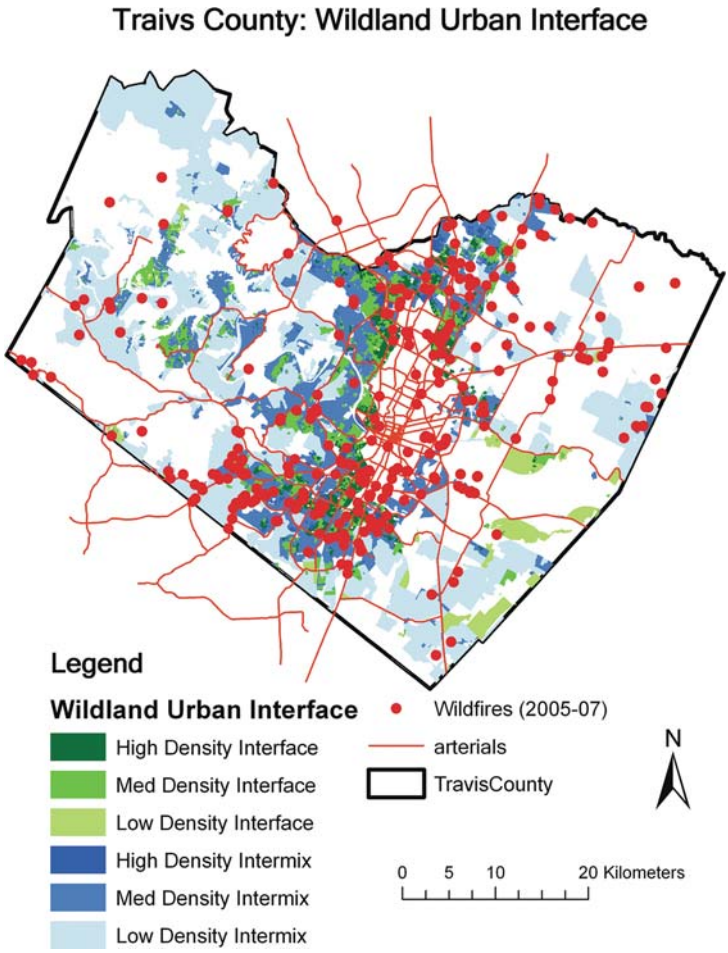

Fig. 10.4 Locations of the 2005–2007 wildfires in relation to Travis County's WUI

the location of the 2005–2007 wildfires in relation to the County's WUI. A clear spatial association appears to exist between the majority of the historical wildfires and human development, with fires apparently concentrated close to, or in, urban areas and the most high-density areas of the WUI.

Elevation was obtained via a digital elevation model (DEM) downloaded from the US Geological Survey's Seamless Data Distribution System (USGS no date). The National Elevation Dataset (NED) 1 arcsec is a raster product that has an approximate 30 m resolution. Both slope and aspect measurements for the study area were derived from this elevation dataset.

Vegetation and land cover data were obtained from the National Land Cover Dataset (NLCD) of 2001. To further refine the NLCD's 30 m spatial resolution and broad land cover/land use categories (e.g., forest, grassland, agricultural uses,

urban, and suburban development) the data was cross-referenced for regional variations using 1 m 2005 Digital Orthophoto Quarter Quadrangles (DOQQs) obtained through the Texas Natural Resource Information System (TNRIS 2008). By performing the cross-referencing, new subcategories of land cover/land use reflecting the local situation were created and their accuracy validated. Details of this process are reported in the following section.

10.5 Wildfire Risk Analysis of Travis County

Three factors that significantly influence and sustain wildfires are topography, fuel supply, and weather conditions. Travis County's wildfire risk was derived by analyzing aspect, slope, and fuel supply data in relationship to different land cover classes. Aspect, derived from DEM data, served as a surrogate for solar heating and vegetation moisture levels. Slope could be classified into different risk levels because uplift of heat along slopes causes wildfires to spread mainly uphill–steeper slopes facilitate the spread of wildfire more efficiently than gentle slopes (Perestrello de Vasconcelos et al. 2001). Since fuel supply data were limited, variation in topography was used to estimate micro-scale spatial variation in heating of fuels. Places receiving more sunshine tend to sustain well-grown vegetation with low moisture content, providing an ideal fuel supply for wildfires. Vacant land data were added to the analysis because they are typically un-cleared prior to development; they support vegetation, and thereby represent a source of fuel. Finally, wildfire risk was related to fuel supplies by generating a location quotient (LQ) of wildfire occurrence for different land cover classes. The latter item requires some explanation.

National Land Cover Dataset (NLCD) categories are generalized and do not reflect local characteristics such as vegetation density and vegetation ignition tendency – criteria that are critical for estimating wildfire risk. Therefore, the dataset underwent a two-step modification before it was used to create an LQ. First, the NLCD was reclassified to reflect local vegetation types. The new "Regional Land Cover Classes" (RLCC) were identified as:

- **H_2O**: Water bodies (not including intermittent and ephemeral streams)
- **MNT**: Maintained grasses (roadside grasses, parks, golf courses)
- **UT**: Urban Trees (groups of trees found in residential and commercial parks)
- **DVL**: Developed land (rooftops, driveways, commercial and residential)
- **ISC**: Impervious surface cover (roads, parking lots)
- **CMNT**: Cement and other artificial coverage (gravel, or not included in ISC)
- **JOP**: Juniper-Oak parks (groups of trees with interspersed grasses)
- **JOW**: Juniper-Oak woodlands (more dense canopies, less open grasses)
- **PR**: Prairie (Blackland Prairie open grasses–limited to eastern Travis County)
- **GRZ**: Grazing, rural (open grasslands–mostly found in western Travis County at higher elevations)

- **SPRS**: Sparse grasses (combined bare soil, rocky outcrops, and sparse grasses)
- **PRD**: Production (mainly agricultural–located near farming operations)
- **AGR**: Agricultural (open fields of continuous crops, visible farming implement footprints)
- **EVRG**: Evergreen (smaller groves of live oak, pine, higher canopies than ash juniper)
- **AQ**: Aquatic vegetation (found near or within water bodies, partial submersion)

Second, the accuracy of the reclassified NLCD data was evaluated to ensure the RLCC accurately reflect the true distribution of regional land cover in the study area. Using random sampling, 50 locations were selected within each of the 15 RLCCs created for the study area, creating 750 sampling sites. These sites were located on the 2005 DOQQs described earlier, and were examined to determine if the derived RLCC matched that found on the DOQQ. The numbers of correctly and incorrectly classified samples were recorded. The NLCD-derived RLCC was found to have an accuracy rate between 76% and 100% (Table 10.1), which was considered sufficient for the purposes of this study.

The LQ for wildfire was then derived by examining the spatial distribution of the RLCCs in relation to wildfire fuel supply. The RLCC was overlaid on a map showing the locations of historic wildfires, and the number of wildfires that occurred in each type of land cover/use recorded. The LQ was then calculated by dividing the percentage of wildfires occurring in each type of land cover/use by the areal percentage of the land cover/use over the entire study area (Table 10.2). The LQ thus reflects the tendency of each type of land cover/use to be impacted by wildfire. An LQ value equal to or less than one indicates that the percentage of wildfires occurring on that specific land cover is not greater than what would be expected given the spatial extent of that land cover within the study area. RLCC with LQ

Table 10.1 The accuracy of land cover classification from NLCD (based on 50 random samples obtained for each category)

Land Cover	Number of correctly classified samples	Accuracy
H_2O	50	1.00
MNT	48	0.96
UT	44	0.88
DVL	50	1.00
ISC	50	1.00
CMNT	50	1.00
JOP	39	0.78
JOW	44	0.88
PR	44	0.88
GRZ	39	0.78
SPRS	46	0.92
PRD	42	0.78
AGR	48	0.96
EVRG	38	0.76

Table 10.2 Wildfire risk: location quotient for different types of land cover based on historical wildfires (2005–2007)

Land cover	Areal percentage (%)	Fire_count percentage (%)	Location quotient (LQ)
H_2O	3.29	0.00	0.00
MNT	10.39	21.59	2.08
UT	6.46	16.19	2.51
DVL	4.10	15.87	3.87
ISC	2.00	13.97	6.99
CMNT	0.09	0.00	0.00
JOP	8.79	4.44	0.51
JOW	22.44	6.35	0.28
PR	0.65	0.32	0.49
GRZ	17.75	8.57	0.48
SPRS	11.64	7.94	0.68
PRD	4.15	0.63	0.15
AGR	6.37	2.86	0.45
EVRG	1.88	1.27	0.68
AQ	0.01	0.00	0.00
Total	100	100	n/a

values greater than one are therefore considered to be at greater risk than those equal to or less than one.

A wildfire risk ranking that combined aspect, slope, and LQ was created, representing each variable's relative contribution to wildfire risk. Slope, presented as a percent, reflects the escalating ability of wildfire to spread as slope increases. Aspect represents the different levels of sunshine a slope might receive. Finally, LQ, calculated as described above, represents the relative activity of wildfire on each land class. The five wildfire risk ranks were: None (0), Low (1), Medium-low (2), Medium-high (3), and High (4). Table 10.3 breaks down the fire risk rankings for the three variables and Figures 10.5, 10.6 and 10.7 utilize these ranks to illustrate the spatial patterns of wildfire risk in Travis County.

Table 10.3 Wildfire risk ranking based on slope, aspect, and Location Quotient for different types of land cover

Wildfire risk level: Reclassified	0 (None)	1 (Low)	2 (Medium-low)	3 (Medium-high)	4 (High)
Slope (%) (areal %)	n/a	0–4.99 (90.31)	5–9.99 (8.42)	10–14.99 (1.13)	≥ 15 (0.15)
Aspect (areal %)	n/a	Northeast, North (21.65)	Northwest, East (24.14)	West, Southeast (25.70)	Southwest, South, Flat (28.51)
Land cover LQ (areal %)	0 (3.38)	> 0 & ≤ 1 (73.67)	> 1 & ≤ 2 (0)	> 2 & ≤ 3 (16.85)	> 3 (6.09)

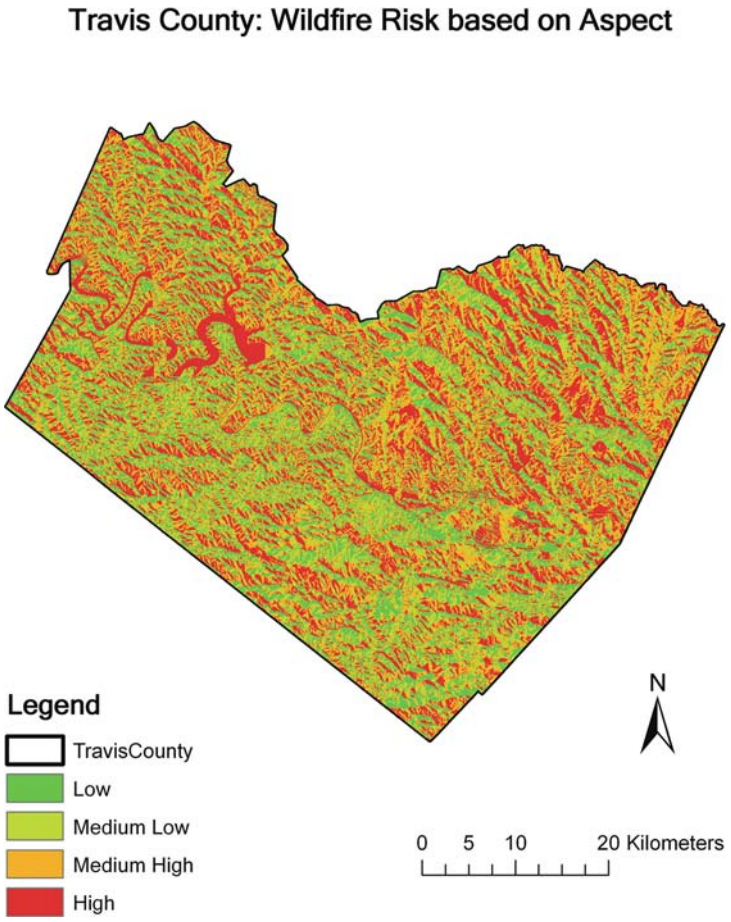

Fig. 10.5 Travis County wildfire risk ranking based on aspect

The fire risk rankings for aspect, slope, and land cover were then combined using GIS raster calculation, generating a data range between 0 and 12. The results were ranked into five categories, from Low to High (Table 10.4). The results indicate that the majority of the county (91.38%) falls in the Low to Medium level of wildfire risk (Fig. 10.8). However, a total of 8.7% of the County's land falls in the Medium-high to High levels of wildfire risk. Mapping this information reveals a clear pattern of High and Medium-high risk areas being prevalent in urbanized locations and in the WUI (Fig. 10.9).

As the population of Travis County continues to grow and developed areas expand, part of that growth is likely to occur on vacant lands. Consequently, vacant lands may indicate the direction of urban growth into the county's WUI. Among the 5548 vacant lots reported in CAPCOG's database, 1543 fall into the Medium-high to

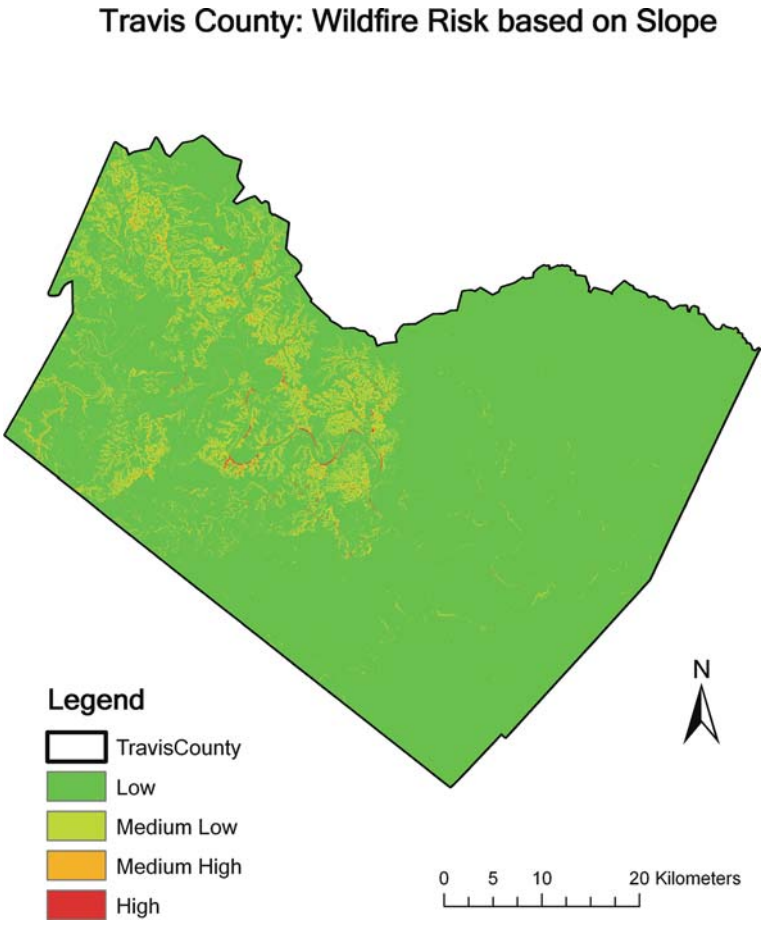

Fig. 10.6 Travis County wildfire risk ranking based on slope

High level for fire risk, with about 30% of the vacant lands located in relatively high fire risk zones. As population and housing move onto these lands, the potential loss from fire increases. Although new development on vacant lands may reduce vegetation density on the land parcel and the areas immediately surrounding it, the fire risk for a specific parcel is unlikely to change dramatically until significant change happens over a larger spatial extent. Thus, land use management designed to improve fire damage control on these vacant parcels, especially those located within the relatively high-risk zones for wildfire, is critical. Figure 10.10 provides a visual display of the spatial relationship between the vacant lands and their calculated fire risk levels.

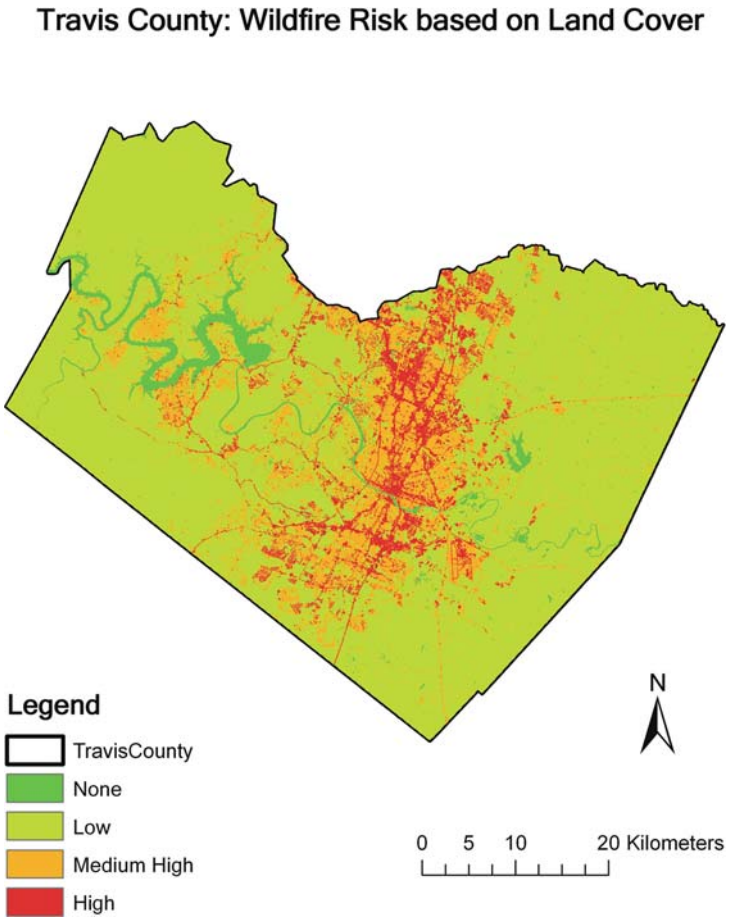

Fig. 10.7 Travis County wildfire risk ranking based on reclassified and cover

Table 10.4 Final wildfire risk ranking for the study area

Risk level	Low	Medium-low	Medium	Medium-high	High
Original combined risk value	2, 3	4, 5	6, 7	8, 9	10, 11, 12
New reclassified risk value	1	2	3	4	5
Areal percentage in Travis County (%)	15.12	42.72	33.46	8.64	0.06

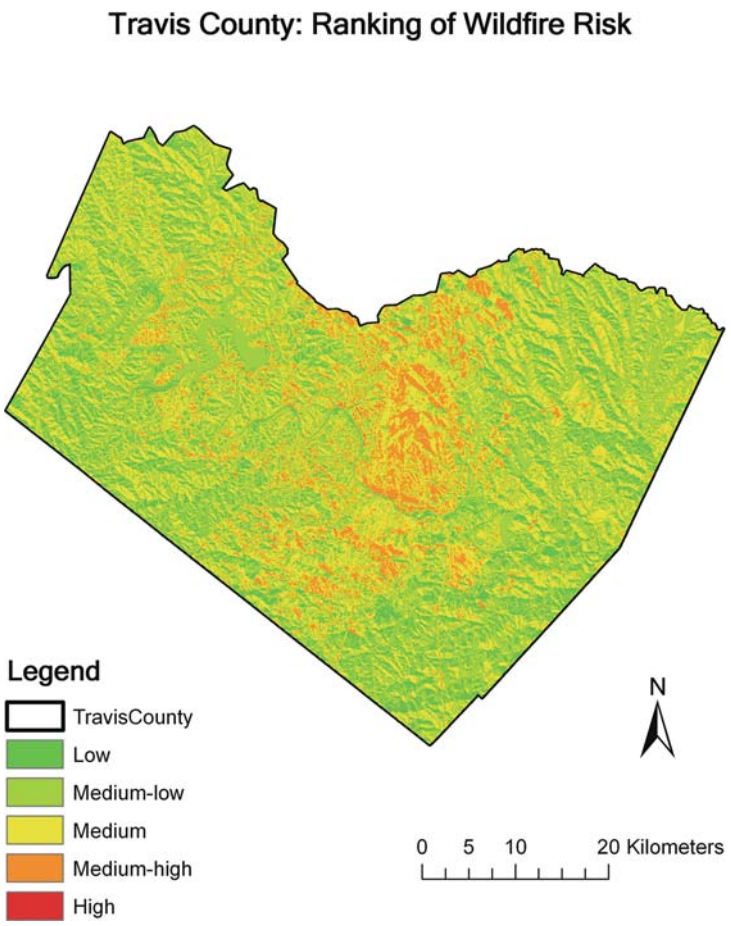

Fig. 10.8 Travis County wildfire risk ranking–overall

10.6 Risk of Wildfires in WUI Areas

As discussed earlier, wildland urban "Interface" and "Intermix" areas were defined following Radeloff et al. (2005) and Stewart et al. (2007). The definition groups all of the census blocks in Travis County into three different types: Interface, Intermix, and non-WUI blocks. Using the zonal statistics function in GIS, census block boundaries were used to define the zones belonging to the different types of WUI areas. The zonal statistics function calculates statistical indicators for all of the raster cells that are within the same zone – the same type of census block in this case. The wildfire risk level indicators derived for each type of census block are: minimum, maximum, mean, and median risk levels, standard deviation of the risk levels, and the majority of the risk levels. Due to space limitations, data for all 11,292 census

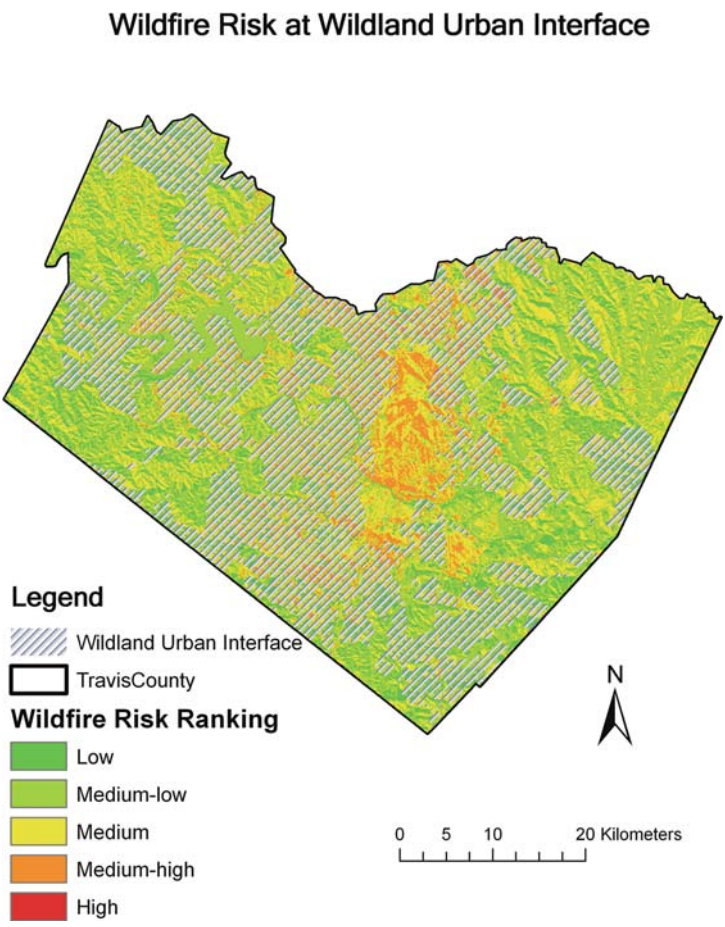

Fig. 10.9 WUI in Travis County and their wildfire risk

blocks are not reported here (but are available from the authors). Instead, Table 10.5 summarizes the different types of census blocks, classified according to their WUI status. Forty-six percent of the land in Travis County is in the WUI areas. More importantly for wildfire management and control, two-thirds of the county population and two-thirds of the housing units are within the WUI areas. These data illustrate that assessing wildfire risk for communities in the WUI is critical in order to appropriately prepare for, respond to, and contain wildfires.

The zonal statistics reported in Table 10.5 summarize the wildfire risk level for census blocks that belong to the same type of WUI category as *the average of the mean*, *the average of the median*, and *the average of the majority* risk levels. Table 10.5 reveals that the high-density WUI blocks (both Interface and Intermix) support more than 30% of the total population and more than 35% of the total

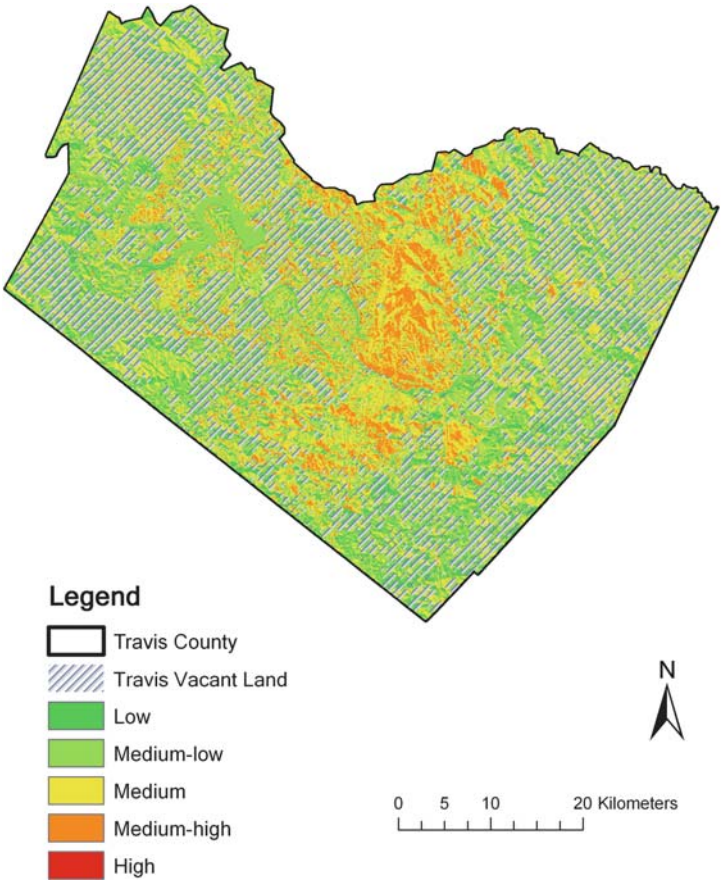

Fig. 10.10 Vacant lands in Travis County and their wildfire risk

housing units in the County. The Table also reveals that, despite the fact that the mean, median, and majority are different ways to represent fire risk for the many cells within each block, the average for the blocks belonging to the same WUI category can serve as an indicator of wildfire risk for each type of WUI area. It is a general trend that the wildfire risk increases from low-density WUI (both interface and intermix) through medium-density to high-density WUI blocks. This trend implies that within the WUI area, the higher the housing (and population) density, the higher the wildfire risk. In addition, compared to the non-WUI areas, blocks within low and medium density WUI areas are at lower risk for wildfire but the blocks within the high density areas are at much higher risk.

To confirm that the above observation was not spurious, further statistical analyses were applied to test for differences in fire risk levels in the different areas. Three statistical indicators for areal fire risk level were examined – the average

Table 10.5 Statistics for the different types of census blocks according to their WUI status

	WUI: interface			WUI: intermix				
	Low density	Medium density	High density	Low density	Medium density	High density	Not WUI	Total
Population size (%)	4463 (0.55)	102,631 (12.63)	209,856 (25.84)	28,137 (3.46)	127,520 (15.70)	65,522 (8.07)	274,151 (33.75)	812,280 (100)
Housing units (%)	1468 (0.44)	39,808 (11.85)	88,281 (26.28)	10,922 (3.25)	50,905 (15.16)	30,831 (9.18)	113,666 (33.84)	335,881 (100)
Number of blocks (%)	119 (1.05)	1665 (14.74)	1814 (16.06)	458 (4.06)	1127 (9.98)	437 (3.87)	5672 (50.23)	11,292 (100)
Area (km^2) (%)	1014 (3.56)	1295 (4.55)	707 (2.48)	6804 (23.91)	3126 (10.98)	252 (0.88)	15,259 (53.62)	28,456 (100)
Average mean risk level	2.80	2.92	3.11	2.41	2.71	3.20	3.04	
Average median risk level	2.80	2.95	3.12	2.41	2.73	3.27	3.04	
Average majority risk level	2.87	2.96	3.13	2.41	2.72	3.27	3.04	

of block mean fire risk, the average of block median fire risk, and the average of block majority fire risk. Non-parametric tests were conducted to compare the fire risk levels for: (1) WUI versus non-WUI areas, (2) high-density versus medium-density versus low-density WUI and non-WUI areas, and (3) high-density-interface versus medium-density-interface versus low-density-interface versus high-density-intermix versus medium-density-intermix versus low-density-intermix WUI and non-WUI areas. A Mann–Whitney (M–W) test and multiple Kruskal–Wallis (K–W) tests were conducted; the M–W test seeks to identify if there is a real difference between the scores of two samples. For example, if observations from two entirely different samples are ranked and mixed together, ranks from one sample should cluster on one end of a scale while ranks from the other sample should cluster on the other end. K–W is an extension of the M–W test to three or more groups of observations (Gravetter and Wallnau 1998; Ott 1984). The results from these two tests are reported in Table 10.6. All three indicators (mean, median, average of majority) are statistically different for the test groups at the 0.01 significance level. These non-parametric tests confirm that the fire risk levels in different types of WUI and non-WUI areas, as measured by each of the three tested indicators, are significantly different.

Examining Table 10.6, the M–W test comparing fire risk levels for WUI and non-WUI areas produced a low average fire risk within the WUI. This result may be due to the large number of Low- and Medium-density WUI blocks (with their associated relatively low fire risk) – 29.83% of the blocks classified as Low or Medium-density WUI, only 19.93% of the blocks classified as High.

Table 10.6 Results of the Mann-Whitney and Kruskal-Wallis tests

	Definition of groups	Average of the mean of risk levels	Average of the median of risk levels	Average of the majority of risk levels
Mann-Whitney	WUI blocks	5285.96	5413.35	5422.18
	Non-WUI blocks	6003.74	5877.51	5868.76
	Z value	−11.70*	−8.21*	−7.85*
Kruskal-Wallis (df = 3)	High-density WUI	6382.05	6293.05	6265.58
	Medium-density WUI	4853.50	5085.08	5106.15
	Low-density WUI	3102.48	3596.86	3661.20
	Non-WUI	6003.74	5877.51	5868.76
	Chi-Square	699.80*	511.44*	463.20*
Kruskal-Wallis (df = 6)	High-density interface WUI	6293.87	6177.63	6149.85
	Medium-density interface WUI	5278.81	5434.64	5470.03
	Low-density interface WUI	4728.34	4795.80	5066.68
	High-density intermix WUI	6748.08	6772.16	6745.97
	Medium-density intermix WUI	4225.15	4568.65	4568.55
	Low-density intermix WUI	2680.03	3251.33	3296.02
	Non-WUI	6003.74	5877.51	5868.76
	Chi-Square	814.22*	606.13*	569.08*

* Indicating significance level of 0.01.

In the K–W test for High versus Medium versus Low-density versus Non-WUI blocks, the Medium and Low-density WUI blocks show considerably lower fire risk than the Non-WUI blocks; but the High-density WUI blocks have much higher fire risk levels than the Non-WUI or other types of WUI blocks. More specifically, as the housing density in the WUI increases, the risk level for wildfire rises sharply. The fire risks in High-density Interface and High-density Intermix areas are significantly higher than all other types of blocks. Moreover, among all the different types of blocks, those in High-density Intermix WUI areas show the overall highest risk for wildfire, higher than those in the High-density Interface areas. Following the definition of High-density Intermix WUI, these blocks are in areas where vegetation covers more than 50% of the land and where the housing density is greater than 741 housing units per km^2. This finding confirms that the fire risk is highest where population and wildland are well-mixed. The large amount of vegetation in these High-density Intermix areas provides the fuel while the high density of housing units puts these blocks at high risk for property damage and loss of life from wildfires.

10.7 Limitations and Recommendations

The research presented here is not without its limitations. For example, wind speed/direction data are important elements when attempting to understand the potential for wildfire spread and duration. While we were able to locate county-wide data reporting monthly changes in wind direction and speed, we were unable to locate data regarding wind conditions at a finer resolution. In order to assess spatial variation in fire risk within/across the county, weather data at a higher spatial resolution is required. General weather conditions through time were also not incorporated into this study – if such information were included, it could add another layer of specificity to the findings.

While forest structure and canopy closure data are frequently incorporated into fire ignition models (Cova et al. 2004), they were not used here due to lack of availability. Other researchers have included road networks, distance to roads, and distance to agricultural fields in their research examining WUI wildfire potential (Perestrello de Vasconcelos et al. 2001). While the use of such data was outside the scope of this paper, they have the potential for revealing interesting spatial patterns if utilized in future research.

Two drawbacks concerning the use of census data must also be recognized. First, such data has limited spatial resolution in exurban areas (where census units can be very large). Second, the census is performed on a decadal basis, therefore has limited temporal resolution during which significant changes can occur (Cova et al. 2004).

The definition of WUI as used in this paper could also be flawed because it is not specific to Central Texas. The housing density criteria used to define the different types of WUI areas were developed based on the nationwide housing density situation in the US; the definition of WUI Interfaces as within 2.4 km of highly vegetation-covered area is based on the firebrand-carrying distance estimated from California data (Radeloff et al. 2005). Firebrands from grassland and bush fires, or from the less dense forest fires of Central Texas may behave differently than those on the west coast.

Given the above, it is recommended that future research consider incorporating the following data to further refine the results: (1) wind speed and direction at a scale finer than county-level, (2) meteorological data (e.g., humidity), (3) forest structure/canopy closure, (4) road networks, (5) distance to roads from ignition points, (6) distance to agricultural fields from ignition points, (7) finer resolution census data (perhaps by performing a survey of residents within their study area, or by processing recently acquired aerial imagery), and finally (8) a WUI definition specific to a study area.

10.8 Conclusion

The increased pace of development in fire-prone areas and exposure of new housing stock to wildfire poses a challenge for land use managers and emergency management officials (Cova et al. 2004). These managers need tools to help them plan for,

and thus mitigate, potential wildfires occurring in their areas of responsibility. With the goal of making new developments *disaster resilient*, it becomes imperative for decision makers to plan for the eventuality of wildfires, rather than simply responding to such fires when they occur (Godschalk et al. 1999).

This study assesses wildfire risk for Travis County, Texas. Historical wildfire data was linked to land cover to estimate the occurrence potential of wildfires on different types of land cover. The results were combined with the wildfire risk estimation derived from topographic characteristics. The final wildfire risk assessment was then related to Travis County's wildland urban Interface (WUI), an area recognized as being at higher risk for wildfire. Although the WUI blocks were not, as a group, subject to a higher fire risk level than the non-WUI blocks, it was confirmed that the high-density WUI areas have much higher fire risk levels than the medium- and low-density WUI blocks or the non-WUI blocks. This interesting pattern may signify the contribution of human activities to the ignition of wildfires – the high-density WUI areas are where sufficient vegetative supplies co-exist with more human activities while the low- and medium-density WUI areas lack human activities. This finding might indicate one "side-effect" of exurbanization in the study area. Exurbanization has been a trend in north America where many middle-class families move into areas that are outside of the city to be closer to nature but are still within commuting distance to the central city (Esparza and Carruthers 2000; Davies and Yeates 2008). Considering that the high-density WUI blocks (both Interface and Intermix) support more than 30% of the total population and more than 35% of the total housing units in Travis County, it is critical that appropriate measures be implemented in these areas to reduce the possibility of wildfire.

Further, the study discovered that the fire risk level in high-density-intermix WUI blocks is higher than that found in high-density-interface WUI blocks. Vegetation coverage is generally denser in WUI Intermix than WUI Interface areas. Therefore, in addition to human activity levels, the supply of fuel is an important factor when calculating fire risk. It can be concluded that as human activities rise in WUI areas (as indicated by increased housing density), controlling the vegetation supply might be an effective tool for fire risk management. Finally, with nearly 30% of the vacant land located in relatively high fire risk zones (especially when many of them are in the UWI areas) it is imperative to employ conscientious planning and preventive measures as development proceeds into these lands.

In 1999, Godschalk et al. wrote, "... geographic information systems and computer models ... [can] assist in guiding new development to safe locations ..." (p. 532). During the past two decades there has been an explosion in the use of GIS by private and governmental entities accompanied by enormous public exposure to maps and images produced by these systems. It is in this setting that we echo Franklin et al. (2000) who wrote that, "these types of analyses are [not only] essential for spatial decision support related to fire management, suppression, prevention, and land-use planning related to fire risk" (p. 1211), but are also becoming routinely expected from an increasingly sophisticated public.

Ultimately, effective mitigation programs must engage the participation of local governments, NGOs, private organizations and individual households (Godschalk

et al. 1999). Wildfire risk analyses such as the one demonstrated in this paper generate informative and compelling maps that can be used to encourage conscientious urban development, regulation of the WUI, scientific management of urban vacant lands, and the participation of local landowners in the protection of their property. These activities are integral necessities if Central Texas' communities are to be prepared for future wildfires.

References

Bradstock, Ross A., Jann E. Williams, and Malcom A. Gill (eds). 2002. *Flammable Australia: The Fire Regimes and Biodiversity of a Continent.* Cambridge University Press: Cambridge, United Kingdom.

Capitol Area Council of Governments (CAPCOG). 2008. Information Clearinghouse-Geospatial Data. http://www.capcog.org/Information_Clearinghouse/Geospatial_main.asp; last updated 2008. Accessed June 25, 2008.

Carapella, Ruth. 1996. Assessing fire risk using a GIS-based approach. *Earth Observation Magazine* 5(8): 22–24.

Cardille, Jeffrey A., Stephen J. Ventura, and Monica G. Turner. 2001. Environmental and social factors influencing wildfires in the Upper Midwest, United States. *Ecological Applications* 11: 111–127.

Christiansen, Julia. 2005. Calculating wildfire hazard levels: Algebraic raster construction using spatial analyst. Paper presented at *ESRI International User Conference,* San Diego, California, July.

Cohen, Jonathan D. 2000. Preventing disaster: Home ignitability in the wildland-urban interface. *Journal of Forestry* 98(3): 15–21.

Colorado State Forest Service (CSFS). 2007. Wildfire. Colorado State Forest Service, Colorado State University, Colorado Springs. http://csfs.colostate.edu/wildfire.htm; last updated October 8. Accessed April 14, 2008.

Cortner, Hanna J., Philip D. Gardner, and Jonathan G. Taylor. 1990. Fire hazards at the urban-wildland interface: What the public expects. *Environmental Management* 14(1): 57–62.

Cova, Thomas J., Paul C. Sutton, and David M. Theobald. 2004. Exurban change detection in fire-prone areas with nighttime satellite imagery. *Photogrammetric Engineering & Remote Sensing* 70(11): 1249–1257.

Davies, S. and Maurice Yeates. 2008. Exurbanization as a component for migration: A case study in Oxford County, Ontario. *Canadian Geographer* 35(2): 177–186.

Davis, James B. 1990. The wildland urban interface: Paradise or battleground? *Journal of Forestry* 88(1): 26–31.

Dennison, Philip E., Thomas J. Cova, and Max A. Mortiz. 2007. WUIVAC: A wildland-urban interface evacuation trigger model applied in strategic wildfire scenarios. *Natural Hazards* 41(1): 181–199.

Esparza, Adrian X. and John I. Carruthers. 2000. Land use planning and exurbanization in the rural mountain west. *Journal of Planning Education and Research* 21(1): 23–36.

Ewert, Alan W. 1993. The wildland urban interface: Introduction and overview. *Journal of Leisure Research* 25: 1–5.

Finney, Mark A. 2005. The challenge of quantitative risk analysis for wildland fire. *Forest Ecology and Management* 211(1–2): 97–198.

Franklin, Janet, Curtis E. Woodcock, and Ralph Warbington. 2000. Multi-attribute vegetation maps of forest service lands in California supporting resource management decisions. *Photogrammetric Engineering & Remote Sensing* 66 (10): 1209–1217.

Godschalk, David R., Timothy Beatley, Philip Berke, David J. Bower, and Edward J. Kaiser. 1999. Natural hazard mitigation: Planning for sustainable communities. In, *Natural Hazard Miti-*

gation: Recasting Disaster Policy and Planning, Chapter 13, pp. 525–552. Washington, DC: Island Press.

Gravetter, Frederick J. and Larry B. Wallnau. 1988. *Statistics for the Behavioral Sciences, 2nd Edition*. St. Paul, New York, Los Angeles, San Francisco: West Publishing Company.

Idaho Department of Lands (IDL). 2006. Summaries of risk and preparedness. *Jerome County WUI Wildfire Mitigation Plan*, Chapter 4, pp. 69–91. http://www.idl.idaho.gov/nat_fire_plan/county_wui_plans/jerome/jerome.htm; last updated November 11. Accessed June 25, 2008.

Ingalsbee, Timothy. 2003. Fuel breaks for wildland fire management: A moat or a drawbridge for ecosystem fire restoration? *Second Annual Wildland Fire Ecology and Fire Management Congress*, Orlando, FL, November 16–20, p. 1F.2. http://ams.confex.com/ams/FIRE2003/techprogram/paper_66008.htm; last update unknown. Accessed June 25, 2008.

Johnson, Angie. 2008. Mapping at local scale for CWPPs. Powerpoint presentation, 2008 Collaboration Workshop–Bringing it all Together, Reno, NV, March 3–4. Healthy Forests and Rangelands: Managing our National Heritage (US Department of Interior and Department of Agriculture). http://www.forestsandrangelands.gov/news/cwpp_workshop_2008.shtml; last updated April 15. Accessed June 25, 2008.

Keeney, Ralph L. 1995. Understanding life-threatening risks. *Risk Analysis* 15(6): 627–637.

Larkin, Thomas J. and George W. Bomar. 1983. *Climatic Atlas of Texas*. Texas Department of Water Resources, Austin, Publication No. LP-192, December. http://www.twdb.state.tx.us/publications/reports/GroundWaterReports/LimitedPublications/LP192.pdf, last update unknown. Accessed June 25, 2008.

Lawrimore, Jay. 2005. Climate of 2000- July Western U.S. wildfires. National Oceanic and Atmospheric Administration, National Climatic Data Center. http://lwf.ncdc.noaa.gov/oa/climate/research/2000/jul/west_fires.html; last updated June 25. Accessed May 3, 2008.

Lindley, T. Todd, Jared L. Guyer, Gregory P. Murdoch, Seth R. Nagle, Kenneth J. Schneider, and Gary D. Skwira. 2007. A Meteorological Composite of the 2005/06 wildfire outbreaks in the Southern Plains. Paper Presented at the Seventh Symposium on Fire and Forest Meteorology, Bar Harbor, ME, October 23–27, p. 10.4. http://ams.confex.com/ams/pdfpapers/126810.pdf; last update unknown. Accessed June 5, 2008.

Manzello, Samuel. 2007. Fires in the wildland-urban interface–experimental investigation of structural ignition in WUI fires. Project Information, Building and Fire Research Laboratory, National Institute of Standards and Technology. http://www2.bfrl.nist.gov/projects/projcontain.asp?cc=8662014000; last updated October 29. Accessed June 5, 2008.

National Interagency Fire Center (NIFC). 2006. Fire Information: Wildland fire statistics. National Interagency Fire Center, Boise, Idaho. http://www.nifc.gov/fire_info/historical_stats.htm; last update unknown. Accessed May 13 May, 2008.

Ott, Lyman. 1984. *An Introduction to Statistical Methods and Data Analysis*, 2nd Edition. Boston: Duxbury Press.

Perestrello de Vasconcelos, Maria José, Sara Silva, Margarida Tomé, and José Miguel Cardoso Pereira. 2001. Spatial prediction of fire ignition probabilities: comparing logistic regression and neural networks. *Photogrammetric Engineering & Remote Sensing* 67(1): 73–81.

Pyne, Stephen J. 2001. The fires this time, and next. *Science* 294: 1005–1006.

Radeloff, Volker C., Roger B. Hammer, Susan I. Stewart, Jeremy S. Fried, S.S. Holcomb, and Jason F. McKeefry. 2005. The wildland-urban interface in the United States. *Ecological Applications* 15(3): 799–805.

Silvis Lab (no date) Texas wildland-urban interface maps, statistics, and GIS data download. http://silvis.forest.wisc.edu/Library/WUI_state_download.asp?state=Texasandabrev=TX, accessed May 2008. Last update, unknown.

Smith, Keith. 2004. *Environmental Hazards: Assessing Risk and Reducing Disaster*, 4th edition. Routledge: London and New York.

Stewart, Susan, Volker C. Radeloff, Roger B. Hammer, and Todd J. Hawbaker. 2007. Defining the wildland-urban interface. *Journal of Forestry* 105(4): 201–207.

Texas Forest Service (TFS). 2007. Protecting your home against wildfires in Texas–everyone's responsibility. *Living on the Edge*, Texas Forest Service Urban Wildland Interface Publication. http://txforestservice.tamu.edu/main/article.aspx?id=1583; last updated September. Accessed May 17, 2008.

Texas Natural Resources Information System (TNRIS). 2008. National Agriculture Imagery Program (NAIP) and DOQQ Imagery. *Strat Map*, Texas Natural Resources Information System. http://www.tnris.state.tx.us/StratMap.aspx?layer=126; last update January 16. Accessed February 13, 2008.

Texas State Data Center and Office of the State Demographer (TSDC/OSD) 2006. New Texas State Data Center Population Projections from The University of Texas at San Antonio. Institute for Demographic and Socioeconomic Research (IDSER), College of Public Policy, University of Texas at San Antonio. http://txsdc.utsa.edu/tpepp/2006projections/summary/; last updated October 19; accessed June 23, 2008.

Thompson, William A., IIan Vertinsky, Hans Schreier, and Bruce A. Blackwell. 2000. Using forest hazard modeling in multiple use forest management planning. *Forest Ecology and Management* 134(1–3): 163–176.

Travis County. 2004. Travis County Parks. Travis County Transportation and Natural Resources Department. www.co.travis.tx.us/tnr/parks/climate.asp; last updated February 2. Accessed May 13, 2008.

Travis County. 2007. Section I: 2006–2010 Consolidated Plan, Amended August 2007.http://www.co.travis.tx.us/health_human_services/CDBG/August07Amendment/ConPlanAug07Amend_SectionI_Introduction.pdf; last updated August 2007; accessed October 15, 2008.

Travis County Health and Human Services and Veterans Service Department (TCHHS). 2006. American Community Survey, Travis County, Texas: Analysis of Trends 2002–2005. Research and Planning Division; http://www.co.travis.tx.us/health_human_services/research_planning/publications/ACS_2005_Report.pdf; last updated November; accessed October 15, 2008.

Trembath, Rick. 2005. Firebrands and long duration smoldering fires: What is the risk? How should we deal with them? *Wildfire News and Notes* 19(2): 2–8.

U.S. Geological Survey (USGS). No date. National Elevation Dataset. USGS Seamless Data Distribution System. http://seamless.usgs.gov/website/Seamless/viewer.htm; last update unknown. Accessed May 3.

Winter, Greg J. and Jeremy S. Fried. 2001. Estimating contingent values for protection from wildland fire using a two-stage decision framework. *Forest Science* 47(3): 349–360

Index